Structural Characterization of Recycled Materials at the NCAT Test Track

by

Miguel Angel Díaz Sánchez

A dissertation submitted to the Graduate Faculty of
Auburn University
in partial fulfillment of the
requirements for the Degree of
Doctor of Philosophy

Auburn, Alabama
December 14, 2019

Keywords: pavement, asphalt, cement,
recycling, reclaiming

Approved by

David H. Timm, Chair, Brasfield & Gorrie Professor of Civil Engineering
Rod E. Turochy, James Madison Hunnicutt Professor of Traffic Engineering
Adriana Vargas, Assistant Research Professor, National Center for Asphalt Technology
Fabricio Leiva, Assistant Research Professor, National Center for Asphalt Technology
April Simons, Assistant Professor of Building Science

Abstract

The functional and structural performance of two pavement recycling techniques: Cold Central-Plant Recycling (CCPR) and Cement Treated Base (CTB) from a Full Depth Reclamation (FDR) process, were evaluated under accelerated pavement testing (APT). Three test sections, consisting of a combination of CCPR and CTB layers built underneath a set of asphalt concrete (AC) layers, were built in 2012 at the National Center for Asphalt Technology (NCAT) Test Track. A total traffic of 20,055,247 ESALs was applied to each test section by a fleet of special tractor trailer rigs manually operated at a target vehicle speed of 45 mph. During this period, the evolution of the performance of each test section was evaluated periodically.

Based on weekly visual inspections and field measurements it was identified that, after over 20 million ESALs, rut depth and ride quality (represented by the international roughness index or IRI) remained well below the limiting criteria used at the Test Track. Periodical falling weight deflectometer (FWD) testing and weekly stress and strain measurements (by means of embedded instrumentation) revealed the structural performance and pavement response of the test sections remained relatively constant over the application of traffic. Laboratory testing and FWD backcalculated modulus showed the CCPR is a temperature-dependent material, with slightly less temperature susceptibility than conventional AC. Similarly, based on the performance measurements, it was determined that the CTB significantly improved the response of the pavement under traffic loading.

The obtained results were used to evaluate the structural contribution of the recycling technologies from a pavement design perspective. Based on empirical pavement design it was determined that the structural layer coefficients of CCPR ranged between 0.30 and 0.35, while those of CTB ranged between 0.20 and 0.25. Additionally, based on mechanistic analyses and the measured pavement responses it was determined that the correct combination of CCPR and CTB may result in a perpetual pavement. Although additional research is needed to support the previous statements, this research provided sufficient information on the performance and failure mechanisms of CCPR and CTB, indicating they may be used for high traffic applications.

Acknowledgements

The author would like to thank Dr. David H. Timm for his guidance and encouragement during the development of this dissertation, and for trusting in him during all these years. Gratitude is also expressed to the advisory committee for their help and direction over the time it took to finalize this dissertation. The author would also like to acknowledge his professors at Auburn University, the staff at the National Center for Asphalt Technology, Dr. Brian Diefenderfer at the Virginia Transportation Research Council, and the Virginia Department of Transportation, for their support of this research. Special thanks are due to his parents Angel and Mayra, and the Diaz Sanchez family for their continuous support and motivation. Finally, to his wife Ximena, and their two daughters Natalia and Ana Lucia, for their unfailing love and continuous encouragement in every step of the way. None of this would have been possible without them.

Table of Contents

List of Tables

List of Figures

List of Abbreviations

AASHTO	American Association of Highway and Transportation Officials
AC/CCPR	Combined layer composed by AC and CCPR
AC	Asphalt Concrete
AMPT	Asphalt Mixture Performance Tester
ANOVA	Analysis of Variance
APA	Asphalt Pavement Alliance
APT	Accelerated Pavement Testing
ARRA	Asphalt Recycling and Reclaiming Association
ASG	Asphalt Strain Gauge
BWP	Between Wheel Path
CBR	California Bearing Ratio
CCPR	Cold Central Plant Recycling
CDF	Cumulative Distribution Function
CIR	Cold In-place Recycling
COV	Coefficient of Variation
CP	Cold Planing
CR	Cold Recycling
CTB	Cement Treated Base
DOT	Department of Transportation
EPC	Earth Pressure Cell
ESAL	Equivalent Single Axle Load
FDR	Full-Depth Reclamation

FEA	Finite Element Analysis
FWD	Falling Weight Deflectometer
GTR	Ground Tire Rubber
H-ASG	Horizontal Asphalt Strain Gauge
HIR	Hot In-place Recycling
HMA	Hot Mix Asphalt
HR	Hot Recycling
IRI	International Roughness Index
ITS	Indirect Tensile Strength
IWP	Inside Wheel Path
LEA	Layered Elastic Analysis
MEPDG	Mechanistic-Empirical Pavement Design Guide
NAPA	National Asphalt Pavement Association
NCAT	National Center for Asphalt Technology
NCHRP	National Asphalt Pavement Association
NDT	Non-Destructive Testing
NMAS	Nominal Maximum Aggregate Size
OWP	Outside Wheel Path
PCA	Portland Cement Association
PPD	Perpetual Pavement Design
RAP	Reclaimed Asphalt Pavement
RAS	Reclaimed Asphalt Shingles
RL	Random Location

RMSE	Root Mean Square Error
SMA	Stone Matrix Asphalt
SN	Structural Number
SSR	Subgrade Stress Ratio
TSR	Tensile Strength Ratio
UCPRC	University of California Pavement research Center
UCS	Unconfined Compressive Strength
V-ASG	Vertical Asphalt Strain Gauge
VDOT	Virginia Department of Transportation
VTRC	Virginia Transportation Research Council
WMA	Warm Mix Asphalt

CHAPTER ONE

INTRODUCTION

1.1 BACKGROUND

With the ever increasing global demand for construction and rehabilitation of transportation infrastructure, a collective necessity for pavement structures capable of meeting the needs of present road users without compromising future generations, becomes evident. The pavement engineering community is challenged with developing innovative technologies and construction methods that take into account environmental, economic and social indicators, targeting sustainable development. In that way, sustainable pavements must systematically minimize the consumption of non-renewable resources, maximizing the reuse of existing materials, while generating a minimum of pollutants and directly benefiting society, in the most cost-effective manner. Multiple innovative pavement recycling and reclamation techniques, using common recycling agents such as hydraulic cement and asphalt binder, meet these requirements.

The environmental, performance, and economic benefits of reusing existing pavement materials have turned the concept of pavement recycling into a popular choice when building new roads or rehabilitating distressed pavement structures. According to the Asphalt Recycling and Reclaiming Association (ARRA), pavement recycling consists of a series of technologies that can be used to rehabilitate distressed pavements or construct

new pavements while reducing costs, construction time, and environmental impacts (ARRA, 2001). For rehabilitation projects, pavement recycling consists of re-mixing the existing pavement materials on-site and reusing them in in the final pavement structure. For new construction projects, pavement recycling allows reusing materials from existing stockpiles of reclaimed asphalt pavement (RAP) and include them to build new pavements. Benefits to using recycling techniques include reduced use of virgin materials, reduced fuel consumption, reduced time of lane closures, reduced emissions related to construction (Nataatmadja, 2001; Thenoux et al., 2007; Stroup-Gardiner, 2011), and large cost savings (Bemanian et al., 2006) allowing highway agencies to better preserve their pavement network.

Although many recycling techniques are continuously developed and fostered by equipment and material manufacturers, according to the ARRA (2001), all pavement recycling techniques may be categorized in three general groups for practical purposes: (1) Hot Recycling, (2) Cold Recycling, and (3) Full-Depth Reclamation. Within these three broad categories, there are a number of sub-categories which further describe pavement recycling depending on the specific method or process used to obtain the recycled material.

The Basic Asphalt Recycling Manual (ARRA, 2001), published by ARRA, establishes a difference between Hot Recycling (HR) and Hot In-Place Recycling (HIR). On the one side, traditional HR is defined as the process of combining RAP with new or "virgin" aggregates, new asphalt binder, and/or recycling agents (as required) in a central plant to produce a recycled asphalt mixture. On the other, HIR is defined as the process of recycling the existing asphalt pavement structure on site, by a heating and softening process that allows scarifying or loosening the existing pavement, which is then thoroughly mixed

and subsequently placed and compacted with conventional HMA paving equipment. A survey conducted by the National Asphalt Pavement Association (NAPA) reported that 97.4% of asphalt concrete producers used RAP in 2018 with 82.2 million tons used that year in hot mix asphalt (HMA) or warm mix asphalt (WMA) production (Williams et al., 2018), making HR the most widely used asphalt recycling method in the United States. This tonnage was a 46.8% increase over the amount recycled in 2009 with less than 0.012% of RAP sent to landfills, corroborating the advantage of pavement recycling.

HIR requires an extensive number of pieces of specialized construction equipment including heaters, scarifiers, mixers, pavers and rollers that may spread over a considerable distance. This sequence of machines is generally referred to as an "HIR train" and its length and composition varies depending on specific construction conditions. In a conventional HIR process the existing pavement is heated and reused as an improved base layer, reactivating the existing asphalt binder in the road by means of engineered additives and rejuvenators that allow for reusing the aged binder in the new mixture. Although new asphalt binder is occasionally added, the main advantage of HIR is that it allows reusing the residual binder in the existing pavement, which in turn generates a low-priced material, even if the HIR process is relatively expensive by itself. Due to all these constraints and complexities, HIR is a slightly less common pavement recycling method than the other.

Full-Depth Reclamation (FDR) is a different recycling technique that allows reclaiming and stabilizing the existing pavement materials, including the full thickness of the asphalt layer and a predetermined portion of the underlying layers (base, subbase, and/or subgrade), to produce an upgraded, homogeneous base material. Unlike HIR, the application of heat is not necessary for the construction of the FDR, and since the process

may be performed regardless of the type of pavement materials found in the roadway, FDR thicknesses may range between 4 and 12 inches (Wirtgen, 2012). The resulting recycled layer may be categorized as a granular material, and can be used as-is or enhanced by the addition of a stabilizing additive to meet the mechanical properties and structural strength required to support the anticipated loads. Commonly used stabilizing additives include portland cement, asphalt emulsion, and foamed asphalt, although other additives such as calcium chloride, magnesium chloride, lime, fly ash, and cement kiln dust may be also used (ARRA, 2001).

The FDR process is relatively simple, which led to the use of a great number of reclamation methods including rippers, scarifiers, and conventional milling machines which in turn tended to increase the relative cost of producing the recycled material (ARRA, 2001). However, the recent development of more advanced reclaiming/stabilizing machines has modernized FDR processes, making it a high-quality, low-cost solution (Wirtgen, 2012). Modern reclaimers have a rotary drum, especially designed to pulverize the existing pavement layers and mix it with the right amount of additive at the same time, in one single pass, achieving higher productivities in the field and an optimum quality of the recycled material. Nonetheless, the process can also be performed in multiple passes of the reclaimer, adding the stabilizing additive independently after the pavement has been initially pulverized to achieve a more uniform application of the additive.

Lastly, the term “cold recycling” or “CR” refers to the rehabilitation of asphalt pavements by recovering and reusing the existing asphalt pavement layers, without the application of heat during the process. Unlike hot recycling (HR), which generally accounts for reusing the residual asphalt binder from the asphalt concrete layers by applying

rejuvenating agents and heat; in CR techniques, the residual asphalt from the bound layers is not considered during the recycling process. The asphalt binder adhered to the aggregates from the reclaimed asphalt pavement (RAP), is assumed to behave as an integral part of the aggregate particle in the final CR mixture.

According to the recycling equipment manufacturer Wirtgen GmbH (Wirtgen, 2012), the recent developments in pavement recyclers have unveiled a wide range of possibilities for pavement preservation and rehabilitation through CR and/or Full Depth-Reclamation (FDR). Even if FDR is categorized as a separate recycling technique, different from traditional CR, the equipment and recycling agents used tend to be very similar, leading to the misconception that both techniques are one and the same. However, according to the ARRA (2001), a distinction must be made as the two processes are conceptually different. Whereas in an FDR process the full thickness of the asphalt pavement and a predetermined portion of the underlying materials is uniformly pulverized to provide the new base material; the concept of CR is limited to using the RAP from the upper asphalt pavement layer to provide this upgraded base material. In that way, the FDR can only be performed "in-place" while the CR can be achieved either "in-plant" or "in-place".

Using a recycling machine and a process similar to the FDR process, but limited to the asphalt concrete layers, CR can be performed "in-place". Alternatively, the RAP materials from an existing road can be hauled to a centrally located facility, where the CR material can be produced "in-plant". Depending on the project conditions, Cold In-Place Recycling (CIR) may be a preferred method due to its relative economic advantages (Wirtgen, 2012). However, in-plant processing or Cold Central Plant Recycling (CCPR)

may offer additional quality and practical benefits which may encourage its use for specific project conditions, including limitations in materials availability and the available time for lane closures. For this, CCPR has been successfully used in many important projects around the world, including the Ayrton Senna Highway in Sao Paulo, one of the most trafficked highways in the world (Wirtgen, 2017).

The CIR process is performed on site, using 100% RAP materials milled directly before the mixing process occurs, as part of the same construction sequence. The thickness of the recycled pavement depends on the type of recycling agent used for the process. In that way, common depths may range between 2-4 inches when the recycling agent is only asphalt emulsion or an emulsified recycling agent; and 5-6 inches when chemical additives, such as portland cement, lime, kiln dust or fly ash are used to improve the early strength gain and resistance to moisture damage (ARRA, 2001). A number of specialized pieces of equipment are required to perform the CIR process, including tanker trucks, milling machines, mobile crushing and screening units, mixers, pavers, and rollers. The equipment formation usually spreads out over a considerable distance in a specific recycling sequence, commonly referred to as the "CIR train". Although the final recycled material is very similar at the back of the CIR train, the construction sequence may present slight variations depending on the type of train and its specific equipment configuration. The CIR trains differ from one another in the way the RAP is removed and sized, the way the recycling additives and modifiers are added, the way the materials are mixed, and the way the recycled material is finally placed. Nonetheless, all these processes are performed by a CIR train in a continuous and iterative process that expands for the complete length of the roadway.

CCPR on the other hand, is a process in which newly milled or existing stockpiled RAP is combined at centrally located plant with the recycling agent (and chemical additives, if needed) to produce a recycled material that can be placed in a conventional asphalt paving process. Since the CCPR process is not performed in-place, the underlying foundational materials can be stabilized or treated, if needed, prior to placement of the CCPR material as an enhanced base layer. Additionally, the CCPR process allows placing thicker or even multiple lifts for a thicker, more robust pavement structure that uses RAP milled in other projects and not necessarily the one coming from the project being built. In that way, the CCPR can be used to produce an enhanced, recycled base course for reconstruction, new construction, lane widening, shoulder strengthening, and other type of projects. Typical layer thicknesses for CCPR range from 2 to 6 inches (ARRA, 2001), but multiple lifts may be used to increase the total thickness of the recycled layer.

1.2 PROBLEM IDENTIFICATION

Among all the recycling techniques described previously, FDR and CCPR are becoming popular solutions and particularly appealing to many agencies (Diefenderfer and Apeagyei, 2011). Both technologies have proven effective in addressing two important needs: (1) recycling the existing pavements and (2) reusing reclaimed materials commonly stockpiled by agencies. On the one hand, FDR allows reusing the existing pavement layers regardless of the type of material in each layer, by means of a relatively simple and cost-effective process, reducing the impact on the road users. On the other, CCPR allows for massively reusing RAP stockpiles obtained from different projects in a cost effective manner and ensuring a homogeneous new base layer.

However, despite some successful experiences evidenced by many highway agencies around the world (Mallick et al., 2002; Mohammad et al., 2003; Romanoschi et al., 2004; Saleh, 2004; Wen et al., 2004; Lane and Kazmierowski, 2005; Bemanian et al., 2006; Lewis et al., 2006; Berthelot et al., 2007; Guthrie et al., 2007; Maurer et al., 2007; Hilbrich and Scullion, 2008; Diefenderfer and Apeagyei, 2011b), CCPR and FDR are still not widely employed in the United States. Its consistent and widespread use is still hindered by the apparent lack of information addressing its structural and functional performance, including the lack of long-term performance data from which to derive the expected service life and a lack of understanding of the failure mechanisms in the field for these technologies. In addition, there are no specific guidelines and procedures to include these two technologies in common pavement thickness design methodologies. For this reason, many pavement engineers may oppose the use of such technologies until more definitive information on the subject is available.

When designing a pavement, engineers require a high degree of certainty to guarantee the selected thicknesses and materials are adequate to withstand the traffic loads and environmental conditions over the design life. However, in the case of these recycled materials, the available research is insufficient to provide this required level of confidence. Although ongoing research is establishing the foundation to address these needs for some recycling techniques, there is limited evidence that substantiates its performance and structural response under high traffic volumes. Furthermore, there is a palpable need for structural design criteria to help pavement engineers advance and design long-lasting recycled pavements.

1.3 OBJECTIVES

Three main objectives were identified for this research and are described as follows:

1. Evaluate the structural and functional performance of CCPR and Cement Treated Base (CTB) from an FDR process under high traffic volumes through accelerated pavement testing (APT).
2. Characterize the structural response of CCPR and CTB from FDR and its evolution under high traffic volumes through APT.
3. Determine the structural contribution of CCPR and CTB from FDR, and how these materials should be considered for structural design according to current pavement design methods.

1.4 SCOPE OF STUDY

To accomplish the aforementioned objectives, the laboratory characterization and field performance of three test sections, built with CCPR and CTB materials at the National Center for Asphalt Technology (NCAT) Test Track, were studied. The test sections were built in 2012 as part of a larger study conducted and sponsored by the Virginia Department of Transportation (VDOT) to evaluate the field performance of CCPR materials under high traffic conditions and evaluate its structural contribution in a pavement structure. The study was originally formulated to address two specific research objectives with paired test sections. Sections N3 and N4 were designed to evaluate the difference between 4 inches and 6 inches of AC over 5 inches of CCPR, while sections N4 and S12 were designed to determine the differences between aggregate base (6 inches) and a cement treated base (CTB) layers (8 inches).

During construction, field samples were collected and used to conduct multiple laboratory tests and evaluate the performance of CCPR and CTB. Laboratory testing for the CCPR and the CTB was conducted at the Virginia Transportation Research Council (VTRC) laboratory. The CCPR was comprehensively evaluated as part of a particular laboratory study conducted by VTRC after construction, while the CTB was tested as part of the design process.

The three test sections were left in place for two research cycles at the NCAT Test Track. During this time, a total of 20,055,247 equivalent single axle loads (ESALs) were applied to each test section by fleet of special tractor trailer rigs manually operated at a target vehicle speed of 45 mph. The sections were instrumented with an arrangement of asphalt strain gauges, earth pressure cells, and temperature measuring devices, which allowed determining the pavement response under the specific climate and traffic conditions of the NCAT Test Track on a weekly basis. Additionally, the functional and structural performance of each test section was monitored on a routine basis over the duration of the study. Weekly visual inspections and performance measurements of rut depth and ride quality were conducted to maintain current and updated data through slightly different dates over the research cycle. Similarly, FWD testing was conducted several times per month on each test section.

1.5 ORGANIZATION OF DISSERTATION

This dissertation was structured as seven independent chapters, including the present introductory chapter, five primary chapters, and a final conclusive chapter. Even if each individual chapter on the body of this dissertation addresses a specific stage of the

investigation, they all follow a logical order to support the final conclusions, included in the seventh and final chapter.

The second chapter presents the literature review, including a brief overview of the most common pavement design methodologies, followed by individual synopses describing the design, construction and structural performance of the two recycling techniques addressed in this investigation: Cold Central-Plant Recycling (CCPR) and Cement-Treated Bases (CTB). The third chapter describes the experimental plan of the investigation, detailing the main characteristics of the VDOT test sections included in the 2012 structural study, the construction process, and the testing plan followed for the study. Chapter four summarizes the results from laboratory testing conducted on the recycled materials as part of design, quality control and construction activities.

Chapter five focuses on the long term structural and functional performance of the three test sections during trafficking, based on the weekly monitoring performed at the NCAT Test Track. The results from non-destructive testing (NDT) and response measurements are presented and analyzed. Furthermore, Chapter Six contains additional analyses, conducted whenever possible, to identify the structural characteristics of the recycled materials based on the results obtained from performance monitoring of the test sections and from the perspective of different pavement design methods.

CHAPTER TWO

LITERATURE REVIEW

2.1 INTRODUCTION

Recent advances in pavement recycling technologies and processes have expanded the possibilities for rehabilitating or reusing distressed pavements while optimizing quality, accelerating construction, reducing costs, and minimizing the environmental impact. Multiple pavement recycling techniques, ranging from the use of Reclaimed Asphalt Pavement (RAP) for asphalt mixtures in new construction projects to recycling the entire pavement structure through a Full-Depth Reclamation (FDR) process in rehabilitation projects, are becoming popular choices in several U.S. states due to their environmental, performance, and economic benefits. However, the widespread use of pavement recycling techniques is hindered by the apparent lack of information addressing structural design and long-term functional performance. In other words, the available information on the topic is still insufficient to provide the level of confidence required by pavement designers to have high confidence in their designs. Based on the available literature, this chapter presents a brief overview of the most common pavement design methodologies, followed by individual synopses describing the design, construction and structural performance of the two recycling techniques addressed in this investigation: Cold Central-Plant Recycling (CCPR) and Cement-Treated Bases (CTB).

2.2 PAVEMENT DESIGN METHODS

Over the last half-century, flexible pavement design has evolved from experience-based thickness selection to more analytically-based engineering approaches (Monismith, 2012). The emergence of the U.S. interstate system in the mid 1950's sparked a renewed interest in the development of better-engineered pavement structures and a uniform set of design standards (Timm et al., 2014). At that juncture, the AASHO Road Test (HRB, 1962) established the foundation for modern pavement design and provided the impetus for the development of the empirical pavement design method adopted by the American Association of Highway and Transportation Officials (AASHTO) in the 1960's. This empirical pavement design method is known today as the AASHTO 93 Pavement Design Guide and is extensively used for the design of pavement structures.

As described by Timm et al. (2014), although mechanistic approaches were developed and validated over the decades following the 1960's, it wasn't until National Cooperative Highway Research Program (NCHRP) Project 1-37A in the 1990's that AASHTO began to seriously develop a mechanistic-empirical pavement design method, which was fully adopted in 2013. Simultaneously, in the early 2000's, the National Asphalt Pavement Association (NAPA), in conjunction with the Asphalt Pavement Alliance (APA), began endorsing the use of a pavement design method based on long-life, or perpetual pavement concepts. Currently, these three design methods (empirical, mechanistic-empirical, and perpetual) constitute the predominant means of designing pavement structures in the world. An understanding of the unique attributes of each design method is relevant for this dissertation to determine a proper procedure to include a CCPR and CTB with a sufficiently high level of confidence.

2.2.1 Empirical Pavement Design

The AASHTO Guide for Design of Pavement Structures (AASHTO, 1993) describes the empirical design method adopted by AASHTO. In the case of flexible pavements, the determination of a pavement thickness is based on empirical correlations obtained at the AASHO Road Test. Heuristic equations associate specified traffic loadings to a corresponding structural number (SN), which in turn defines the structural capacity required for the pavement. The SN of a pavement structure can then be determined as the mathematical summation of the individual thicknesses of each layer multiplied by two empirical coefficients, a layer coefficient (a_i) and a drainage coefficient (m_i), which account for the layer-specific structural contribution and the drainage capabilities, respectively. In the same way, the SN can also be used to represent the structural capacity of each layer in the pavement cross-section as the product of the layer thickness and the corresponding layer and drainage coefficients. Hence, a direct correlation may be established between the structural layer coefficient and the measured elastic modulus of each layer. Based on such correlation, the structural layer coefficient may be used to empirically describe the structural contribution of a specific pavement layer under traffic loading.

The layer coefficients used today are largely based on analytical projections of the results obtained during the AASHO Road Test and fail to consider the more recent advances in pavement recycling techniques. Some layer coefficients have been proposed for a limited number of recycled materials, though the recommended values are mostly based on the results from laboratory testing. The most appropriate way of determining the structural contribution of a recycled pavement layer would be to study its performance under realistic conditions that roughly replicate the AASHO Road Test. By evaluating the

evolution of pavement properties and distresses under representative traffic loading, it would be possible to estimate layer coefficients for the recycled layers. The obtained field-based layer coefficients may be sufficiently reliable to be used as an input in the empirical pavement design method.

2.2.2 Mechanistic-Empirical Pavement Design

One of the main disadvantages of the AASHTO 93 Pavement Design Method is that it is based on the results of a field test, and therefore its applicability is limited to the specific conditions of the test. For this reason, the NCHRP developed the Mechanistic-Empirical Pavement Design Guide (MEPDG), which incorporates project-specific considerations and nationally calibrated models to predict pavement performance over time (Applied Research Associates, 2004).

The MEPDG consists of a multi-step analysis procedure that incorporates project-specific material properties, local weather conditions, and precise load spectra to predict the long-term performance of the pavement, based on mechanistic models and empirical experimental results. For a defined pavement structure, mathematical models, such as layered elastic analysis (LEA) or finite element analysis (FEA), are used to calculate the structural response of each pavement layer, according to their specific material properties, under different loading and environmental conditions. The obtained stresses, strains and deflections are projected over the design period and correlated to empirically-derived and locally-calibrated transfer functions, which allow predicting the development of distresses over time. Distresses are sequentially added until the damage exceeds allowable limiting criteria established on the basis of rideability. Pavement failure is therefore defined as a

distress threshold beyond which the pavement structure is expected to be reconstructed or rehabilitated. Due to the complex and extensive procedures and analyses required by the MEPDG, a pavement design software, known as the AASHTOWare Pavement ME Design Software, has been developed and is currently supported by AASHTO (AASHTO, 2017).

Although national and local calibration of the MEPDG have been performed, none of these calibrations considered recycled materials. Furthermore, the MEPDG provides little if any guidance for using these materials. Ongoing research under NCHRP Project 09-51 aims to propose material properties and associated test methods and distress models for predicting the performance of CIR and FDR with asphalt binder as stabilizing agent (NCHRP, 2017). However, CCPR and CTB materials do not seem to be addressed. An efficient way of determining the structural contribution of recycled pavement layers would be to compare the performance predicted by the AASHTOWare Pavement ME Design Software and the performance measured in the field under known traffic and environmental conditions leading to the ultimate failure of the pavement. However, performing a local or material-specific calibration would require extensive long-term performance data, including the moment of final pavement failure.

2.2.3 Perpetual Pavement Design

Although the MEPDG is a substantial improvement over its predecessor, the AASHTO 93 Pavement Design Method, it is still based on empirical equations that correlate pavement responses to its long-term performance and failure. An alternative approach, known as perpetual pavement design, considers limiting the critical stresses, strains and deflections

to a level below which structural damage does not accumulate and therefore substantial structural distresses should be eradicated over the service life of the pavement.

While the concept of perpetual pavements was introduced in 2000 by the Asphalt Pavement Alliance (APA, 2002), the Perpetual Pavement Design (PPD) concept is based on a mechanistic-empirical approach. However, instead of correlating pavement responses to damage as the MEPDG, the objective of PPD is to define a pavement structure in which the vast majority of expected loads produce stresses, strains and deflections lower than those which would cause structural damage on the pavement. Most approaches to PPD focus on limiting the pavement responses related to the most common structural pavement distresses; structural rutting and bottom-up fatigue cracking. A comprehensive overview of PPD was presented by Newcomb et al. (Newcomb et al., 2010). Although several limiting criteria for PPD have been proposed over the years, most recent studies utilize measured and simulated control strain distributions to evaluate the pavement structure (Willis and Timm, 2010; Castro et al., 2017). A PPD software, known as PerRoad, has been developed under support of the APA, and has been recently updated to incorporate control strain distribution evaluations.

As for the two previous pavement design methods, the information addressing the use of recycled materials in PPD is very limited. An efficient way of determining the structural contribution of such materials in PPD would be to analyze the measured and predicted structural responses of pavement sections under realistic traffic conditions. These stresses, strains, and deflections may then be compared to the limiting criteria developed for each condition to assess the applicability of PPD for the structural design of pavements containing recycled materials.

2.3 COLD CENTRAL PLANT RECYCLING

Cold central-plant recycling (CCPR) is an innovative cold recycling (CR) alternative that constitutes an environmentally-friendly and cost effective solution that allows for reusing large amounts of stockpiled RAP as an enhanced base layer for a new pavement (Wirtgen, 2012). According to the ARRA (2001), CCPR is categorized as a CR technique in which the asphalt recycling process takes place in a central location by means of a stationary cold mixing plant or a CIR train, minus the milling machine, setup in a stationary configuration. In that way, due to its fabrication process and depending on the type of additive selected, the CCPR mix can be used immediately or it can be stockpiled for later use in other applications (ARRA, 2001).

2.3.1 CCPR Production Process

For the production of the CCPR, the RAP obtained from milling operations or cold planning (Figure 2.1) is transported to the cold mixing plant facility and carefully stockpiled to avoid excessive contamination. If necessary as part of the job mix formula, new aggregates can also be stockpiled at the plant site. Depending on the type and origin of the RAP being used, additional crushing and/or fractionating may be required at the plant site to achieve the specified gradations needed for the CCPR mixture (ARRA, 2001).

Figure 2.1 Cold Planning Machine (ARRA, 2001)

As shown in Figure 2.2 and 2.3, traditional CCPR plants consist of a number of cold feed bins for the RAP and the new aggregate (if used), a computer controlled belt scale, a computer controlled dosing system for the recycling additive, a pugmill mixer, and either an optional hopper for temporary storage of the CCPR or a conveyor/belt stacker that allows stockpiling the CCPR (ARRA, 2001). In that way, during production the RAP (and the aggregates, if necessary) is loaded into the cold feed bins where it is weighted by the belt scale and transported into the mixing unit. At this stage, the recycling additives are added and thoroughly mixed with the RAP materials to provide a uniform mixture. The new material is subsequently transported by a conveyor/belt into a storage hopper or directly discharged to the ground to form a stockpile or into a dump truck for hauling to the job site. In a conventional CCPR mixing plant the RAP is loaded into the cold feed bins, weighted in a conveyor equipped with a load cell before being introduced into a

mixer. In this closed twin shaft pugmill mixer, the RAP is combined with asphalt emulsion, foamed asphalt, and/or portland cement to produce a homogeneous CCPR material. The CCPR material is transported by a loading belt into dump trucks or stockpiled at the plant facility. However, stockpiling the CCPR material is not recommended when asphalt emulsion is used as the primary recycling additive (Asphalt Academy, 2009). According to the ARRA (2001), asphalt emulsions and emulsified recycling agents are commonly used for the production of a CCPR, although portland cement, fly ash, and lime have also been successfully used. Due to the recent advancements in asphalt foaming technologies, the use of foamed asphalt, with portland cement as a mineral additive, has increased significantly (Wirtgen, 2012).

Figure 2.2 Conventional CCPR Plant (ARRA, 2001)

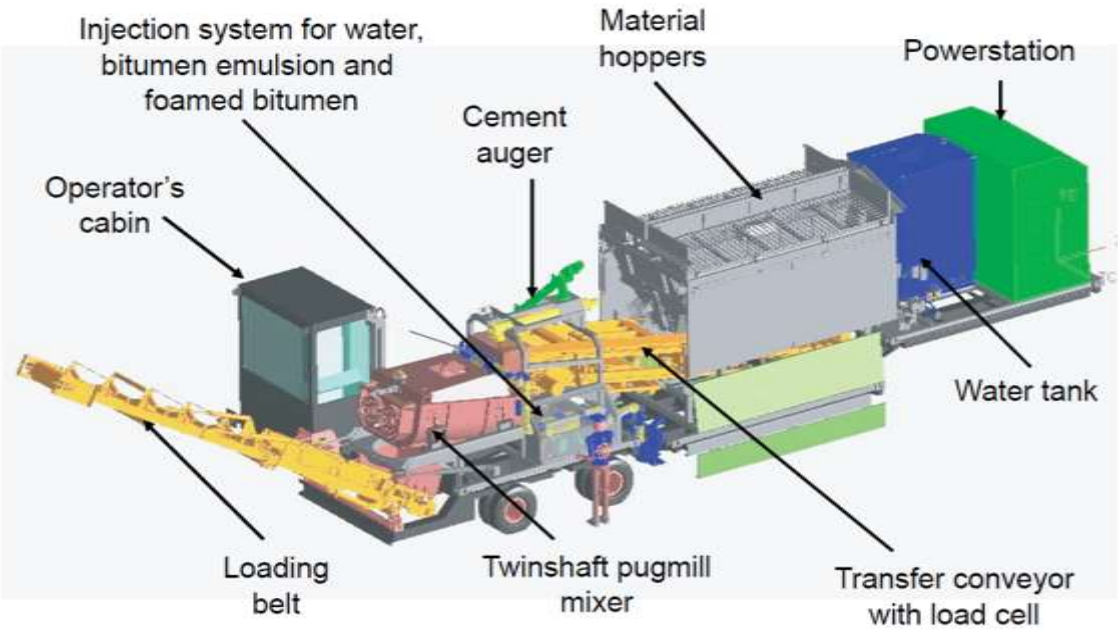

Figure 2.3 Mixing Plant for CCPR (Asphalt Academy, 2009)

The CCPR mixing process is different from the normal mixing process used for conventional asphalt concrete production. For the production of HMA or WMA the aggregates and the RAP need to be consistently and thoroughly coated by the asphalt binder during the mixing process, in order to provide a sufficiently thick asphalt film around the aggregates that ensures the adequate performance of the asphalt concrete. However, in the case of the CCPR, during the mixing process, the distribution of the asphalt binder in the mixture occurs differently, depending on the type of recycling agent used. On the one hand, asphalt emulsions disperse preferentially amongst the finer particles, but not exclusively, partially coating the larger aggregate particles, which promotes a chemical bond between the asphalt binder and the aggregate particles. On the other, foamed asphalt adheres to the finer particles (portland cement) to form a strong and homogeneous asphalt mastic that produces "spot welds" between the larger aggregate particles (Asphalt Academy, 2009).

In all cases, the plant used for the production of the CCPR must be capable of accurately proportioning and blending the recycling agent, the added water, and the active filler (portland cement) with the RAP materials, to continuously produce a consistent and homogeneous recycled material. For this, the South African Asphalt Academy (2009) recommends controlling the temperature and moisture content of the RAP material at the time of mixing. In the case of CCPR with foamed asphalt, if the temperature of the aggregate is below 50°F, the mastic will not disperse properly in the mix as the foaming process is directly affected by the temperature. Similarly, the moisture content of the recycled material affects directly the performance of the CCPR in the field as it influences the dispersion of the foamed asphalt and the compaction effort required to achieve adequate density.

After production, the CCPR material can be transported by dump trucks to the roadway, while avoiding excessive handling that could lead to segregation of the loose material (Asphalt Academy, 2009). Placement of the CCPR layer is usually performed with a conventional asphalt paver, while compaction can be performed with conventional tandem rollers capable of compacting the material to the desired field-density.

2.3.2 Asphalt Foaming

Although emulsified asphalt, fly ash, and lime are commonly used for the production of CCPR, foamed asphalt has become one of the preferred recycling agents recently, and has generally been combined with portland cement (ARRA, 2001). Asphalt foaming is a physical-chemical process in which asphalt binder, cold water, and compressed air are mixed in a specially designed chamber to produce an abundant foam of asphalt bubbles, as

shown in Figure 2.4. As the hot asphalt binder is mixed with cold water, a thermal shock is generated from a swift heat and energy transfer. These thermodynamic interactions cause a temporary expansion of the effective surface of the asphalt binder and a temporary state of reduced viscosity. This momentary expanded state enhances the dispersion and uniform mixing of the asphalt binder with colder particles at ambient temperatures (Jenkins and Van de Ven, 2001).

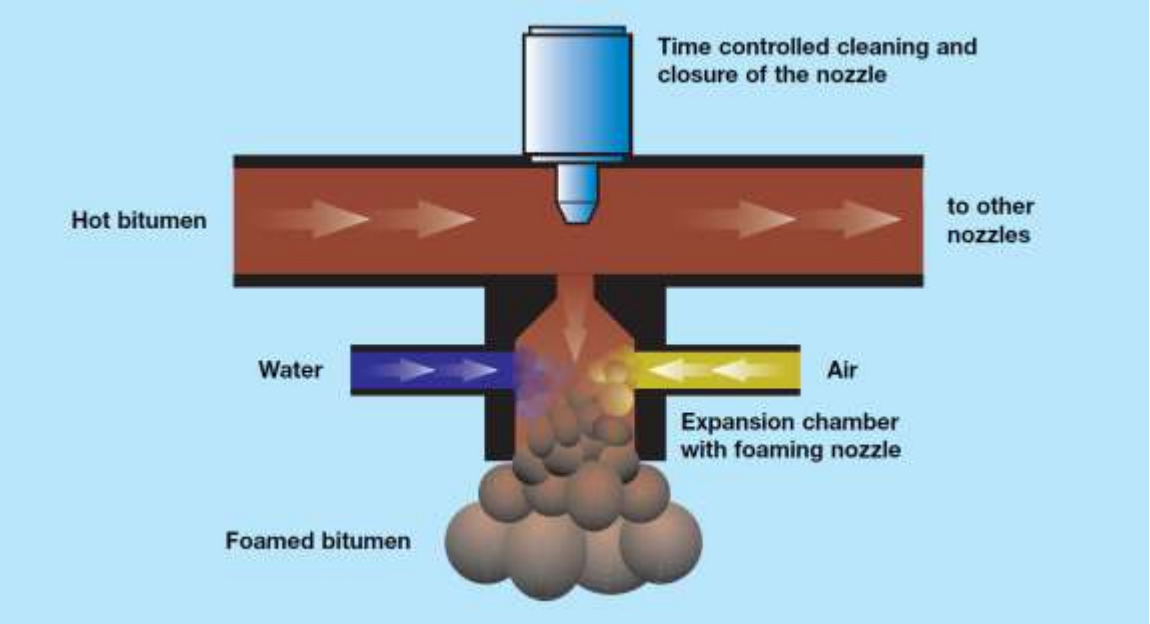

Figure 2.4 Asphalt Foaming Schematic (Wirgten, 2002)

When combined with foamed asphalt, portland cement acts as an active filler and enhances the dispersion of the asphalt binder in the mixture, especially in the case of coarser materials with less than 5% passing the 0.075 mm sieve (Wirtgen, 2012). The combination of foamed asphalt with portland cement has shown to be very effective in improving the strength, stiffness, and permanent deformation of foamed asphalt mixes (Fu et al., 2010). A series of studies conducted at the University of California Pavement

Research Center (UCPRC) demonstrated that foamed asphalt and portland cement both serve the purpose of bonding the larger particles together, but their roles are complementary rather than interchangeable. The bonds formed by portland cement are strong but brittle compared to the weaker, more ductile bonds formed by foamed asphalt (Fu et al., 2010). Additionally, it is believed that due to pozzolanic action, portland cement provides irregularities on the surface of larger particles where foamed asphalt droplets tend to adhere more firmly (Wirtgen, 2012). In that way, when used together foamed asphalt and portland cement it is possible to optimize the mixture and take advantage of the individual benefits of each material. While portland cement reduces water susceptibility and increases short and long-term strength, foamed asphalt improves the flexibility of the stabilized material. The result is a pavement layer with improved mechanical properties and enhanced structural performance when compared to a conventional base layer (Jenkins and Van de Ven, 2001).

2.3.3 Structural Performance of a CCPR

Although cold recycling with foamed asphalt is a widely used technique in multiple countries around the world (Mohammad et al., 2003; Diefenderfer at al., 2012; Chen et al., 2006; Menendez et al., 2006; Saleh et al., 2004; Fernandez, 2013; Loizos et al., 2007), the available literature addressing the structural characteristics of CCPR materials with foamed asphalt is limited. As cited by Halles et al. (2013), there is not currently a specific methodology for determining the structural contributions of CCPR though some previous studies have investigated its fundamental behavior in the laboratory and the in the field. Halles et al. (2013) studied the stiffness evolution of foamed bitumen mixtures using the

indirect tensile fatigue test and found that once the mixture reached a constant value, the stiffness either increased or decreased depending on the applied stress level which allowed it either to continue curing or induce damage, respectively. These findings were in general agreement with those made by others (Loizos et al., 2007; Bowering and Martin, 1976; Jones et al., 2008; Fu et al., 2010). Romanoschi, et al. (2004) investigated full-depth reclaimed pavement (FDR) in a full-scale experiment using a heavy vehicle simulator under fixed environmental and loading conditions. Their material included 50% RAP, 37% base material and 12% A-7-6 soil stabilized with a PG 64-28 foamed asphalt (Romanoschi et al., 2004). They found similar rutting performance between pavements rehabilitated with FDR and the control without FDR (Romanoschi et al., 2004). More recent laboratory studies, conducted by Diefenderfer and Link (2014), determined the dynamic modulus (E*) of lab-compacted CCPR specimens over a range of temperatures and frequencies, finding the CCPR exhibited traits very similar to conventional asphalt concrete (AC) materials in that it was possible to create E* master curves that resembled those of AC materials, as shown in Figure 2.5.

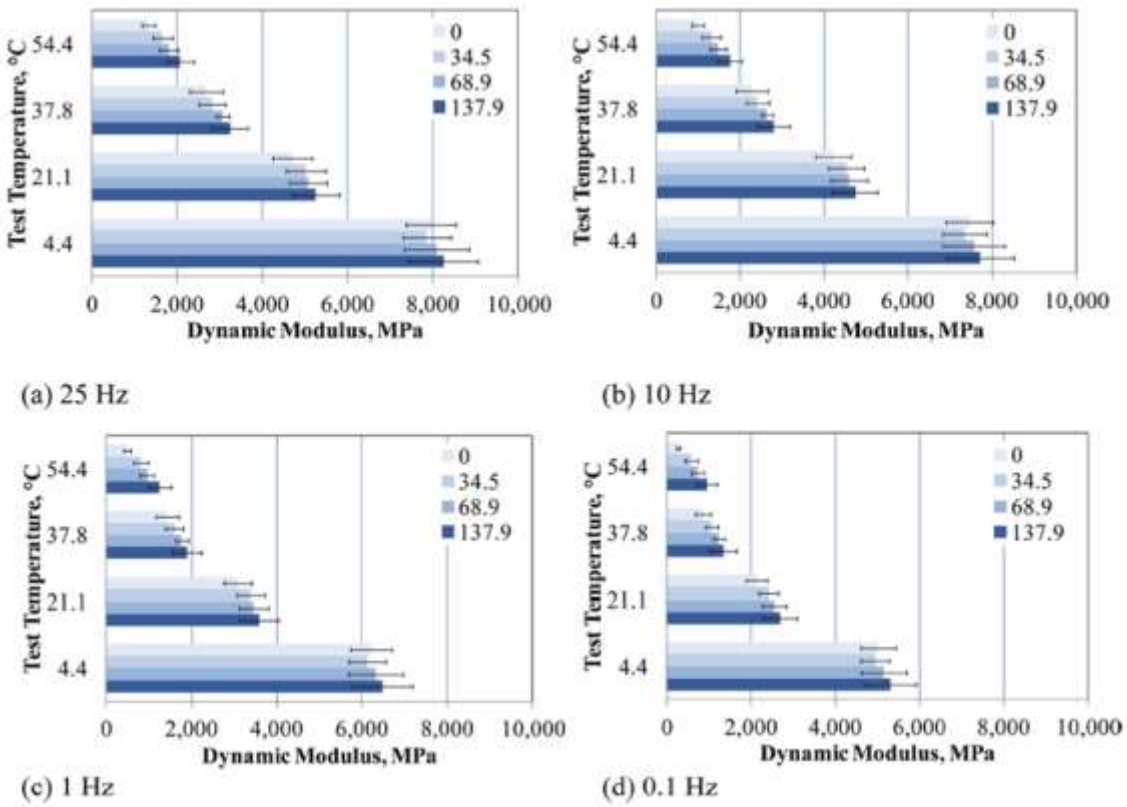

Figure 2.5 Results of Dynamic Modulus Testing at Four Confinemente Pressures: (a) 25 Hz, (b) 10 Hz, (c) 1Hz, and (d) 0.1 Hz (presented by Diefenderfer and Link, 2014)

The structural contribution of cold recycled materials using foamed asphalt fluctuates between that of a granular base and that of conventional asphalt concrete (Khosravifar et al., 2013). Commercial manuals suggest considering resilient modulus values ranging between 145 ksi and 290 ksi, with corresponding layer coefficients from 0.20 to 0.38 (Wirtgen, 2012). However, as mentioned by Khosravifar et al. (2013), the modulus for foamed asphalt recycled materials, including RAP and quality aggregates, ranged from 100 ksi to 800 ksi, even though lower values in the vicinity of 40 ksi have also been reported by Jenkins and Van de Ven (2001). In any case, the obtained resilient moduli are much greater than typical values used for granular base materials (20 ksi to 40 ksi).

Triaxial testing conducted by Jenkins and Van de Ven (2001) has shown that foamed asphalt recycled materials may exhibit a granular nature in terms of stress dependency, as described by Figure 2.6. However, due to the rheological characteristics of the asphalt binder, the stiffness of such materials is temperature sensitive and decreases with increasing temperature (Khosravifar et al., 2013). Master curves developed by Kim et al. (2009) for foamed asphalt cold-in-place recycling, and shown in Figure 2.7, were relatively flat compared to conventional AC mixtures, supporting the fact that even if foamed asphalt mixtures behave as temperature-dependent materials, they may not behave exactly like typical AC.

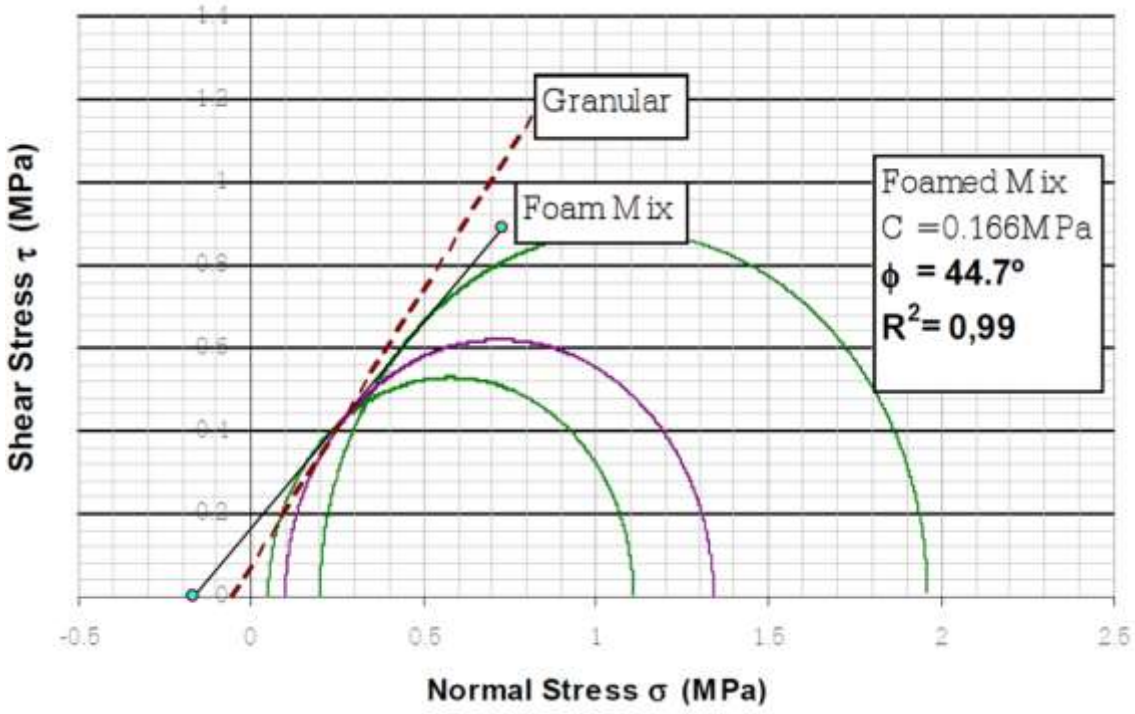

Figure 2.6 Mohr-Coulomb Circles for Foamed Mix and Granular Material (presented Jenkins and Van de Ven, 2001)

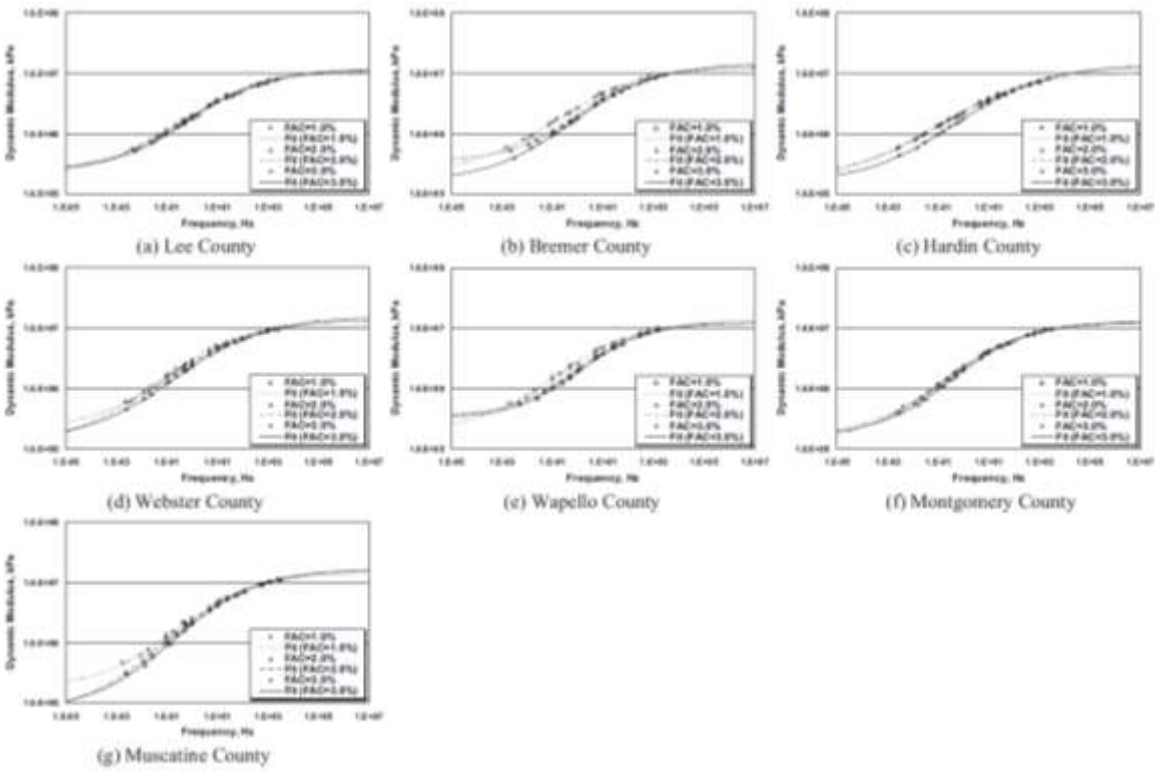

Figure 2.7 Master Curves at Three Foamed Asphalt Contents from Seven Different RAP Sources (presented by Kim et al., 2009)

A number of structural layer coefficients for materials recycled with foamed asphalt have been proposed in the literature over the years. The main results found in the literature reviewed are summarized in Table 2.1. Tia and Wood (1983) suggested using structural layer coefficients ranging from 0.25 to 0.40 for an artificially aged paving mixture recycled with foamed asphalt. Similarly, based on pavement deflection measurements in two road projects in Indiana, Van Wyk et al. (1983) and Van Wijk and Wood (1983) estimated an average layer coefficient of CIR with foamed asphalt between 0.26 and 0.37, with values as low as 0.10 and as high as 0.43. Marquis et al. (2003) determined the layer coefficient varied from 0.22 to 0.35 for three foamed asphalt recycling projects in Maine. Seebaly et al. (2004) recommended a layer coefficient of 0.26 for CIR with foamed asphalt in Nevada.

Based on the results of full-scale accelerated pavement testing (APT) in Kansas, Romanoshi et al. (2004) recommended a structural layer coefficient of 0.18 for full-depth reclamation using foamed asphalt. Loizos and Papavasiliou (2006) and later Loizos et al. (2007) followed an analytical approach based on multilayer elastic analysis to estimate a structural layer coefficient at approximately 0.25 for a CIR-foam constructed on a major highway in Greece. More recently, Diefenderfer and Apeagyei (2014) used deflections testing and laboratory measurements of the resilient modulus and indirect tensile strength of CCPR-foam field cores to estimate a layer coefficient ranging from 0.36 to 0.48. However, the deflection measurements were also affected by an underlying FDR layer.

Table 2.1 Layer Coefficients for Materials Mixed with Foamed Asphalt

Source	Material	Recycling Method	Suggested Layer Coefficient
Tia and Wood (1983)	Artificially aged paving mixture	Laboratory Mixing	0.25 – 0.40
Van Wyk et al. (1983)	RAP	CIR	0.26 – 0.37
Marquis et al. (2003)	RAP	CIR	0.22 – 0.35
Seebaly et al. (2004)	RAP	CIR	0.26
Romanoschi et al. (2004)	RAP and Granular base	FDR	0.18
Loizos and Papavasiliou (2006) Loizos et al. (2007)	RAP	CIR	0.25
Diefenderfer and Apeagyei (2014)	RAP	CCPR	0.36 – 0.48

In general, layer coefficient values ranging between the layer coefficients of a granular base (0.06 – 0.14) and those of AC (0.35 – 0.54) have been recommended. However, this range is wide and the values selected may be under- or over-estimating the true structural capacity of a CCPR-foam layer, resulting in non-optimized thickness designs. Furthermore, only two of the studies found in the literature specifically considered CCPR materials (Diefenderfer and Link, 2014 and Diefenderfer and Apeagyei, 2014).

While there have been both laboratory and field investigations of CCPR, longer-term experiments under higher traffic volumes have been lacking for CCPR specifically, and other recycled materials in general, and have limited CCPR's use on a wider basis.

2.4 CEMENT-TREATED BASE

According to the Portland Cement Association (PCA), a cement-treated base (CTB) is a mixture of aggregate material and/or granular soils combined with measured amounts of portland cement and water that hardens after compaction and curing to form a durable paving material (PCA, 2017). In that way, a CTB is a cost effective solution that allows reusing existing soils and base materials, with a relatively small addition of virgin materials, to provide a more efficient and durable base compared to conventional granular bases. Due to its increased rigidity, the CTB distributes the stresses induced by traffic loads over a larger area, significantly reducing the stresses applied to the underlying layers and the deflection of the upper layers. However, in the same way as any portland cement-based material, the CTB may be prone to cracking which should be considered in the design.

2.4.1 FDR with Portland Cement

Full-Depth Reclamation (FDR) is a recycling technique that allows reclaiming and stabilizing the existing pavement materials, including the full thickness of the asphalt layer and a predetermined portion of the underlying layers (base, subbase, and/or subgrade), to produce an upgraded, homogeneous base material. Unlike the case of hot-in-place recycling (HIR), the application of heat is not necessary for the construction of the FDR, and since the process may be performed regardless of the type of pavement materials found in the roadway, FDR thicknesses may range between 4 and 12 inches (ARRA, 2001). The resulting recycled layer may be categorized as a granular material, and can be used as-is or enhanced with the addition of a stabilizing additive to meet the mechanical properties and structural strength required to support the anticipated loads (Wirtgen, 2012). Commonly used stabilizing additives include portland cement, asphalt emulsion, and foamed asphalt, although other additives such as calcium chloride, magnesium chloride, lime, fly ash, and cement kiln dust may be also used (ARRA, 2001). Figures 2.8 shows conventional pavement reclaimers used to perform an FDR process, while Figure 2.9 shows the resulting reclaimed material mixed with portland cement.

Figure 2.8 FDR Reclaimer (ARRA, 2001)

Figure 2.9 FDR with Cement (Wirtgen, 2012)

The FDR process is relatively simple, which led to the use of a great number of reclamation methods including rippers, scarifiers, and conventional milling machines which tended to increase the relative cost of producing the recycled material (ARRA, 2001). However, the recent development of more advanced reclaiming/stabilizing machines, has modernized FDR processes, making it a high-quality, low-cost solution (Wirtgen, 2012). New generation pavement reclaimers have a rotary drum, especially designed to pulverize the existing pavement layers and mix it with the right amount of additive at the same time, in one single pass, achieving higher productivities in the field and an optimum quality of the recycled material (Wirtgen, 2012). The process can also be performed in multiple passes of the reclaimer, adding the stabilizing additive independently after the pavement has been initially pulverized to achieve a more uniform application of the additive (Wirtgen, 2012).

2.4.2 Portland Cement in a CTB

Portland cement is the most commonly used stabilizing agent in the world (Wirtgen, 2012). Its primary function in a CTB is to increase the compressive and tensile strength of the pavement layer. Typical cement contents in a CTB range from 3% to 10%, resulting in 7-day unconfined compressive strengths (UCS) between 300 and 800 psi (PCA, 2017). Nonetheless, the compressive and tensile strength achieved by a CTB is determined by the portland cement content, the type of material, and the density of the compacted material (PCA, 2017). As portland cement comes in contact with water, the hydration process initiates and crystalline bonds begin forming between particles as the material is mixed.

Because of the hydration process, the timing of compaction plays a major role in determining the ultimate strength of a CTB.

Like any cement-treated material, including concrete, a CTB is influenced by the behavior of portland cement. In that way, a CTB constantly continues to gain strength as the hydration process continues for a long period of time. Similarly, since the hydration process is also an exothermic process, the CTB mixture is prone to shrinkage and drying, which may potentially lead to shrinkage cracking of the CTB layer. As described by Cho et al. (2006), the possibility of reflection cracking in the AC layer is a great concern for CTB layers. A crack may appear in the CTB at its early age, as a result of uncontrolled drying shrinkage, and subsequently propagate into the asphalt concrete layers causing reflection cracking (as illustrated in Figure 2.10), which in turn may lead to the failure of the pavement (Cho et al., 2006). Design and construction considerations based on the recommendations from Wirtgen (2012) need to be taken into account to avoid early damage of the pavement caused by the cement hydration process of the constructed CTB layer.

Figure 2.10 Reflection Cracking in a Cement-Treated Base (Sebesta, 2006)

2.4.3 Structural Performance of a CTB

Due to the widespread use of CTB there have been numerous studies addressing its structural performance, with diverging, and even conflicting results. The results are summarized in Table 2.2.

Table 2.2 Layer Coefficients for Cement Treated Materials

Source	Material	Recycling Method	Suggested Layer Coefficient
Lofti and Witczak (1985)	Dense-graded limestone base with 4% cement	Laboratory Mixing	0.27
Janoo (1994)	RAP	FDR	0.13 – 0.19
Puppala et al (2011)	RAP with 2% cement	FDR	0.15 – 0.21
Puppala et al (2011)	RAP with 4% cement	FDR	0.16 – 0.22

An early study presented by Lofti and Witczak (1985) reported the resilient modulus of a dense-graded limestone base material treated with an approximate portland cement content of 4.5%. The resilient modulus measured in the laboratory reached a value of 1,260 MPa, which in turn was correlated to an approximate layer coefficient of 0.27 (Lofti and Witczak, 1985).

A study was also conducted by Janoo (1994) to assess the structural performance of reclaimed asphalt concrete (RAP) treated with portland cement in real test sections built in New Hampshire. Modulus results were obtained from FWD backcalculation and

correlated to a layer coefficient ranging between 0.15 and 0.19 (Janoo, 1994). Additional California Bearing Ratio (CBR) testing was conducted in the laboratory and the results were correlated to a layer coefficient of 0.13.

Another study was conducted by Taha et al. (2002) to assess the structural performance of RAP and virgin aggregate combinations with portland cement contents as high as 7%. Unconfined compression strength testing was used to determine resilient modulus values as high as 3,719 MPa, indicating the modulus increases significantly as the cement content is increased.

Gnanendran and Woodburn (2003) conducted resilient modulus, CBR and unconfined compressive strength testing on cement treated RAP materials in Australia. The obtained resilient moduli ranged between 310 and 590 MPa for portland cement contents raging between 0% and 3%, and stress levels varying from 0 to 140 kPa. These results were used by Puppala et al. (2011) to assess the reliability of their research, in which the structural contribution of cement-treated RAP materials was descried as structural layer coefficient ranging between 0.15 and 0.21 for cement contents of 2%, and between 0.16 and 0.22 for cement contents of 4%.

2.5 SUMMARY

This chapter provided a brief overview of the most common pavement design methods, including the AASHTO 93 pavement design method, the mechanistic-empirical pavement design method, and the perpetual pavement design method. Additionally, after a description of the material properties and construction processes of the two main recycling techniques included for this study, a literature-based summary of their documented

structural performance was presented. The available literature on the structural performance of the two recycling techniques addressed in this investigation: Cold Central-Plant Recycling (CCPR) and Cement-Treated Bases (CTB) is relatively limited. However, it was sufficient to provide a general understanding on the common design considerations currently used.

CHAPTER THREE

EXPERIMENT PLAN

3.1 INTRODUCTION

As part of the fifth research cycle at the NCAT Pavement Test Track, twenty new experimental pavement test sections were built, including seven instrumented test sections, identified as “structural sections”, which allowed measuring the structural response of the pavement layers under traffic loading. Three sections included in this structural study were sponsored by the Virginia Department of Transportation (VDOT) to investigate the structural and functional performance of different pavement structures containing Cold Central Plant Recycled (CCPR) materials using 100% RAP and foamed asphalt under high traffic applications. Although the VDOT test sections were originally intended to withstand one research cycle, they exhibited good performance under traffic loading, and VDOT decided to leave the test sections in place to withstand an additional research cycle for a total trafficking of approximately twenty-million equivalent single axle loads (ESALs). This chapter contains a detailed description of the VDOT test sections included in the 2012 structural study, the construction process, and the experimental plan followed for the study and structural characterization of this innovative pavement recycling technology under high traffic applications.

3.2 TEST FACILITY

The NCAT Pavement Test Track, operated by the National Center for Asphalt Technology (NCAT), is a 1.7 mile closed loop full-scale flexible pavement test facility located in Opelika, AL. This unique accelerated pavement testing (APT) facility combines real-world pavement construction with live heavy trafficking for rapid testing and analysis of asphalt pavements, allowing highway agencies to improve their mixture specifications, construction practices, and pavement design methods (West et al., 2012). Figure 3.1 shows an aerial photograph of the NCAT Pavement Test Track.

Figure 3.1 Aerial Photograph of the NCAT Test Track (West et al., 2012)

Consisting of forty-six individual two-hundred foot test sections, with twenty-six sections located on the two straight segments and twenty sections distributed amongst the two curves, the NCAT Pavement Test Track has been continuously sponsored during six consecutive three-year research cycles. Over the multiple research cycles, select test

sections have been replaced and reconstructed, while certain test sections have been left in-place for continued traffic loading. During each research cycle, once reconstruction had been completed, all test sections were loaded with approximately ten-million ESALs over a two-year period, with applied traffic similar to open access highways. Live traffic was applied by means of special tractor trailer rigs manually operated at a target vehicle speed of 45 mph, on a daily basis (sixteen hours a day, five days a week). The trucks consisted of a 12,000-lb steer axle, a 40,000-lb tandem axle, and five 20,000-lb single axles, which allowed attaining 10 million ESALs over the two-year period of each research cycle.

During each trafficking phase, samples of the mixtures obtained during construction were tested and analyzed at the NCAT's state-of-the-art laboratory, located in Auburn, AL. Similarly, the performance of each test section was assessed through weekly performance measurements that included international roughness index (IRI), rut depth measurement, crack mapping, and a program of regular falling weight deflectometer (FWD) testing. Additionally, the pavement structural response was measured weekly, for selected test sections containing embedded instrumentation, known as the "structural sections".

The fifth research cycle began in 2012, with the reconstruction of twenty new experimental test sections between the months of August and September. The 2012 structural study consisted of seven new instrumented structural sections. Four sections constituted the "green group" experiment sponsored by four agencies (Alabama DOT, Alabama Department of Environmental Management, North Carolina DOT, and South Carolina DOT) and three sections were sponsored by the Virginia DOT. While the "green group" experiment focused on assessing the effect of multiple combinations of sustainable

technologies, such as recycled asphalt shingles (RAS), high reclaimed asphalt pavement (RAP) contents, and ground tire rubber (GTR) modified asphalt binders on the performance of asphalt pavements; the VDOT sections were conceived to investigate the functional and structural performance of Cold Central-Plant Recycled (CCPR) materials under high traffic conditions. Each structural test section of the 2012 structural study contained a minimum of twelve asphalt strain gauges (ASG) located at the bottom of the asphalt bound layer and two earth pressure cells (EPC) located on top of the base and subgrade layers, respectively. Additionally, a minimum of four temperature probes were installed at various depths within the structure, to measure in-place temperatures of the asphalt layers. It is important to mention that the "green group" test sections were beyond the scope of this study and only the three VDOT sections were considered for this dissertation.

3.3 TEST SECTIONS

The three VDOT structural sections were part of larger scale study initiated by VDOT in 2011 with the construction of a field project on Interstate-81(I-81) to evaluate CCPR along with several other in-place recycling techniques (Diefenderfer et al., 2012). Construction using a CCPR process proved viable and the preliminary performance data through 34 months of service indicated excellent performance (Diefenderfer and Apeagyei, 2014). In conjunction with these promising initial results from the I-81 field project, VDOT was interested in developing a companion study that would evaluate different thicknesses of HMA over a CCPR layer and the inclusion of a cement-stabilized base layer underneath the CCPR layer. This companion study was meant to answer questions about optimizing surfacing thickness, potentially validate results from the I-81 site and provide information

regarding both the CCPR and cement-stabilized materials under accelerated loading conditions. To that end, VDOT sponsored the construction of the three VDOT structural test sections as part of the 2012 research cycle, identified as N3, N4, and S12. Sections N3 and N4 were adjacent to each other on the north tangent of the Test Track while the third section, S12 was near the end of the south tangent, as shown in Figure 3.2.

Figure 3.2. VDOT Test Sections at the NCAT Test Track (not to scale)

3.3.1 Pavement Cross-Sections

The pavement cross sections in this study are shown in Figure 3.3 and the as-built properties are presented in Table 3.1. Section N3 consisted of three asphalt concrete layers placed over a fourth layer of CCPR. Similarly, sections N4 and S12 consisted of two asphalt concrete layers (top and bottom) placed over a third layer of the same CCPR material, with the exception that section S12 contained a Cement Treated Base (CTB) as a base layer. Each section featured stone-matrix asphalt (SMA) surface and Superpave

dense-graded AC layers above the CCPR layer. Sections N3 and N4 were constructed on top of a crushed granite aggregate base layer while S12 was built on a CTB layer. The stabilization of the CTB was done in-place where approximately 6" of crushed granite aggregate base and 2" of the subgrade were treated in place with 4% Type II cement. All three sections were constructed on the same subgrade native to the Test Track and classified as an A-4 soil (Taylor and Timm, 2009). Originally, the VDOT study was formulated to address two specific research objectives with paired test sections. Sections N3 and N4 were designed to evaluate the difference between 4 inches and 6 inches of AC over 5 inches of CCPR, while sections N4 and S12 were designed to determine the differences between aggregate base (6 inches) and the cement treated base (CTB) layers (8 inches).

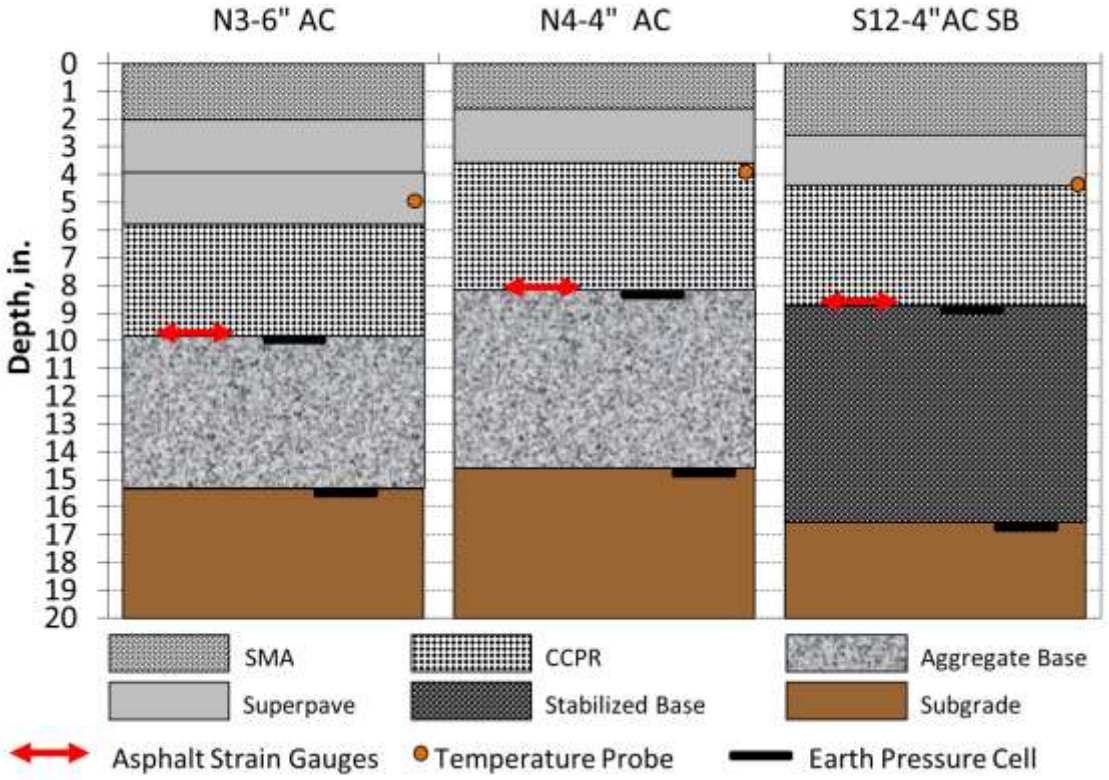

Figure 3.3 VDOT Experiment Average As-Built Thicknesses and Depth of Instrumentation

Table 3.1 VDOT Experiment As-Built Layer Properties

Section	N3-6 in. AC	N4-4 in. AC	S12-4 in. AC SB
Layer Description	Lift 1-19 mm NMAS SMA with 12.5% RAP and PG 76-22 binder		
Binder Content, %	6.1	6.0	6.1
Air Voids, %	4.3	4.7	4.2
Layer Description	Lift 2-19 mm NMAS Superpave with 30% RAP and PG 67-22 binder		
Binder Content, %	4.6	4.6	4.7
Air Voids, %	7.1	7.4	6.7
Layer Description	Lift 3-19 mm NMAS Superpave with 30% RAP and PG 67-22 binder		
Binder Content, %	4.4	NA	NA
Air Voids, %	6.4	NA	NA
Layer Description	CCPR-100% RAP with 2% foamed PG 67-22 binder and 1% Type II hydraulic cement		
Layer Description	Crushed granite aggregate base (CGAB)		6 in. CGAB + 2 in. subgrade stabilized in-place with 4% Type II hydraulic cement
Layer Description	Subgrade – AASHTO A-4 Soil		

It is important to note that the thicknesses presented in Figure 3.3 correspond to the average as-built thickness of measurements taken at 12 distinct locations within each test section, and therefore account for the natural variation due to standard construction practices. The figure also shows the depth of instrumentation used in this investigation. Six horizontal asphalt strain gauges oriented in the longitudinal direction (parallel to traffic) were placed at the bottom of the CCPR layer to capture bending of the asphalt-bound layers. Six vertical strain gauges were installed to capture vertical deflection of the asphalt-bound layers. However, the vertical strain gauges were only functional for a short period of time (i.e., a few weeks), preventing the development of meaningful vertical strain data over time. Earth pressure cells were placed at the top of the base and subgrade layers to capture vertical pressures transmitted through the sections. Temperature probes were installed after paving at the middle of the composite AC/CCPR to measure mid-depth temperature during testing. The instrumentation followed previous Test Track practice as described by Timm (2009).

3.3.2 Structural Design of the Test Sections

The three test sections were designed to mimic the cross section of the VDOT field project on Interstate-81. As explained by Timm et al. (2018), the expected service life of the test sections may be easily determined by following procedures in the AASHTO 1993 Pavement Design Guide (AASHTO, 1993) and using VDOT's typical design parameters for asphalt pavements (VDOT 2000 and 2015). In that way, the structural numbers for Sections N3, N4, and S12 were calculated as 5.1, 4.2, and 5.5, respectively. Based on these structural numbers, and assuming a conservative soil support of 9,400 psi (approximately 1/3 of FWD of the values reported by Taylor and Timm (2009)), the pavement structure should withstand between 3 and 16 million ESALs (Timm et al. (2018).

3.3.3 Design of the Pavement Materials

The design of the CCPR was performed by personnel from the Virginia Transportation Research Council (VTRC), while the CTB was designed by a third party (Diefenderfer et al., 2016). According to Diefenderfer et al. (2016), the CCPR mix design parameters were determined to be 2% foamed asphalt, with a carefully selected PG 67-22 binder with adequate foaming characteristics, and 1% Type II portland cement. The criteria recommended in the Wirtgen design method (Wirtgen GmbH, 2012) were met, with an average ITS value of 83 psi and a TSR of 76%. In the case of the CTB, the optimum Type II portland cement content was 4%, with an optimum moisture content of 8.0%, which yielded an average compressive strength of 256 psi after 7 days.

3.4 CONSTRUCTION PROCESS

The three test sections were built between July and August 2012. Initially, the existing test sections from the previous research cycle were milled using a Roadtec, Inc. RX-600 cold planer equipped with a direct loading conveyor belt as shown in Figure 3.4. The milled RAP was then transported to a designated disposal area. Once the RAP had been successfully removed from the test sections, heavy construction equipment was used to remove the existing base materials and reach the desired subgrade level. From there, the base corresponding to each test section was built to the desired thickness.

Figure 3.4 Initial Milling of the Test Sections

3.4.1 Construction of the CTB

The cement stabilization in section S12 was performed in-place, following conventional FDR construction practices. For its construction, a calibrated cement-distributer truck applied Type II cement, at a rate of 4% by weight, to the previously moistened surface of the section, as shown in Figure 3.5. A Wirtgen WR-2000 reclaimer, connected to a water truck, was used to pulverize approximately 6 inches of the crushed granite aggregate base and 2 inches of the subgrade while mixing the cement and the water, as shown in Figure 3.6. Compaction was performed by a 6-ton vibratory soil compactor. The compacted material was thoroughly leveled by a motorgrader before final compaction was applied. A nuclear density gauge was used to monitor field densities during and after compaction. After construction, the CTB was allowed to cure for approximately three weeks before the CCPR layer was placed.

Figure 3.5 Cement Application Process

Figure 3.6 Pulverization and Mixing of the CTB

3.4.2 Construction of the CCPR

The CCPR for the three test sections was produced and placed on the same day. The RAP used for the construction of the CCPR was originally obtained by VDOT during a pavement recycling project performed in 2011 on I-81 in Virginia and consisted of a combination of surface, intermediate, and base AC mixtures commonly used in Virginia (Diefenderfer et al., 2011). Prior to being transported to the production plant located on-site at the NCAT test track, the RAP had been stockpiled in Virginia for nearly two years (Diefenderfer and Link, 2014). The RAP was transported from Virginia to the Test Track, where it was fractionated on-site by means of large-scale processing plant, as shown in Figure 3.7. The different RAP fractions were combined according to the CCPR mix design using a Wirtgen KMA 220 mobile cold recycling mixing plant located on-site, shown in Figure 3.8. At the mobile plant, the fractionated RAP was mixed with 2% foamed asphalt

and 1% Type II portland cement, and the resulting CCPR was loaded into dump trucks by means of wheeled loaders. The Wirtgen (2012) Cold Recycling Manual describes that one of the main benefits of the CCPR process with foamed asphalt is that it may be temporarily stockpiled before being placed. However, due to the nature of the project, it was decided to transport and place the CCPR material immediately, so the effect of stockpiling the CCPR was not directly studied. In that way, the trucks hauled the CCPR to each test section and transferred the material into a conventional asphalt paver, which uniformly spread the material, as shown in Figure 3.9. The CCPR layer was finally compacted by a 13-ton double-drum vibratory roller while constant density measurements were performed using nuclear density gauge. Some project specifications require the application of a tack coat over the CCPR, while others are unclear over the matter. However, based on VDOT requirements for the test sections at the test track, a tack coat or a prime coat were not applied to the surface of the CCPR.

Figure 3.7 On-Site RAP Fractionating Plant

Figure 3.8 On-Site Cold-Recycling Mixing Plant

Figure 3.9 CCPR Construction Using Conventional Paving Equipment

3.4.3 Construction of the AC Layers

The AC layers in the VDOT test sections were built in accordance with strict quality procedures and under constant monitoring from NCAT personnel, as described by West et al. (2018). Through a competitive bidding process through Auburn University, a local contractor, East Alabama Paving Company, was charged with the production and construction of all the AC layers for the fifth reconstruction of the Test Track. To ensure the quality and consistency of the materials, a special production sequence was followed to produce and place each asphalt mixture. This procedure, thoroughly described by West et al. (2018), included the individual calibration of the cold feed bins for each individual stockpile at the plant, as well as extensive precautions to ensure a uniform gradation,

optimum aggregate coating, and homogeneous mix temperature for each material. Each asphalt mixture was produced initially as a “trial mix”, for preliminary testing and evaluation to determine the necessary adjustments in plant settings for the subsequent production of the final asphalt mixture to be placed on the Test Track. The asphalt mixtures were transported by the contractor in end-dump haul trucks to the test site. A Roadtec SB2500 material transfer machine operated form the track inside lane was used to transfer the asphalt mixtures into the paver hopper, avoiding the circulation of the haul trucks over the test sections. A Roadtec RP190e asphalt paver was used to place the material and was the only machine that operated on the actual test sections, as shown in Figure 3.10.

The compaction process was conducted in accordance with common practice, and included breakdown, intermediate, and finish rolling operations. Initial or breakdown compaction was accomplished by at least three passes of a steel-wheeled vibrating tandem roller. Intermediate or secondary compaction was performed by a rubber-tired roller until the desired density was achieved. Final compaction or finish rolling was performed by a smaller static steel wheel roller.

(a) **(b)** **(c)**

Figure 3.10 Rolling Operations Performed by (a) Tandem Vibratory, (b) Rubber Tire, and (c) Static Steel Wheel Rollers

Figure 3.11 Construction of the AC Layers

3.5 INSTRUMENTATION

The instrumentation of the VDOT sections was based on the instrumentation system that had been previously developed and improved in previous research cycles at the Test Track. The instrumentation system and methodology, thoroughly detailed by Timm (2009), has proven to be robust and effective in gathering data for mechanistic pavement analysis (West et al., 2018).

3.5.1 Instrumentation

Figure 3.12 illustrates the instrumentation arrangement used for the VDOT sections. A total of 14 structural response measurement devices were installed in the outside wheelpath (OWP) for each test section. Devices 1, 2, 3, 10, 11, and 12 were horizontal asphalt strain gauges (H-ASG), while devices 4–9 were vertical asphalt strain gauges (V-ASG). Additionally, the instrumentation arrangement featured two earth pressure cells (EPC) to measure vertical pressure at the CCPR/base interface (identified as gauge 13) and the base/subgrade interface (identified as gauge 14).

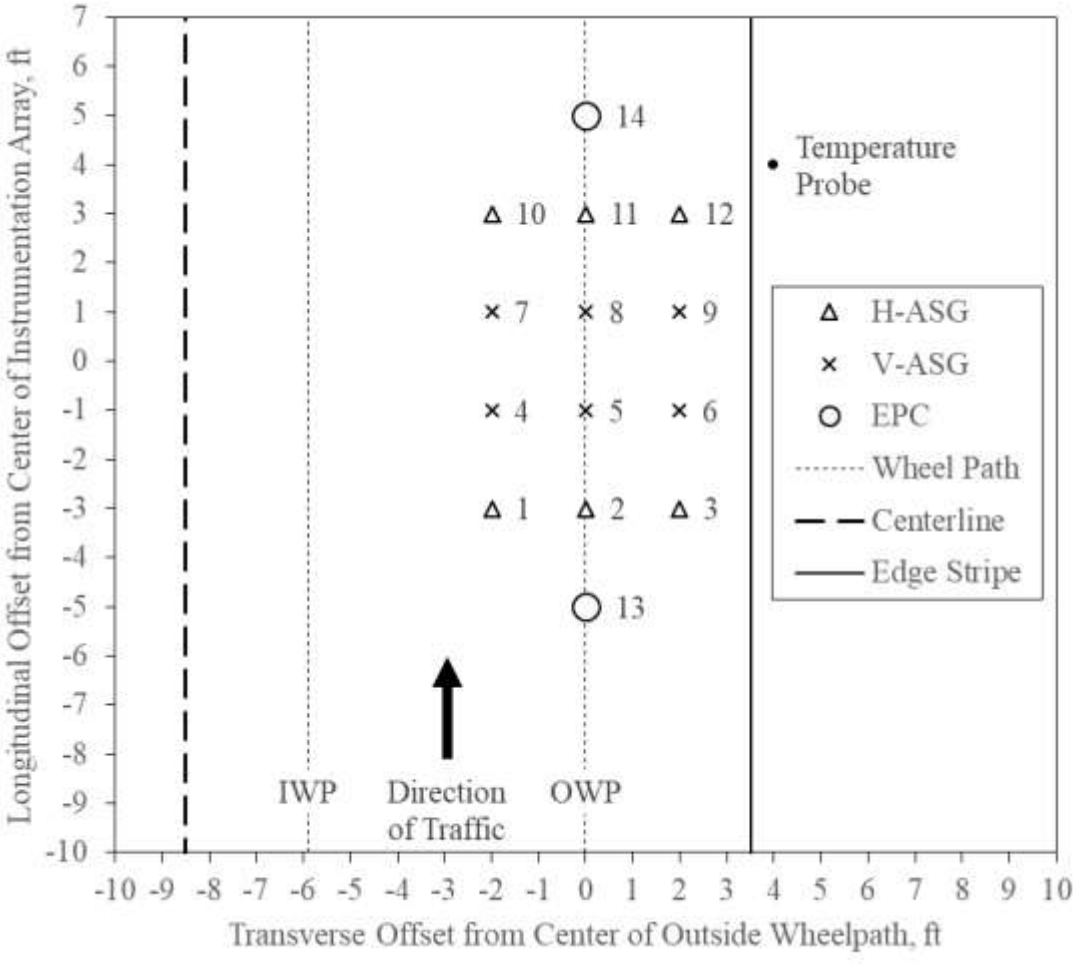

Figure 3.12 Instrumentation Arrangement for the Test Sections

The six H-ASG were installed at the CCPR/base interface and in the direction parallel to traffic to measure longitudinal strains and capture bending of the asphalt bound layers. Previous research at the Test Track had revealed that asphalt strain gauges located in the longitudinal direction yielded greater strain measurement than those located in the direction transverse to traffic. For this reason, H-ASG in the transverse direction were not used in this study. The six V-ASG were also installed at the CCPR/base interface to capture the vertical deflection of the asphalt-bound layers. However, all the V-ASG were only functional for a short period of time (i.e., a few weeks), preventing the development of meaningful vertical strain data over time. All the gauges were centered around the OWP, with gauges located at the center and two feet on either side of the wheelpath. The specific location of the gauges was devised to secure positive measurements of the maximum strain, despite the effects of natural wheel wander, and to provide adequate redundancy to the system by placing two mirrored sets of gauges (Timm, 2009).

The two EPC were installed in the center of the OWP and at different depths in the pavement structure to measure the vertical pressure at the interfaces between the asphalt bound and unbound materials, and between the base and the subgrade. These measurements were deemed important toward the prediction of base and subgrade rutting and to assess the effectiveness of the granular base and/or the CTB in dissipating stresses. Previous research at the Test Track had revealed no significant differences in measured vertical stresses on the inside and outside wheelpaths, which led to only place the two EPC at the center of the OWP. Figure 3.13 shows the instrumentation arrangement on the test sections.

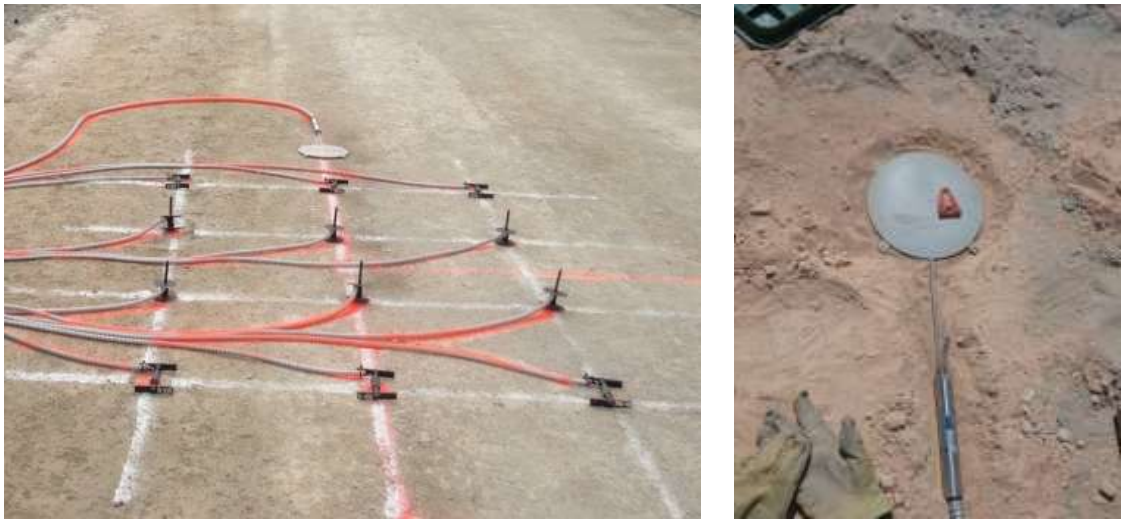

(a) **(b)**

Figure 3.13 Gauges at the (a) CCPR/Base and (b) Base/Subgrade Interfaces

After paving operations were completed, a multi-depth temperature probe was also installed on each test section to measure the temperature at four different depths within the pavement structure. Six Campbell-Scientific model 108 thermistor temperature measuring units, with an accuracy of ± 0.3°C, over the range of temperatures observed in the field, were bundled together into one larger probe that allowed measuring the thermal gradients within the pavement structure. An individual temperature probe was custom built for each test section to measured temperatures at different depths as described in Table 3.2.

Table 3.2 Temperature Probe Depths

Section	Depth of Temperature Probe, inches					
	Probe 1	**Probe 2**	**Probe 3**	**Probe 4**	**Probe 5**	**Probe 6**
N3	0.0	2.9	5.8	7.8	9.8	12.8
N4	0.0	1.8	3.6	5.9	8.2	11.2
S12	0.0	2.2	4.4	6.6	8.7	11.7

3.5.2 Data Collection and Processing

The strains and pressures induced to the pavement layers were collected for each test section on a weekly basis for a minimum of three passes of each truck at the test track. The strain and pressure measurements were then evaluated to determine the 95th percentile under each axle. Previous research at the test track had determined that the 95th percentile represented the "best hit" on each particular date and therefore provided reliable strain and stress information (Willis and Timm, 2009). Mid-depth pavement temperatures were also recorded during each strain and stress measurement. All the strain, stress, temperature and traffic information was archived in a Microsoft©Access database for further analysis and evaluation.

3.6 TRAFFIC CHARACTERIZATION

Traffic was applied by a fleet of 5 triple-trailer trucks configured to apply one steer axle (11,000 lb), one drive tandem axle (40,000 lb) and five single axles (20,750 lb/axle) per vehicle pass, which corresponded to approximately 10 ESALs per truck pass. Two shifts of professional drivers operated four trucks pulling triple flatbed trailers (shown in Figure 3.14) and one truck pulling a triple box trailer from 5:00 a.m. until approximately 10:40 p.m., Tuesday through Saturday. In that way, the trucks operated at approximately 45 mph for 16 hours per day and five days per week, to apply approximately 10 million ESALs during each research cycle. The specific axle weights for each of the five trucks are shown in Table 3.3. By the end of the first research cycle, and based on the adequate performance observed for the three test sections, VDOT decided to continue traffic operations and extend the study over a second research cycle.

Figure 3.14 Heavily Loaded Triple-Trailer used for Trafficking at the NCAT Test Track (West et al., 2018)

Table 3.3 Axle Weights (lbs.) for the Truck Fleet

Truck	Axle 1	Axle 2	Axle 3	Axle 4	Axle 5	Axle 6	Axle 7	Axle 8
	Steer	Tandem	Tandem	Single	Single	Single	Single	Single
1	10,150	19,200	18,550	21,650	20,300	21,850	21,100	19,966
2	11,000	20,950	20,400	20,950	21,200	21,000	20,900	20,900
3	10,550	20,550	21,050	21,000	21,150	21,150	21,350	20,850
4	10,550	21,050	20,700	21,100	21,050	21,050	20,900	21,050
5	11,200	19,850	20,750	20,350	20,100	21,500	19,500	20,300
AVG	**10,680**	**20,320**	**20,290**	**20,760**	**20,760**	**21,310**	**20,550**	**20,613**
COV	**3.9%**	**3.9%**	**4.9%**	**2.2%**	**2.5%**	**1.7%**	**3.6%**	**2.2%**

For the first research cycle, trafficking of the test sections began on October 23rd, 2012 and continued for approximately 2 years until October18th, 2014. The total traffic applied to the sections at this stage was 10,045,790 ESALs. Traffic resumed for the second research cycle in October 2015 after a planned one-year break dedicated to forensic evaluation of other test sections and reconstruction activities at the Test Track. Traffic was continued until November 30th, 2017 for the application of an additional 10,009,457 ESALs. By the time of this study, a total of 20,055,247 ESALs had been applied to the sections.

3.7 PERFORMANCE MONITORING

The functional and structural performance of the test sections was routinely monitored with a comprehensive range of surface measurements and non-destructive testing (NDT). Traffic operations were stopped every Monday to perform such measurements at the Test Track. All the testing was performed in-house by NCAT personnel, and following the procedures defined for previous research cycles.

3.7.1 Functional Performance Testing

The functional performance testing included a thorough visual inspection, rut depth, ride quality, texture, reflectivity, and friction measurements conducted a different time intervals to maintain current and updated data through slightly different dates over the two research cycles. The sections were visually inspected by qualified personnel to identify and draw up surface cracking. The individual cracks were marked on the pavement surface every week, which allowed producing reliable cracking maps and identifying the evolution of each

crack over time. The crack maps identified on the pavement surface were captured by a continuous digital imaging system in an automated road analyzing vehicle. These crack maps were then used to establish the magnitude of cracking as a percentage of the total pavement area by means of an algorithm developed by test track personnel. For this research cracking failure was defined at 25% of lane area or 50% of wheel path area.

Additionally, the automated road analyzing vehicle, shown in Figure 3.15, was used to determine rut-depth and ride quality (represented as the International Roughness Index or IRI) every week. For this research, rutting failure was set at 0.5 in and ride quality failure was set at 170 in/mile.

Figure 3.15 Automated Road Analyzing Vehicle at the NCAT Test Track

3.7.2 Falling-Weight Deflectometer Testing

Falling-Weight Deflectometer (FWD) testing was conducted several times per month on each test section. On each date, three FWD tests were performed on the inside wheel path (IWP), outside wheel path (OWP) and between the wheel paths (BWP), at four different longitudinal stations for a total of 12 FWD tests on each section for every test date. As shown in Figure 3.16, each 200-ft test section was subdivided into three different 50-ft subsections, excluding 25-ft of pavement on both ends, considered as non-tested transition areas. Within each 50-ft subsection, a random location (RL1, RL2, and RL3) was determined at the start of the first research cycle and maintained for the duration of the entire study. The final random location (RL4) was located in the middle of the instrumentation array.

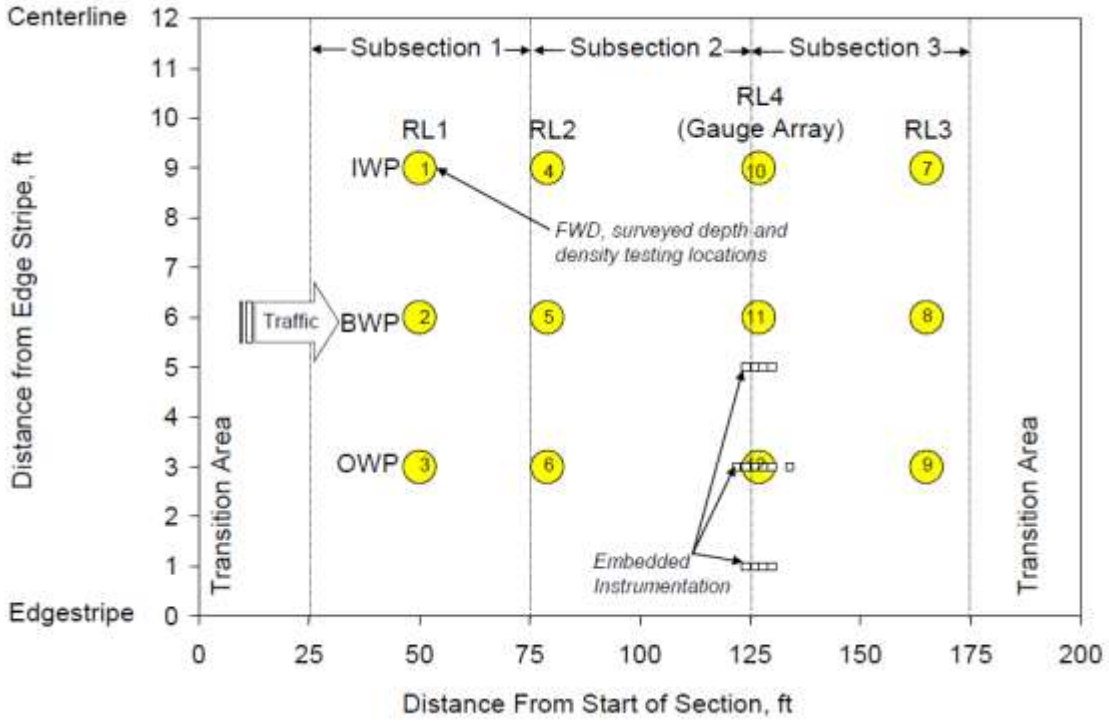

Figure 3.16 Random Location and Instrumentation Schematic (West et al., 2018)

Testing was conducted using a Dynatest 8000 FWD with a 5.91-in radius split plate and nine deflection sensors, spaced at 0, 8, 12, 18, 24, 36, 48 and 72 in. from the load center. Figure 3.17 shows a test of the FWD being performed, where the white line marked on the pavement surface corresponds to one of the longitudinal random locations. Although three replicates at four load levels ranging from 6,000 to 16,000 lb were obtained through the research cycle, only the data obtained for the second load level (approximately 9,000 lb) were used for this study. The FWD was submitted to monthly relative calibration and annual reference calibration according to the AASHTO R32 methodology. Pavement temperatures were recorded from FWD-mounted devices (air temperature and pavement surface temperature). Additionally, a corresponding mid-depth pavement temperature from the embedded temperature probe was recorded during each FWD test.

Figure 3.17 Dynatest Model 8000 FWD on the NCAT Test Track (West et al., 2018)

Backcalculation was conducted using Evercalc® 5.0 and considered each section as a three-layer structure, where the top layer was defined as the combination of the AC and the CCPR, the aggregate base (Sections N3 and N4) or the CTB (Section S12) was considered as the second layer, and the subgrade represented the third layer. Previous research had demonstrated that the CCPR would exhibit a behavior similar to that of AC (Kim et al., 2009), so it seemed rational to combine the AC and CCPR layers for the backcalculation process. Subsequent laboratory testing performed by VDOT confirmed that the CCPR exhibited behavior consistent with AC materials and supported the use of the combined AC/CCPR layer for backcalculation purposes (Diefenderfer and Link, 2014). Only backcalculated moduli corresponding to a root mean square error (RMSE) of less than 3% were considered for the analysis.

3.8 SUMMARY

Three test sections were built in 2012 at the NCAT Test Track as part of larger study conducted and sponsored by the VDOT to evaluate the field performance of CCPR materials under high traffic conditions and evaluate its structural contribution in a pavement structure. The study was originally formulated to address two specific research objectives with paired test sections. Sections N3 and N4 were designed to evaluate the difference between 4 inches and 6 inches of AC over 5 inches of CCPR, while sections N4 and S12 were designed to determine the differences between aggregate base (6 inches) and a cement treated base (CTB) layers (8 inches).

The three test sections were left in place for two research cycles at the Test Track. During this time, a total traffic of 20,055,247 ESALs was applied to each test section by

fleet of special tractor trailer rigs manually operated at a target vehicle speed of 45 mph. The sections were instrumented with an arrangement of asphalt strain gauges, earth pressure cells, and temperature measuring devices, which allowed determining the pavement response under the specific climate and traffic conditions of the Test Track on a weekly basis. Additionally, the functional and structural performance of each test section was monitored on a routine basis over the duration of the study. Weekly visual inspections and performance measurements of rut depth and ride quality were conducted to maintain current and updated data through slightly different dates over the research cycle. Similarly, FWD testing was conducted several times per month on each test section.

CHAPTER FOUR

LABORATORY EVALUATION

4.1 INTRODUCTION

The materials used for the construction of the three VDOT sections were evaluated in the laboratory for the design and as part of standard Test Track quality control procedures. Certain materials were evaluated more in-depth in particular laboratory studies. Laboratory testing for all the asphalt mixtures was performed at the NCAT laboratory while the CCPR and the CTB were tested at the Virginia Transportation Research Council (VTRC) laboratory.

The CCPR was comprehensively evaluated in the VTRC laboratory after construction. The CTB, on the contrary, was only tested as part of the design process and no samples were taken during or after construction. Therefore, while extensive information may be available for the CCPR, the laboratory data available for the CTB is limited to only the average 7-day compressive strength of 256 psi, obtained during the design phase.

The laboratory evaluation of the CCPR was summarized by Diefenderfer al. (2016) and Diefenderfer and Link (2014). The laboratory characterization of the asphalt mixtures had been previously reported by West et al. (2018) and a detailed description is beyond the scope of this report.

4.2 DESIGN OF THE CCPR MATERIAL

The CCPR was designed at the Virginia Transportation Research Council (VTRC) Laboratory using the procedures described by in the Wirtgen manual (Wirtgen Group, 2010). Based on the recommendations included in this manual, foamed asphalt was selected as the primary recycling agent to achieve the desired laboratory properties of the CCPR. Hydraulic cement was used as the active filler to reduce the moisture susceptibility of the material and increase its early age strength (Diefenderfer and Link, 2014).

4.2.1 Gradation of the CCPR

As shown in Figure 4.1, the gradation of the RAP material used for the CCPR does not comply with the target gradation suggested by Wirtgen (Wirtgen Group, 2012). Based on the Wirtgen recommendations for foamed asphalt stabilization, RAP material with such characteristics requires additional blending with an imported gravel (Wirtgen Group, 2012). However, the original gradation of the RAP from the VDOT I-81 project was conserved to replicate the sections built during the project. The gradation of typical RAP materials according to Wirtgens' experience is also shown in the Figure as a dotted curve, which only matches the RAP used for this study for the finer particles. For this, it may be inferred that the recommended gradations presented by Wirtgen are specific for in-place recycling and/or stabilization, and therefore do not account for the fractionating process followed at the Test Track. Furthermore, the discrepancy between the RAP gradation and the recommendations may provide a good insight into the applicability of the mentioned gradation envelopes for CCPR materials.

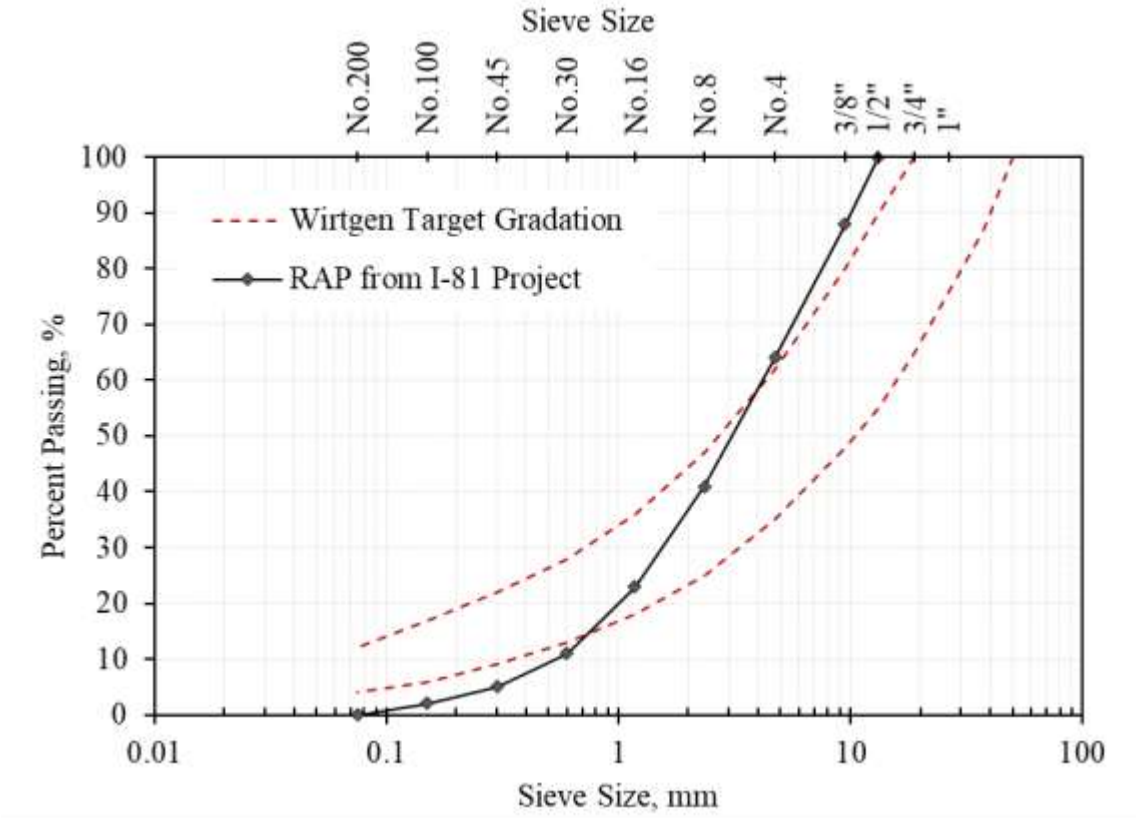

Figure 4.1 RAP Gradation (Adapted from Diefenderfer and Link, 2014)

As mentioned before, the RAP materials were fractionated at an on-site plant. The resulting gradation of the final CCPR material is presented in Figure 4.2. It can be seen that after the fractionation process, the gradation of the CCPR material was considerably improved as large lumps of asphalt concrete may have been disintegrated into smaller particles. The new gradation is within the limits recommended by Wirtgen (2012) with a 12.5 mm nominal maximum aggregate size (NMAS) and approximately 8.7% passing the 0.075 mm (No. 200) sieve. According to Wirtgen (2012), the most critical requirement for the gradation is the percent passing the 0.075 mm (No. 200) sieve, as it is necessary for the dispersion of the small foam droplets that bind together the CCPR. In the case of the CCPR built at the Test Track, this parameter was successfully met.

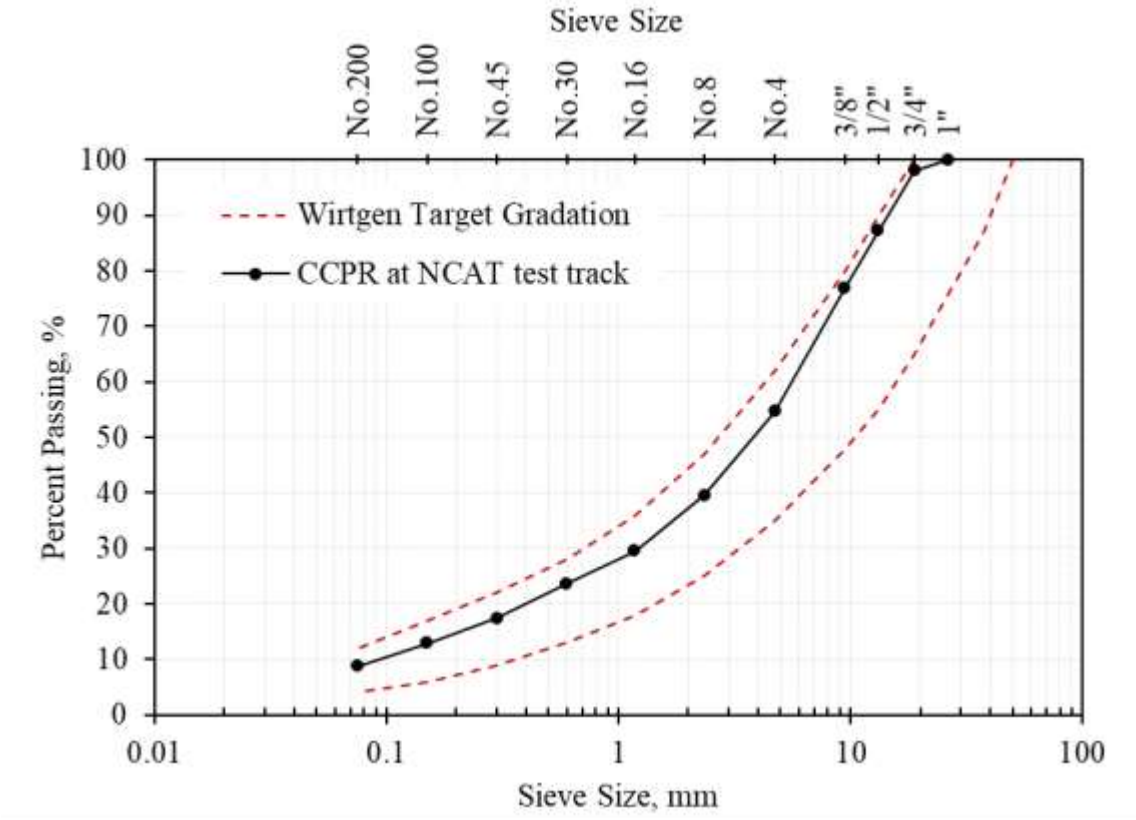

Figure 4.2 CCPR Gradation (Adapted from Diefenederfer et al., 2017)

4.2.2 Design Parameters

The required design parameters were met for a combination of 2.0% foamed asphalt and 1.0% hydraulic cement by weight. These proportions with laboratory mixed CCPR yielded a dry indirect tensile strength (ITS) greater than 45 psi and a tensile strength ratio (TSR) greater than 70%, as recommended by Wirtgen (Wirtgen Group, 2012). Verification tests were performed during construction to verify the properties of the in-place material at the Test Track. The results, presented in Table 4.1, yielded a dry ITS of 94.7 psi and a TSR of 77.6%. Such values were considered satisfactory as they complied with the recommendations in the literature.

Table 4.1 ITS and TSR Results during Construction

Condition	Dry			Soaked		
Specimen	**1A**	**2A**	**3A**	**1B**	**2B**	**3B**
ITS (psi)	95.5	94.3	94.2	76.5	71.9	72.0
Mean ITS (psi)	94.7			73.5		
TSR (%)	77.6					

The average measured binder content for the CCPR was 7.73%. The average binder content had been previously measured for the RAP materials used for the production of the CCPR with a resulting value of 5.77%. Based on these results, it was determined that the design dosage of 2.0% foamed asphalt was achieved during production and the built CCPR reflected the design properties.

4.3 DYNAMIC MODULUS TESTING

Dynamic modulus testing was performed on the CCPR material collected at the on-site plant during construction of the Test Track. The samples were placed in sealed buckets to preserve the moisture of the material during transportation to the on-site laboratory were specimens were tested.

4.3.1 Specimen Fabrication

At the on-site laboratory, the necessary buckets were unsealed and the loose CCPR material was combined to create one larger batch of approximately 25-kg, sufficient for fabricating 16 dynamic modulus specimens. Specific attention was given to conserving the moisture content of the CCPR during this fabrication process. The specimens were fabricated using a gyratory compactor so that all specimens had a similar bulk density as that of the

specimens used for the mixture design. In that way, a calculated mass of material was added to a 150-mm diameter gyratory compactor mold and compacted to a desired height of about 170 mm, which corresponded to a density of approximately 135 to 137 lb/ft^3. The number of gyrations needed to fabricate the dynamic modulus specimens ranged from 30 to 50 gyrations. After compaction, all the specimens were cured in a forced draft oven for 72 hours at 104°F. Finally, the specimens were stored at approximately 70°F and 70% relative humidity for approximately six months prior to testing. This long time between fabrication and testing was a result of a backlog of other testing in the laboratory rather than a predetermined curing or waiting period.

4.3.2 Testing

The compacted specimens were cored and trimmed to produce the definitive test specimens having a diameter of 4 inches and a height of 6 inches. The dynamic modulus testing was performed using an asphalt mixture performance tester in accordance with AASHTO TP79 – Standard Method of Test for Determining the Dynamic Modulus and Flow Number for Asphalt Mixtures Using the Asphalt Mixture Performance Tester (AMPT) (AASHTO, 2013), with some modifications specific for the CCPR material. The test was conducted in the axial mode and considering a reduced set of temperatures (40, 70, 100, and 130°F), six loading frequencies (25, 10, 5, 1, 0.5 and 0.1 Hz), and four levels of confinement (0, 5, 10, and 20 psi). Five replicates were tested for each temperature-frequency-confinement condition, reusing the specimens through the testing routine. For each specimen, the order of temperature was increased as the order of frequency decreased within each temperature

to minimize the potential for earlier tests to influence later ones negatively by permanent sample deformation.

4.3.3 Results

The results of the dynamic modulus testing are summarized in Figures 4.3, 4.4 and 4.5. Figure 4.3 shows the results of the dynamic modulus testing for the four confining pressures at the four test temperatures. Each of the six figures represents an individual confining pressure from 0.1 Hz (Figure 4.3 (a)) to 25 Hz (Figure 4.3 (d)). The error bars represent plus/minus one standard deviation of the data obtained. All the figures show a similar trend, where modulus values are higher for lower temperatures and lower for higher temperatures. The average unconfined dynamic modulus at 10 Hz (Figure 4.3 (e)), which as mentioned before correlates well with highway traffic conditions, was 1,083 ksi for 40°F, 612 ksi for 70°F, 330 ksi for 100°F, and 145 ksi for 130°F. Comparable trends were also observed at all levels of confinement. Based on these results, it may be inferred that the CCPR is a temperature-dependent material, similar to conventional AC materials. Comparable results in terms of temperature-dependency and magnitude have been reported in the literature (Cross and Jakatimah, 2007; Kim et al., 2009; Diefenderfer et al., 2016). From this, it may be inferred that, in terms of temperature-dependency, the CCPR may have a similar behavior as an AC material.

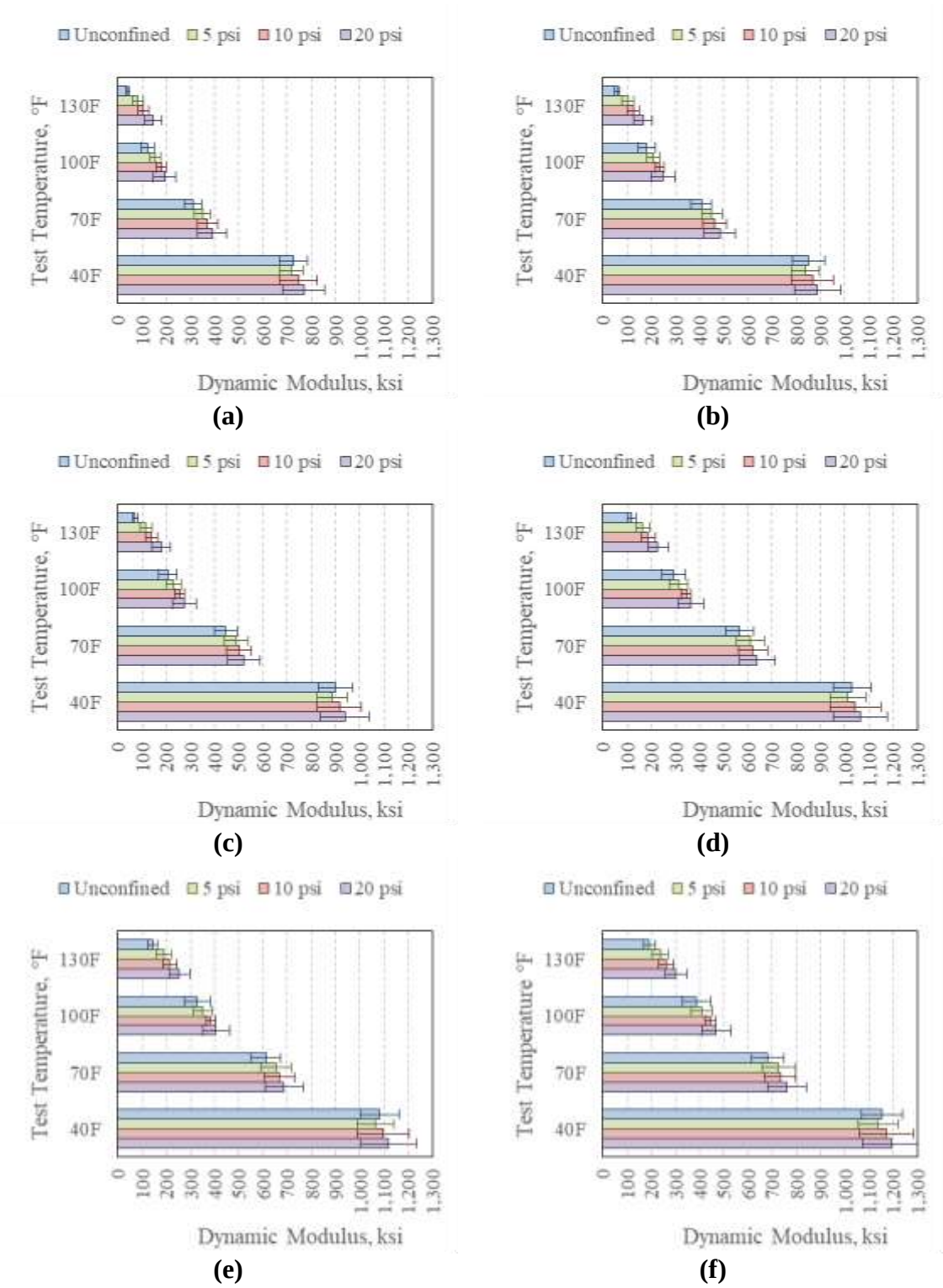

Figure 4.3 Dynamic Modulus vs. Temperature at Six Test Frequencies: (a) 0.1 Hz, (b) 0.5 Hz, (c) 1 Hz, (d) 5 Hz, (e) 10 Hz, and (f) 25 Hz

Figure 4.4 shows the results of the dynamic modulus testing for the four confining pressures at the six test frequencies. Each figure represents an individual test temperature. All the Figures show a similar trend and a direct correlation between test frequency and dynamic modulus value. Although the magnitude of the difference in modulus values is lower than that observed in Figure 4.3, the dynamic modulus seems to constantly increase with increasing test frequency. The average unconfined dynamic modulus at 70°F (Figure 4.4 (b)), was 310 ksi for 0.1 Hz, 407 ksi for 0.5 Hz, 447 ksi for 1 Hz, 565 ksi for 5 Hz, 612 ksi for 10 Hz, and 681 ksi for 25 Hz. Comparable constant increasing trends were also observed at all test temperatures. Based on these results, it may be inferred that the CCPR is a frequency-dependent material, similar to conventional viscoelastic pavement materials.

Finally, Figure 4.5 shows the results of the dynamic modulus testing for the four test temperatures at the six test frequencies. Each figure represents an individual confinement level. All the figures show a similar trend and a direct correlation between test frequency, test temperature, and dynamic modulus value. The effect seems to be confirmed, the dynamic modulus of the CCPR is affected by temperature and loading frequency. As temperature increases, dynamic modulus of the CCPR decreases, and as test frequency increases, dynamic modulus of the CCPR increases. Comparable trends were also observed at all levels of confinement.

Based on all these results, it may be inferred that the CCPR is a temperature-dependent material and exhibits a viscoelastic behavior during traffic loading, similar to conventional AC materials. By a simple visual inspections, the dynamic modulus results and the trends observed suggest that the CCPR may be considered as an AC material for structural pavement design purposes.

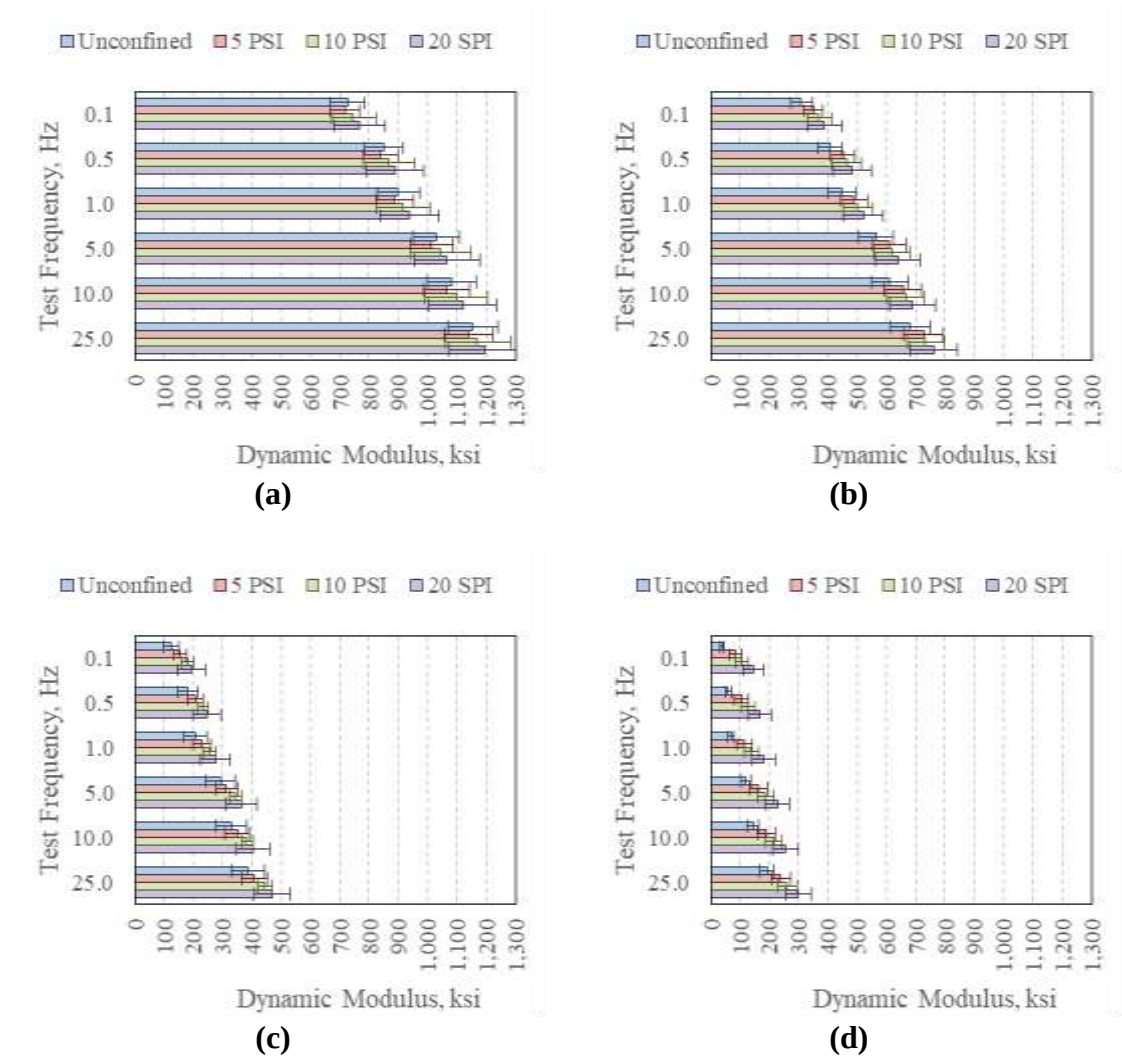

Figure 4.4 Dynamic Modulus vs. Test Frequency at Four Temperatures: (a) 40°F, (b) 70°F, (c) 100°F, and (d) 130°F

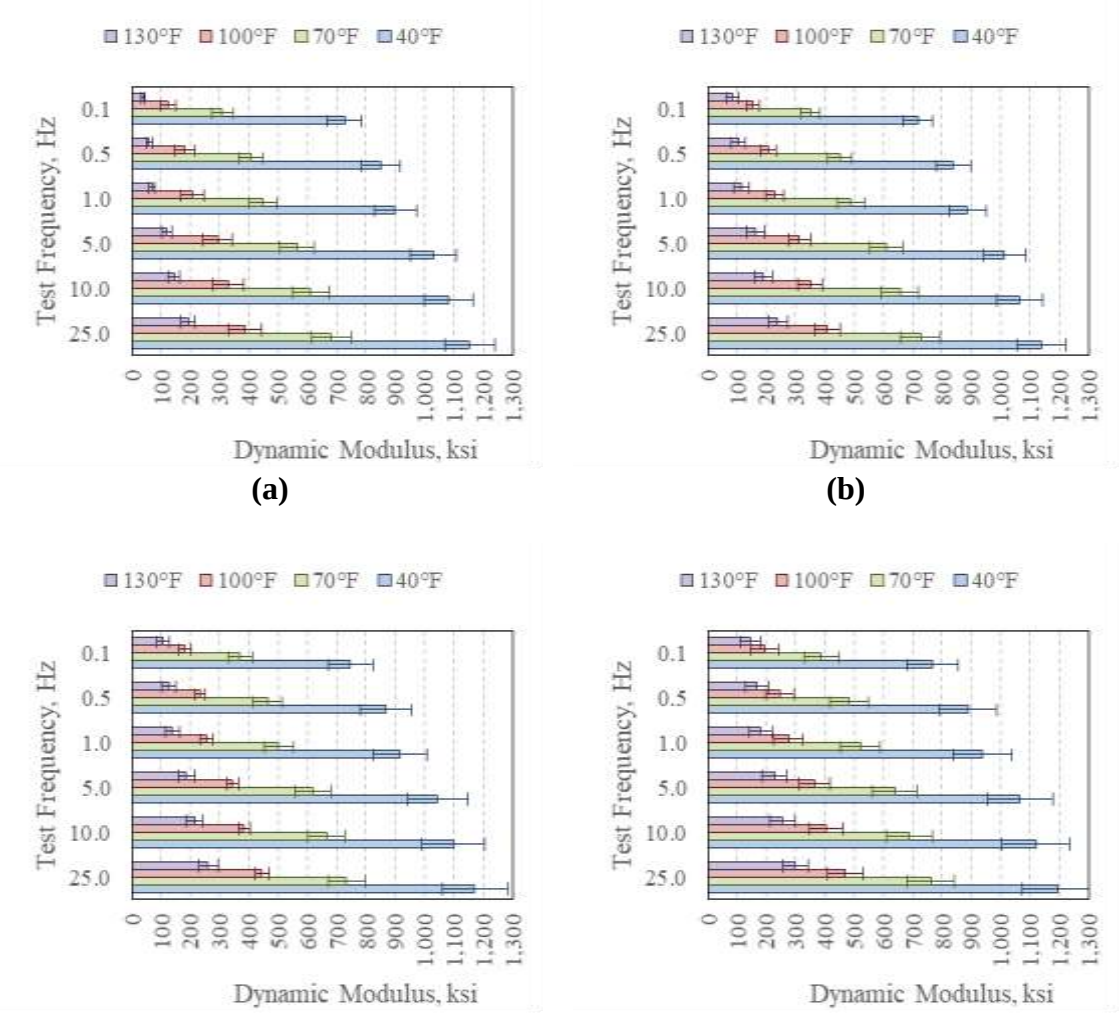

Figure 4.5 Dynamic Modulus vs. Test Frequency at Four Confinement Pressures: (a) Unconfined, (b) 5 psi, (c) 10 psi, and (d) 20 psi

4.3.4 Effects of Temperature and Confinement

A statistical analysis was conducted to investigate the influence of temperature and confinement on the stiffness of the CCPR. The results of this statistical analysis have been previously presented by Diefenderfer and Link (2014).

Testing Variability

The dynamic modulus coefficient of variation (COV) for the five replicates of all tests ranged from approximately 5% to 25%. The results are summarized in Figure 4.6. Higher COVs were found for the higher temperatures and for the lower test frequencies. Such conditions generally yielded the lowest dynamic modulus values and therefore minor differences, even similar in magnitude as those obtained for other test conditions, had a greater impact on the COV.

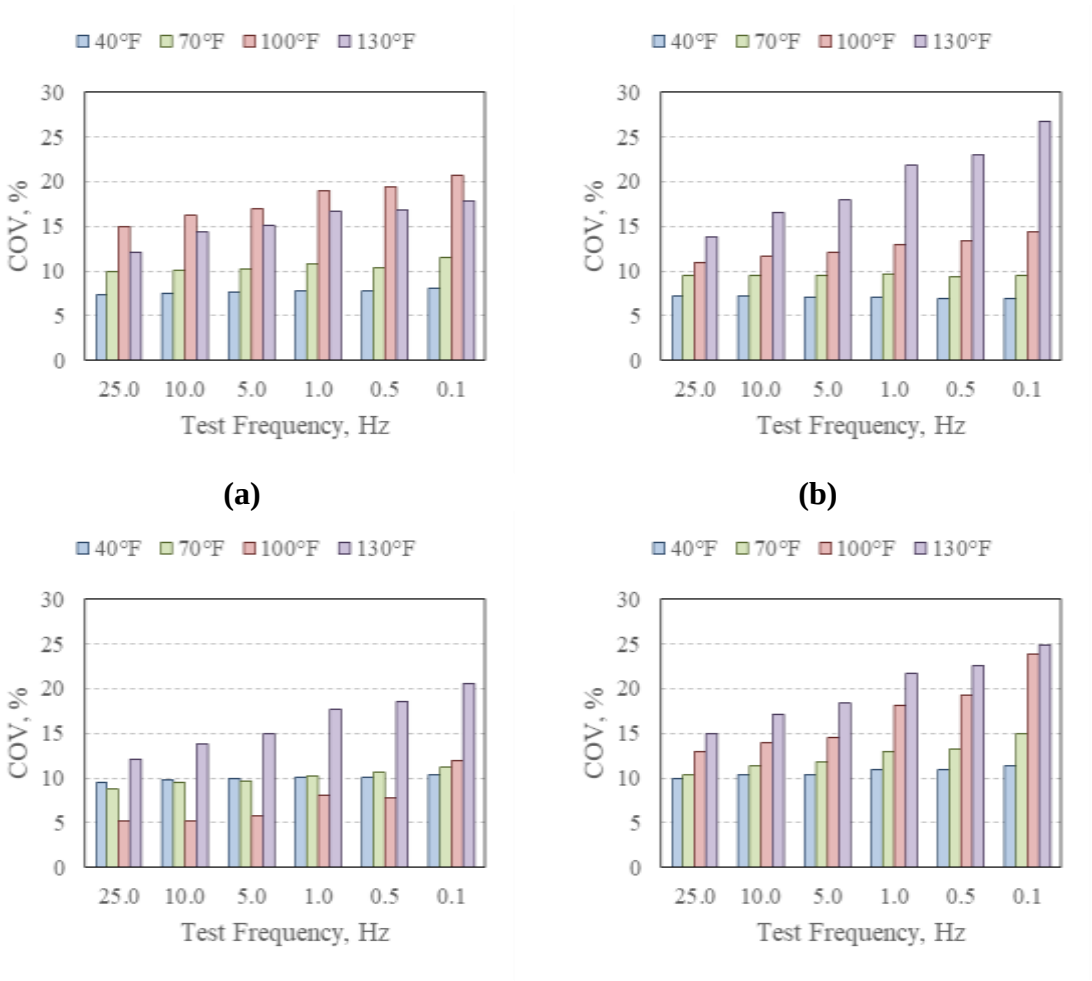

Figure 4.6 COV vs. Test Frequency at Four Confinement Pressures: (a) Unconfined, (b) 5 psi, (c) 10 psi, and (d) 20 psi

In general, higher COVs were obtained for the 20 psi confinement pressure. However, the highest COV obtained was 26.6% and corresponds to a confinement pressure of 5 psi, a test frequency of 0.1 Hz and a temperature of 130°F. The effect of the confinement pressure on the COV is better explained by Figure 4.7. For each test temperature, a similar parabolic trend was observed, with relatively higher COVs for the lowest and highest confinement conditions and lower COVs (0 psi and 20 psi) for the intermediate confinement conditions (5 psi and 10 psi).

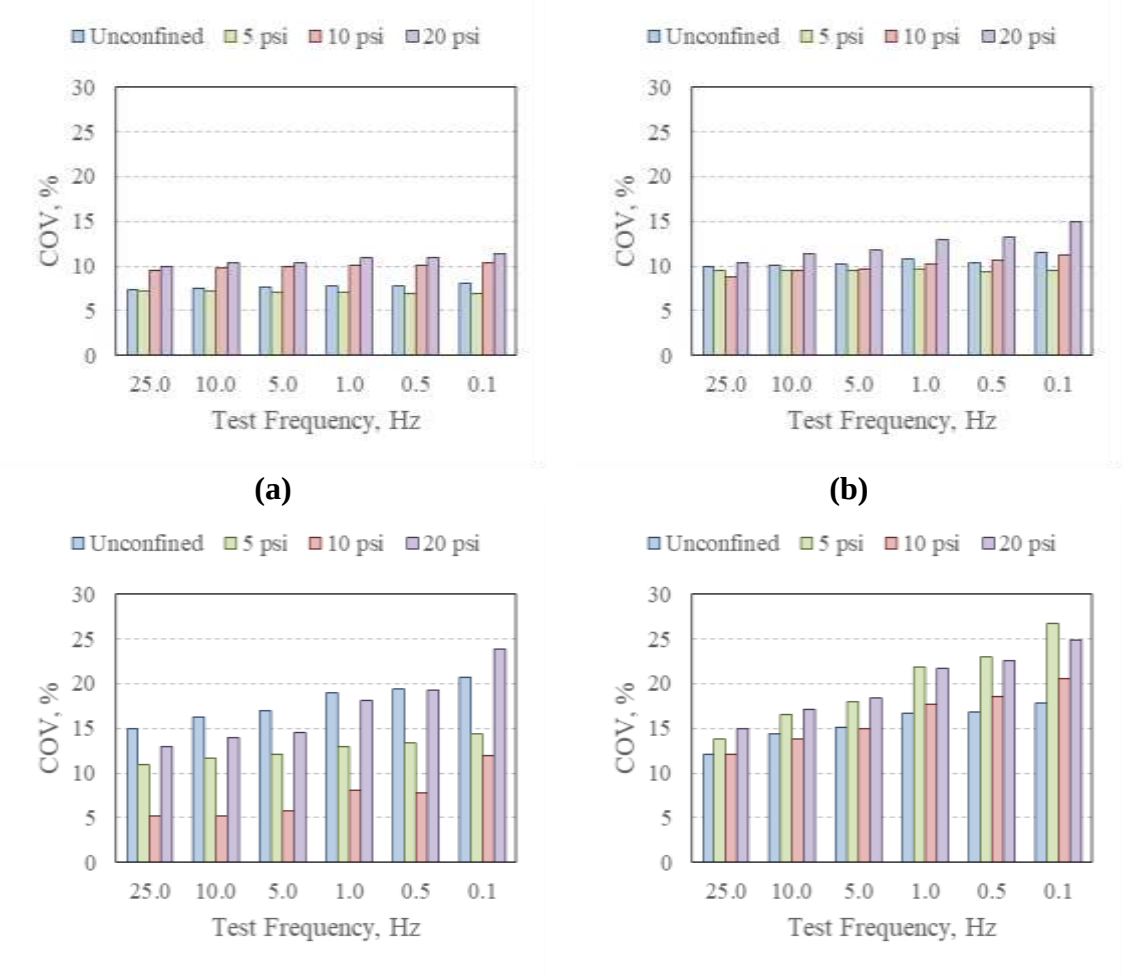

Figure 4.7 COV vs. Test Frequency at Four Test Temperatures: (a) 40°F, (b) 70°F, (c) 100°F, and (d) 130°F

A study conducted by Bonaquist (2011) to investigate the repeatability for dynamic modulus testing on conventional AC materials reported that the COV increased as the stiffness of the materials decreased. This conclusion was based on testing conducted on AC mixtures at temperatures of 40°F, 70°F, and 100°F, and found COVs ranging from 6% to 24% depending on the NMAS of the material. Figure 4.8 shows the COV of the CCPR at a test frequency of 10 Hz and for all confinement levels. The red horizontal lines represent the COV suggested by Bonaquist (2011) for an AC material with a NMAS of

12.5 mm, and for the corresponding dynamic modulus magnitude observed for the CCPR at each test temperature. Although in all cases the COV of the CCPR tends to be greater than the COV suggested for AC materials, the average difference did not exceed 30%, indicating the COV for the CCPR may be similar to that of AC mixtures.

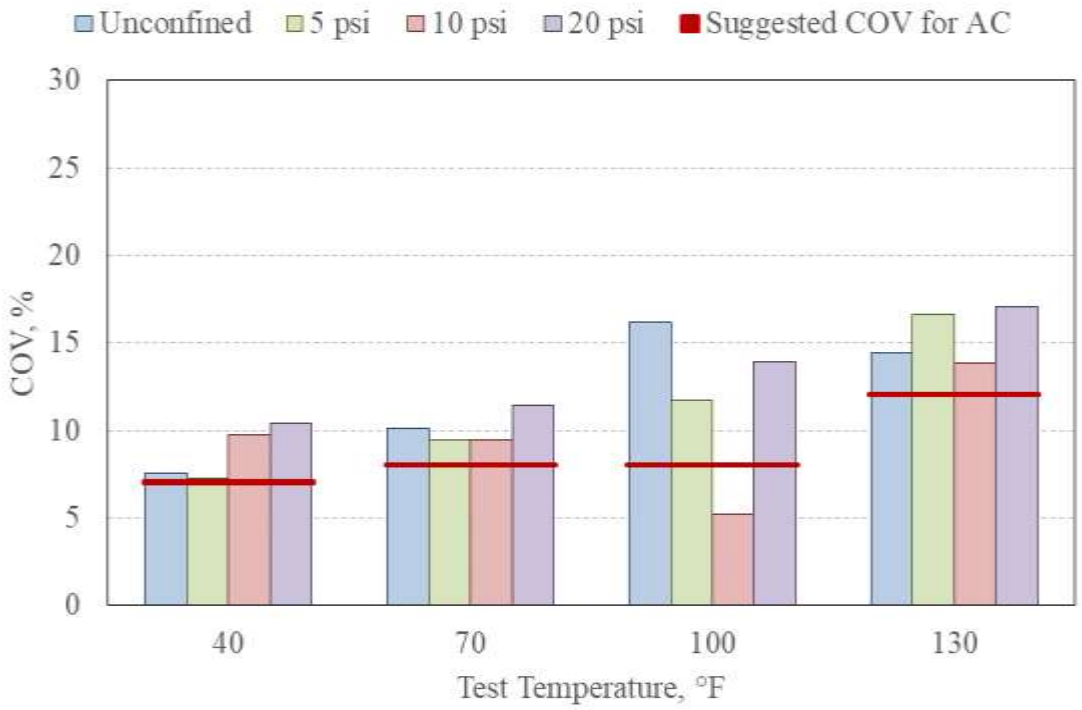

Figure 4.8 COV vs. Test Temperature for a Test Frequency of 10 Hz

Effect of Temperature

A statistical analysis was conducted by Diefenderfer and Link (2014) to investigate the influence of temperature and confinement on the stiffness of the CCPR. To consider the effects of temperature, a two tailed student's t-test was conducted to compare the mean dynamic modulus results at consecutive neighboring temperatures for each test frequency and confinement level. In that way, for each test frequency and confinement level, the

results at 70°F were compared to the results at 40°F and 100°F, while the results at 100°F were only compared to the results at 130°F. If statistical differences were found between two consecutive test temperatures, then it was safe to assume that the differences across larger temperature intervals would be statistically significant as well. The analysis revealed statistically significant differences, at a 95% confidence level (α=0.05), between all dynamic modulus values, except for one irregular measurement corresponding to the confinement pressure of 5 psi, a test frequency of 0.1 Hz and a temperature of 130°F. As stated before, these result also presented the highest coefficient of variability (COV) and therefore was ruled out from the analysis.

The results from this statistical analysis are consistent with the observations made in the previous sub-section. The significant differences in dynamic modulus values across testing temperatures suggest that the CCPR is behaving as a temperature dependent material. Furthermore, the fact that these differences are true for all confinement levels and for all testing frequencies suggests that the CCPR may be considered as a thermorheologically simple material. In that way, the CCPR seems more similar to AC materials as its performance is directly affected by temperature regardless of the confinement and loading conditions in the pavement structure.

Effect of Confinement

An analysis of variance (ANOVA) was conducted at a 95% confidence level (α=0.05) to determine the effects of confinement level on the dynamic modulus results. The ANOVA allowed determining if the differences between the average dynamic modulus at the four levels of confinement were statistically significant for the six test-frequencies and for the

four test temperatures. The results of a subsequent multiple-comparison Tukey-Kramer test, at a significance level (α) of 0.05, are presented in Table 4.2, using grouping letters for test frequencies of 25, 10, 1, and 0.1 Hz. Same grouping letters indicate that the differences in mean dynamic modulus values are not statistically significant.

Table 4.2 Tukey-Kramer Test Results (Adapted from Diefenderfer and Link, 2014)

	Confinement Pressure, psi	**Test Temperature, °F**								
		40	**70**		**100**		**130**			
25 Hz	0	A	A		A		B			
	5	A	A		A		B	A		
	10	A	A		A			A		
	20	A	A		A			A		
10 Hz	0	A	A		A		C			
	5	A	A		A		C	B		
	10	A	A		A			B	A	
	20	A	A		A				A	
1 Hz	0	A	A		B		C			
	5	A	A		B	A	C	B		
	10	A	A		B	A		B	A	
	20	A	A			A			A	
0.1Hz	0	A	B		B		C			
	5	A	B	A	B	A		B		
	10	A	B	A		A		B	A	
	20	A		A		A			A	

As inferred from the table, the effect of confinement pressure on the dynamic modulus is only evident at high temperatures and low frequencies. In fact, the differences in dynamic modulus at different confinement levels were not statistically significant at all test frequencies for test-temperatures of 40°F. On the contrary, significant differences were

found in the dynamic modulus at different confinement levels for test-temperature of 130°F. These differences increased as test-frequencies decreased (Diefenderfer and Link, 2014).

4.3.5 Dynamic Modulus Mastercurve

Figure 4.9 shows the dynamic modulus master curves for the four levels of confinement. These results are consistent with the observations from the previous section in this dissertation, with dynamic modulus values that are visually different at lower reduced frequencies, and become less evident for higher reduced frequencies. The dynamic modulus master curve of the CCPR resembles that of conventional AC materials, for which a similar dependency to confinement has been reported repeatedly in the literature (Zeiada et al., 2011; Lacrois et al., 2011; Pellinen and Witczak, 2002). Similar results had been reported for laboratory- and field- samples of CCPR by Schwartz and Khosravifar (2013), finding that temperature and loading rate had a greater influence on the dynamic modulus than confining stresses.

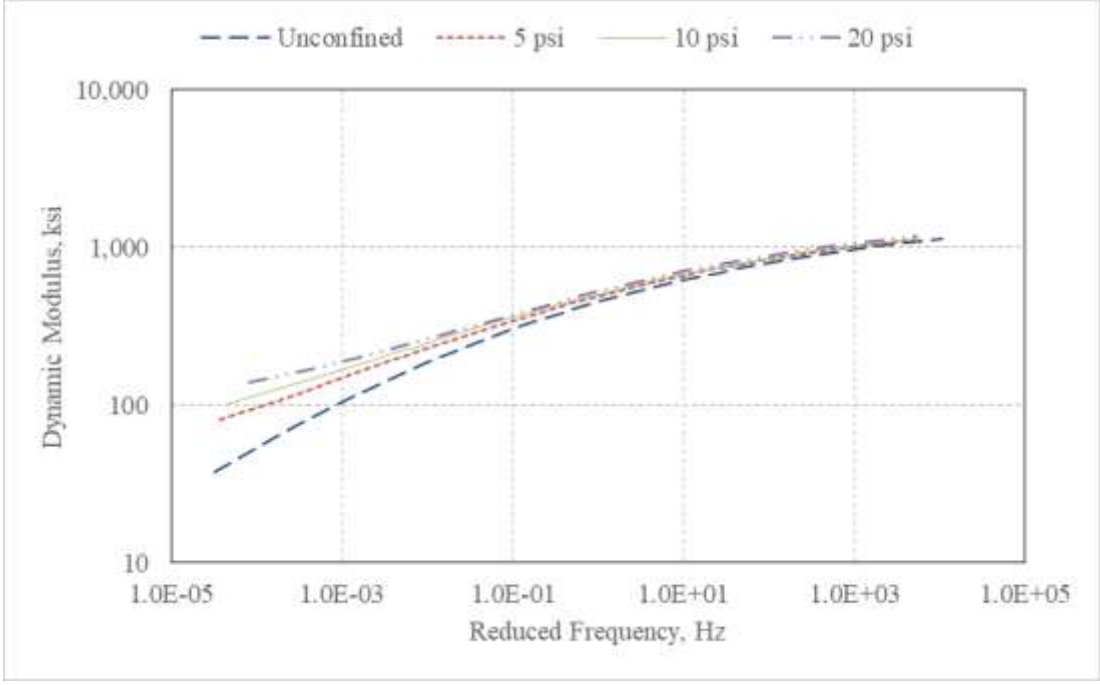

Figure 4. CCPR Dynamic Modulus Master Curves at Different Levels of Confinement

Based on these laboratory results, it may be inferred that the CCPR is a thermorheologically simple and viscoelastic material with a behavior to loading and temperature relatively similar to that of AC materials. Although the temperature- and frequency- dependence of CCPR is not as marked as for AC materials, it seems reasonable to assume both materials may be modeled and analyzed with a similar approach.

From the perspective of pavement design, CCPR may be considered as a material with similar characteristics as conventional AC. Furthermore, similar pavement responses may be expected under traffic loads. In that way, it can be safely postulated that CCPR should be analyzed with the same conventions and using the same correlation functional forms as those established for AC materials. The structural contribution of the CCPR may then be expressed as a layer coefficient in the empirical pavement design method, or as a linear elastic material in LEA for mechanistic-empirical and perpetual pavement design

methods. Furthermore, the correlations and analysis used for each pavement design method, may be the same as those used for conventional AC materials.

4.4 SUMMARY

The CCPR was comprehensively evaluated in the laboratory prior, during and after construction. The CTB, on the contrary, was only tested as part of the design process and no samples were taken during or after construction. Therefore, while extensive information may be available for the CCPR, the laboratory data available for the CTB is limited to only the average 7-day compressive strength of 256 psi, obtained during the design phase. The AC mixtures were designed and evaluated in the laboratory as part of customary quality control activities during Test Track construction.

The RAP used for the CCPR was originally obtained from a pavement recycling project on I-81 in Virginia and consisted of a combination of surface, intermediate, and base AC mixtures (Diefenderfer et al., 2011). As described by Diefenderfer et al. (Diefenderfer et al., 2016), the RAP was milled in 2011 and was stockpiled for approximately two years before being hauled to the project site in Alabama for construction, where it was crushed and fractionated, achieving a gradation slightly finer than the recommendations from Wirtgen GmbH (2012), with a 12.5 mm NMAS and nearly 9% passing the 0.075 mm sieve. The RAP materials were individually sampled at the mobile plant during construction, placed in sealed buckets to preserve their moisture content, and transported to the on-site lab where laboratory-mixed CCPR specimens were fabricated. Dynamic modulus testing was conducted on the test specimens using an AMPT, in accordance with AASHTO TP79 (AASHTO, 2009), slightly modified to considered a

reduced set of four different temperatures, six different loading frequencies, and four levels of confinement. Testing was conducted in the axial mode at temperatures of 40°F, 70°F, 100°F, and 130°F, loading frequencies of 25, 10, 5, 1, 0.5, and 0.1 Hz; and confinement levels of 0, 5, 10 and 20 psi. For each temperature-frequency-confinement condition, a total of five replicates were tested. The specimens were reused while increasing the temperature and decreasing the frequency to minimize potential damage of the samples.

The results show that the dynamic modulus of the CCPR is affected by temperature and loading frequency. As temperature increases, dynamic modulus of the CCPR decreases, and as test frequency increases, dynamic modulus of the CCPR increases. Comparable trends were also observed at all levels of confinement. Based on these results, it may be inferred that the CCPR is a temperature-dependent material and exhibits a viscoelastic behavior during traffic loading, similar to conventional AC materials.

The dynamic modulus master curves of the CCPR were defined for the four levels of confinement. The resulting dynamic modulus master curves resemble that of conventional AC materials. Based on these laboratory results, it may be inferred that the CCPR is a thermorheologically simple viscoelastic material with a behavior to loading and temperature relatively similar to that of AC. Although the temperature- and frequency-dependence of CCPR is not as marked as for AC materials, it seems reasonable to assume both materials may be modeled and analyzed with a similar approach for pavement design.

CHAPTER FIVE

FUNCTIONAL AND STRUCTURAL PERFORMANCE

5.1 INTRODUCTION

During the two research cycles at the NCAT Test Track, the structural and functional performance of the three VDOT test sections was monitored periodically. A comprehensive range of surface measurements, non-destructive testing (NDT), and pavement response measurements were performed at different time intervals to maintain current and updated data through slightly different dates over the two research cycles. The functional performance was determined by rut depth measurements and ride quality, defined as the International Roughness Index (IRI) for each test section. Additionally, the test sections were carefully inspected for the appearance of surface cracks on a weekly basis. However, by the time of this dissertation, no cracks were identified on any of the three test sections.

Falling-weight deflectometer testing was also conducted several times per month to assess the structural performance of the three test sections and its evolution over the two research cycles. Finally, the structural response of each test section was measured under real-traffic conditions. For this, the stresses and strains at different depths within the pavement structure were measured on a weekly basis by means of the previously embedded asphalt strain gauges (ASG) and earth pressure cells (EPC).

5.2 FUNCTIONAL PERFORMANCE

The functional performance of the test sections was determined by three main characteristics: (1) cracking performance, (2) rutting performance, and (3) ride quality or pavement smoothness. Although these three characteristics may be the end result of the structural performance of each test section, they ultimately define the serviceability of the pavement and the user perception of its functionality. The following sub-sections describe each of these characteristics for the VDOT test sections at the NCAT Test Track.

5.2.1 Cracking

Through the end of trafficking (November 30th, 2017), no surface cracking was detected on any of the test sections. Figures 5.1 through 5.3 show the test sections at the end of the 2015 research cycle, after approximately 20 million ESALs. The transverse pavement markings in yellow indicate the beginning of each test section, while the horizontal markings correspond to the random testing locations selected at the beginning of the first research cycle. The circular irregularities observed for section N4 in the foreground of Figure 5.2 correspond to the extracted cores as part of quality control procedures at the Test Track. The large discontinuity observed in section S12 at the foreground of Figure 5.3 corresponds to localized rehabilitation activities performed during the one-year break between the two research cycles. This was due to a rough spot, situated approximately 40 to 60 feet into the section S12, which was identified immediately after initial construction in 2012. During the one-year break after trafficking for the first research cycle ended, the transition zone leading into section S12 was milled and inlaid as part of reconstruction activities, resulting in the irregularly colored pavement surface observed in Figure 5.3.

Figure 5.1 Section N3 at the End of the 2015 Research Cycle

Figure 5.2 Section N4 at the End of the 2015 Research Cycle

Figure 5.3 Section N5 at the End of the 2015 Research Cycle

5.2.2 Rutting

The rutting performance of the test sections over the two research cycles is presented in Figure 5.4. The first research cycle is identified as the “2012 Research Cycle” since traffic operations began in 2012. Similarly, the second research cycle is identified as the “2015 Research Cycle” since traffic operations began in 2015. The shaded area corresponds to the planned one-year break dedicated to forensic evaluation of failed test sections from previous research cycles and reconstruction activities for the 2015 research cycle. It is important to mention that 10,045,790 ESALs were applied during the 2012 research cycle, while 10,009,457 ESALs were applied as part of the 2015 research cycle. As mentioned previously, by the time of this study, a total of 20,055,247 ESALs had been applied to each of the test sections.

The figure shows two evident increases in mean rut depth noted between 3 and 4.5 million ESALs and between 8 and 9 million ESALs. This may be attributed to an increase in pavement temperatures over the summer months of the first two year trafficking cycle. The mid-depth pavement temperatures for the three test sections are presented in Figure 5.5, with overlapping trends that correlate with the two significant increases in rut-depth observed in Figure 5.4. Over the second research cycle, the data seems more erratic, and although some increases may be observed between 13 and 15 million ESALs (during the first summer of the second research cycle), the mean rut depth seems to maintain more constant values. The overall trend over the two research cycles is consistent with common behavior of AC pavements subjected to high traffic, where excessive densification occurs in the initial service stage, causing a reduction of the air voids in the AC layer from 7% or 8% after construction, to 4% or 5% in the first two years of operation (Brown et al., 2009).

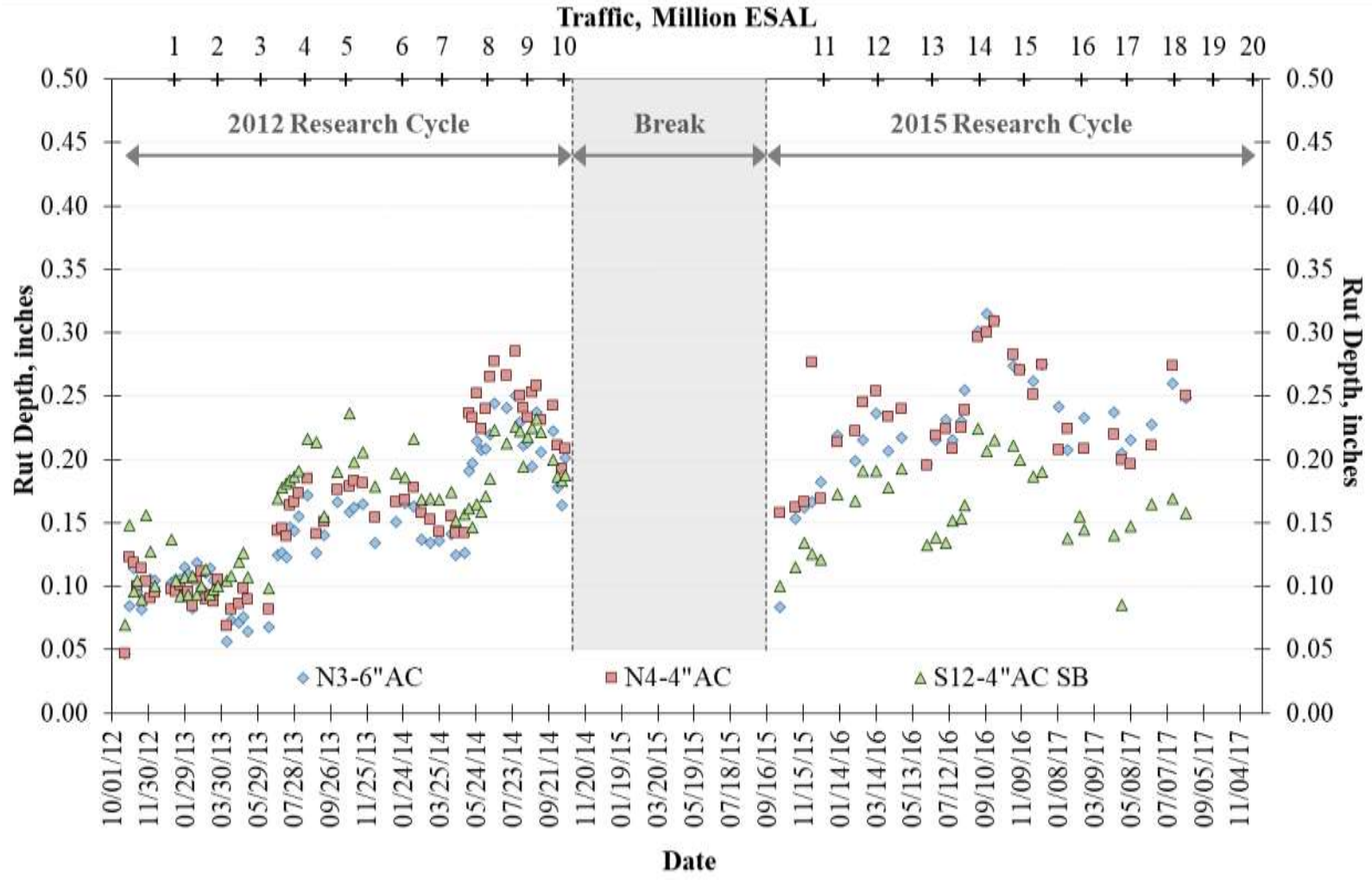

Figure 5.4 Rutting Performance

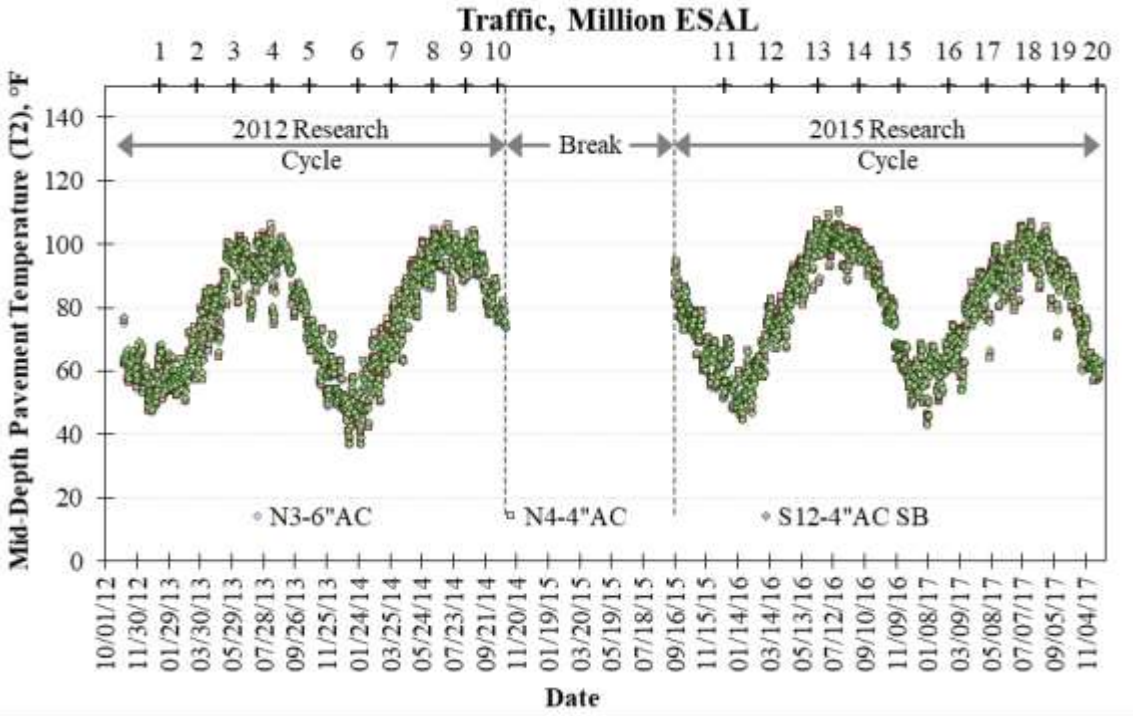

Figure 5.5 Mid-Depth Pavement Temperature over Time

By the end of trafficking, the mean rut depth of the three test sections was well below the failure criteria of 0.5 inches, established at the NCAT Test Track. In fact, the mean rut depths at the end of the two research cycles was less than two-thirds of the rutting failure limit, which indicates the test sections had a very good rutting performance after more than 20 million ESALs. According to most CCPR design manuals (Wirtgen, 2012 and Asphalt Academy, 2009), the main failure mechanism in CCPR layers under high traffic conditions is rutting. However, the rutting performance for the CCPR test sections included in this study follows the same trend as that observed for conventional AC pavements (Brown et al., 2009). In that way, based on these results, it may be inferred that the CCPR may have an adequate rutting performance under high traffic applications.

5.2.3 Ride Quality

Figure 5.6 shows the measured international roughness index (IRI) over the two research cycles as an indication of pavement smoothness. Once again, the shaded area represents the planned one-year break between the 2012 and 2015 research cycles. As identified in the figure, the three test sections show relatively little change in smoothness over the entire duration of this study. In all cases, the measured IRI was maintained below the failure threshold of 170 in/mile established at the NCAT Test Track. Section N4 seems to be the more constant over the two research cycles, closely followed by section N3, which started showing a slight increase in IRI by the end of the second trafficking cycle.

Section S12, which included the CTB, had an initial roughness of nearly double the other two test sections since the beginning of the study. This was caused by a localized rough spot, situated approximately 40 to 60 feet into the test section, which was identified immediately after construction. This rough spot increased significantly the average measured IRI. However, the measured IRI did not change appreciably during the 2012 research cycle, indicating the ride quality was maintained over the first 10 million ESALs. During the one-year break, the transition zone leading into section S12 was milled and inlaid as part of reconstruction activities, noticeably improving the ride quality of the test section over the second research cycle. The measured IRI was reduced approximately 25% between the end of the 2012 research cycle and the beginning of the 2015 research cycle. Furthermore, a similar trend was observed over the second research cycle, without any significant variations of the measured IRI values for section S12. Despite the high IRI values reported since the beginning, the IRI in section S12 did not seem to change significantly over time, except for the improvement from milling between test cycles.

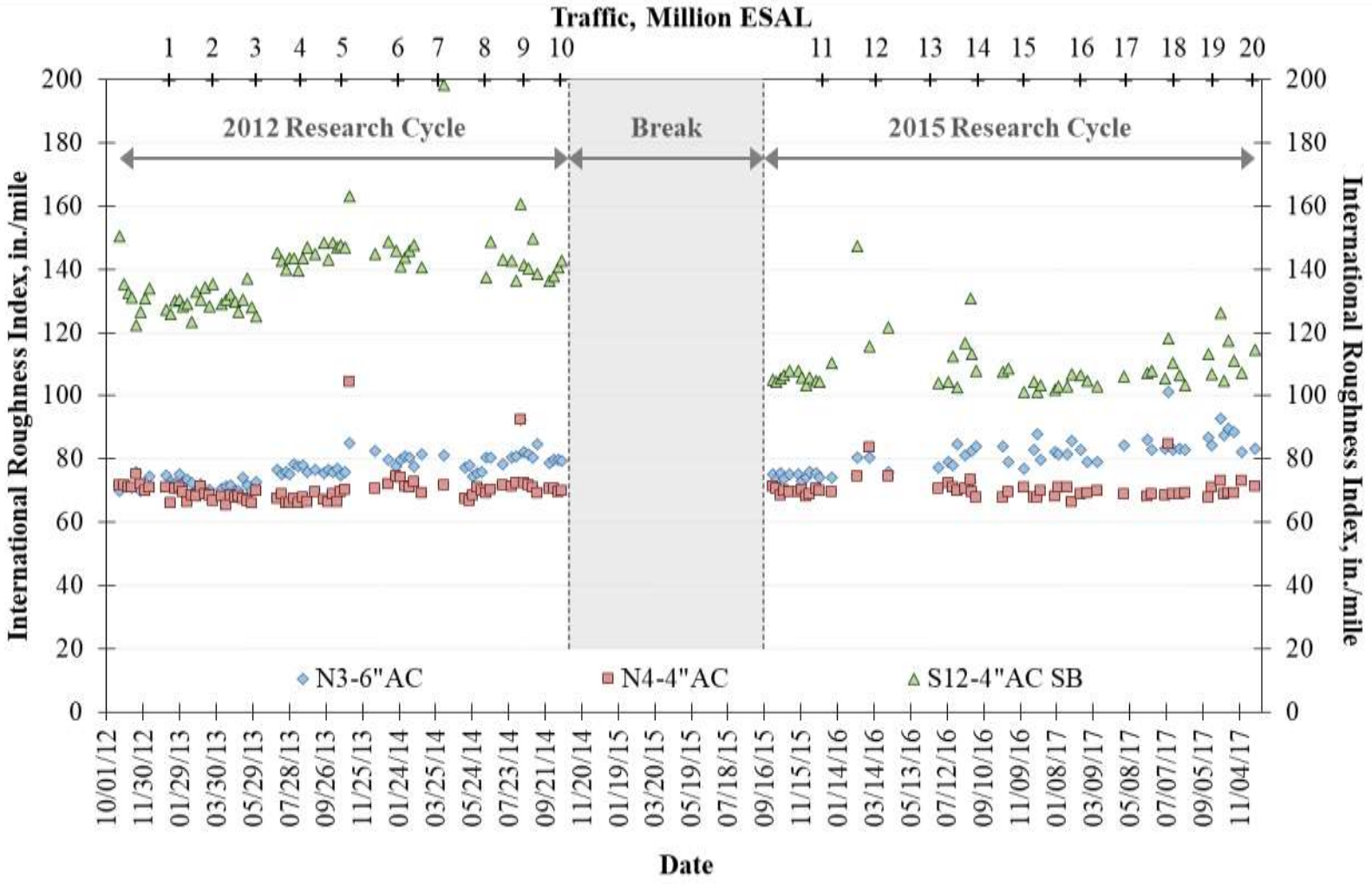

Figure 5.6 Ride Quality

A subsequent analysis was performed to evaluate the evolution of ride quality over the duration of the study in section S12 by determining the difference between the measured IRI and the average IRI obtained for the first five IRI measurements for each research cycle. This difference was identified as ΔIRI and the results are presented in Figure 5.7, where linear trendlines were plotted to illustrate the evolution of ΔIRI over time. This difference showed an increasing trend for the 2012 research cycle, while relatively no change was observed for the 2015 research cycle. Nonetheless, statistical testing (t-test) revealed that the ΔIRI observed for both research cycles were comparable at a 95% confidence level. Therefore, it may be concluded that the IRI in section S12 had no significant change over the duration of the two research cycles.

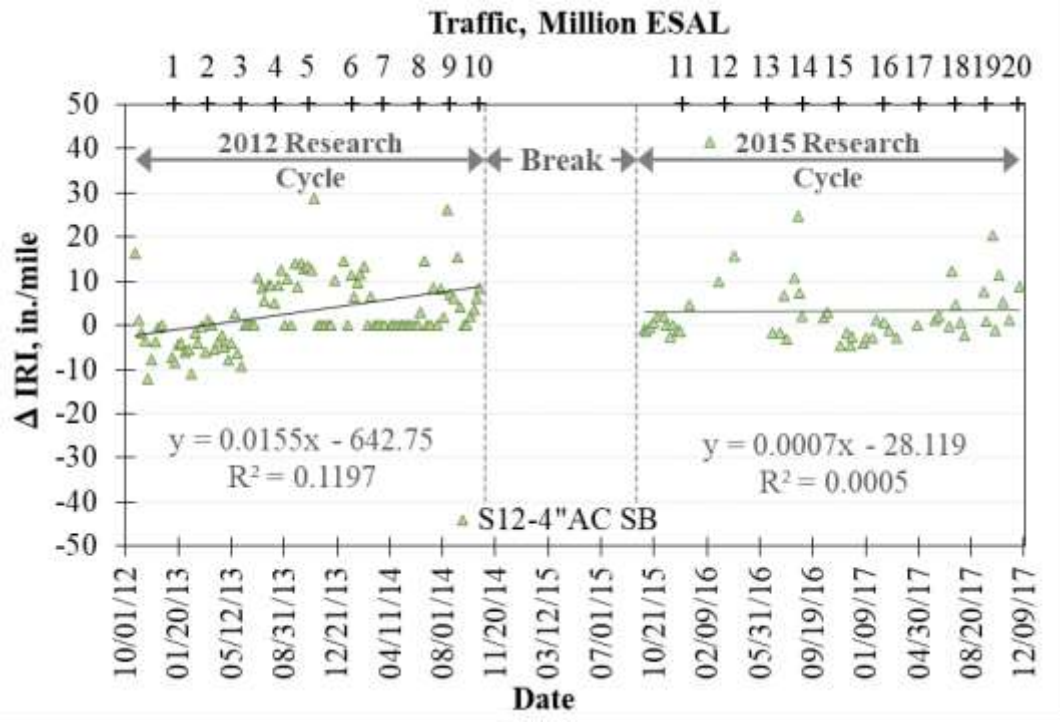

Figure 5.7 Evolution of IRI in Section S12

Section N3 shows initial IRI values similar to those obtained for section N4. The measured IRI values for section N4 seem to remain constant over the duration of the study. On the contrary, the measured IRI values for section N3 show a slightly increasing trend which may indicate pavement damage may occur in the long term. Even if the measured IRI values for both sections are well below the Test Track failure threshold, by the end of the 20 million ESALs, the IRI in section N3 is 10% greater than the IRI in section N4. To further evaluate this observation, a statistical comparison (t-test) was conducted on the average IRI measurements for each research cycle, revealing a significant difference, at a 95% confidence level, between the measured IRI in sections N3 and N4. Additionally, the mathematical differences between the measured IRI for sections N3 and N4 was calculated and an individual cumulative distribution function (CDF) was obtained for each research cycle. Figure 5.8 shows the obtained CDF and includes the average difference calculated for each research cycle. The results indicate that the IRI in section N3 is statistically greater than the IRI in section N4, and this difference increases for the 2015 research cycle when compared to the 2012 research cycle. In fact, the average difference increases nearly 4.9 in./mile between the 2012 and the 2015 research cycles, indicating that the IRI in section N3 is increasing at a faster rate than that in section N4. However, from a practical perspective, this observed increase of 4.9 in./mile is insignificant and does not allow for establishing a robust conclusion at this stage.

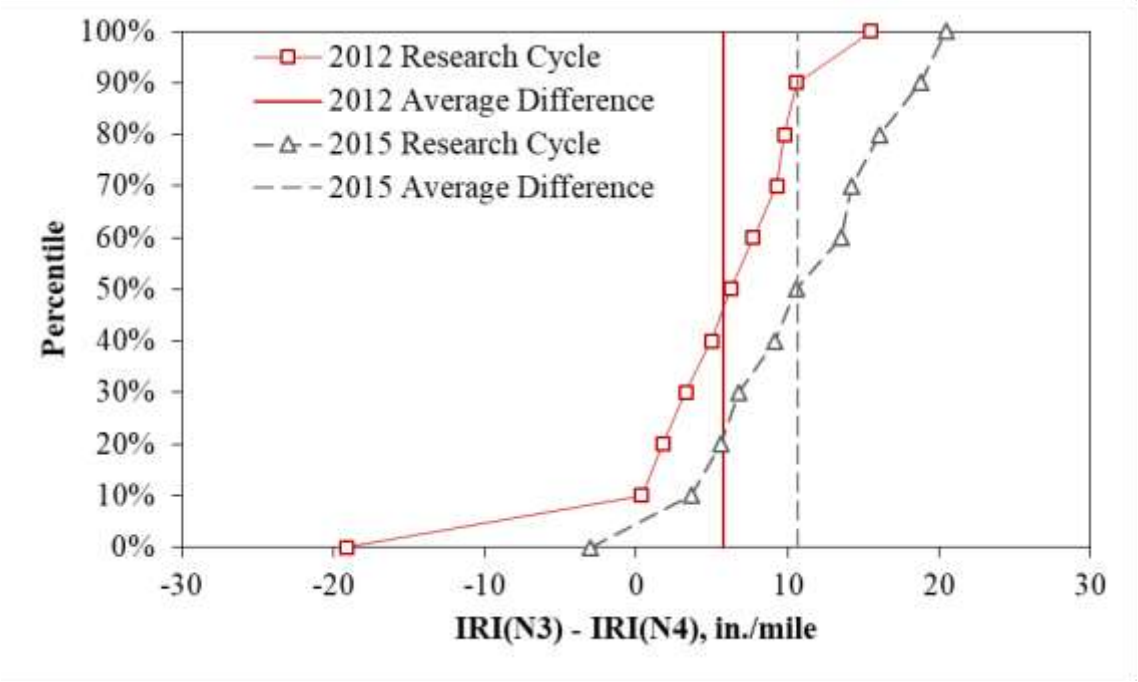

Figure 5.8 CDF Plot for IRI Differences between Sections N3 and N4

Peters-Davis and Timm (2009) documented a performance-based method to recalibrate the structural asphalt layer coefficient based on the converting measured IRI to a pavement serviceability index (PSI). Considering the IRI correlates to the structural integrity of the pavement, its variation over time may be considered as a reduction of the structural capacity of the pavement due to traffic loading. However, in the case of the three test sections in this study, the variation in measured IRI over time is minimal and is insufficient to be attributed to structural decay of the test sections. On the contrary, the results indicate that the structural capacity of the three test sections was maintained over the duration of the study and all three pavement structures are adequate to withstand the applied traffic loads. Although the CCPR test sections performed very well, withstanding more than 20 million ESALs without significant damage, more conclusions may be achieved by analyzing the structural performance and the pavement responses.

5.3 STRUCTURAL PERFORMANCE

The concept of structural performance for this study refers to the capacity of the pavement structure to withstand the traffic loads over time without experiencing significant structural damage. This structural capacity is in turn quantified by the elastic modulus of the pavement layers and their change as loads are applied over time. Based on the deflection measurements obtained from frequent FWD testing performed as part of Test Track operations, the elastic modulus of the pavement layers was backcalculated considering a three-layer structure consisting of the AC/CCPR lifts as layer one, the aggregate base (N3 and N4) or CTB (S12) as layer two, and the subgrade as layer three. Based on the laboratory results previously obtained and considering the temperature- and frequency-dependent behavior observed in the laboratory for the CCPR, it was decided to combine the AC and CCPR layers into one single AC/CCPR layer for the backcalculation process. In that way, the structural capacity of the pavement was assessed by simply analyzing the backcalculated modulus of two pavement layers over time: (1) the AC/CCPR and (2) the CTB.

5.3.1 Effect of Pavement Temperature on AC/CCPR Backcalculated Modulus

The backcalculated modulus values obtained for the AC/CCPR layer are greatly affected by pavement temperature. Figure 5.9 shows the backcalculated AC/CCPR modulus during the two research cycles. Each research cycle is clearly identified while the shaded area represents the planned one-year break between both research cycles. A seasonal variation is evident, with lower elastic modulus values obtained during the summer months and higher results corresponding to the months with lower registered temperatures.

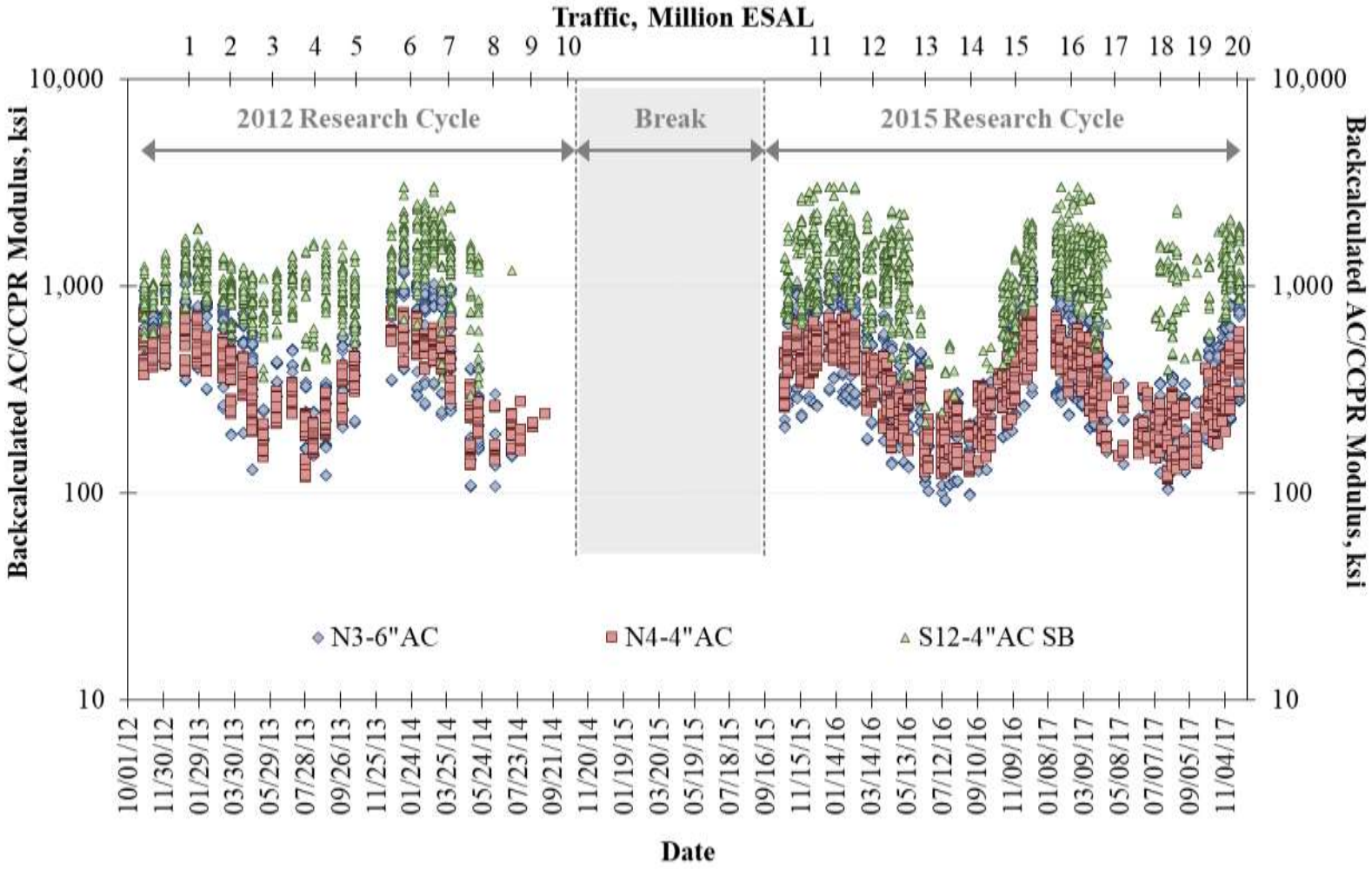

Figure 5.9 Backcalculated AC/CCPR Modulus vs. Date

The seasonal variability of the backcalculated modulus is more evident for the second research cycle. However, this may be attributed to changes in the backcalculation process based on findings reported by Timm and Tutu (2017). This new methodology, adopted only for the 2015 research cycle, allowed determining an optimum backcalculation cross sections to account for the effect of the stiff subgrade at the Test Track and the CTB.

As mentioned before, as FWD testing was being performed, pavement temperatures from the embedded temperature probes were recorded. In that way, three individual pavement temperatures were recorded for each drop of the FWD. The temperature at the middle of the AC layers was recorded by the second temperature probe within each pavement section, and identified as T2. Similarly, the temperature at the AC/CCPR interface was recorded as T3, while the temperature within the CCPR layer was recorded as T4. Figures 5.10 to 5.12 show the three measured pavement temperatures for each FWD drop during the two research cycles for each test section, where each data point corresponds to the average recorded temperature for the duration of each FWD test. The trends are similar to the trends described in previous sections of this dissertation, and the results are consistent with previous research at the Test Track, where temperatures decrease with increasing depth within the pavement structure. In that way, the temperatures in the middle of the AC layers (T2) are higher than the temperatures in the middle of the CCPR layer (T4).

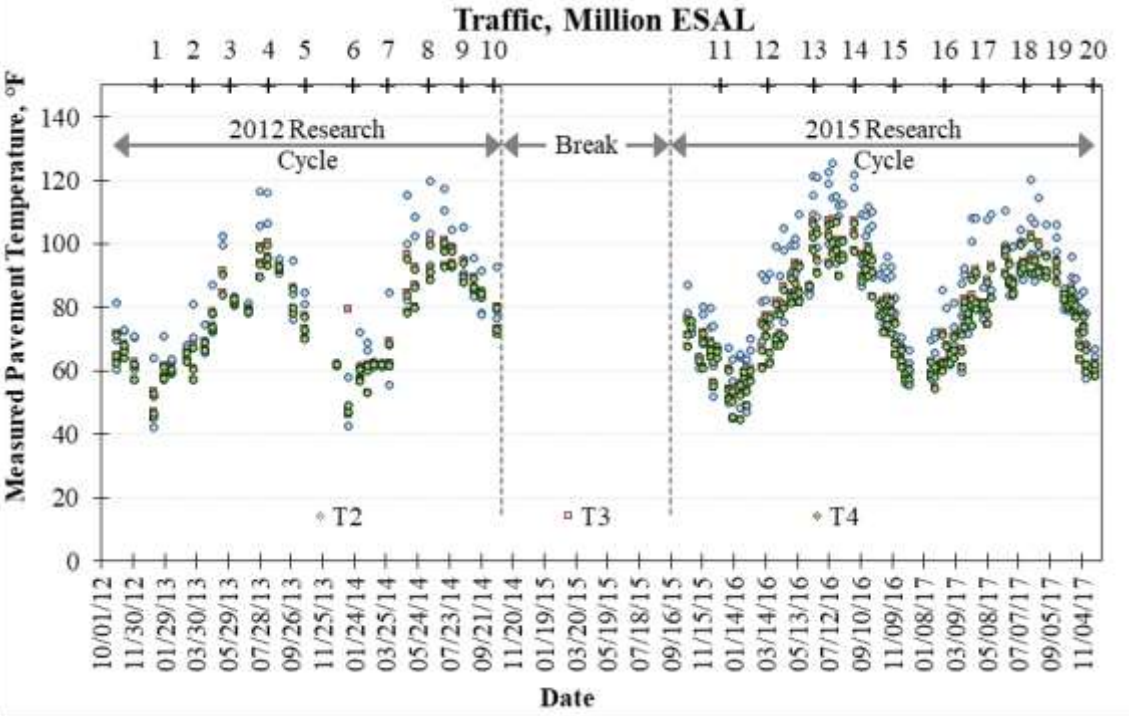

Figure 5.10 Pavement Temperatures for Section N3

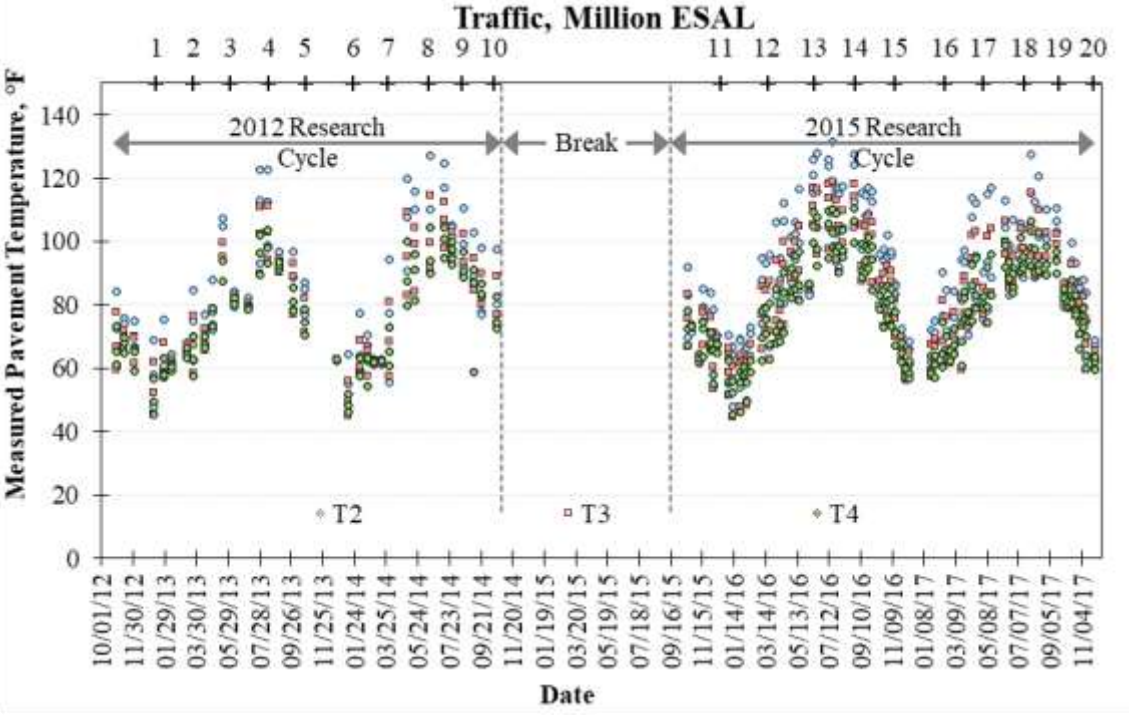

Figure 5.11 Pavement Temperatures for Section N4

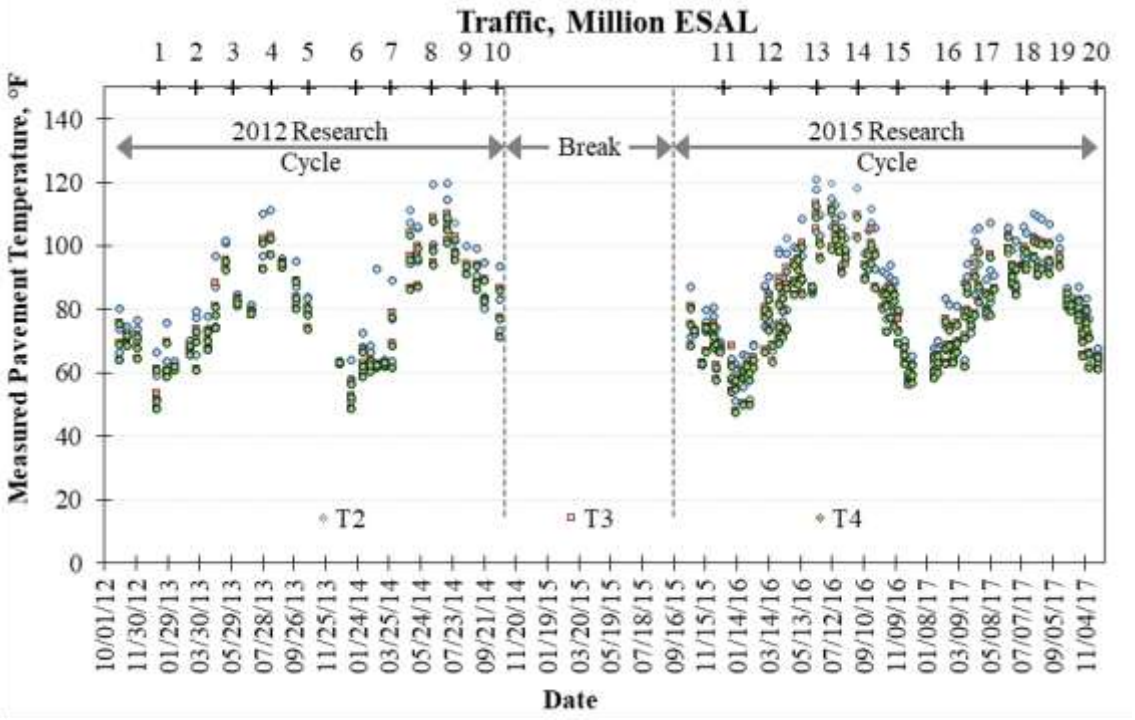

Figure 5.12 Pavement Temperatures for Section S12

The backcalculation procedure considered one single AC/CCPR layer; however, a relatively small, but sufficiently evident temperature difference was detected within the layer, specifically between temperatures T2 and T4. Therefore, it was deemed necessary to determine and quantify the effect of pavement temperature on the backcalculated elastic modulus. Figure 5.13 shows the effect of pavement temperature at the middle of the AC layers (T2) on the backcalculated modulus for the three test sections. The negative slope of the linear trendlines indicate the magnitude of the effect of the temperature on the backcalculated modulus. Similarly, Figures 5.14 and 5.15 show how the backcalculated modulus for the test sections is affected by the temperature at the AC/CCPR interface (T3) and at the middle of the CCPR layer (T4).

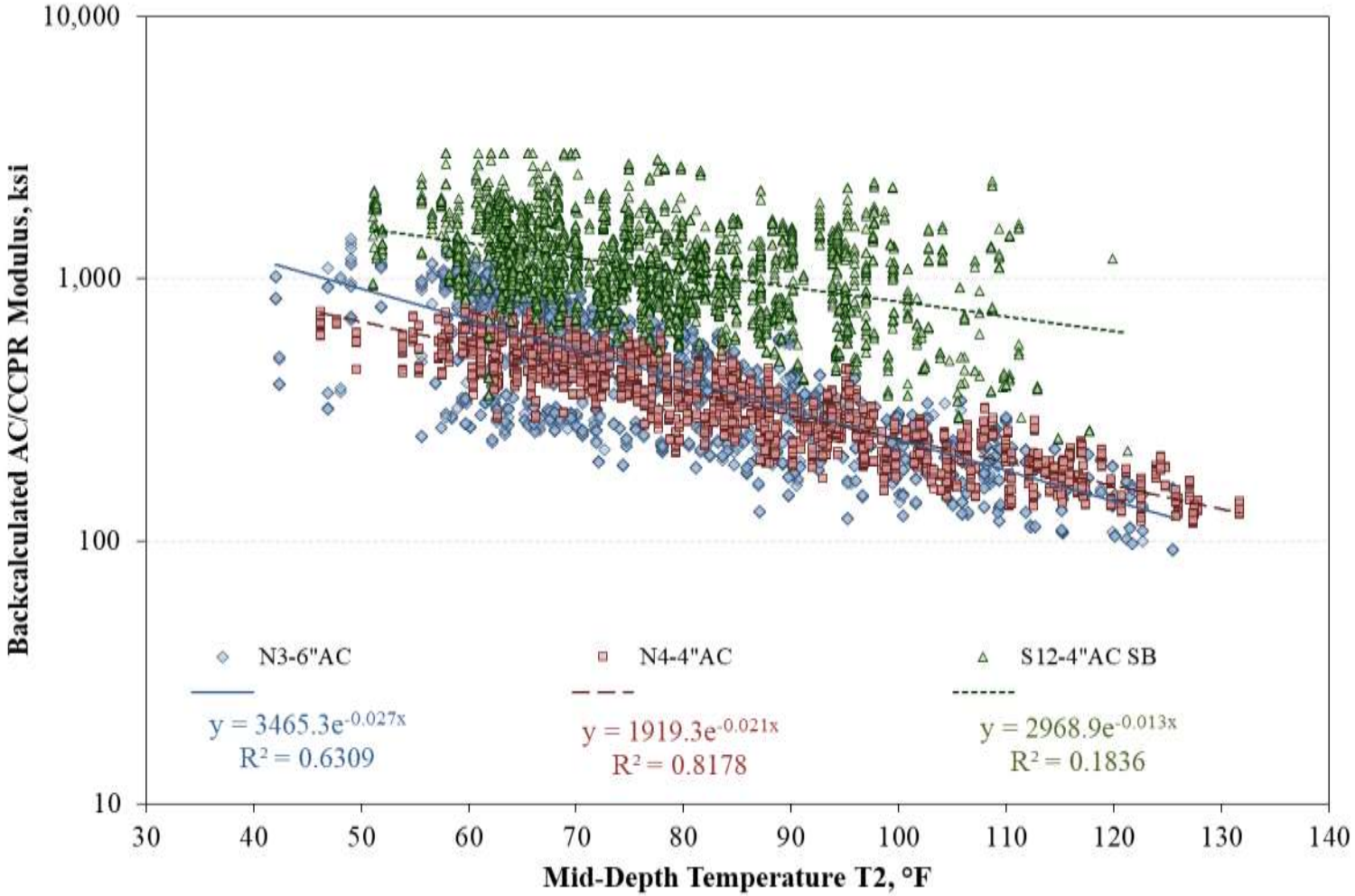

Figure 5.13 Backcalculated AC/CCPR Modulus vs. Mid-Depth Pavement Temperature (T2)

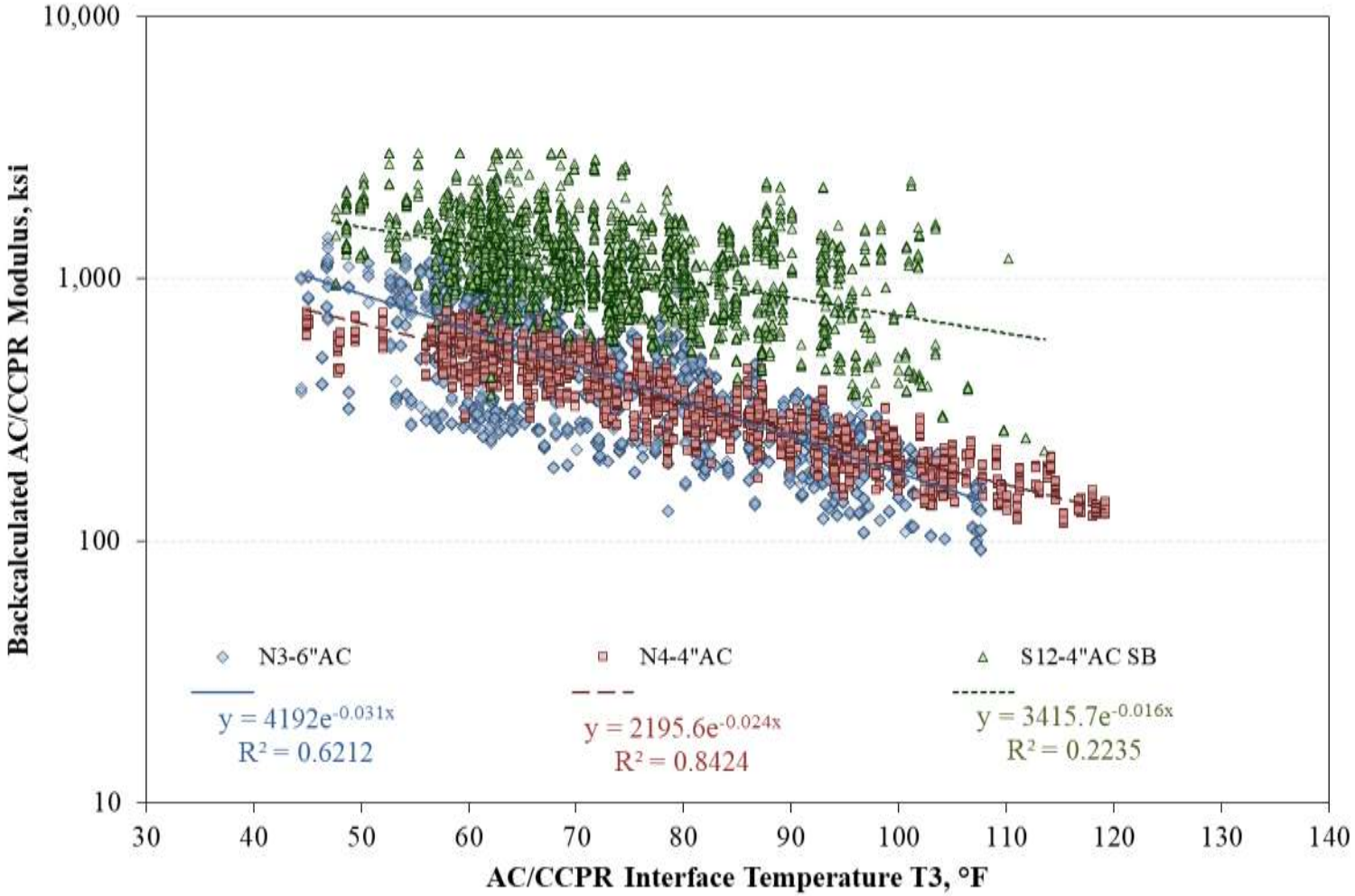

Figure 5.14 Backcalculated AC/CCPR Modulus vs. Pavement Temperature at the AC/CCPR Interface (T3)

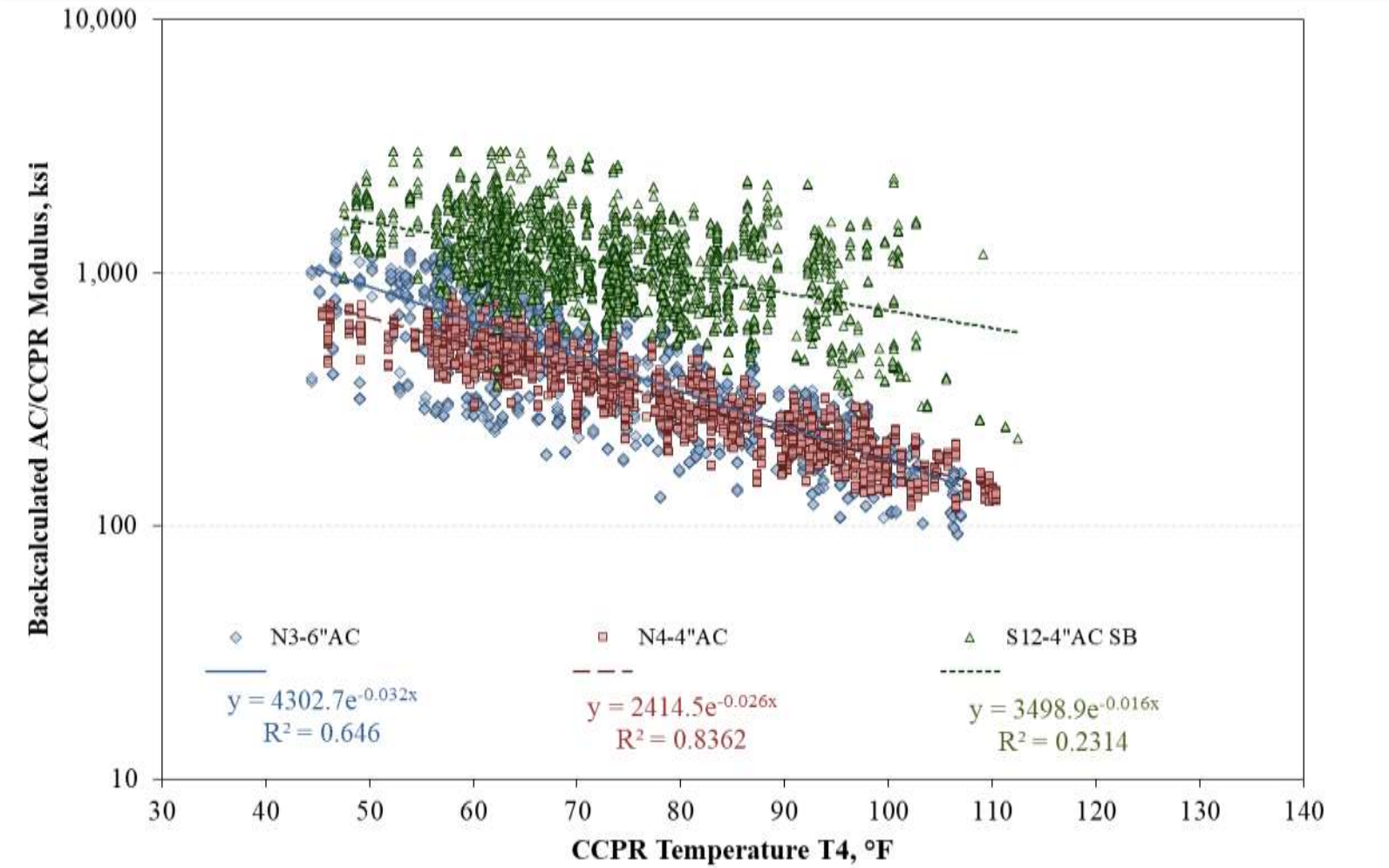

Figure 5.15 Backcalculated AC/CCPR Modulus vs. Pavement Temperature at the Middle of the CCPR Layer (T4)

The results seem to be consistent in all cases and for all the pavement temperatures recorded. Sections N3 and N4, over the aggregate base, show a strong influence of pavement temperature on the elastic modulus of the AC/CCPR, demonstrated by the exponential regression equations and corresponding coefficients of determination (R^2). The thicker AC section (N3) appears to be slightly more temperature sensitive (i.e., steeper slope) than the thinner AC section (N4). This may be due to the effect of the additional 2 inches of AC in section N3 and the relatively higher percentage of CCPR conforming the AC/CCPR layer in section N4. These results are consistent with previous findings at the NCAT Test Track that described a reduction in temperature-sensitivity in high RAP sections due to the presence of a larger amount of aged binder (West et al., 2012).

Section S12, having the CTB, shows a higher modulus and much less temperature sensitivity than the other two sections. The exponential regression coefficient is less than half that obtained for the other two sections and the corresponding R^2 is significantly lower. It is believed that the increased modulus and lower temperature sensitivity is an artifact of the backcalculation process whereby the AC/CCPR was given a higher apparent modulus to adjust for smaller measured deflections on the CTB. Similarly, the wider range of backcalculated moduli values observed for S12 may be attributed to backcalculation process and the relatively small deflections obtained.

When analyzing each test section individually across T2, T3, and T4, the location of the pavement temperature seems to have an effect on the results, as explained by the variations in the R^2 of the three different regression models. In the case of section N3, the exponential regression model considering pavement temperature T2 revealed an R^2 of 0.63. However, the R^2 increases to 0.65 when the regression is based on pavement temperature

T4 and is 0.62 when the regression is based on pavement temperature T3. Similar variations are observed for the other two test sections, where the three temperatures show relatively similar correlation with the data. The coefficients of determination obtained for each model are summarized in Table 5.1. Each test section corresponds to a row in the table and the three different R^2 values obtained in the previous figures for temperatures T2, T3, and T4 are presented. In all cases, the coefficient of determination obtained for T4 seems slightly higher than that obtained for T2, which at first glance would seem to indicate T4 has a more significant influence on the backcalculated AC/CCPR modulus. However, a more in-depth analysis was performed to substantiate this observation.

Table 5.1 Coefficients of Determination for Different Pavement Temperatures

Section	Coefficient of Determination (R^2) for Exponential Regression		
	T2	T3	T4
N3	0.63	0.62	0.65
N4	0.82	0.84	0.84
S12	0.18	0.22	0.23

To determine if the depth of the measured pavement temperature had a significant effect on the backcalculated modulus, and in order to select a reference temperature for subsequent analyses, a multiple regression analysis was performed. Three linear regression models were generated, one for each test section, considering the backcalculated modulus as the dependable variable and the temperatures T2, T3 and T4 as the explanatory variables, as described by Equation 5.1. In that way, for each test section, an individual regression

coefficient was assigned to each pavement temperature considered in the analysis (T2, T3 and T4). A simple comparison between the three regression coefficients ($\beta_{T2}, \beta_{T3}, \beta_{T4}$), for each test section, allowed determining which pavement temperature had a higher effect and better correlation on the backcalculated AC/CCPR modulus.

$$\log(E_{AC/CCPR\,i}) = \alpha + \beta_{T2}T2_i + \beta_{T3}T3_i + \beta_{T4}T4_i + \varepsilon_i \qquad \textbf{(Equation 5.1)}$$

Where:

$E_{AC/CCPR\,i} =$	Backcalculated modulus for sections N3, N4, and S12
$\alpha =$	Intercept of the linear regression
$\beta_{T2}, \beta_{T3}, \beta_{T4} =$	Regression coefficients for temperatures T2, T3, and T4
$T2_i, T3_i, T4_i =$	Temperatures T2, T3, and T4
$\varepsilon_i =$	Residual for the linear regression

The results are presented in Table 5.2. For each test section the corresponding regression coefficients for pavement temperatures T2, T3 and T4 are complemented by star signs indicating the individual p-value for each statistic and its specific standard error in parentheses. All regression coefficients, except for β_{T3} in sections N3 and S12, revealed p-values below 0.01, indicating a strong evidence of the effect of each regression coefficient in computing the dependable variable, which confirms previous observations that temperature has a significant effect in the backcalculated modulus of the AC/CCPR. Based on the fact that β_{T3} was the only regression coefficient with p-values greater than 0.1, it may be inferred that temperature T3 is having a less important effect on the backcalculated modulus, when compared to the other two temperatures T2 and T4.

Table 5.2 Linear Regression Coefficients for the Three Linear Regression Models

Section	Regression Coefficients for Dependent Variable: $\log(E_{AC/CCPR\,i})$		
	β_{T2}	β_{T3}	β_{T4}
N3	-0.0147*** (0.00142)	-0.00128 (0.00394)	-0.0135*** (0.00391)
N4	-0.0143*** (0.00145)	0.0143*** (0.00320)	-0.0244*** (0.00197)
S12	0.0153*** (0.00239)	0.000308 (0.00726)	-0.0325*** (0.00652)

Standard errors in parentheses
* $p < 0.10$, ** $p < 0.05$, *** $p < 0.01$

Higher magnitude regression coefficients in Table 5.2 indicate a greater influence of the corresponding pavement temperature in the backcalculated modulus for each specific test section. In that way, a simple analysis "column by column" in Table 5.2 revealed that T4 may be having a greater effect than the other two temperatures, since the obtained regression coefficients (β_{T4}) are significantly greater for sections N4 and S12. Nonetheless, the standard errors are also significantly greater for β_{T4} than for the other two regression coefficients. Furthermore, β_{T4} values vary greatly within test sections (i.e. β_{T4} for section S12 is two times greater than for section N3), indicating the effect of T4 is more significant for section S12 than on section N4, and on section N4 than on section N3. Although T4 may have a greater influence in the backcalculated modulus for sections S12 and N4, its effect is not consistent for all three test sections considered in the analysis. In fact, as T4 was measured at the middle of the CCPR layer, the observed differences may be caused by the presence of the stiffer CTB layer in section S12 or by the reduction in AC thickness in section N4.

Regression coefficient β_{T2}, corresponding to temperature T2, seems to have the most consistent effect in all test sections, with magnitudes ranging between 0.0143 and 0.0153, p-values lower than 0.01, and relatively small standard errors. Based on the previous observations, it may be inferred that temperature T2 has a better, more consistent correlation with the backcalculated modulus. Therefore, it seems appropriate to select temperature T2 as the reference temperature for further analyses on the test sections.

5.3.2 Structural Performance of the AC/CCPR

Temperature T2 was selected as the pavement temperature for further analyses. As shown in Figure 5.13, for each test section, the measured AC/CCPR modulus was expressed as a function of mid-depth pavement temperature according to equation 5.2.

$$E_{AC/CCPR@T} = k_1 e^{k_2 T} \qquad \textbf{(Equation 5.2)}$$

Where: $E_{AC/CCPR@T} =$ Backcalculated modulus at the test temperature (ksi)

$T =$ Mid-Depth Temperature T2 (°F)

$k_1, k_2 =$ Regression coefficients for temperature T2

To objectively evaluate the evolution of the AC/CCPR modulus over time, it was necessary to normalize the measured values to a reference temperature. A reference temperature of 68°F was selected, following the recommendations of the AASHTO 93 pavement design guide. Temperature-normalization was performed by mathematically dividing the modulus at the reference temperature ($E_{AC/CCPR@68°F}$) by the modulus at the

measured temperature ($E_{AC/CCPR@T}$), using Equation 5.2. This ratio was then solved for the temperature-normalized modulus to obtain Equation 5.3, which was used to calculate a temperature-normalized modulus for each measured modulus. This constitutes a practical method to eliminate the effect of temperature for the analysis of backcalculated modulus over time, describing the evolution of the structural capacity of the pavement structure over time with minimal influence of the climate and temperature conditions.

$$E_{AC/CCPR@68°F} = E_{AC/CCPR@T} \cdot e^{k_2(68°F-T)} \quad \textbf{(Equation 5.3)}$$

Where: $E_{AC/CCPR@68°F} =$ Temperature-normalized modulus (ksi)

$E_{AC/CCPR@T} =$ Backcalculated modulus at the test temperature (ksi)

$T =$ Measured mid-depth pavement temperature T2 (°F)

$k_2 =$ Section specific regression coefficient

The normalized AC/CCPR modulus over time are presented in Figure 5.16. Test sections having an aggregate base (N3 and N4) show virtually no change in modulus over time. However, the modulus for section S12 over the CTB show a clear increase over time, which may be attributed to the presence of the CTB. It was postulated that this behavior may be the result of two different effects. On one hand, the backcalculation process may be attributing certain CTB properties to the AC/CCPR layer. On the other hand, the CTB may be curing over time, as described by Diefenderfer and Apeagyei (2014), which in turn would result in reduced pavement response measurements that will be explored in the next sections of this dissertation.

Certain scatter of the data may be observed, especially for the normalized modulus in section S12. Although the scatter is much less than that observed in Figure 5.7, the effect of seasonal variation is still evident and slightly lower normalized modulus values are obtained for the summer months. This is especially evident for section S12 during the 2015 research cycle, where normalized modulus values are significantly lower in the summers of 2016 and 2017. This effect may also be attributed to the change in the backcalculation process mentioned previously. However, the differences were deemed satisfactory for practical purposes since the effect is minimal on the overall behavior of the normalized modulus over time.

To evaluate the evolution of the temperature normalized modulus over time, linear trendlines were plotted for each test section. A significant negative slope would indicate the structural decay of the corresponding test section. In that way, a visible reduction in the normalized modulus over time could be interpreted as progressive structural damage in the test sections, and therefore a loss of structural capacity of the AC/CCPR layer. However, despite the variability of the normalized modulus values, the resulting slopes were positive indicating no structural damage was induced to the sections by the applied traffic. In any case, all three test sections appear to be healthy from a structural standpoint.

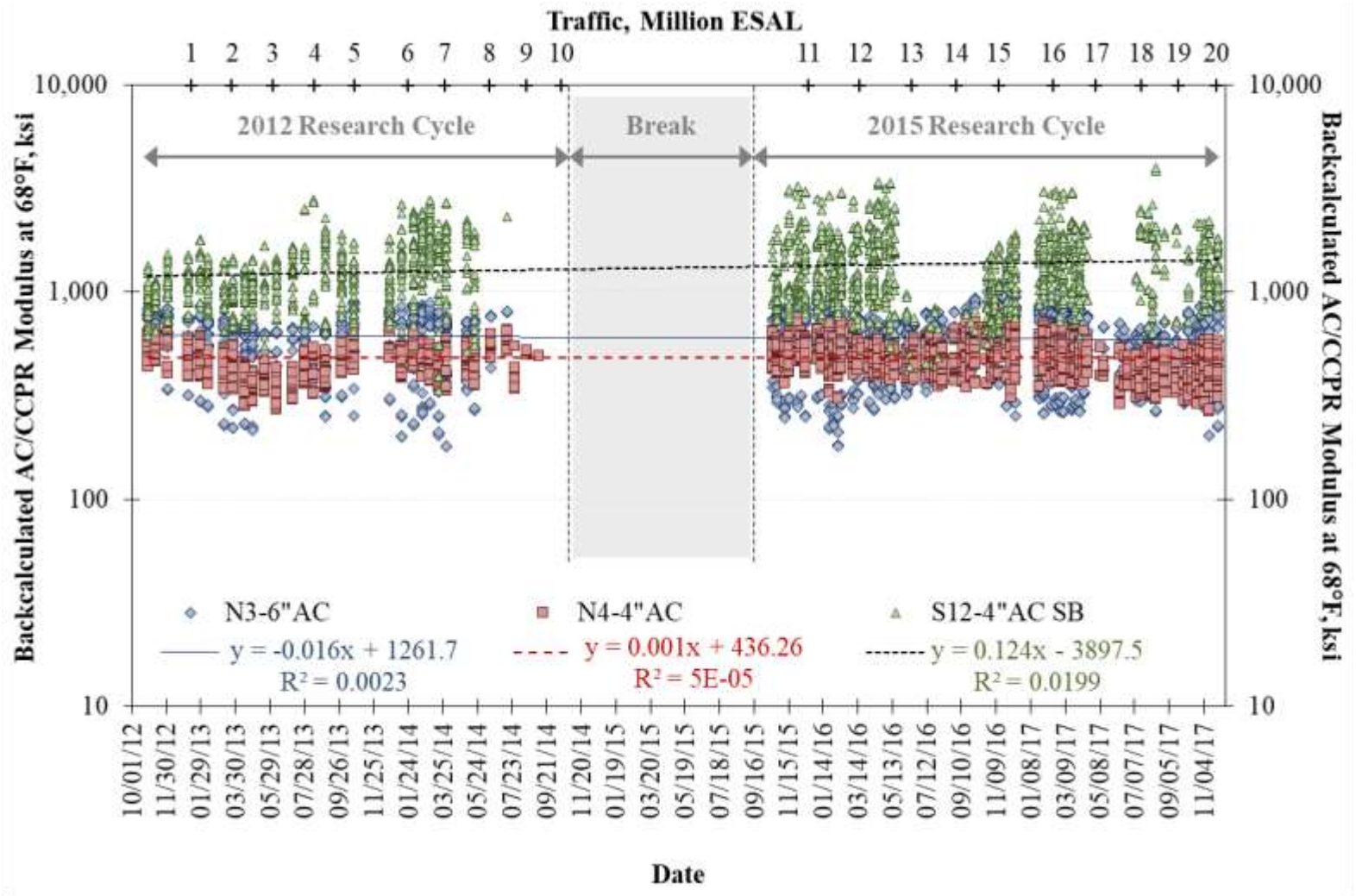

Figure 5.16 Temperature Normalized AC/CCPR Modulus vs. Date

5.3.3 Effect of Pavement Temperature on Backcalculated Base and CTB Modulus

As part of the backcalculation procedure, the modulus of the second pavement layer for the test sections was also determined. As explained previously, in the case of sections N3 and N4 this third layer corresponded to the granular base, whereas in the case of section S12 it corresponded to the CTB. Figure 5.17 shows the effect of mid-depth pavement temperature (T2) on the backcalculated modulus of the granular base and the CTB. There seems to be no evident correlation between mid-depth temperature and backcalculated modulus, corroborating the fact that both layers, the granular base and the CTB, are not thermally dependent materials. For that reason, no temperature correction was necessary to analyze the results and to identify the evolution of the modulus over time.

The evolution of the backcalculated modulus over time is presented in Figure 5.18. The backcalculated modulus for the granular base, obtained for sections N3 and N4, are very similar. Both sections were built with the same granular material and with similar as built thicknesses, which explains the almost identical results obtained. The backcalculated modulus for the CTB in section S12 are considerably higher than those obtained for the granular base. The cement is considerably stiffening the CTB creating a rigid layer from a structural perspective. A similar increasing trend, as that mentioned for the AC/CCPR in section S12, is observed for the CTB. As mentioned before, this may be attributed to the curing process of the CTB over time. However, in the case of the CTB, the backcalculated modulus values show significantly more scatter, with specific values even lower than those obtained for the granular base. Further analyses on the specific base materials would allow discerning the cause of such variations.

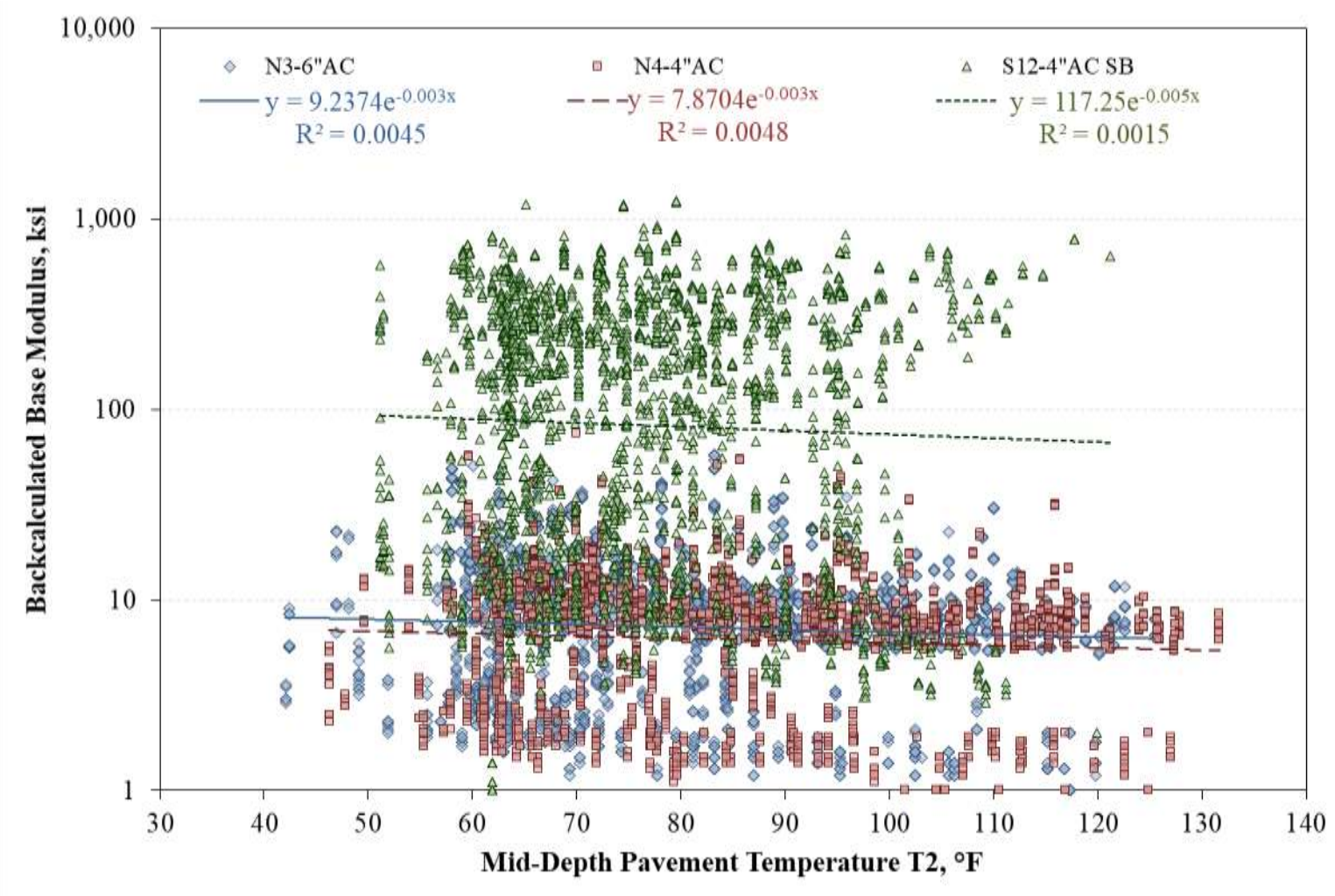

Figure 5.17 Effect of Temperature on the Granular Base and the CTB

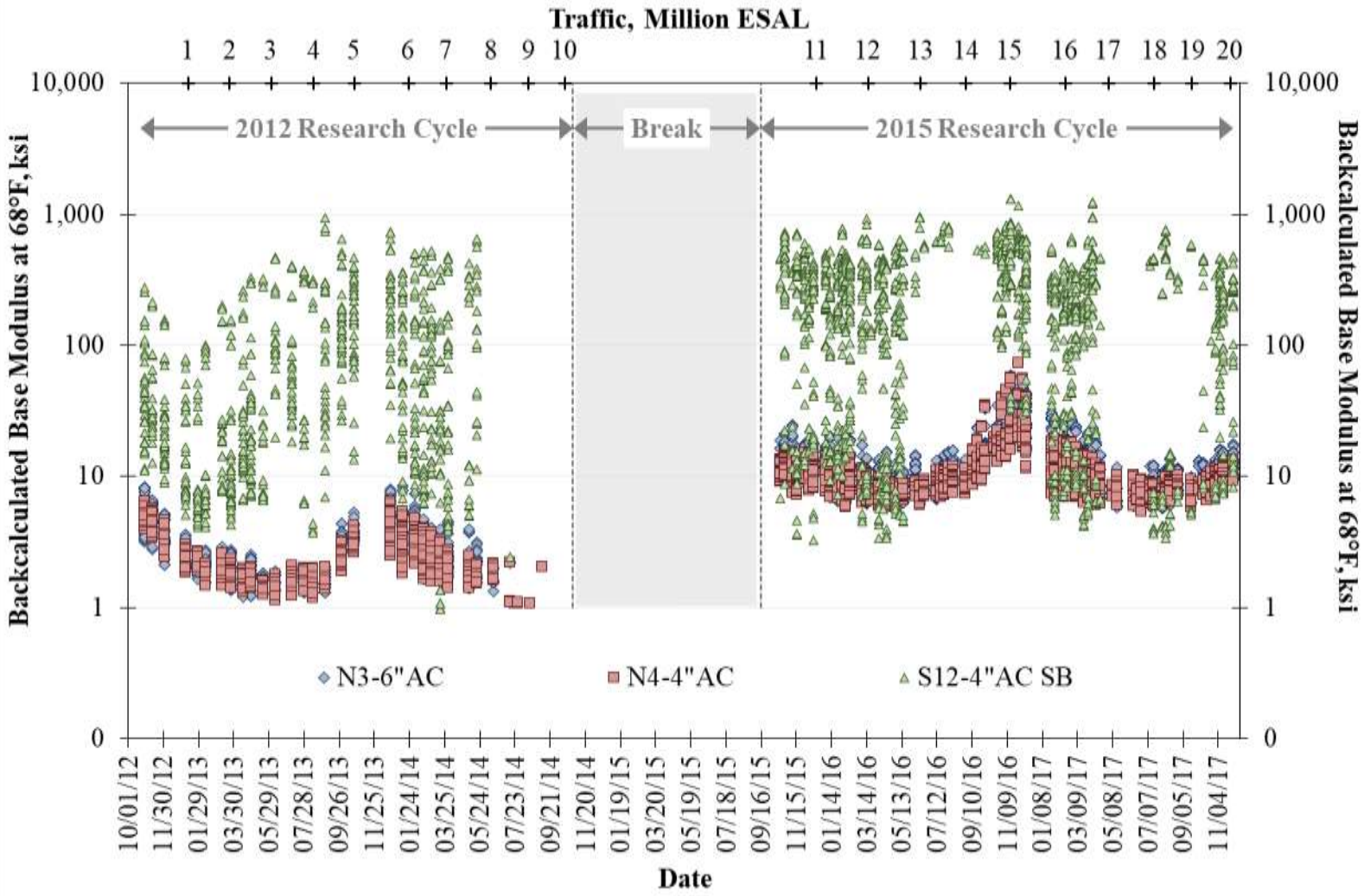

Figure 5.18 Backcalculated Base Modulus vs. Date

5.3.4 Structural Performance of the Granular Base

Although it was impossible to establish a direct correlation between mid-depth pavement temperature and the backcalculated modulus of the granular base, a certain level of seasonality was observed for sections N3 and N4. This seasonality became more evident when the vertical scale was changed as shown in Figure 5.19. However, based on the considerably low slope obtained when the effect of mid-depth temperature was analyzed, this seasonality cannot be attributed to the effect of pavement temperature on the granular base. The backcalculated modulus values obtained for the granular base during the months of September, October, November and December 2016 are significantly greater than those obtained for all other dates, including the same months in other years. A similar behavior was observed for all load levels. As exemplified by Figure 5.20 for section N3, the backcalculated base modulus values obtained in December 2016 are significantly greater than those obtained for the same month in the years 2012 and 2015. This same trend was also observed for section N4, and for the months of September, October, and December in both test sections. The measured mid-depth pavement temperatures for those months was very similar in all three years shown in the figure. This seems to indicate that even if the seasonality observed for sections N3 and N4 corresponds to the seasonality observed for pavement temperature, the backcalculated base modulus may have been affected by other factors. The linear trendlines included for each FWD testing date in Figure 5.19 seem to indicate the backcalculated modulus decreases as the load level increases. This trend seems to be consistent in the three dates presented in the figure, regardless of the clear difference in magnitude observed for the 2016 results.

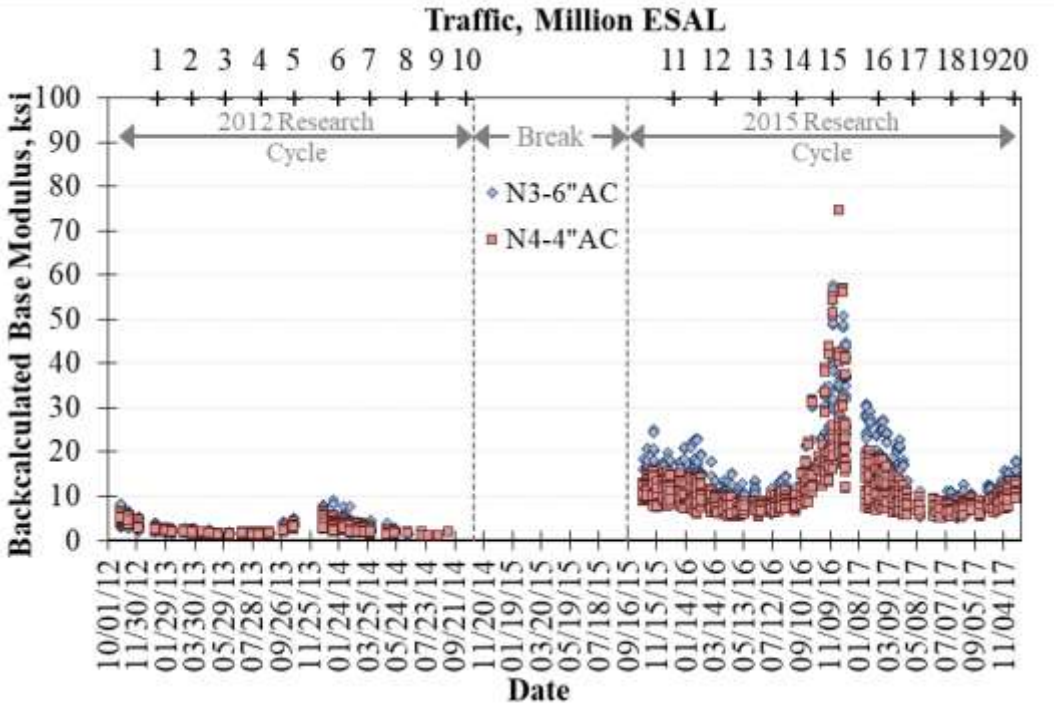

Figure 5.19 Results for Section N3 in the December 2012, 2015 and 2016

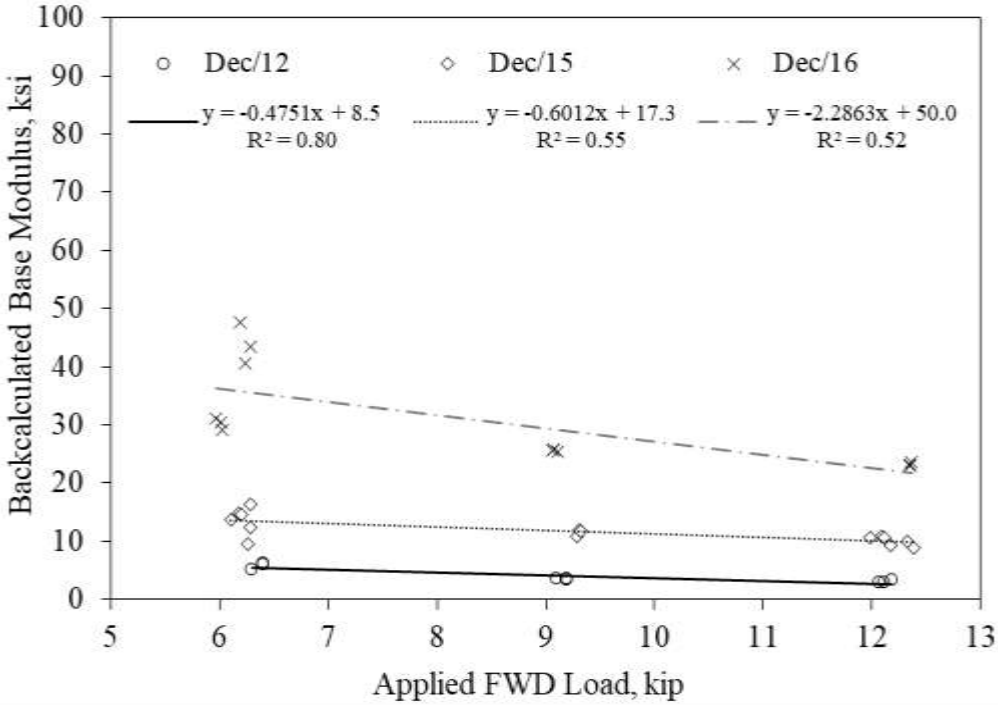

Figure 5.20 Results for Section N3 in the December 2012, 2015 and 2016

A sensitivity analysis, considering all FWD load levels, revealed that the backcalculated modulus of the granular base in sections N3 and N4 was directly affected by the load level. The effect of load level was assessed in each test section for different combinations of testing date, wheel path and random location. In all cases, the same trend was identified, where increased load levels generated lower backcalculated base modulus values. Figure 5.21 exemplifies this effect for two illustrative combinations. The data specified as "Case 1" corresponds to section N3, random location 2 (RL2), outside wheel path (OWP), and tested on March 17th 2014. In a similar way, "Case 2" corresponds to section N4, random location (RL3), inside wheel path (IWP), and tested on April 10th 2017. These two cases are presented only as examples, but showed the same trend as that observed for all other combinations analyzed.

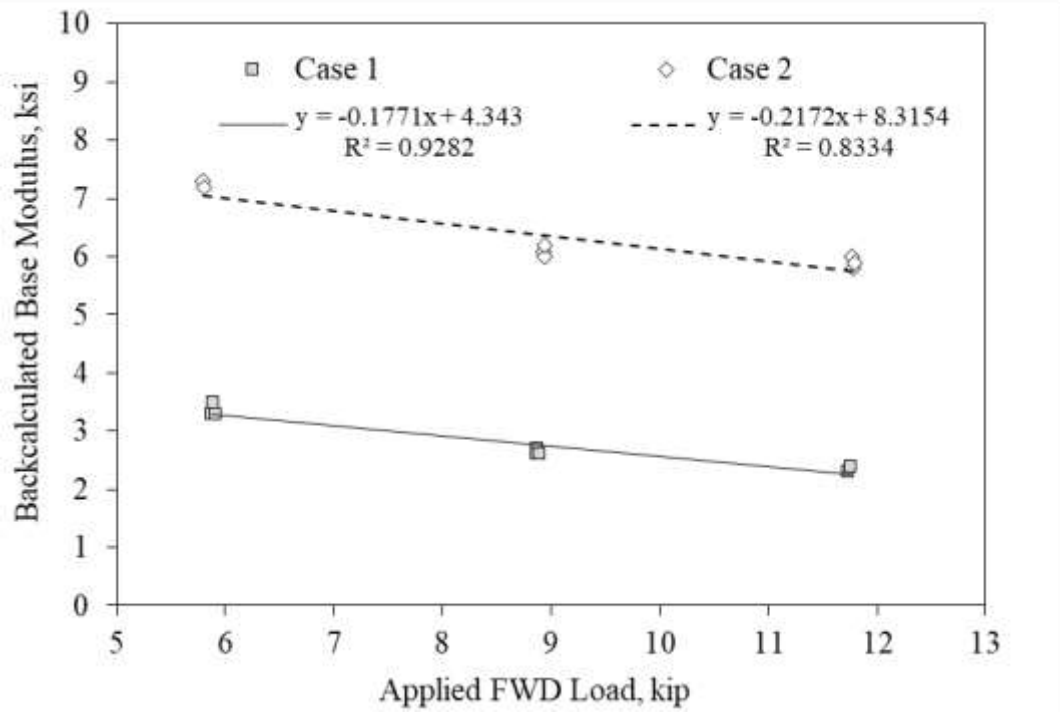

Figure 5.21 Effect of Load Level for Two Different Conditions

In all cases, the backcalculated modulus of the granular base layer decreased as the applied FWD testing load increased. This behavior is consistent with stress softening materials for which larger induced stresses tend to reduce its elastic modulus. This stress softening phenomenon in the granular base explained the results and the seasonality observed previously for sections N3 and N4. It was established in previous sections of this dissertation that the AC/CCPR layer, built above the granular base layer, showed substantial temperature-dependence. In that way, during the colder months, the AC/CCPR layer, with a relatively higher modulus, was capable of absorbing a larger portion of the load-induced stresses applied to the pavement. In turn, the stress-softening granular base layer was subjected to lower induced stresses which tended to increase its modulus. Conversely, during the warmer months, the less stiff AC/CCPR layer transferred larger magnitude stresses to the granular base, which in turn exhibited lower modulus values. For these reasons, even if the granular base is not a temperature-dependent material, its stress softening characteristics generate cyclical variations in the backcalculated modulus, which are indirectly correlated to mid-depth temperature of the AC/CCPR layer.

5.3.5 Structural Performance of the CTB

The backcalculated CTB modulus obtained for section S12 did not show an evident cyclic seasonality as that observed for the base in sections N3 and N4. This may be attributed to the relatively larger scatter observed for the results in section S12 for the two research cycles. To exclude the effect of the observed scatter, a relatively unsophisticated analysis was performed by only considering one specific testing location and analyzing its evolution over a simplified date scale consisting of one single testing date for each month over the

duration of the study. This analysis was individually repeated for multiple testing locations to establish wether the observed trends were sufficiently consistent to make conclusive remarks. An example of the results is presented in Figure 5.22, for the specific condition between wheel paths (BWP) in random location 2 (RL2). A similar behavior was observed for all the conditions analyzed. Linear trend lines were plotted for each research cycle, revealing similar slopes for both research cycles, but more scatter for the 2015 research cycle. In all cases, the backcalculated CTB modulus showed a relatively constant increase over time. However, it was found that specific testing variables such as wheel path and random location had a significant effect on the results. This led to perform a more in depth analysis of the results, which will be summarized in the following discussion.

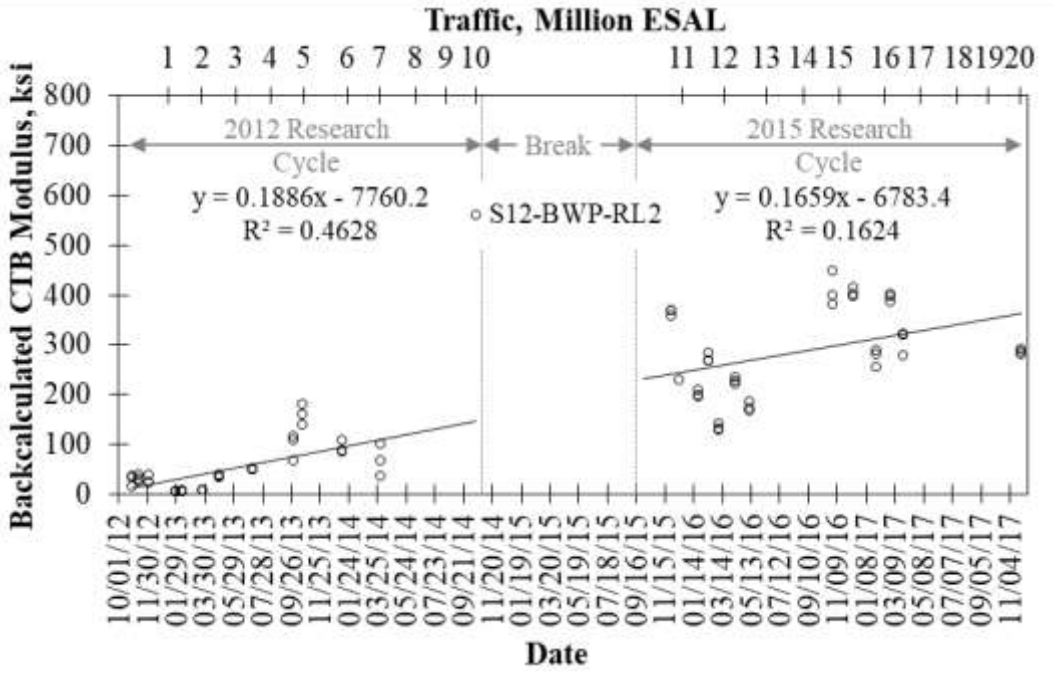

Figure 5.22 Backcalculated CTB Modulus vs. Simplified Date for BWP-RL2

Initially, a sensitivity analysis, similar to the one performed in the previous subsection of this dissertation, was performed on section S12 to assess the effect of FWD load level on the backcalculated CTB modulus. As a mere example, Figure 5.23 shows the effect of the load level on the CTB modulus for the outside wheel path (OWP) in random location 3 (RL3) for four different testing dates. These results are a general representation of the trends observed for the data. It was impossible to establish a robust correlation between load level and backcalculated CTB modulus. In some cases, the backcalculated CTB modulus slightly increased with increasing load levels, while in other cases it seemed to decrease. However, in most cases, these increasing or decreasing trend was specifically attributed to specific outlying results that skewed the linear trend line in one or other direction. Furthermore, from a practical perspective, the changes within the three load levels were relatively small, which in turn would not allow to establish a generalized trend.

The results presented in Figure 5.23 seem to corroborate the observations made previously that the backcalculated modulus of the CTB seemed to increase over time. Regardless of the load level, the results obtained at the beginning of the 2012 research cycle were lower than those obtained for the 2015 research cycle. In fact, the backcalculated modulus seems to increase significantly between November 2012 and December 2015. On the contrary, the results obtained for June 2016 were very similar to those obtained for December 2015, showing the backcalculated CTB may have reached a relatively constant value after the first research cycle. As mentioned before, two possible explanations were postulated for this phenomenon, including the progressive curing of the CTB and/or the change in the backcalculation procedure.

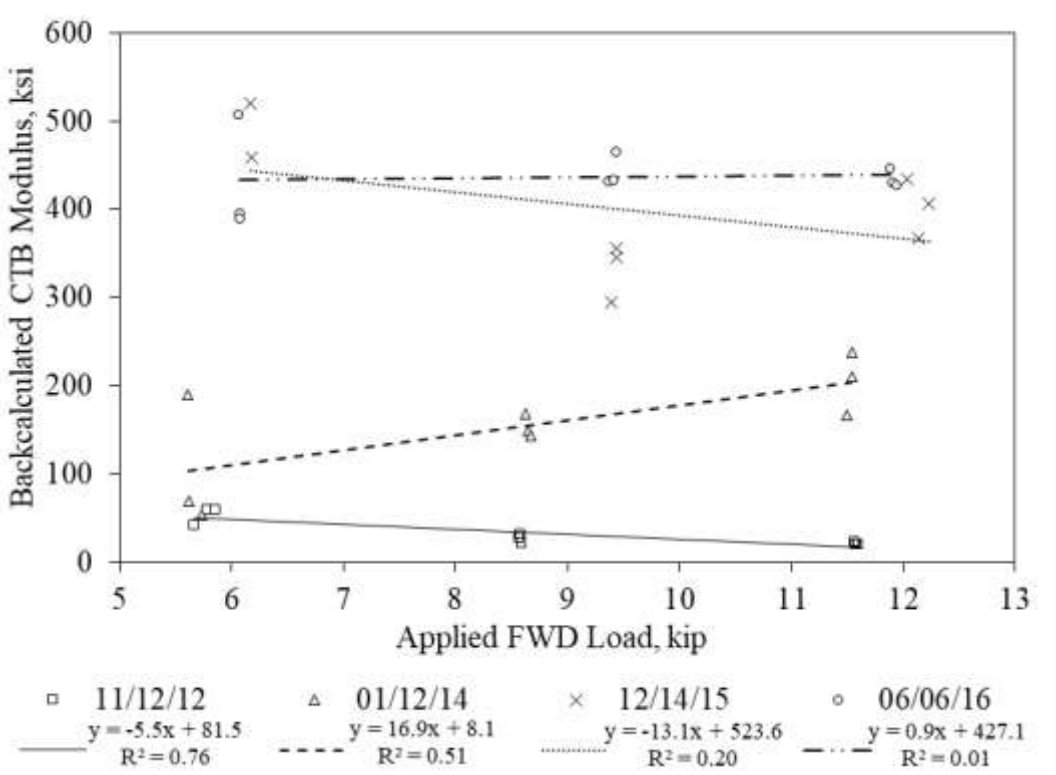

Figure 5.23 Effect of Load Level on the CTB

Based on these results, it was established that the CTB did not show a stress softening behavior as that observed previously for the granular base. In that way, the backcalculated modulus of the CTB was not affected by the applied load and seems to have remained relatively constant regardless of the load level used for FWD testing. It was postulated that the variability observed for the backcalculated CTB modulus in both research cycles may have been a result of this condition. Since the upper AC/CCPR layer was found to be temperature-dependent, its modulus consequently showed a relative cyclic seasonality over the two research cycles. However, the CTB, which showed to be independent from temperature and/or stress, maintained a constant modulus throughout the same period, thus generating erratic backcalculation results as observed for section S12.

When considering all the data obtained for all three load levels, the average backcalculated modulus and its standard deviation are nearly doubled between the 2012 and 2015 research cycles. For the 6,000 lbs load level, average backcalculated modulus (and corresponding standard deviation in parentheses) increase from 127.7 ksi (154.15 ksi) to 322.93 ksi. Similarly, an increase from 98.31 ksi (131.76 ksi) to 252.28 ksi (213.12 ksi) was observed for the 9,000 lbs load level, while an increase from 86.18 ksi (126.04 ksi) to 245.96 ksi (211.27 ksi) was observed for the 12,000 lbs load level. Statistical testing on these averages revealed that the results for the 9,000 lbs and 12,000 lbs load levels were similar at a 95% confidence level, while the results obtained for the 6,000 lbs load level were significantly greater. In fact, a pairwise comparison allowed grouping the 9,000 lbs and 12,000 lbs load levels within each individual research cycle, while the 6,000 lbs load level was assigned to an individual grouping in both cases. In that way, it was confirmed that using the 9,000 lbs load level as originally defined, produced sufficiently consistent results for the CTB and could be used for subsequent analyses. Figure 5.24 shows the effect of the load level on the backcalculated modulus for each research cycle, where markers with the same shape and color indicate the groupings obtained from a Tukey pairwise comparison at a 95% confidence level.

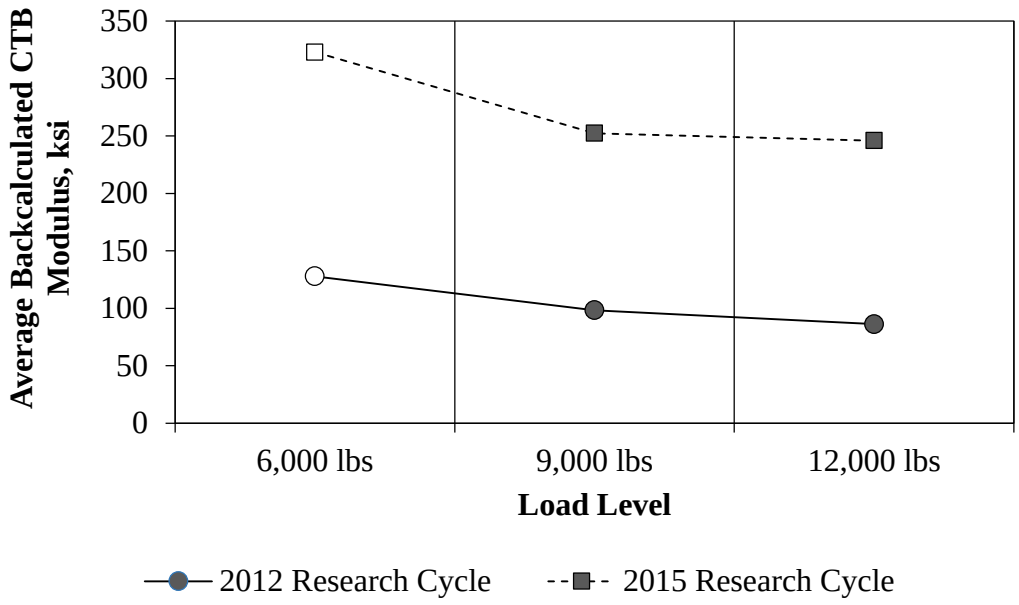

Figure 5.24 Main Effects Plot for Load Level

A subsequent analysis was performed considering only the 9,000 lbs load level, to study the effect of longitudinal random location on the backcalculated CTB modulus. Although it was difficult to identify substantial differences from a visual sensitivity analysis, the results showed relatively more scatter for random location 1 (RL1) than for any other random location. Statistical analysis on the average results obtained for each research cycle revealed that RL1 was statistically different from the other random locations at a 95% confidence level. This differences was observed for the 2012 research cycle, and was maintained for the 2015 research cycle, even with the significantly greater scatter identified previously. Figure 5.25 shows the effect of random location on the average backcalculated CTB modulus for both research cycles, where markers with the same shape and color indicate the groupings obtained from a Tukey pairwise comparison at a 95% confidence level.

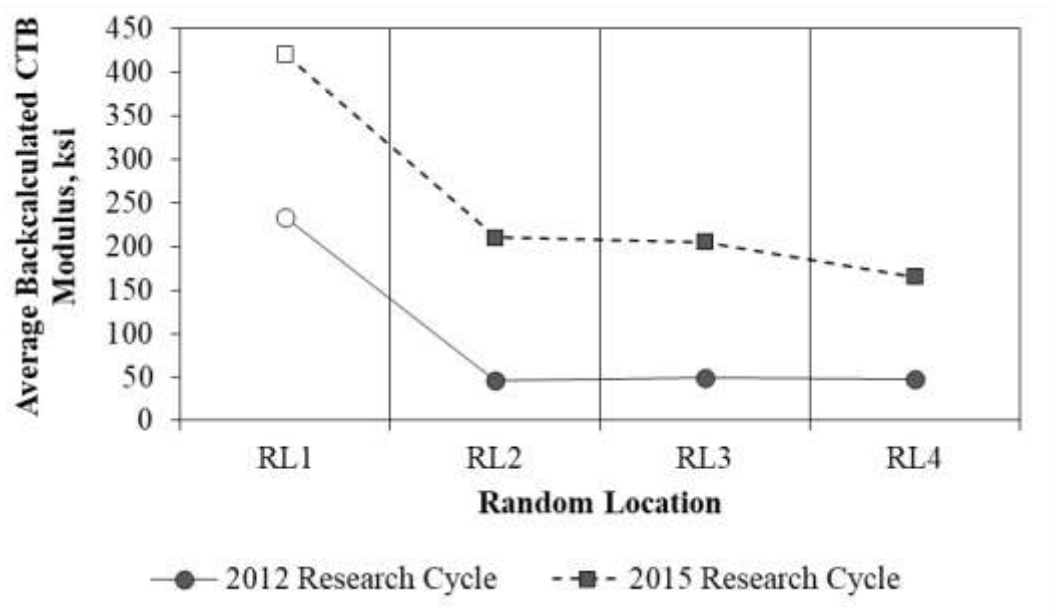

Figure 5.25 Main Effects Plot for Random Location

Besides the difference observed for RL1, the other three random locations showed very similar results, indicating that the modulus of the CTB is relatively homogeneous in the longitudinal direction. Furthermore, the backcalculated CTB modulus values obtained for RL4, located over the gauge array, are comparable to those obtained for the RL2 and RL3, indicating the properties of the CTB at the gauge array are similar to those of the entire test section. This is important because it corroborates that the installation of the strain gauges and pressure plates did not affect the integrity of the CTB layer.

A final analysis was performed to evaluate the effect of the wheel path on the backcalculated CTB modulus. Figure 5.26 shows the main effects plot for the three different transverse locations: (1) inside wheelpath or IWP, (2) outside wheelpath or OWP, and (3) between the wheelpaths or BWP. Markers with the same shape and color indicate the groupings obtained from a Tukey pairwise comparison at a 95% confidence level, while

different lines indicate the research cycle. Statistical analysis on the average results obtained for each research cycle, revealed that the three wheel paths are statistically different at a 95% confidence level when compared to the other wheel paths in the same research cycle. Interestingly, the average backcalculated modulus obtained for the IWP seemed to be statistically similar in both research cycles, and relatively lower than the other two wheel paths. .

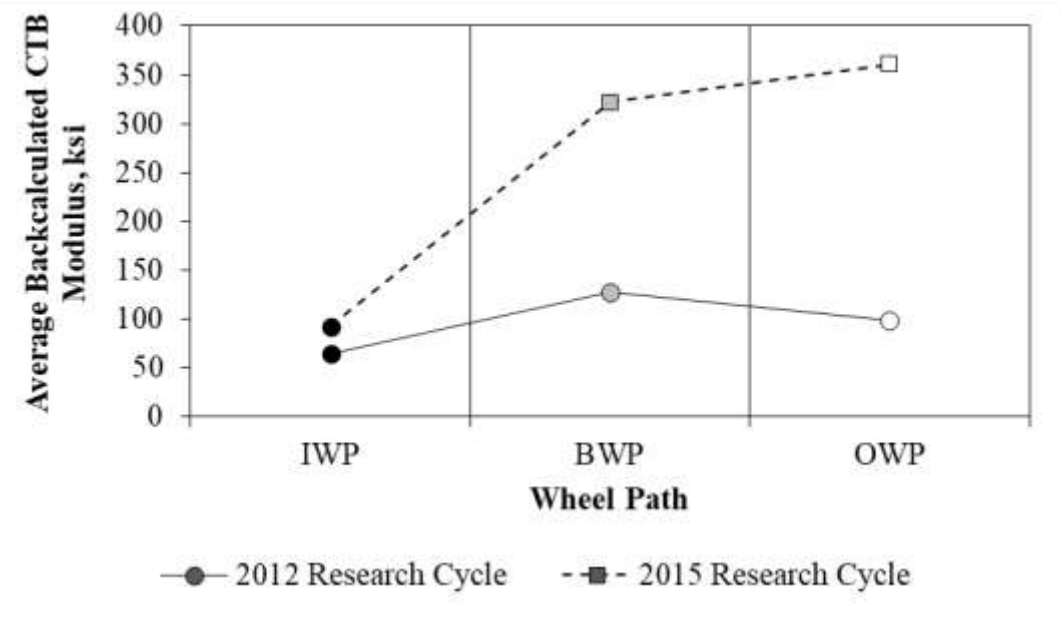

Figure 5.26 Main Effects Plot for Random Location

The analyses performed were insufficient to identify a clear and compelling effect of the wheel path and/or the random location on the backcalculated CTB modulus. In that way, the variability observed for the results could not be attributed to a specific location within the test section. And, since the CTB was found to be independent from the applied stresses, the variability observed for the backcalculated CTB modulus could not be

attributed to the effect of FWD loading. It was postulated that the erratic results observed for the CTB were a product of the backcalculation process, where the layer with relatively increased stiffness may have affected the backcalculation results. To verify this, layered elastic analysis was used to calculate the theoretical surface deflections obtained for the pavement structure in section S12, for a load similar to that applied by the FWD. For this, WESLEA for Windows was used to model a pavement structure consisting of three different layers: (1) a 9-inch AC/CCPR, (2) an 8-inch CTB, and (3) a Subgrade. The modulus values of the AC/CCPR layer and the subgrade were fixed at 400 ksi and 10 ksi, respectively, while the modulus of the CTB was varied between 0.05 and 3 times the modulus of the upper AC/CCPR layer. The load was simulated as a 9,000 lbs steer axle with a tire pressure of 82 psi, which would be equivalent to the 5.91-inch plate used for FWD testing. The results are shown in Figure 5.27, where multiple theoretical deflection basins were plotted for different modulus ratios. This modulus ratio was defined as the ratio between the CTB modulus and the AC/CCPR modulus (E_{CTB} / $E_{AC/CCPR}$). In that way, different deflection basins were calculated for modulus ratios of 0.05, 0.5, 1, 1.5, 2, and 3.

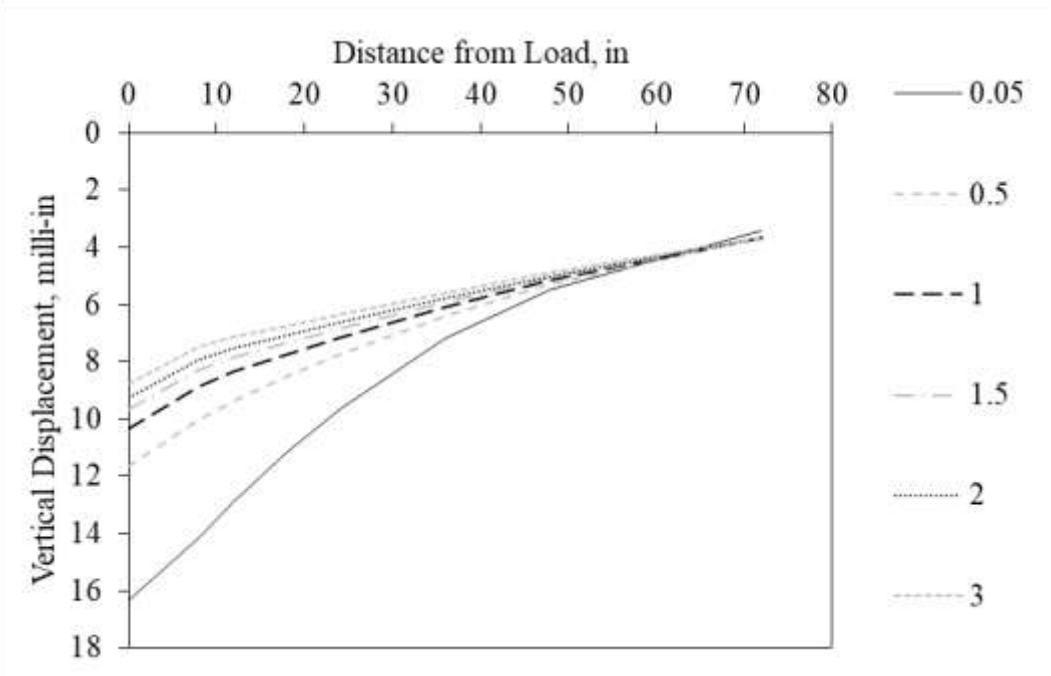

Figure 5.27 WESLEA Deflection Basin Simulations for Different CTB Modulus

Although the layered elastic model used is only a mere approximation of FWD testing and its results could not be directly compared with the results obtained from real FWD testing, the analysis was found sufficient to validate the cause of the backcalculated CTB modulus results. As expected, lower modulus ratios corresponded to larger vertical displacements. For a modulus ratio between 0.05 and 0.5, which would correspond to CTB modulus values closer to those of a granular base, the theoretical deflection basins were substantially different. However, for modulus ratios larger than 1, the theoretical deflection basins became very similar. In fact, the difference between the maximum deflection at the center of the load for modulus ratios of 1 and 3 was less than 2 milli-in. Figure 5.28 shows the how the effect of the modulus ratio on the theoretical vertical deflection for four different offsets from the applied load.

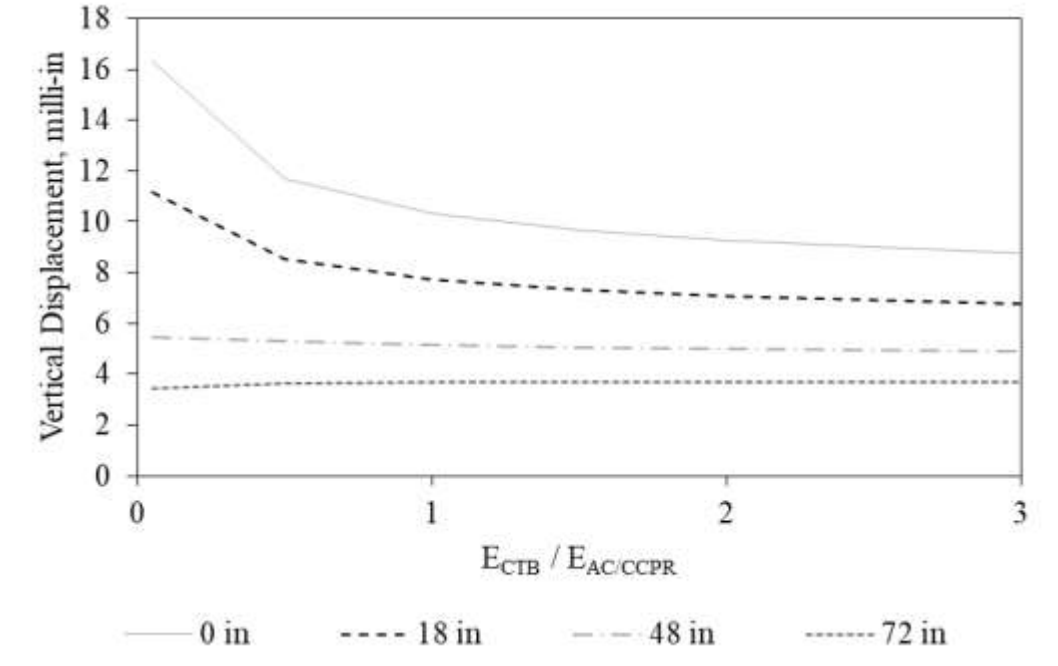

Figure 5.28 Vertical Deflection vs. CTB Modulus for Different Offsets

Figure 5.28 corroborates the observations made previously. The vertical displacements for higher modulus ratios, equal or larger than 1, seem to become very similar. A relatively large variation in the modulus ratio caused fairly similar deflections. In other words, for modulus ratios larger than 1, a relatively small variation in the vertical deflection would correspond to a significant increase in the modulus ratio. This would explain the relatively large scatter observed for the backcalculated CTB modulus. Since the backcalculation process is based on layered elastic theory, and the CTB was substantially stiffer than the AC/CCPR layer, a minor variation in the measured FWD deflection may have caused a large variation in the backcalculated modulus values. This would have caused considerably different backcalculated CTB modulus for adjacent FWD tests performed nearly at the same time. Furthermore, since the properties of the CTB made

it independent from temperature and loading, this difference in the backcalculated modulus would have remained constant throughout the duration of the study, which is consistent with the observations made previously. In that way, it may be inferred that the variability observed for the backcalculated CTB values for both research cycles was caused by the effect of the stiffer layer in the backcalculation process.

5.3.6 Structural Performance of the Subgrade

As mentioned before, the subgrade was considered as the third pavement layer for backcalculation purposes. As shown in Figure 5.29, the backcalculated subgrade modulus was not affected by pavement temperature, expressed by the relatively small slope of the exponential trendlines obtained for each test section. The figure shows a certain level of scatter, however this was found to be only a visual effect caused by the scale of the vertical axis in the plot. In fact, the backcalculated subgrade modulus values in the three test sections are fairly similar and seem to be contained in relatively narrow range between 20 ksi and 50 ksi. The evolution of the backcalculated subgrade modulus over time is presented in Figure 5.30.

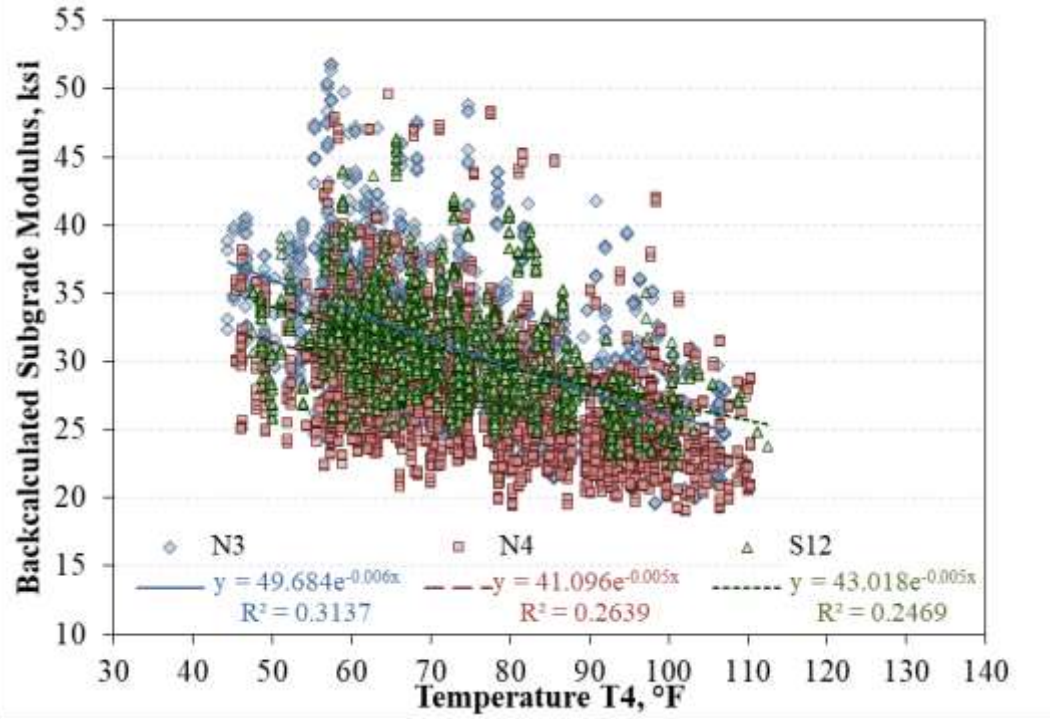

Figure 5.29 Effect of Temperature on Subgrade

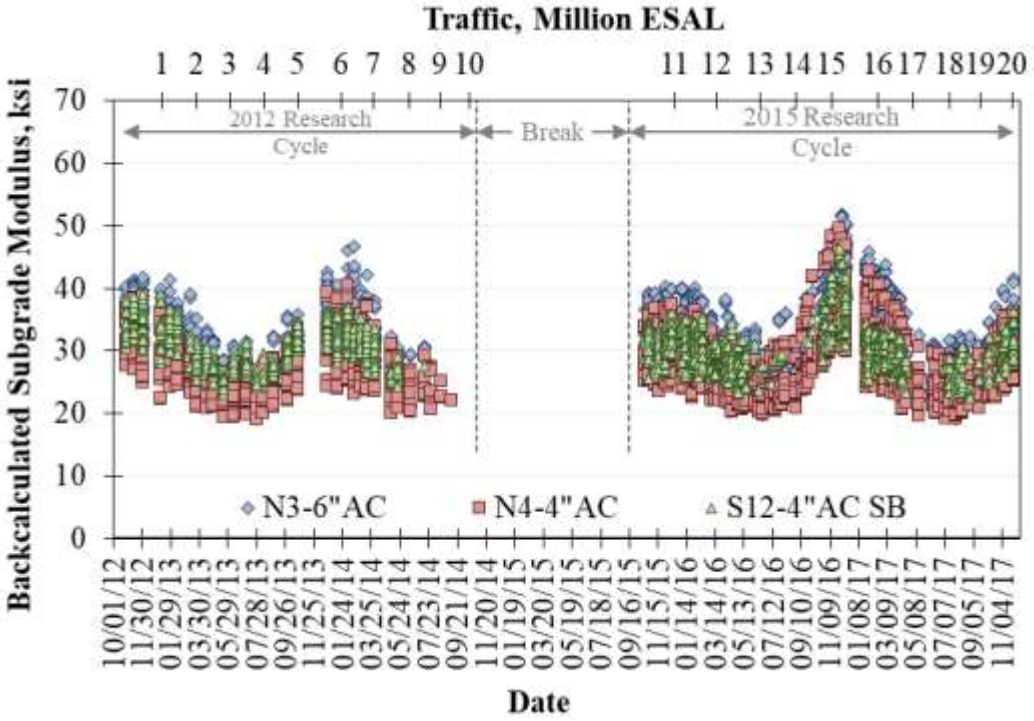

Figure 5.30 Backcalculated Subgrade Modulus vs. Date

The backcalculated subgrade modulus showed a relative seasonality for the three test sections. The subgrade was classified by Taylor and Timm (2009) as an A-4 soil. Therefore, it was expected that the subgrade would behave as a stress softening material, exhibiting a cyclic stiffness as that observed for the granular base in sections N3 and N4. However, for practical purposes of this dissertation, the seasonality shown by the backcalculated subgrade modulus may be neglected since the range of variation is relatively small. In fact, the average backcalculated subgrade modulus (and corresponding standard deviation in parentheses) were relatively similar for all three sections, with values of 31.6 ksi (5.6 ksi) for section N3, 27.8 ksi (4.9 ksi) for section N4, and 30.9 (3.7 ksi) for section S12. Even if the average backcalculated subgrade moduli are statistically different at a 95% confidence level, this difference was relatively small for practical purposes. A more detailed analysis of the subgrade at the Test Track was beyond the scope of this dissertation; however, an in-depth study was presented by Taylor and Timm (2009).

5.4 PAVEMENT RESPONSE

For each test section, the behavior of the pavement layers under traffic was documented through weekly measurements of the strains and stresses induced by traffic loads, at different depths within the pavement structure. As mentioned before, horizontal stresses and strains in the asphalt bound layers illustrate how the pavement structure copes with fatigue cracking, while vertical stresses and strains in the base and subgrade layers are representative of the rutting endurance of the pavement structure. In that way, longitudinal strains at the bottom of the CCPR layer were documented to describe the effect of loading

on the fatigue resistance of the pavement structure. Similarly, vertical stresses were documented to describe effect of loading on the structural rutting of the pavement structure.

5.4.1 Longitudinal Strain in Bound Layers

Figure 5.31 shows the tensile strain response at the bottom of the CCPR versus mid-depth pavement temperature. Given the negative exponential relationship between backcalculated modulus and temperature obtained for the three test sections, a strong correlation between the temperature and pavement response was also expected. Exponential regression equations and trendlines illustrate this correlation. An exponential model was chosen in accordance to previous research and common practices at the Test Track. As anticipated, the benefit of the additional 2 inches of AC in section N3 (6 in. AC) as compared to section N4 (4 in. AC) is clear across the temperature spectrum. At 68°F, section N3 had approximately 40% lower strain than section N4. Both N3 and N4 exhibited similar temperature sensitivity as demonstrated by the comparable exponential coefficients in their respective regression equations.

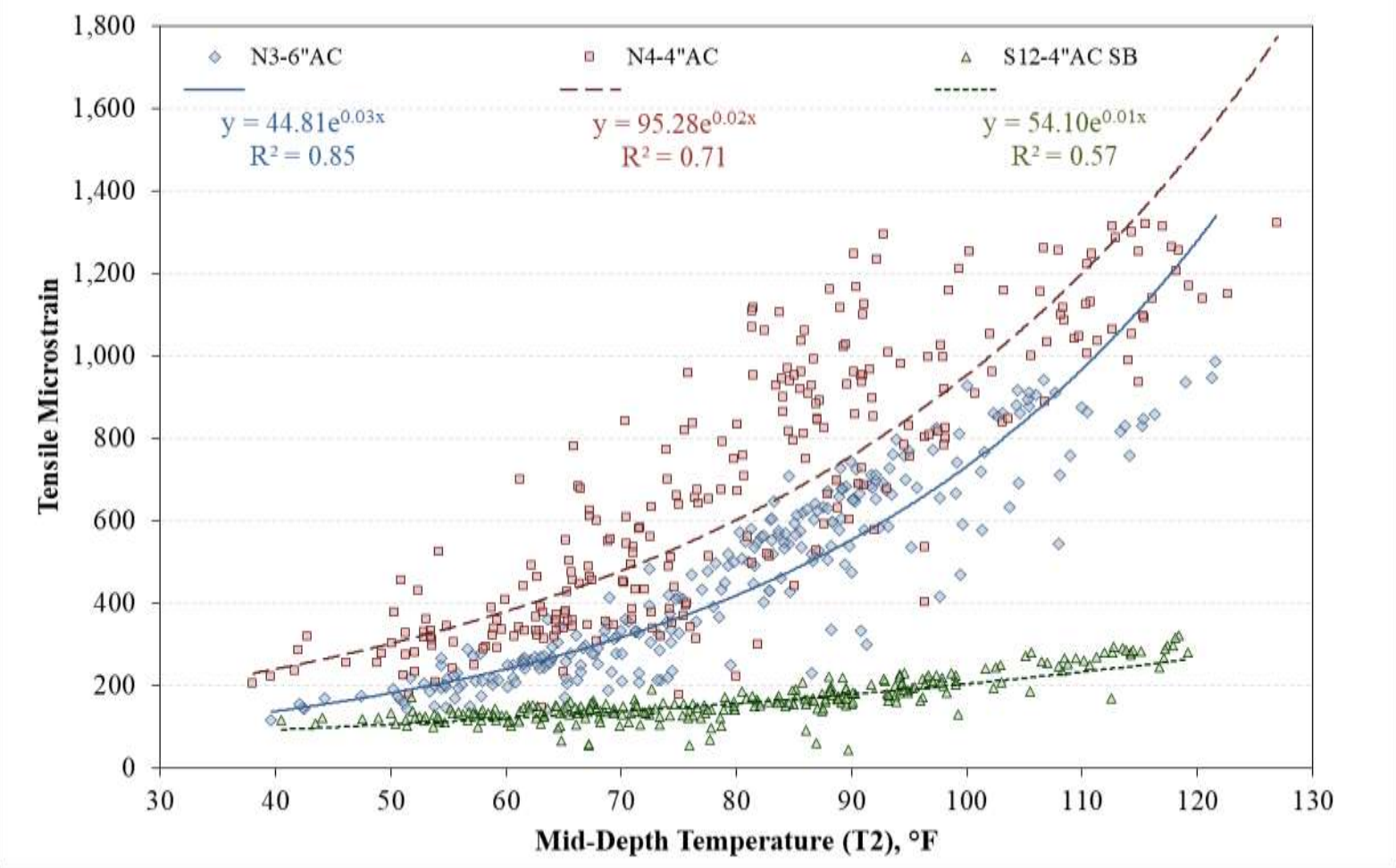

Figure 5.31 Tensile Microstrain vs. Mid-Depth Pavement Temperature

Section S12, on the other hand, presented a relatively different response when compared to the other two sections. The strain magnitude is significantly lower and the response seems to be considerably less temperature sensitive. As the tensile strain is a direct function of the underlying supporting material, and the CTB in section S12 is much stiffer than the granular base in sections N3 and N4, it is reasonable to assume that the stiffer CTB is limiting, to an extent, the tensile strain in the CCPR layer. This is consistent with the results obtained for the backcalculated modulus.

When analyzing the correlation between tensile microstrain at the bottom of the AC/CCPR layer and temperature, a clear difference was found between the two research cycles. Figure 5.32 shows the effect of temperature on the tensile microstrain response for each test section and for each research cycle at the Test Track. Regression models, including a categorical variable to define each research cycle, were created. The results for the interaction between the response and categorical variables revealed a statistical difference between the slopes in each research cycle. This indicates the magnitude and the temperature susceptibility of the tensile strains increased for the 2015 research cycle. From a pavement analysis perspective, this would suggest the capacity of the pavement structure to withstand fatigue cracking may be decreasing over time, in comparison to conventional AC pavements where fatigue cracking is attributed to multiple load repetitions that exceed the tensile strength of the AC material. In the case of the three test sections this seems to be true as the tensile strains measured for the 2015 research cycle are slightly higher. However, from a practical perspective, this relatively small increase seems insufficient to indicate with certainty that fatigue damage is occurring. In fact, the increase seems substantially low when considering the high level of traffic applied to the pavement.

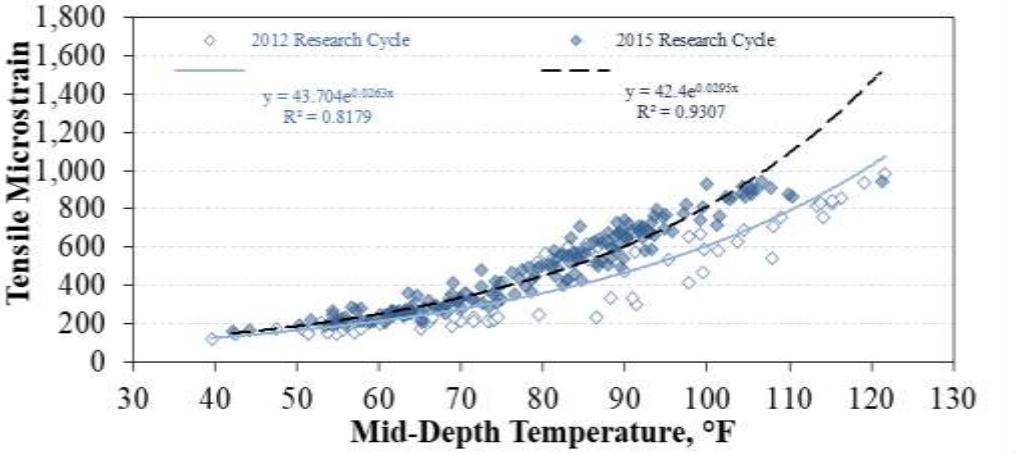

(a)

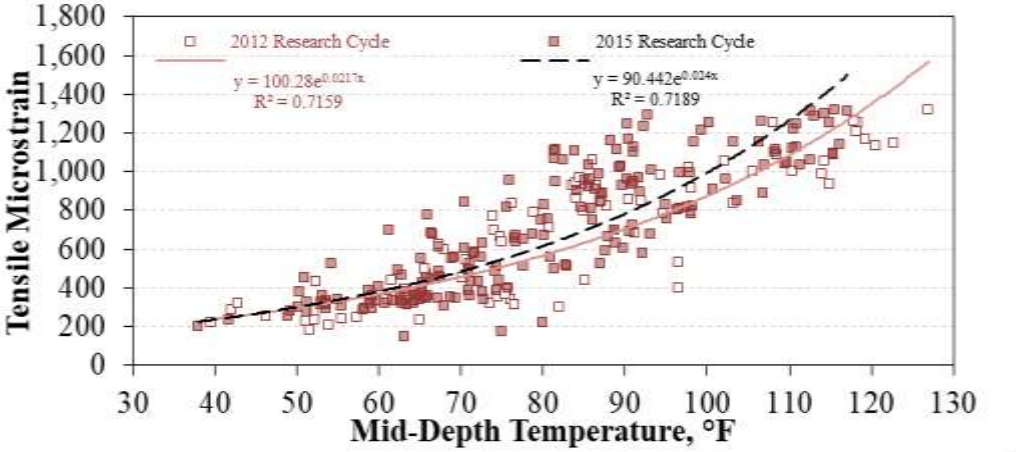

(b)

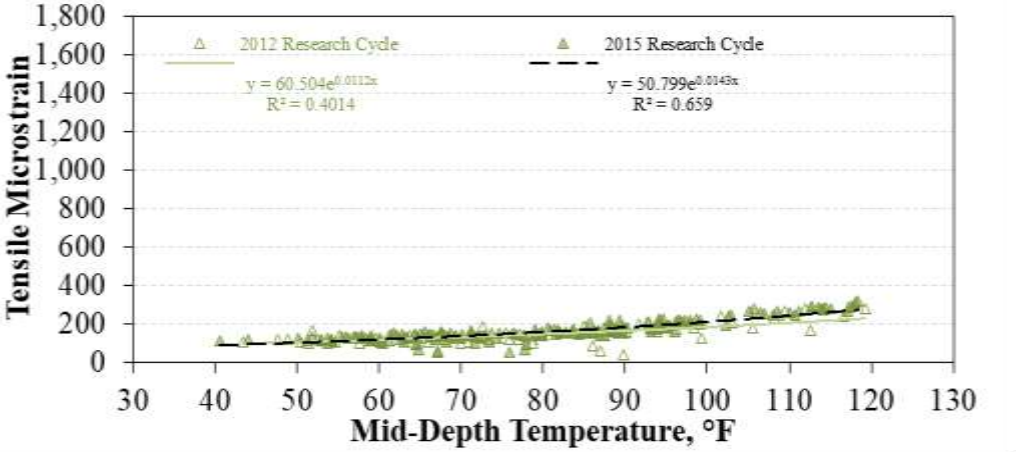

(c)

Figure 5.32 Tensile Microstrain vs. Mid-Depth Pavement Temperature for Test Sections (a) N3, (b) N4, and (c) S12

Although the change in the slope of the temperature-strain curve observed for section S12 was statistically significant, the variation in the tensile strain magnitude between the two research cycles is less than 10% than that observed for the other two test sections. In that way, the rate of change in tensile strains for section S12 was significantly lower than that observed for the other two test sections. It was postulated this may be attributed to the stiffer CTB layer, which may have limited the deformations in the pavement structure, thus reducing the strains. This effect would be consistent with the results obtained from backcalculation, and will be addressed in greater detail in the following.

To evaluate the evolution of tensile strains over time, a similar temperature normalization procedure as that performed for the backcalculated AC/CCPR modulus was performed and the tensile strains were normalized to a reference temperature of 68°F. As explained previously, the measured strains were expressed as a function of mid-depth pavement temperature for each test section, according to equation 5.4.

$$L_{AC/CCPR@T} = k_1 e^{k_2 T} \qquad \textbf{(Equation 5.4)}$$

Where: $L_{AC/CCPR@T} =$ Longitudinal strain at the test temperature (microstrain)

$T =$ Mid-Depth Temperature T2 (°F)

$k_1, k_2 =$ Regression coefficients for temperature T2

To objectively evaluate the evolution of the longitudinal strains over time, it was necessary to normalize the measured values to a reference temperature. A reference temperature of 68°F was selected, following the recommendations of the AASHTO 93 pavement design guide. Temperature-normalization was performed by mathematically dividing the longitudinal strain at the reference temperature ($L_{AC/CCPR@68°F}$) by the longitudinal strain at the measured temperature ($L_{AC/CCPR@T}$), using Equation 5.4. This ratio was then solved for the temperature-normalized modulus to obtain Equation 5.5, which was used to calculate a temperature-normalized longitudinal strain for each measured longitudinal strain. This constitutes a practical method to eliminate the effect of temperature for the analysis of longitudinal strains over time, describing the evolution of the structural capacity of the pavement structure over time with minimal influence of the climate and temperature conditions.

$$L_{AC/CCPR@68°F} = L_{AC/CCPR@T} \cdot e^{k_2(68°F-T)} \quad \textbf{(Equation 5.5)}$$

Where: $L_{AC/CCPR@68°F} =$ Temperature-normalized strain (microstrain)

$L_{AC/CCPR@T} =$ Measured strain at the test temperature (microstrain)

$T =$ Measured mid-depth pavement temperature T2 (°F)

$k_2 =$ Section specific regression coefficient

Figure 5.33 shows the tensile strains over time, including linear trendlines to illustrate the variation of the normalized strains over time. Sections N3 (6 in. AC) and N4 (4 in. AC) show an increase in normalized strain over time. The slope and relatively low R^2 corresponding to N3 indicate relatively little change in strain over time. The slope of N4 is greater and has a corresponding lower R^2 than N3, which may indicate some damage may be occurring in this section and has not yet been detected by FWD testing. The small slope and low R^2 corresponding to section S12 (4 in. AC and CTB) indicate no appreciable change over time and a healthy pavement structure.

Although the strains have been normalized to a reference temperature, temperature seasonality still seems to be affecting the results, especially for sections N3 and N4. In both cases, normalized strains are higher in the warmer months and slightly lower during the colder months. This cyclical behavior is consistent with the trends observed for the backcalculated AC/CCPR modulus, indicating the AC/CCPR layer is less stiff during the warmer months, inducing higher tensile strains. The effect in section S12 is less evident.

To better visualize the trends of the tensile strains for each test section, the temperature-normalized strains were considered as a time series which could be decomposed into two components: (1) the trend, and (2) the cycle. Time series decomposition is a statistical procedure commonly used to examine the nature of the seasonal component in a data series over time. This allowed to generate two plots for each test section: (1) a smooth representation of the trend with better sensitivity to long-term variations, and (2) the daily and seasonal fluctuations attributed to temperature variations. The trend component is presented in Figure 5.34 for all three test sections, while the cyclical component is shown in Figure 5.35 for each section individually.

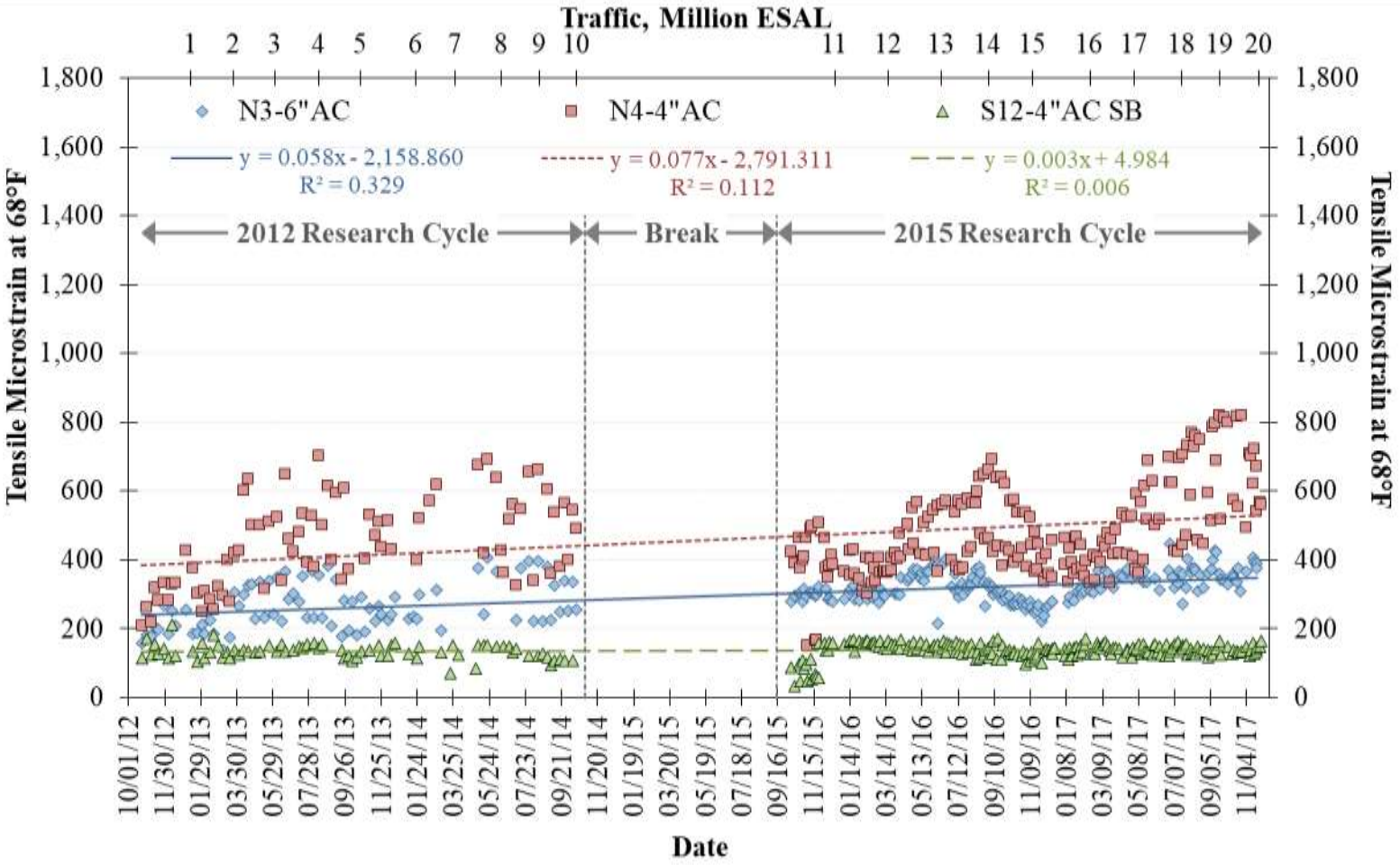

Figure 5.33 Temperature Normalized Tensile Microstrain over Time

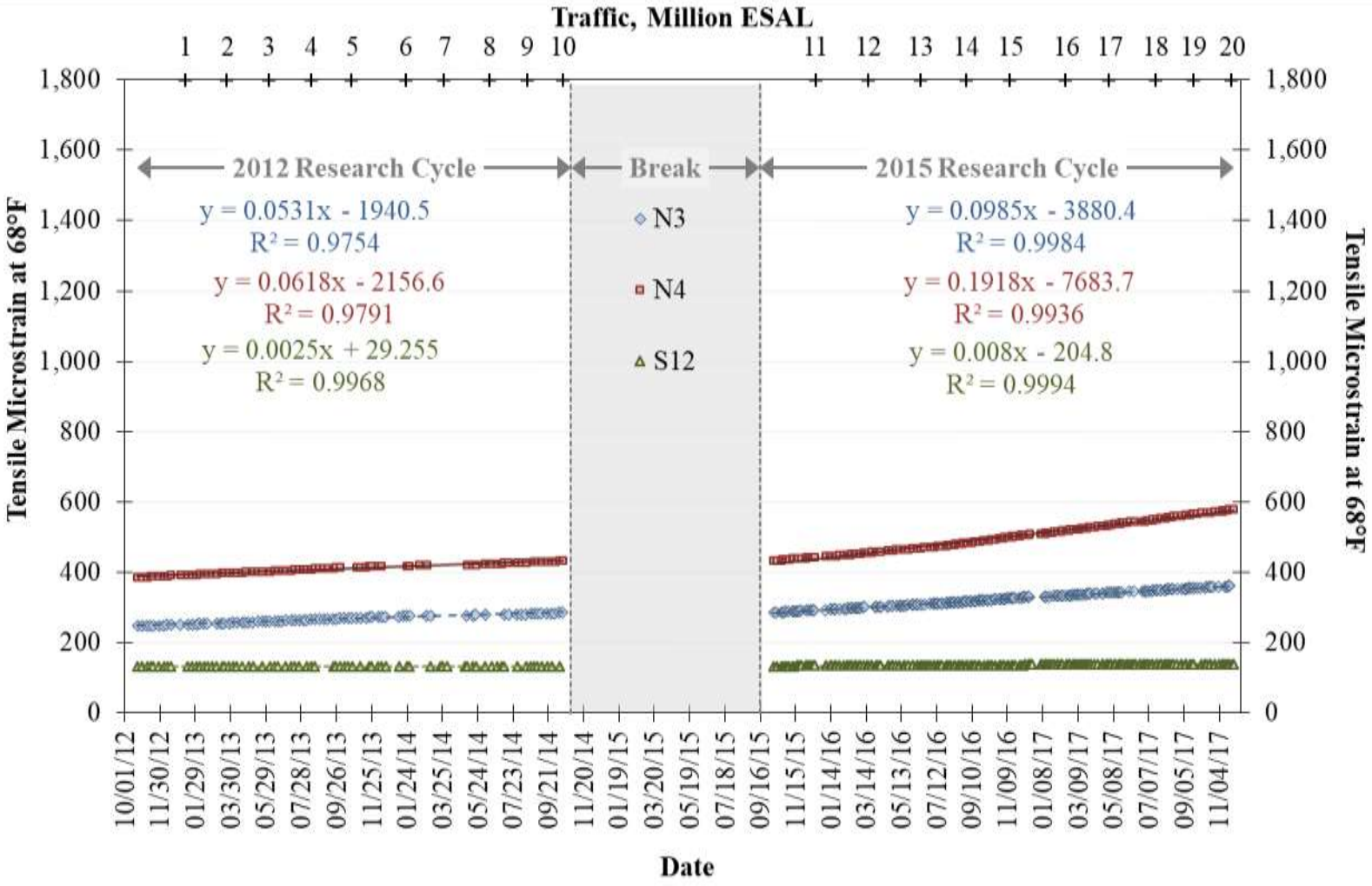

Figure 5.34 Tensile Strain Trend Component (from Time Series Decomposition)

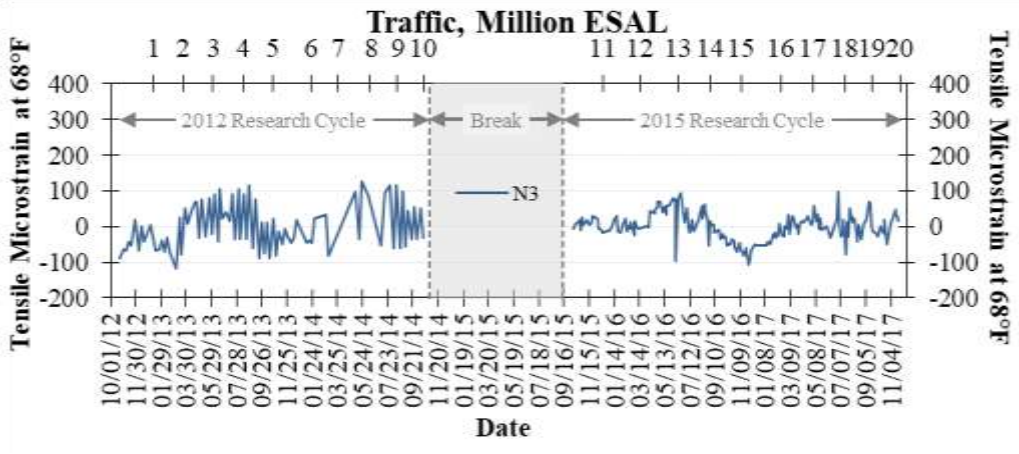

(a)

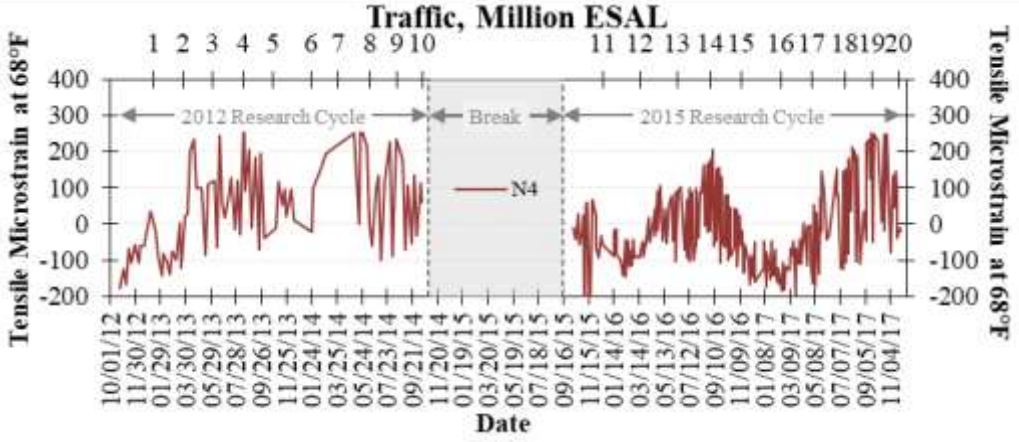

(b)

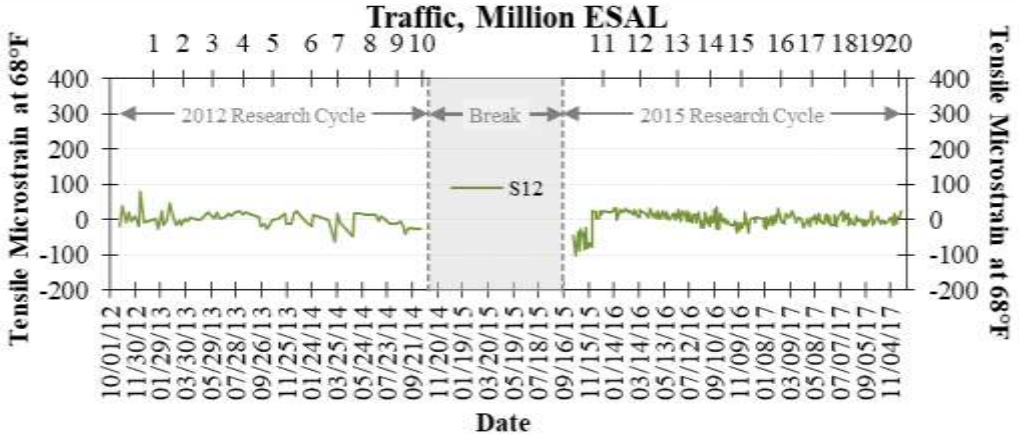

(c)

Figure 5.35 Tensile Strain Cyclical Component (from Time Series Decomposition) for Test Sections (a) N3, (b) N4, and (c) S12

Individual linear trend lines were plotted in Figure 5.34 for each test section and for each research cycle to illustrate the magnitude of the variation in tensile strain over time. In all cases, the obtained coefficients of determination were relatively high, indicating the equation of each linear trendline is sufficiently accurate in predicting the real trend observed in the figure. The slope of each equation represents an indicator of the evolution of strains in each test section. A positive slope indicates tensile strains are increasing over time. Section N4 shows the steepest slopes for both research cycles. In fact, the slope for section N4 increased considerably for the 2015 research cycle by a factor of over 200%, indicating the rate of tensile strain increase was accelerated after the first research cycle. When compared directly to section N3, the higher slopes and the significant increase in the rate of tensile strain increase observed for section N4, may be attributed to the 2-inch thickness differences between the two sections.

Section N3 shows a more moderate rate of tensile strain increase when compared to section N4. Even if the evolution of tensile strain over time, described by the slope of the linear trend lines, was similar for sections N3 and N4 during the 2012 research cycle, the rate of tensile strain increase in section N3 only increased 85% for the 2015 research cycle. This seems relatively low when compared to the 200% increase observed for section N4. In fact, for traffic levels below 10 million ESAL, the rate of strain increase in sections N3 and N4 was very similar. However, after 10 million ESAL, the rate of tensile strain increase changed for both test sections, showing a greater influence on section N4. Nonetheless, it is important to mention that both sections were performing well by the end the 2015 research cycle and none of them had exhibited any sign of damage after 20 million ESAL, indicating the pavement had an adequate structural integrity.

Section S12 stands out due to the lower slopes obtained for the linear trendlines in both research cycles. Even if the slope seems to increase nearly 200% for the 2015 research cycle, it still remains considerably lower than that obtained for the other two test sections (approximately $1/7^{th}$ of the value obtained for section N3). This indicates that the tensile strains at the bottom of the AC/CCPR layer in section S12 are not being affected by the application of over 20 million ESAL, and tensile strains remained relatively constant as traffic increased. From a pavement design perspective, this low variation in tensile strains at the bottom of the bound layers may be indicating that the induced strains on section S12 may be below the endurance limit of the AC/CCPR. Based on this it was postulated that section S12 may be showing characteristics consistent with perpetual pavements where tensile strains are usually low. However, the evolution of tensile strain, by itself, is insufficient to reach a robust conclusion at this stage and a more detailed analysis of this theory is presented in the following section of this dissertation.

The results described previously are consistent with the results obtained for the backcalculation. The stiffer CTB layer seems to affect the AC/CCPR layer by reducing the tensile strains in section S12. This is consistent with the elevated AC/CCPR modulus values obtained for this section. A stiffer pavement would be expected to have more limited deformation when the traffic load is applied, resulting in lower stresses and strains on each pavement layer. In the case of section S12, the stiff CTB layer may be acting as a large rigid slab that distributes stresses evenly in a greater area of influence, which in turn limits the bending of the pavement structure under loading, thus reducing the tensile strains on the upper layers.

By analyzing the cyclical component of the tensile strains, presented in Figure 5.35, two different sub-components were identified: (1) a broad seasonal sub-component, and (2) recurrent weekly fluctuations. On the one hand, the larger seasonal oscillations describe the effect of the warmer months on strains, validating the temperature susceptibility of the AC/CCPR layer, previously described for the backcalculated modulus and initially detected for the tensile strains. The recurrent weekly fluctuations, on the other hand, are consistent with the way measurements were taken during the research cycle. As mentioned before, strain measurements were performed on weekly basis, alternating measurements in the morning hours one week, and in the afternoon the next. The observed variability was caused by this slight temperature changes from morning to afternoon.

The cyclical component is significantly less evident for section S12. In fact, the seasonal sub-component is almost invisible and the fluctuations seem to be only related to the weekly fluctuations caused by the data collection process. This corroborates that the strains at the bottom of the AC/CCPR layer in section S12 are less susceptible to temperature, as mentioned previously. It may be inferred that, once again, the rigid CTB layer is affecting the stress distribution in the pavement structure. As described in previous sections of this dissertation, the CTB is not a temperature-dependent layer, and this may be translating to the more consistent strain results observed in Figure 5.35(c). In that way, the rigid CTB layer reduces the temperature susceptibility of the entire pavement structure, causing more consistent, and lower, strains regardless of the pavement temperature. This would also be consistent with the previous theory that section S12 may be behaving as a perpetual pavement.

5.4.2 Stress on Base and CTB

There is an evident correlation between the measured stresses and the mid-depth temperature (T2), as shown in Figure 5.34. As the loads are applied to the surface of the pavement, stresses are dissipated through the AC/CCPR layer. Therefore, the stress at the top of the base layer should be a direct function of the thickness of the AC/CCPR layer. In that way, it would be expected that sections N4 and S12, having comparable AC/CCPR thicknesses, would yield similar vertical stress measurements. Consequently, lower vertical stresses would have been expected for section N3, with two additional inches of AC. However, the results seem contradictory, with similar vertical base stresses for sections N3 and N4, and considerably lower stresses in section S12. Nonetheless, the vertical stresses in the three test sections showed a strong and very similar correlation to temperature, as expressed by the similar slopes observed for the three test sections in Figure 5.36.

A statistical comparison was performed between the equations obtained in Figure 5.34 for test sections N3 and N4. The slopes and y-intercepts in the equations were found statistically different, at a 95% confidence level. The results indicated the vertical base pressure for section N4 was slightly greater than that measured in section N3. However, the vertical base pressure in section N3 showed more susceptibility to mid-depth pavement temperature than that observed for section N4. These results seemed more reasonable, since the greater AC thickness in section N3, would have reduced the vertical stresses in the subgrade by absorbing a larger portion of the stresses induced to the underlying layers. Simultaneously, due to this increased AC thickness, a larger portion of the AC/CCPR layer consisted of a much more temperature-dependent material, which in turn would have attributed more temperature-susceptibility to the AC/CCPR layer.

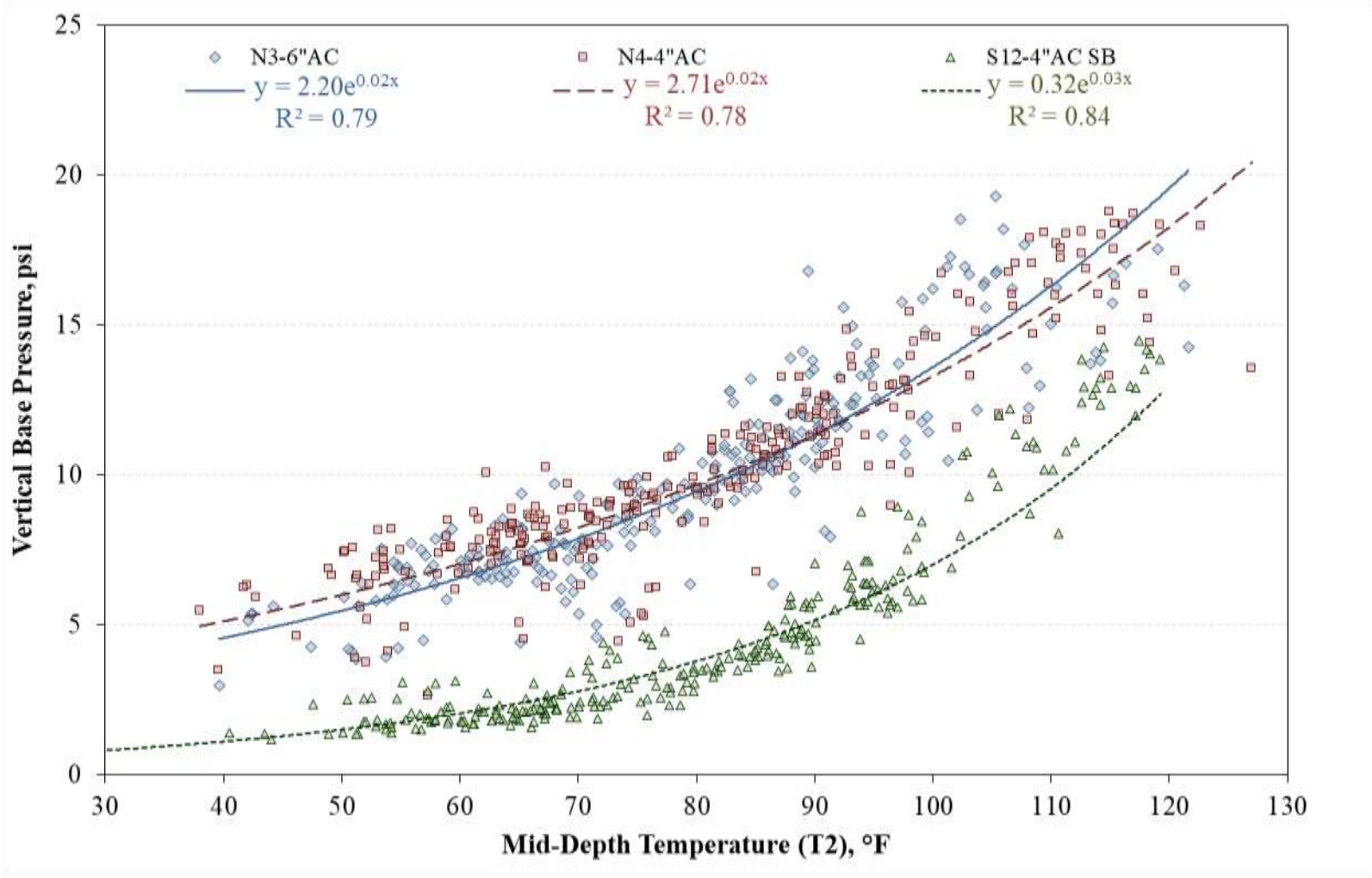

Figure 5.36 Effect of Pavement Temperature on Measured Stress at the Top of the Base Layer

The base pressures were normalized to a reference temperature of 68°F, following a similar procedure as the one described previously. For this case, the measured stresses were expressed as a function of mid-depth pavement temperature for each test section, according to equation 5.6.

$$\sigma_{Base@T} = k_1 e^{k_2 T} \quad \textbf{(Equation 5.6)}$$

Where: $\sigma_{Base@T} =$ Vertical stress at the test temperature (psi)

$T =$ Mid-Depth Temperature T2 (°F)

$k_1, k_2 =$ Regression coefficients for temperature T2

To objectively evaluate the evolution of vertical stresses over time, it was necessary to normalize the measured values to a reference temperature. A reference temperature of 68°F was selected, following the recommendations of the AASHTO 93 pavement design guide. Temperature-normalization was performed by mathematically dividing the vertical stress at the reference temperature ($\sigma_{Base@68°F}$) by the vertical stress at the measured temperature ($\sigma_{Base@T}$), using Equation 5.6. This ratio was then solved for the temperature-normalized modulus to obtain Equation 5.7, which was used to calculate a temperature-normalized vertical stress for each measured vertical stress. This constitutes a practical method to eliminate the effect of temperature for the analysis of vertical stresses over time, describing its evolution over time with minimal influence of the climate and temperature conditions.

$$\sigma_{Base@68°F} = \sigma_{Base@T} \cdot e^{k_2(68°F-T)}$$ **(Equation 5.7)**

Where: $\sigma_{Base@68°F} =$ Temperature-normalized vertical stress (psi)

$\sigma_{Base@T} =$ Measured vertical stress at the test temperature (psi)

$T =$ Measured mid-depth pavement temperature T2 (°F)

$k_2 =$ Section specific regression coefficient

The temperature-normalized vertical stresses over time are presented in Figure 5.37. Individual linear trendlines were generated for each test section and for each research cycle, and the corresponding equations and R^2 are presented next to the reference test section marker and in its corresponding research cycle. The temperature-normalized stresses in section N3 and N4 seemed to increase over the two research cycles, while those obtained for section S12 remained relatively constant. Additionally, some level of cyclic seasonality was also observed for sections N3 and N4, but it was attributed to the scale of the plot since the observed variability is small in magnitude. The relatively steeper slopes observed for the 2012 research cycle seem to flatten for the 2015 research cycle. It was postulated that the steeper slopes observed for the 2012 research cycle may be attributed to the densification of the AC/CCPR layer with traffic, which could cause increased stresses while the materials rearrange, until achieving a more compressed (and stable) state after approximately 10 million ESAL, when the stresses achieve a constant state. Conversely, the vertical stresses for section S12 seem to reduce during the first research cycle and tend to stabilize for the 2015 research cycle. These effects are studied in the following paragraphs.

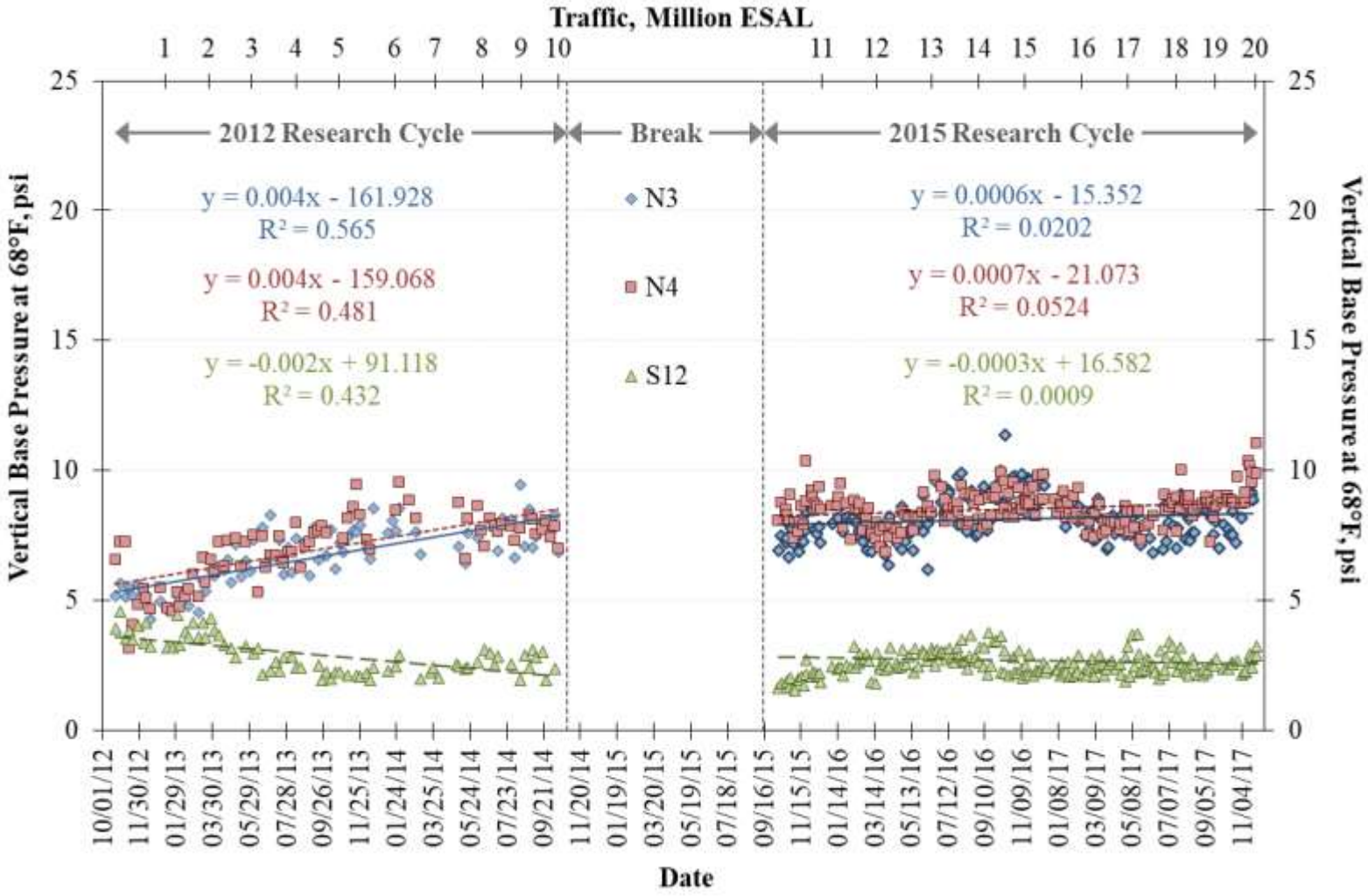

Figure 5.37 Evolution of Stresses at the Top of the Base Layer over Time

Even if the measured vertical stresses for sections N3 and N4 are statistically different, from a practical perspective the results seemed very similar. Using WESLEA for Windows, layered elastic analysis was conducted to study this effect, modeling each test section in three different layers: (1) a 6-inch (N3) or 4-inch (N4) AC/CCPR, (2) a 6-inch granular base, and (3) a Subgrade. The modulus of the AC/CCPR, granular base, and the subgrade were fixed at 400 ksi, 9 ksi and 8 ksi, respectively, based on the findings from the previous sections in this dissertation. The load was simulated as a single axle with a load magnitude of 5,000 lbs and a tire pressure of 100 psi to emulate the traffic loading at the test track. The resulting vertical stresses on top of the base were 9.25 psi and 16.36 psi for sections N3 and N4, respectively. In that way, layered elastic analysis indicated that the stresses in section N4 should have been 1.77 times greater than in section N3. However, the difference observed in the previous figure is substantially smaller. These results seem to indicate that the sensitivity and precision of the pressure measurement, apparently, were not sufficient to capture the expected reduction in base pressure from the additional 2-inch AC thickness in section N3.

The measured base pressure for section S12 was significantly lower than that observed for the other two test sections. Theoretically, the results obtained for section S12 should have been similar to those obtained for section N4 since both sections had an AC/CCPR layer of similar thickness above the pressure plate, where measurements were taken. Once again, layered elastic analysis with WESLEA for Windows was used to understand these results, based on the same concept of the modulus ratio described previously. In this case, the pavement model consisted of three different layers: (1) a 9-inch AC/CCPR, (2) an 8-inch CTB, and (3) a Subgrade. The modulus values of the

AC/CCPR layer and the subgrade were fixed at 400 ksi and 10 ksi, respectively, while the modulus of the CTB was varied between 0.05 and 3 times the modulus of the upper AC/CCPR layer. The load was simulated as a 5,000 lbs tandem axle with a tire pressure of 100 psi to emulate the traffic loading at the test track. The vertical stresses and displacements on top of the CTB were calculated at 2-inch intervals from underneath the applied load to a distance of 30 in. in the direction of traffic. Figure 5.38 shows the theoretical vertical stresses and displacements obtained with the model for six different modulus ratios. As stated previously, this modulus ratio was defined as the ratio between the CTB modulus and the AC/CCPR modulus (E_{CTB} / $E_{AC/CCPR}$), and the figure shows the results obtained for modulus ratios of 0.05, 0.5, 1, 1.5, 2, and 3.

As expected, vertical stresses and displacements tend to decrease as the distance from the load increases, indicating the effect of the load has less impact further away from the load. However, the simulations showed that if the modulus ratio increases, the vertical stresses tend to increase while the vertical displacements tend to decrease. This results seem consistent since a stiffer CTB layer would limit the deflections at the interface of the AC/CCPR layer and the CTB and, since the load level is maintained, the stresses would increase as the AC/CCPR layer would be obligated to absorb the same load with less allowable deformation. However, the results obtained for the pressure measurements seem contradictory as the CTB layer is showing lower pressure results than the less stiff granular base. Initially, these results raised concerns about the validity of the measured base stresses and the functionality of the pressure plates was questioned. However, a detailed analysis of the base and subgrade stresses, and the data acquisition and processing, revealed that the obtained results were valid and consistent.

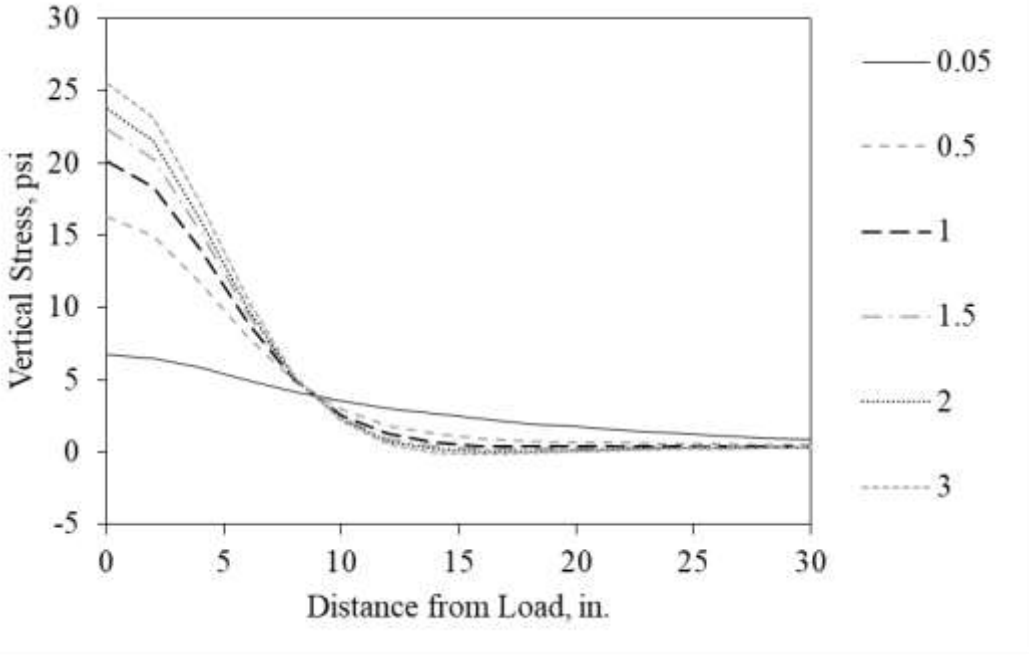

(a)

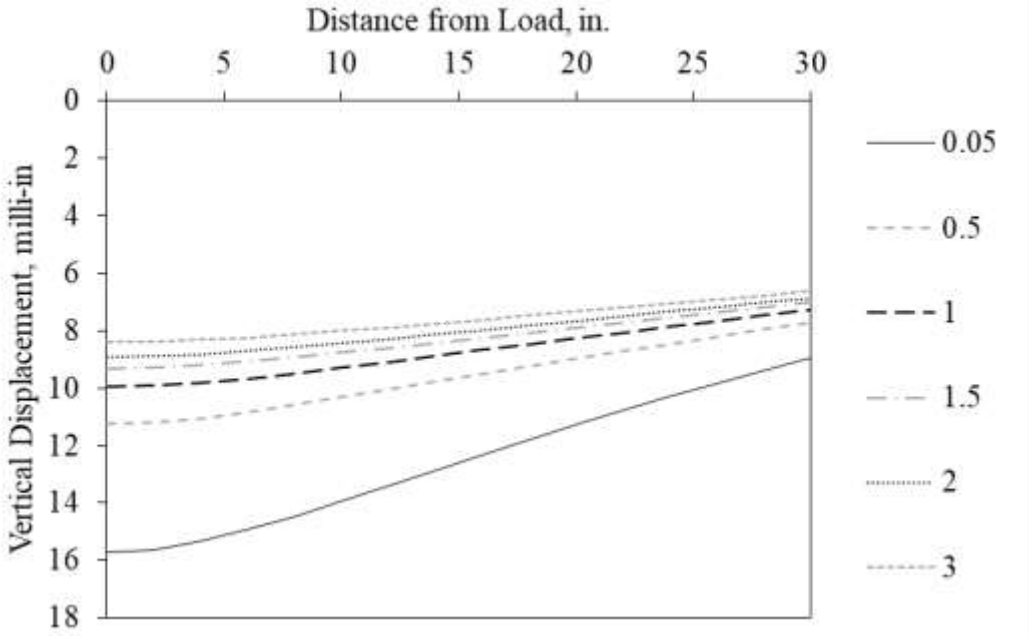

(b)

Figure 5.38 Vertical (a) Stresses and (b) Displacements from LEA

Figure 5.39 shows a direct comparison between the measured vertical pressures on top of the CTB and on top of the subgrade for section S12 on the 2015 research cycle. Although the results for the measured vertical pressures on top of the subgrade will be formally presented in the following sub-section of this dissertation, they were considered here to expand on the current analysis. Only the 2015 research cycle was included since previous observations showed that the data for this second research cycle were more consistent and had lower variability. As expected, the vertical base pressure showed more temperature susceptibility than the subgrade pressures, as explained by the steeper slope observed in Figure 5.39(a) and the more evident seasonality in Figure 5.39(b).

Figure 5.39(c) shows the temperature-normalized base and subgrade vertical pressures, obtained by means of the same temperature-normalization procedure described previously, are very similar and the trends seem to overlap over the 2015 research cycle. Statistical testing (t-test) revealed that the average temperature-normalized base and subgrade vertical pressures are statistically the same at a 95% confidence level. These are conflicting results since they seem to indicate that the 9-inch CTB had no effect in reducing the vertical pressures in section S12. However, the exponential trendlines in Figure 5.39(a) seem to intersect at a temperature near the reference normalization temperature of 68°F, indicating that for pavement temperatures higher than this reference temperature, the measured vertical pressure was higher on the base than on the subgrade, while the results were very similar for temperatures lower than this reference. In that way, if a different reference temperature would have been selected for the normalization process, the results for the vertical base pressure would have been greater.

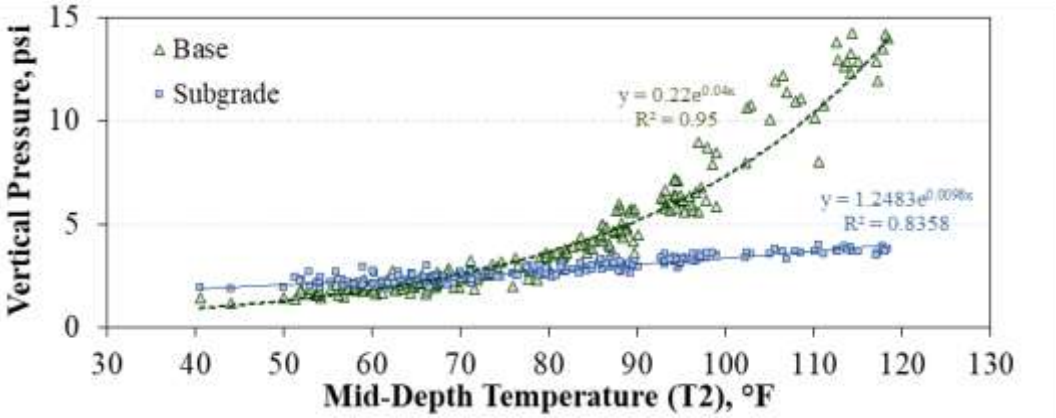

(a)

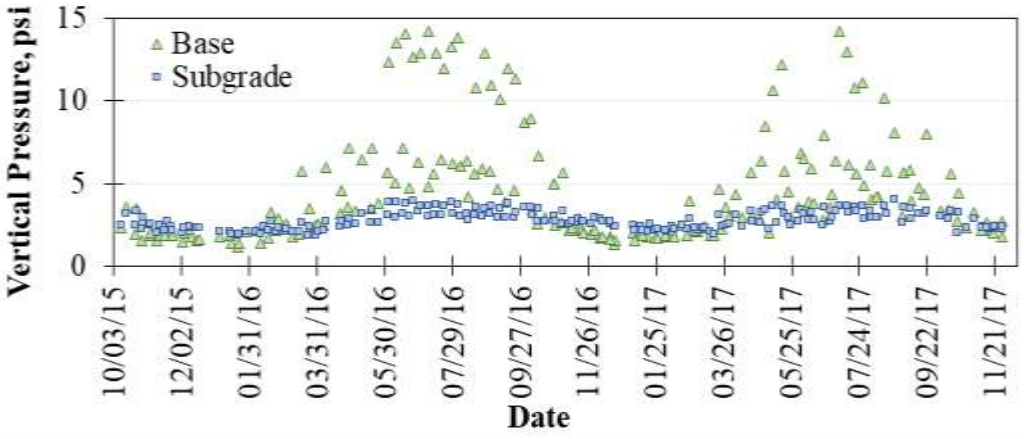

(b)

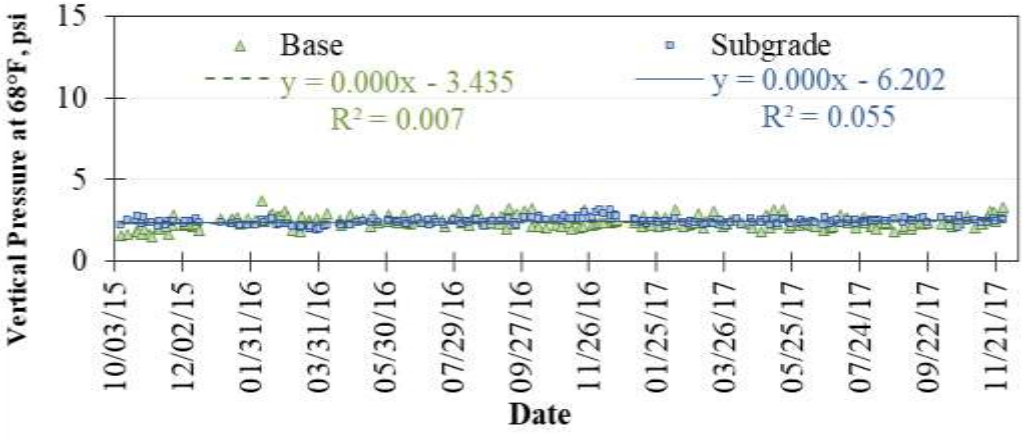

(c)

Figure 5.39 Effect of (a) Temperature, and Date on (b) Measured and (c) Normalized Vertical Pressures for Section S12

Even if the temperature-normalized base and subgrade pressures were slightly unusual, the similarities found between the both measurements were attributed to the effect of pavement temperature on the AC/CCPR and the marginal effect of pavement temperature and/or applied stress on the CTB. However, the results obtained for the pressure measurements in section S12 seem contradictory when compared with section N4. The layered elastic modelling performed previously showed that section S12, with a stiffer CTB as the second layer and a correspondingly higher modulus ratio, should have presented higher vertical stresses than section N4, which contained a lower modulus ratio. It was postulated that this conflicting results were caused by the way the pressure measurement itself is performed.

The pressure plates used at the Test Track measure the fluid displacement caused by the deformation between two parallel circular plates. This absolute deformation is transformed into a voltage reading which was then correlated to an applied pressure over the area of the plate. In that way, when the pressure plate is placed horizontally over the base or CTB layer, it provides an indirect measurement of the applied stress based on the effective vertical displacement over the area of the circular plate. To corroborate this effect, layered elastic theory was used to create an independent layered elastic model for sections N4 and S12. The pavement structure was idealized as a three layer pavements consisting of three layers: (1) AC/CCPR, (2) granular base (N4) or CTB (S12), and (3) Test Track subgrade. To recreate the pavement conditions at the location of the pressure measurement, the model considered realistic pavement conditions including the specific layer thicknesses measured over the gauge array, and the average temperature-normalized backcalculated modulus values obtained for the 2015 research cycle for each layer.

The model generated for section N4 consisted in an 8.17-inch AC/CCPR layer with a modulus of 400,560 psi, a 6.41-inch granular base with a modulus of 11,150 psi, and a modulus of 28,301 psi was assigned to the subgrade. Analogously, the model generated for section S12 consisted in an 8.74-inch AC/CCPR layer with a modulus of 914,420 psi, a 7.81-inch CTB with a modulus of 281,758 psi, and a modulus of 30,727 psi was assigned to the subgrade. The load was simulated as a 5,000 lbs single axle with a tire pressure of 100 psi to emulate the traffic loading at the test track. A graphical representation of the models is presented in Figure 5.40. The obtained vertical stresses on top of the CTB were 8.76 psi for section N4 and 14.62 psi for section S12. These theoretical results seem to oppose the measured vertical stress measurements, which revealed significantly lower stresses for section S12. However, a subsequent analysis was performed by modeling the pressure plate as an individual layer with a thickness of 0.1 in. and the same properties as the granular base or the CTB. Vertical displacements were measured at the top and at the bottom of this "pressure plate layer" so that the final difference between these displacements would indicate the final thickness of the pressure plate in its compressed state. In that way, for section N4 the vertical displacements were 5.83 milli-in and 5.79 milli-in. for the top and bottom measurements, respectively; which in turn indicated that the final thickness of the "pressure plate layer" was 0.06 milli-in. Meanwhile, the vertical displacements for section S12 were 3.42 milli-in and 3.41 milli-in, for the top and bottom measurements, respectively; which corresponded to a final thickness of the "pressure plate layer" of 0.09 milli-in. Therefore, the absolute deformation of the pressure plate layer for section N4 was 0.04 milli-in, while only 0.01 milli-in were calculated for section S12.

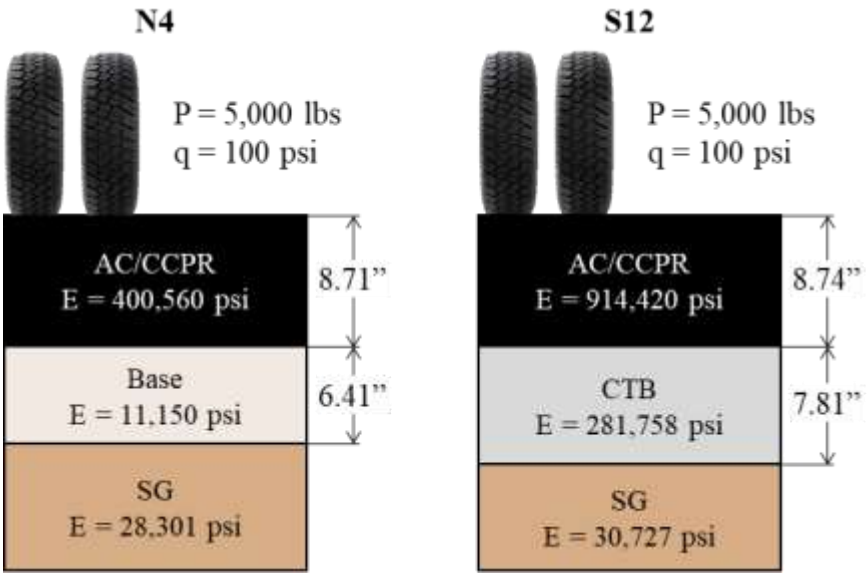

Figure 5.40 Layered Elastic Models of N4 and S12 used in the Analysis

These results would corroborate the theory presented previously, attributing the inconsistent results to the way the pressure measurement was performed within the pressure plate. When the load was applied, the pressure plate detected the relative vertical displacement of the two parallel plates on top of the base layer. For section S12 this displacement would have been relatively lower because of the stiffer underlying CTB layer, the pressures reported would have been reduced. In that way, the measured pressures on top of the CTB may not be an actual representation of the real stress condition at that location, since the increased stiffness of the underlying layer may have created lower vertical relative displacements which in turn led to the significantly lower vertical pressure measurements obtained for section S12. This effect would also explain the relatively similar vertical pressure obtained for the base and the subgrade for section S12.

Despite this unique outcome, the vertical stresses for section S12 seem to have reduced during the 2012 research cycle until they tended to level off after 10 million ESAL. This was consistent with previous observations made for the backcalculated modulus. It was postulated that the slight reduction in base pressure observed may have been caused by of some sort of stiffening over time of the CTB, consistent with the curing process of the portland cement. As cement materials hydrated during the first two years and the CTB became more rigid, and the measured vertical displacements (and therefore the reported vertical stresses) tended to reduce gradually. However, once the hydration process reached a certain threshold nearly two years after construction, the CTB would also have reached its peak stiffness. Beyond that point, the CTB would have stopped to become more rigid, explaining the opposing, more natural trend with a relatively constant slope observed for the 2015 research cycle.

5.4.3 Stress on Subgrade

The subgrade pressure measurements more clearly show the differences between the test sections. Figure 5.41 show subgrade pressure measurements versus temperature. Sections N3 and N4 are slightly more distinguishable and follow similar trends with respect to temperature, though N3 has much greater scatter, explained by its corresponding lower R^2. As described previously, based on the interaction of the response and categorical variables in a simple regression analysis it was determined that the slopes and y-intercepts of the regression equations for sections N3 and N4 are statistically different at a 95% confidence level. The subgrade pressure in section S12 is significantly lower and less responsive to temperature than the other two test sections.

The temperature-normalized subgrade pressure measurements are plotted in Figure 5.42. Section N4 shows very little change in pressure over time with no evident trend that may indicate the state of the base or the subgrade may have been affected by the application of traffic loads. Section N3 on the contrary, shows a peculiar behavior with very erratic data for the 2012 research cycle, which seems to become more consistent during the 2015 research cycle. In fact, for the 2015 research cycle, the temperature-normalized subgrade stresses for sections N3 and N4 seem to overlap, without any evidence of possible damage in the subgrade. These results seem more consistent with the results observed for the base pressures, indicating that the apparent sensitivity and precision of the pressure measurement was not sufficient to capture the expected reduction in base pressure from the additional AC thickness in section N3. It was postulated that some measurement errors or problems during data acquisition may have occurred during the 2012 research cycle.

Section S12 shows a decreasing trend, reflecting the curing process of the CTB and a certain stiffening over time during the 2012 research cycle. The trend seems to level off for the 2015 research cycle, which in turn would be consistent with the curing and stiffening process of the CTB described previously. In any case, the considerably low stress values observed for section S12, especially at the end of the first research cycle and during the second research cycle, seem to contribute to the theory that section S12 may be behaving as a perpetual pavement. Lower vertical displacements on top of the subgrade indicate the test section has an adequate resistance to structural rutting.

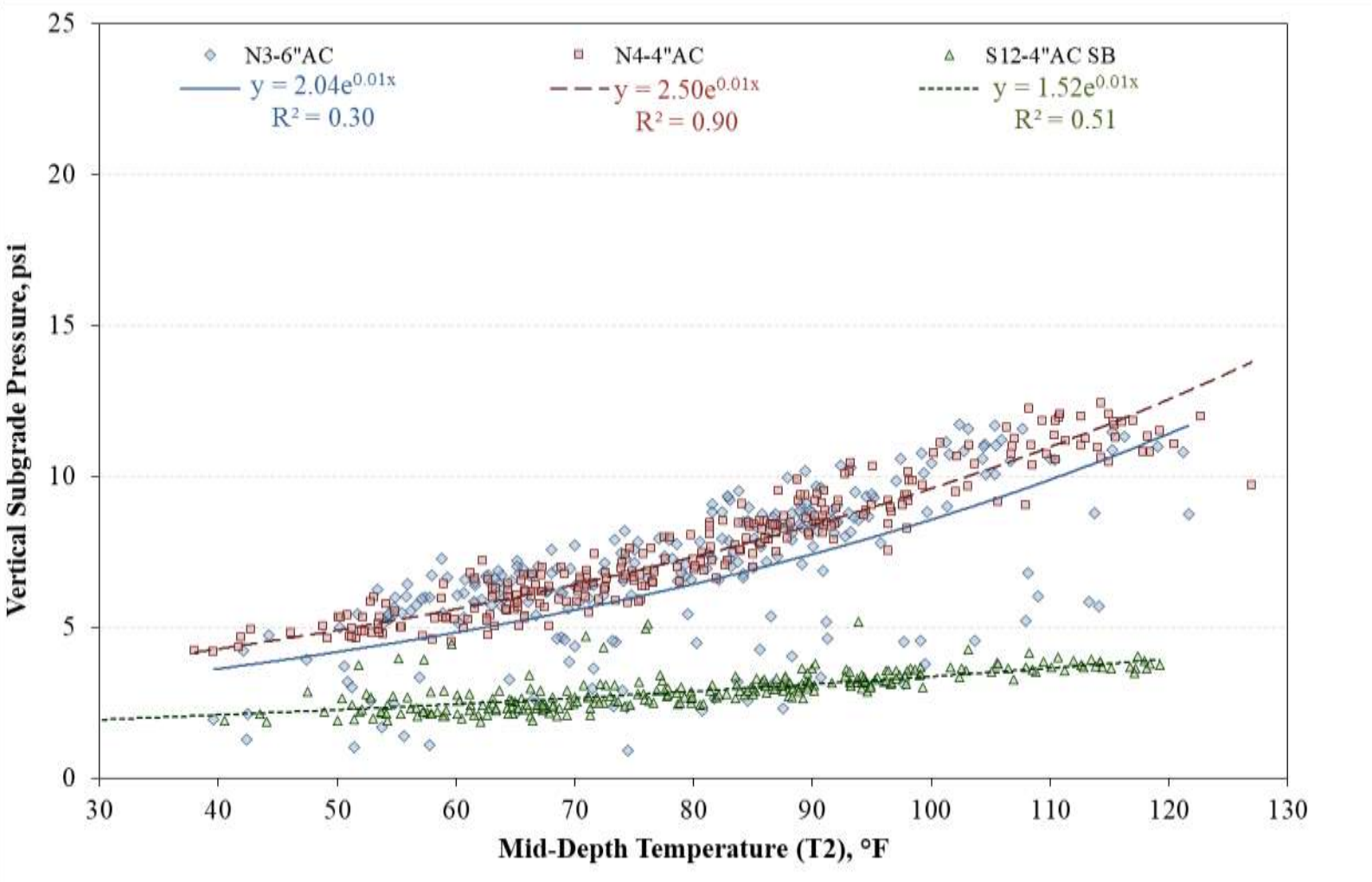

Figure 5.41 Effect of Pavement Temperature on Measured Stress at the Top of the Subgrade Layer

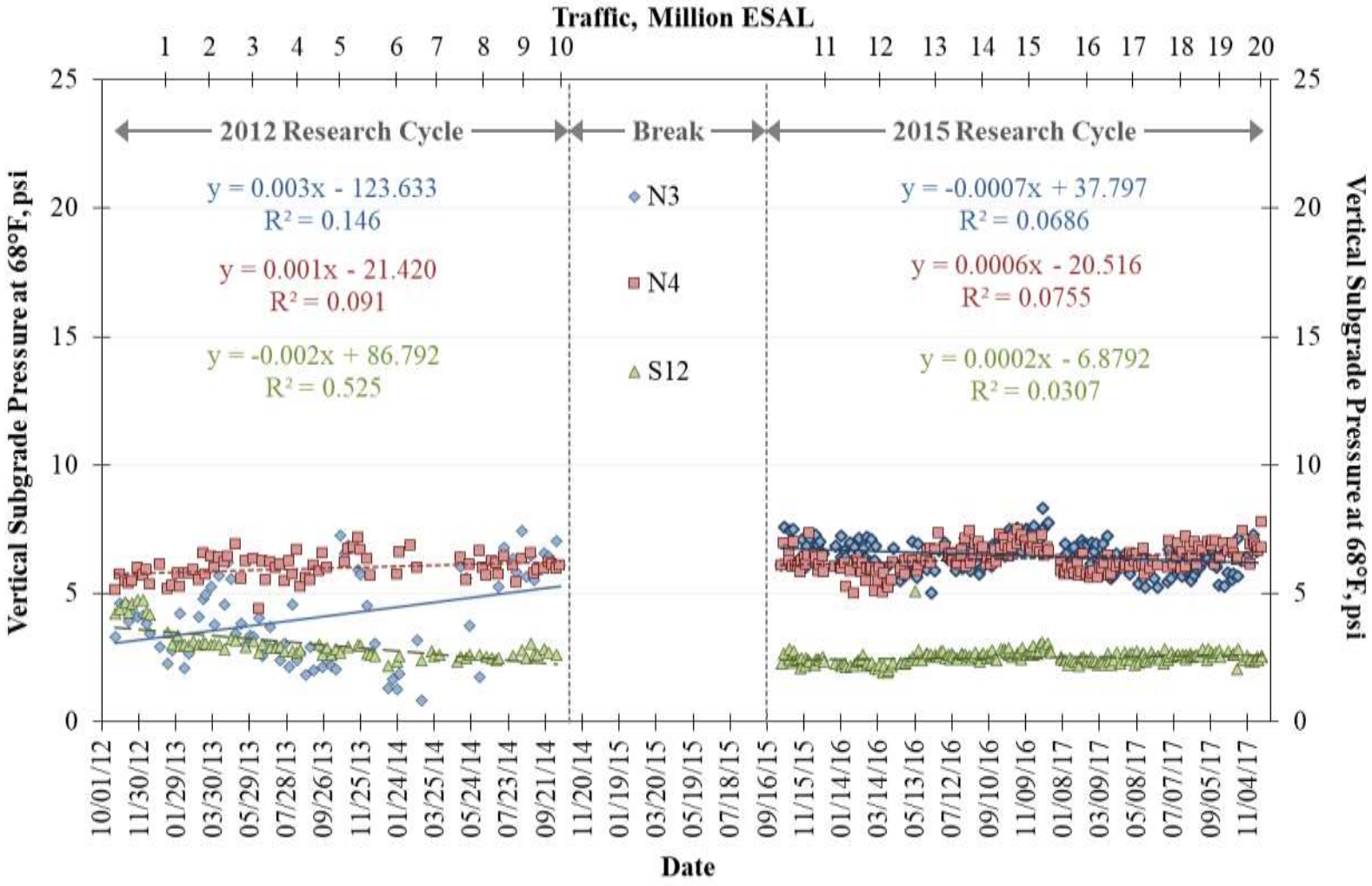

Figure 5.42 Evolution of Stresses at the Top of the Subgrade over Time

5.5 SUMMARY

The structural and functional performance of the three test sections was monitored on a weekly basis over two APT research cycles. After the application of approximately 20 million ESALs, the three test sections behaved very well, showing no visible cracking and excellent functional performance. Measured rut depths were considerably below the failure threshold defined at the Test Track and the sections exhibited very little variation in pavement smoothness over time, indicating the three pavement structures were behaving adequately.

Pavement modulus was backcalculated considering a three-layer structure consisting of the combined AC/CCPR lift as layer one, the aggregate base (N3 and N4) or CTB (S12) as layer two, and the subgrade as layer three. Sections N3 and N4, over the aggregate base, showed a strong influence of mid-depth pavement temperature on the modulus, and the thicker AC section (N3) was found slightly more temperature sensitive than the thinner AC section (N4). This was attributed to the effect of the additional 2 inches of AC in section N3 and the relatively higher percentage of CCPR conforming the AC/CCPR layer in section N4.

Section S12, having the CTB, showed a higher modulus and much less temperature sensitivity than the other two sections. It was postulated that the increased modulus and lower temperature sensitivity was an artifact of the backcalculation process whereby the layers were given a higher apparent modulus to adjust for smaller measured deflections on the CTB. The obtained backcalculated modulus values were normalized to a reference temperature of 68°F, and the sections having an aggregate base (N3 and N4) showed virtually no change in modulus over time. However, the modulus obtained for section S12,

over the CTB, showed an increasing trend over time which may be attributed to the curing process of the CTB. It was postulated that this behavior may be the result of two different effects. On one hand, the backcalculation process may be attributing higher layer modulus to compensate for the relatively low deflections caused by the presence of the CTB. On the other hand, the CTB may have been curing over time, which in turn resulted in increasing backcalculated modulus for all layers. In any case, all three sections appear to be healthy from a structural standpoint.

The measured stresses and strains in different layers of the pavement structure were analyzed. The test sections having an aggregate base (N3 and N4) showed a strong correlation between the temperature and horizontal strains at the bottom of the AC/CCPR layer. The benefit of the additional 2 inches of AC in section N3 (6 in. AC) as compared to section N4 (4 in. AC) was evident across the temperature spectrum. When normalized at 68°F, section N3 had approximately 40% lower horizontal strains than section N4. Section S12, on the other hand, presented a relatively different response, with strain magnitudes significantly lower and a response considerably less temperature-sensitive. As the tensile strain is a direct function of the underlying supporting material, and the CTB in section S12 is much stiffer than the granular base in sections N3 and N4, it was postulated that the stiffer CTB was limiting, to an extent, the tensile strain in the CCPR layer.

Stress measurements at the top of the base/CTB and subgrade, revealed the sensitivity and precision of the pressure measurement equipment was not sufficient to capture the expected reduction in base pressure from the additional AC thickness in section N3 when compared to N4. The measured base and subgrade pressures for section S12 were significantly lower than in the other two sections. It was established that the increased

stiffness of the CTB may have created lower vertical displacements directly above the pressure plate, leading to the significantly lower vertical pressure results obtained for section S12. However, the evolution of temperature-normalized base and subgrade pressures over time in section S12 seemed to indicate some sort of stiffening over time, consistent with a curing process of the CTB. It was postulated that the relatively low strains and vertical displacements observed for section S12 may be indicating that the section may possibly behave as a perpetual pavement.

CHAPTER SIX

STRUCTURAL CHARACTERIZATION AND DESIGN

6.1 INTRODUCTION

The previous sections in this report have focused on summarizing and analyzing the results obtained as part of the research on recycled materials conducted at the Test Track. As described previously, laboratory testing provided knowledge on the characteristics and expected behavior of the materials used for the construction of the three test sections. Additionally, the structural and functional performance of the three test sections was monitored periodically to evaluate the evolution of the pavement under high traffic conditions. It was then determined that the three test sections behaved adequately, and all three sections have endured more than 20 million ESALs without any visible signs of damage. Based on the results obtained from this study, this sixth chapter focused on investigating the structural contribution of the CCPR and CTB to determine how these two recycled materials may be incorporated in common flexible pavement design practices, based on the most popular pavement design methodologies: (1) Empirical AASHTO 93 pavement design, (2) Mechanistic-Empirical pavement design, and (3) Perpetual pavement design. In that way, the laboratory and field performance results were evaluated from a pavement design perspective and, whenever it was possible, a practical approach was recommended to consider these materials in the different design methodologies.

6.2 AASHTO 93 PAVEMENT DESIGN METHOD

As mentioned before, the AASHTO Guide for Design of Pavement Structures (AASHTO, 1993) is based on empirical equations that associate specified traffic loadings to a corresponding structural number (SN), which in turn defines the structural capacity required for the pavement. This SN is calculated as the mathematical summation of the individual thicknesses of each pavement layer multiplied by two empirical coefficients, a layer coefficient (a_i) and a drainage coefficient (m_i), which account for the layer-specific structural contribution and the drainage capabilities, respectively. A direct correlation may be established between the structural layer coefficient and the measured elastic modulus of each pavement layer. Based on such correlation, the structural layer coefficient may be used to empirically describe the structural contribution of a specific pavement layer under traffic loading.

The layer coefficients used for the AASHTO 93 flexible pavement design method are largely based on analytical projections of the results obtained during the AASHO Road Test (HRB, 1962), an accelerated pavement testing program conducted in the early 1960's, to some extent comparable to the research conducted at the NCAT Test Track. Therefore, to determine the structural contribution of the recycled materials included in this study, the pavement performance results presented in the previous chapter were used to estimate a structural layer coefficient for each recycled layer. The obtained field-based layer coefficients may be sufficiently reliable to be used as an input in the AASHTO 93 empirical pavement design method.

6.2.1 Structural Layer Coefficient of the CCPR

The structural layer coefficient of the CCPR was determined considering only test sections N3 and N4, since these two test sections are similar and the only difference between the two is the additional two inches of AC in section N3. Section S12 was not considered in this analysis to avoid the possibly distorting effect of the CTB, which is addressed in the following sub-section.

The procedure for determining the layer coefficient of the CCPR was described by Díaz et al. (2017), and is based on the equations reported by Schwartz and Khosravifar (2013) and presented as Equation 6.1. As reported by Diefenderfer and Apeagyei (2014), this relationship was based on graphical correlations between the layer coefficient and the elastic modulus of AC from the AASHO Road Test.

$$a = 0.1665 \times \ln(\mathrm{E}) - 1.7309 \qquad (6.1)$$

Where: a = Layer coefficient for AC

E = Elastic Modulus of the AC (ksi)

The temperature-normalized backcalculated modulus values obtained for the combined AC/CCPR layer on each testing date were considered as the "E" parameter in Equation 6.1. Subsequently, using the layer coefficient (a) computed from Equation 6.1, the AC/CCPR layer SN was calculated according to Equation 6.2. The SN for the AC layer was then determined from Equation 6.3, using an AC layer coefficient of 0.54, as determined in a previous layer coefficient calibration performed at the Test Track (Peters and Timm, 2011). The layer coefficient for the CCPR layer was finally calculated using

Equation 6.4. It should be pointed out that using 0.54 for the hot mix AC layers is conservative relative to using the most common value of 0.44, because more structural capacity is attributed to the AC layers and less to the CCPR. Had 0.44 been used for the AC layers, the CCPR structural coefficient would have been greater. Furthermore, these results were based on the backcalculated AC/CCPR modulus obtained from the 9,000 lb load level. Considering other load levels would increase the backcalculated layer coefficient of the CCPR, which in turn is also a conservative approach.

$$SN_{AC/CCPR} = D_{AC/CCPR} \times a \quad (6.2)$$

Where: $SN_{AC/CCPR}$ = AC layer coefficient determined for the first approach

a = Layer coefficient of the AC/CCPR from Equation 6.1

$D_{AC/CCPR}$ = AC/CCPR thickness (N3=9.84 in. and N4=8.17 in.)

$$SN_{AC} = 0.54 \times D_{AC} \quad (6.3)$$

Where: SN_{AC} = Structural Number for the AC layer

D_{AC} = AC thickness (N3=5.81 in. and N4=3.59 in.)

$$a_{CCPR} = \frac{(SN_{AC/CCPR} - SN_{AC})}{D_{CCPR}} \quad (6.4)$$

Where: a_{CCPR} = Layer coefficient for the CCPR-foam

D_{CCPR} = CCPR thickness (N3=4.03 in. and N4=4.58 in.)

Following the previous procedure, individual layer coefficients were determined for every testing date at every testing location and considering each temperature-normalized modulus. The results obtained for both test sections are presented in Figure 6.1. The calculated layer coefficients show considerable variability over time, similar to that observed before for the backcalculated modulus. Furthermore, a similar trend is observed for the linear trendlines included in the figure. However, the insignificant slope of the linear trendlines and the low magnitude of their corresponding coefficients of determination (R^2) clarify that the layer coefficients are not significantly increasing or decreasing over time and the average values may be used for further analyses.

The average layer coefficients were determined as 0.38 for section N3 and 0.37 for section N4, with corresponding standard deviations of 0.14 and 0.06, respectively. These values are within the range described in the available literature and it was esteemed they adequately represent the structural capacity of the CCPR. Although a statistical analysis (t-test) revealed that these two values were different at a 95% confidence level (α=0.05, p-value$\leq$0.001), it was reasoned that the difference was not necessarily significant for practical purposes. The difference between the mean layer coefficient obtained for each test section is only 0.01, which would not represent a drastic variation of the SN for design purposes. Furthermore, the obtained layer coefficients obtained in both test section seem relatively similar and appear to have maintained a constant trend over the two research cycles, suggesting that the CCPR layer was capable of withstanding a high level of traffic (over 20 million ESAL) without a showing significant deterioration or loss of its structural capacity.

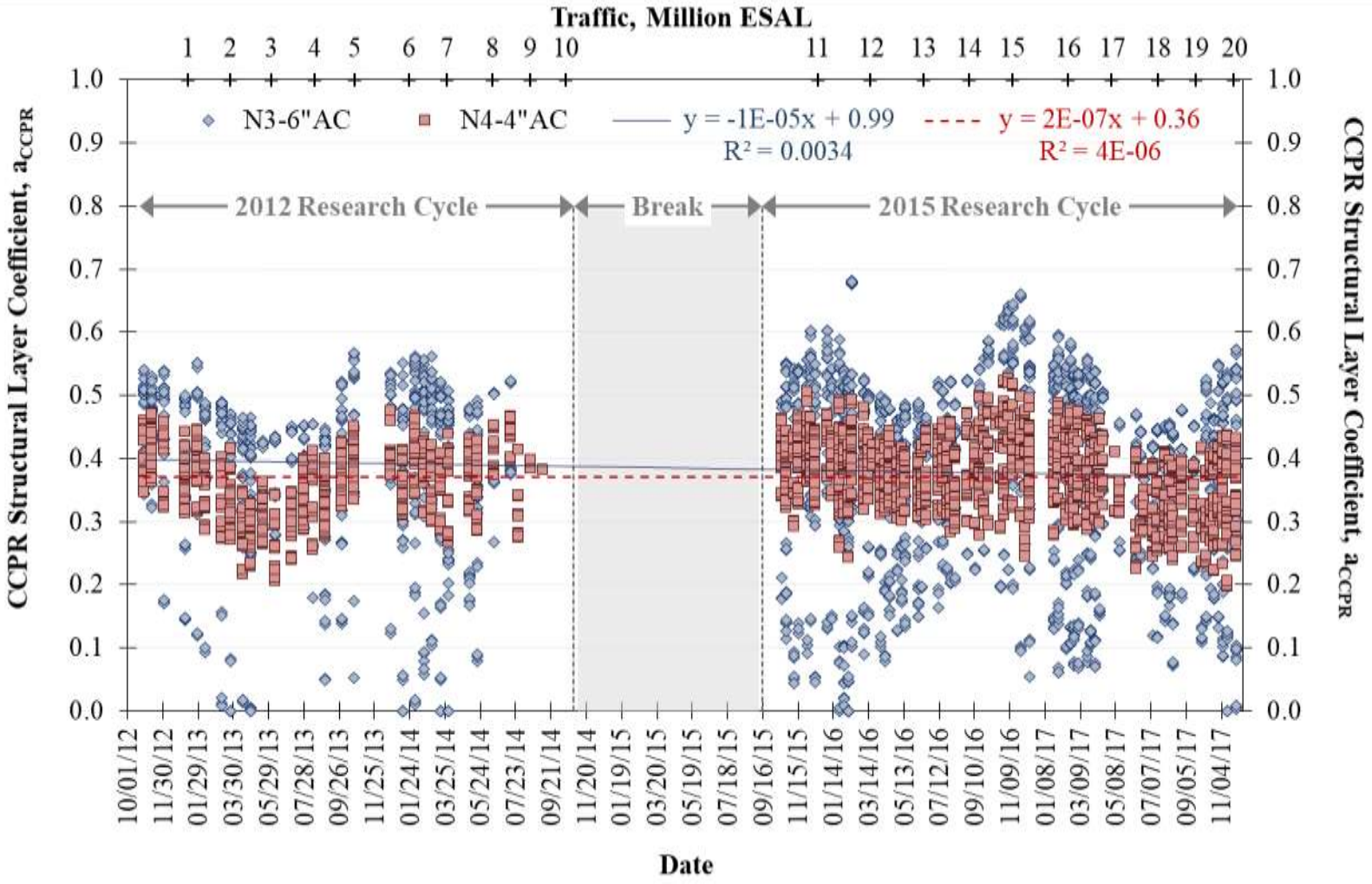

Figure 6.1 CCPR Structural Coefficient vs. Date/Traffic

Although the average layer coefficient was slightly lower for section N4, the lowest values were obtained for section N3, approaching zero in multiple occasions. This is also consistent with the greater standard deviation obtained previously and the significant scatter observed in Figure 6.1 for section N3. Further analyses were performed to evaluate influence of the random location and/or the wheel path on the results obtained for N3.

Figure 6.2 shows the effect of the wheel path on the layer coefficient for section N3. The lower values correspond to the inside and outside wheel paths (IWP and OWP, respectively), while relatively higher and more consistent results were obtained between the wheel paths (BWP). Furthermore, linear trendlines plotted for each data set, revealed a positive slope for the BWP location. Conversely, the IWP and OWP locations showed a slightly negative slope. This seems reasonable since traffic loads are directly applied in the inside and outside wheel paths where the truck tires line up, theoretically inducing more damage in these areas. In that way, the relatively more erratic data and the negative slopes observed in the figure would be an indication of such effect. Nonetheless, the slopes of the trendlines are minimal and at the end of the second research the CCPR layer coefficients vary between 0.003 and 0.555 for the IWP and between 0.008 and 0.682 for the OWP, revealing significant variability in the results. Due to this variability and based on the difference between minimum and maximum values observed, it is impossible to establish with sufficient certainty that the wheel path had an effect on the calculated layer coefficients for the CCPR.

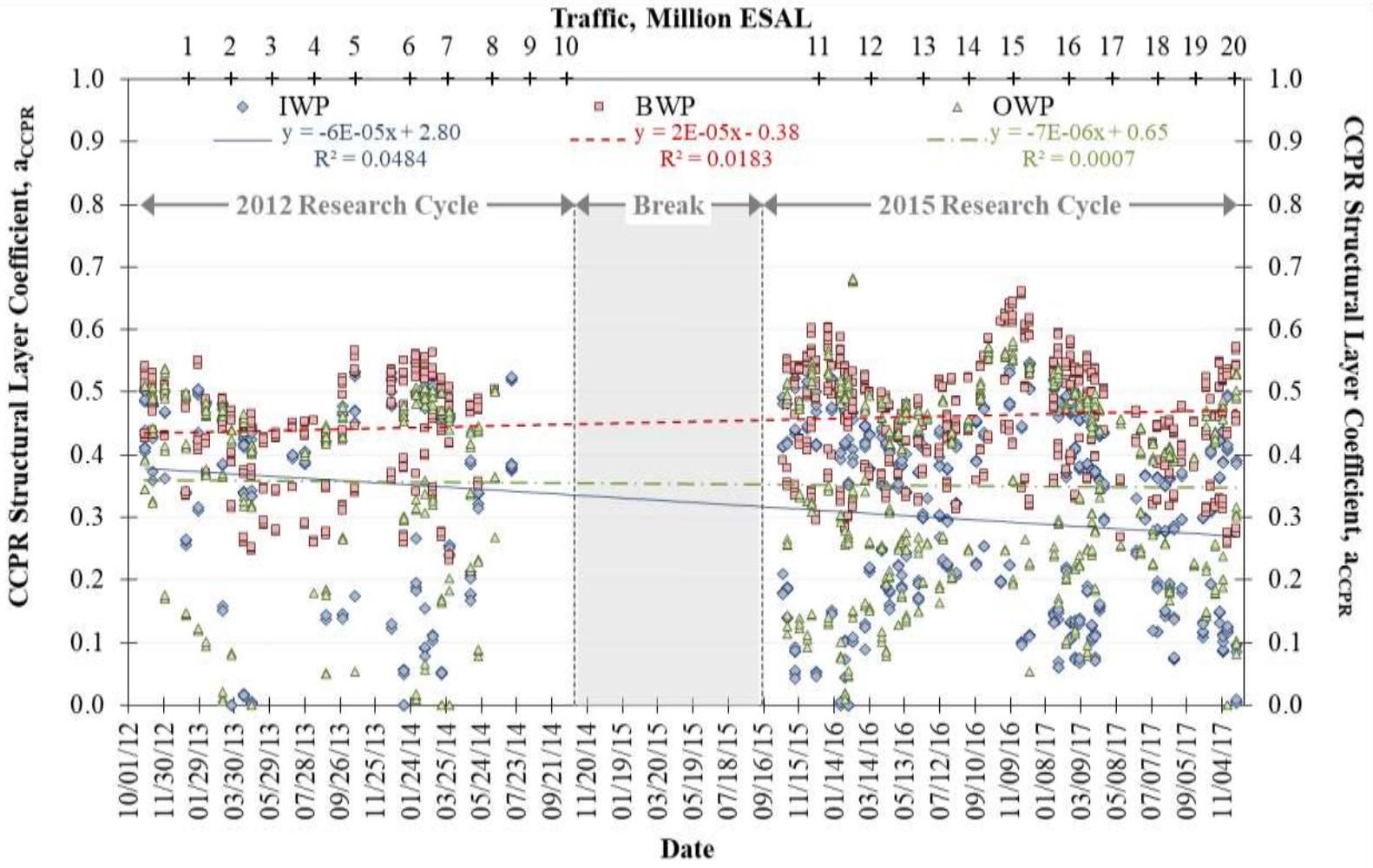

Figure 6.2 Effect of Wheel Path in Section N3

Figure 6.3 shows the effect of the random FWD testing location for section N3. As it can be seen in the figure, most of the lower results were attributed to random location 4 (RL4). Certain low values were also identified for more recent dates in random location 3 (RL3). Conversely, random locations 1 and 2 (RL1 and RL2, respectively) showed very similar and relatively consistent results for the duration of this study. It was postulated that RL4 may coincide with a localized distressed area within section N3, warranting additional exploration in the near future. If RL4 is removed from the analysis, the average layer coefficient for section N3 increases to 0.43, with a correspondingly lower standard deviation of 0.11. This relatively high layer coefficient approaches the value of 0.44 recommended by AASHTO for conventional AC (AASHTO, 1993).

Figure 6.4 shows the results for RL4 identifying the three different wheel paths with different colors. As shown in the figure, relatively low layer coefficients correspond to the IWP and OWP, while more consistent results are visible for the BWP. The average layer coefficient for the BWP is 0.35, with a standard deviation of 0.05, while in the case of the IWP and OWP, the average layer coefficients (and corresponding standard deviations in parentheses) are 0.17 (0.09) and 0.16 (0.07), respectively. These results seem to indicate that the localized distresses in RL4 are only limited to the IWP and OWP. If only these two wheel paths are removed from the analysis, the average layer coefficient of section N3 is reduced to 0.42 with a standard deviation of 0.11. Since the OWP in RL4 corresponds to the location of the gauge array, it was postulated that the presence of the strain gauges and pressure plates may somehow be the cause of the localized lower layer coefficients obtained for the section.

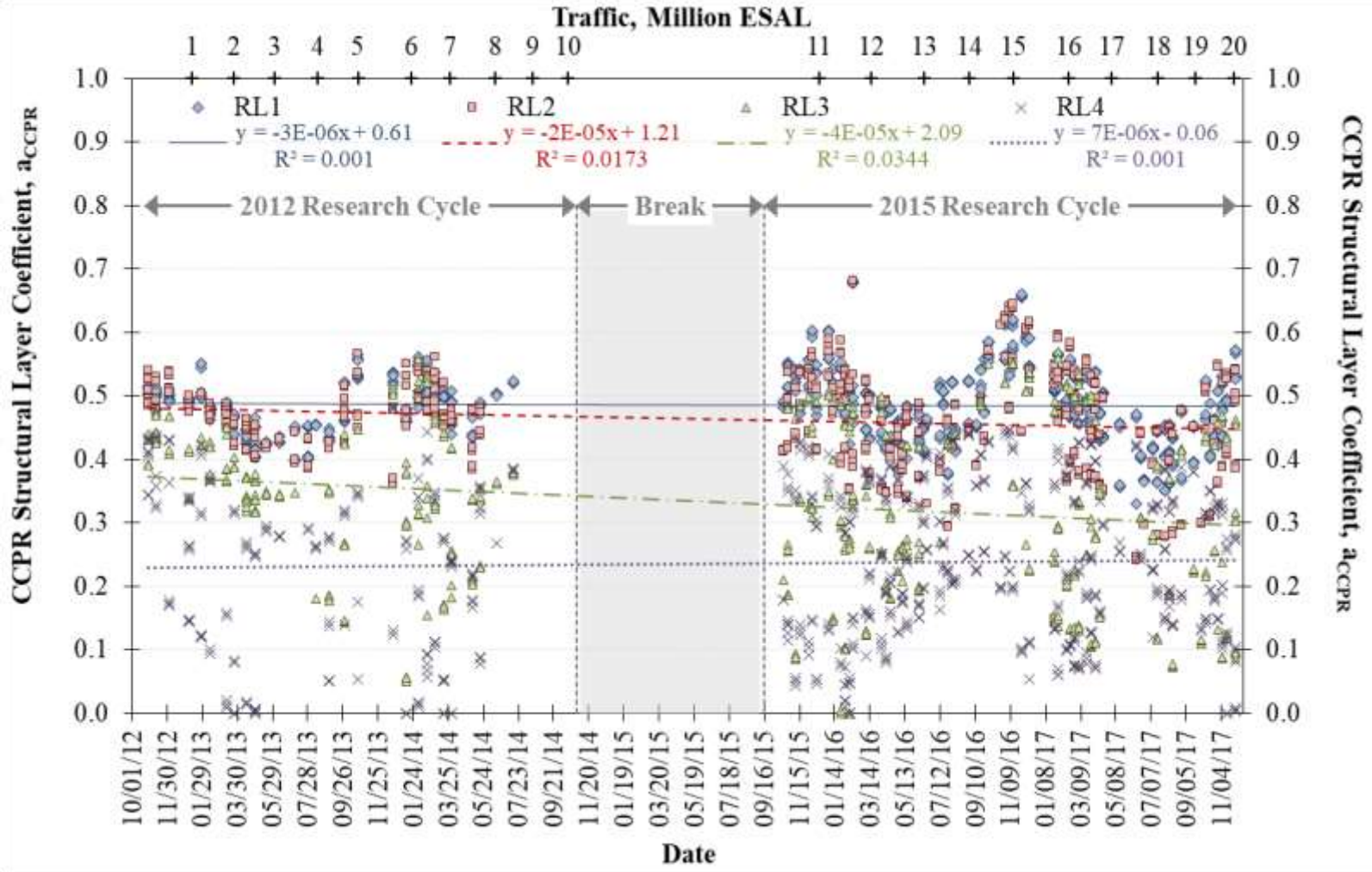

Figure 6.3 Effect of Random Location in Section N3

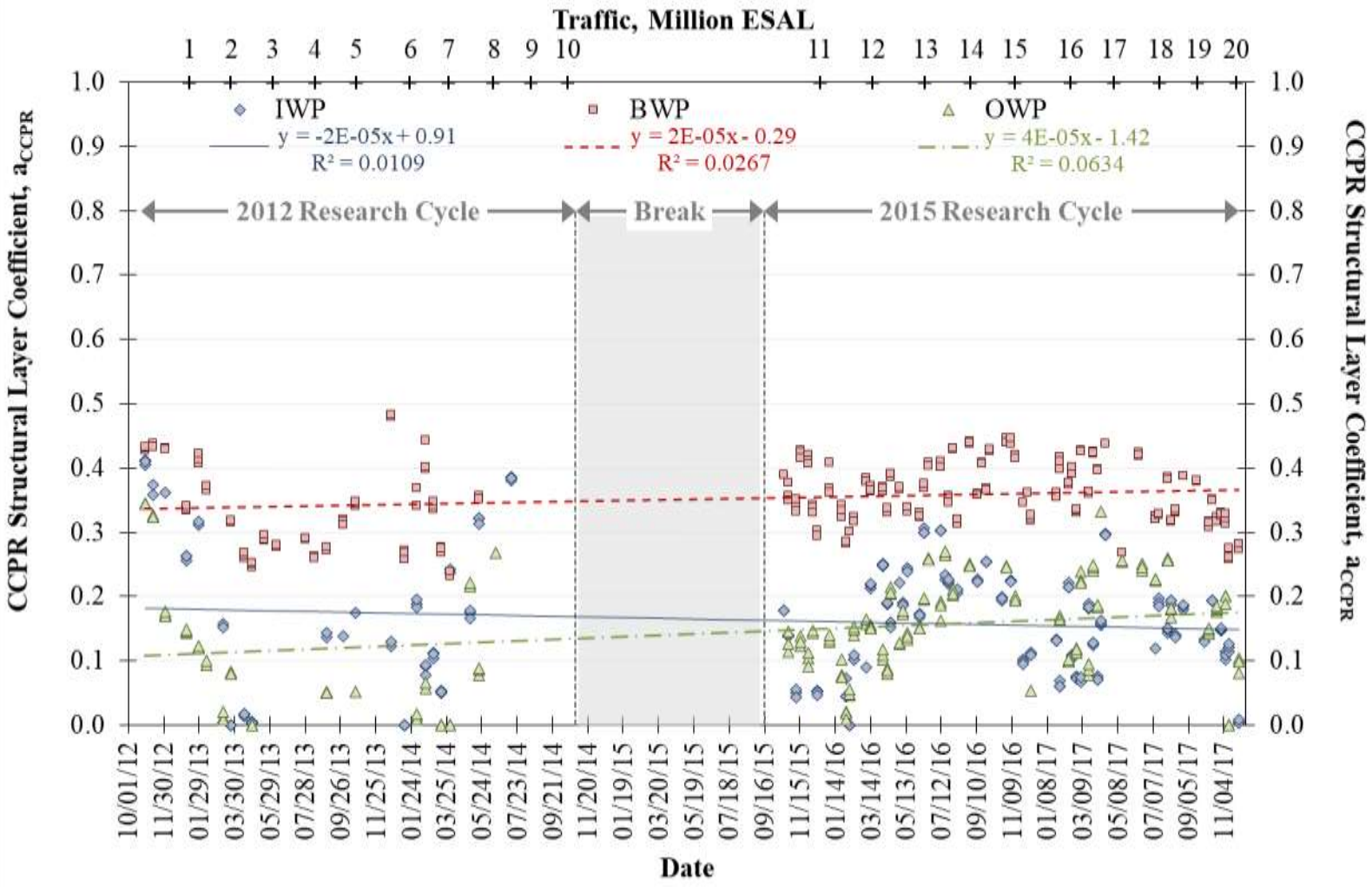

Figure 6.4 Effect of Wheel Path for RL4 in Section N3

Although FWD testing location has a significant effect on the calculated layer coefficient for section N3, the variations may be considered as natural variations obtained from common construction practices. Therefore, for practical design purposes, the spatial variability observed for section N3 would describe more realistically the overall structural capacity of the CCPR in the test section. In that way, it was decided to include RL4 in the analysis, as it would provide a more conservative layer coefficient from a structural design perspective. Based on all this results, it was reasoned that a structural layer coefficient ranging between 0.30 and 0.35 would be appropriate for design purposes.

6.2.2 Structural Layer Coefficient of the CTB

The structural layer coefficient of the CTB was determined based on the modulus values obtained for the second backcalculation layer in section S12, corresponding to the CTB layer. An individual layer coefficient was calculated for each FWD testing date using Equation 6.5. This equation, included in the AASHTO flexible pavement design guide, was originally determined for granular base materials according to the nomographs presented in the design guide and based on the results from the AASHO Road Test. However, the equation allows correlating the stiffness of the first unbound layer and its structural contribution to the overall pavement structure. Therefore, even if the equation was not originally established for cement-treated materials, it was considered it would be sufficiently adequate to explain the structural contribution of the CTB. In any case, the layer coefficient results obtained with this equation should be on the conservative side when it comes to defining the structural contribution of the CTB.

$$a_2 = 0.249 \times \ln(\mathrm{E}) - 0.977 \quad (6.5)$$

Where: a_2 = Layer coefficient for base layers

E = Elastic Modulus of the CTB (psi)

The results are presented in Figure 6.5 and linear trendlines have been generated for each individual research cycle. The layer coefficients showed an increasing trend over the 2012 research cycle and seemed to exhibit a slight decreasing trend afterwards. Although the corresponding coefficients of determination (R^2) are considerably low, which indicates the observed trends are not sufficiently significant to reach a robust conclusion at this stage, it was postulated that the initial increasing trend may be attributed to the curing process of the CTB, while the slight decrease observed after the first two years may be explained as a gradual loss in the structural contribution of the CTB. These results would be consistent with previous observations made for the CTB backcalculated modulus. The relatively small slope of the linear trendline for the 2015 research cycle would indicate that the rate of loss in structural capacity of the CTB is minimal, with only a 6% reduction in the average layer coefficient after 10 million ESALs, from 0.31 at 10 million ESALs to 0.29 after 20 million ESALs. The significant scatter and low values observed for the CTB layer coefficients correspond to the scatter in backcalculated CTB modulus observed previously.

When considering all the data, the average layer coefficient for the CTB is 0.28, with a standard deviation of 0.14. This result is consistent with previous findings from Lofti and Witczak (1985) for a cement-treated, dense-graded, limestone granular base, for which a layer coefficient of 0.27 was obtained directly from resilient modulus testing. However, when analyzing the layer coefficients for each research cycle individually, the results

showed significant differences. The average layer coefficient (and corresponding standard deviation in parenthesis) obtained for the 2012 research cycle was 0.21 (0.13), while that obtained for the 2015 research cycle was 0.32 (0.13). On the one hand, layer coefficients of 0.21 had been previously reported as the maximum range limit by Puppala et al. (2011) for a cement-treated RAP base with 2% cement, who also reported a lower limit of 0.15. On the other, layer coefficient values as large as 0.32 were not found in the literature for cement-treated materials. Therefore, it may be inferred that the layer coefficients obtained in this study are on the high end of the values reported in the literature.

At the beginning of this study, daily average layer coefficients were approximately 0.15, consistent with other results found in the literature (Janoo, 1994; and Taha et al., 2002). However, by the end of the first research cycle, after two years of trafficking and 10 million ESALs, the daily average layer coefficients increased to approximately 0.27, which was also consistent with other results found in the literature (Lofti and Witczak, 1985). Although the difference in average layer coefficients observed within the first research cycle is relatively significant (0.12), sufficient evidence was found in the literature to validate both results. It was postulated that the effect of long-term curing of the CTB was the cause for the variability in the results found in the literature. In that way, in the early stages of the life of the pavement the layer coefficient of the CTB was in the vicinity of 0.15. Conversely, after approximately two years of curing, the average layer coefficient of the CTB reached a peak value in the vicinity of 0.26, after which it began to gradually decrease in a more conventional behavior of loss of structural capacity with increasing traffic. Based on these results, it was reasoned that a structural layer coefficient ranging between 0.20 and 0.25 would be appropriate for practical design purposes.

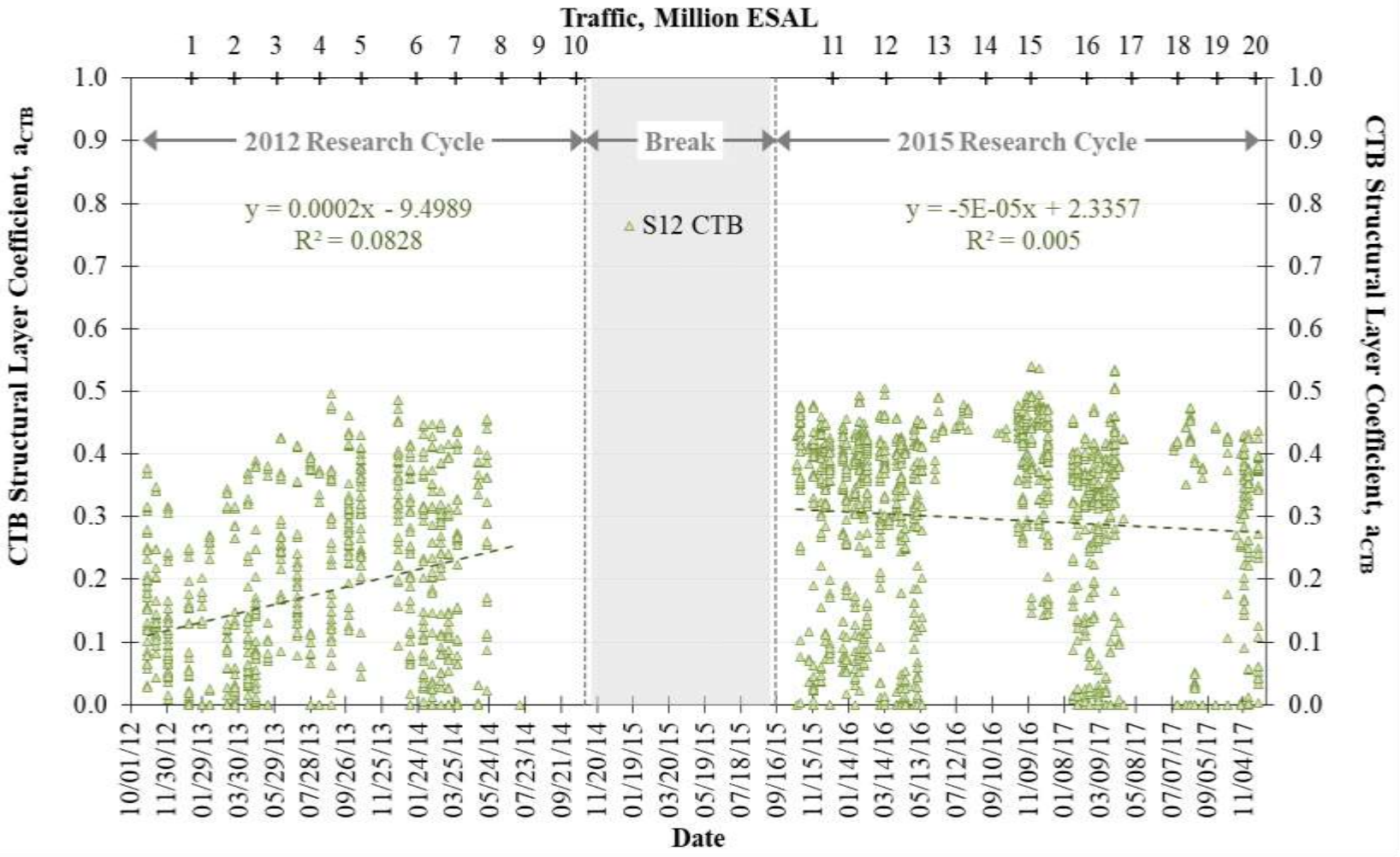

Figure 6.5 CTB Structural Coefficient vs. Date/Traffic

6.2.3 Structural Evaluation of the Test Sections

In the previous subsections of this report, it was suggested that, for pavement design purposes, the layer coefficients of the CCPR should range between 0.30 and 0.35, while the layer coefficients of the CTB should range between 0.20 and 0.25. Based on these results, and considering the average design thicknesses of the three test sections, a structural number was computed for each test section. The lowest layer coefficients in the proposed range were selected for this analysis as they provided a more conservative approach. Additionally, a layer coefficient of 0.54 was used for the AC layer and a layer coefficient of 0.14 was conservatively selected for the granular base.

The resulting structural numbers found for each test section were subsequently used to estimate the allowable number of ESALs each test section should withstand before failure. Since the purpose of this analysis was to evaluate the pavement structures in each test section from a pavement design perspective, the values recommended in the AASHTO 93 design guide were used as inputs in the design equation. The parameters selected included a reliability of 90%, and overall standard deviation of 0.45, an initial serviceability of 4.2 and a terminal serviceability of 2.5, for a serviceability loss of 1.7. The average backcalculated subgrade modulus obtained for the two research cycles for each test section were used to determine the design resilient modulus (M_R) of the subgrade. According to AASHTO 93 pavement design guide recommendations, the measured subgrade modulus were affected by an adjustment factor of 0.33 and the obtained design M_R were 10,423 psi for section N3, 9,062 psi for section N4, and 10,182 psi for section S12. The results are presented in Figure 6.6, including the structural number (on the left axis) and the allowable ESAL (on the right axis) for each test section.

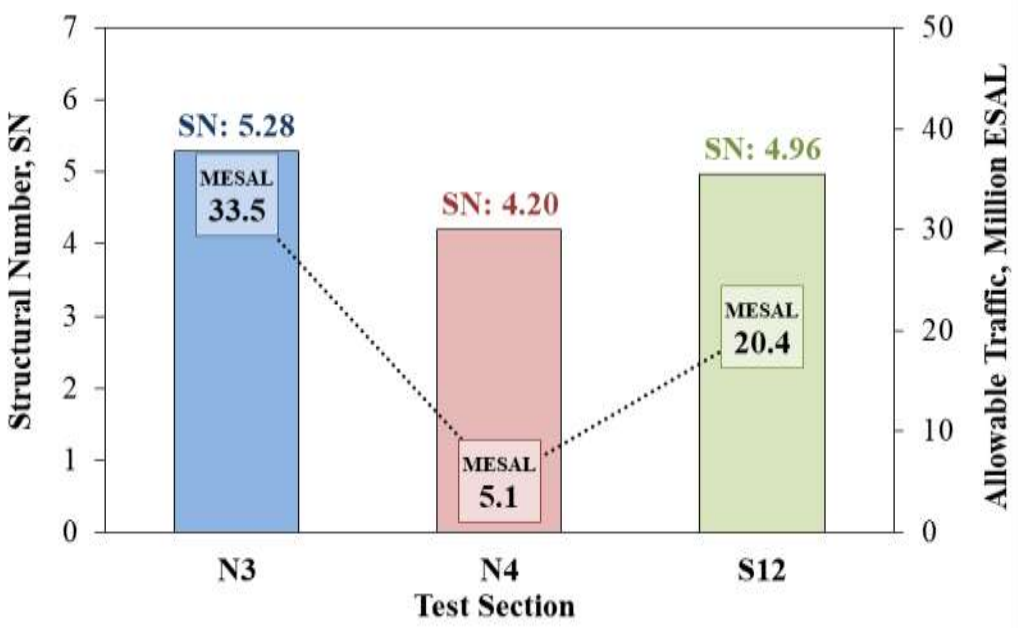

Figure 6.6 Pavement Structural Numbers and Corresponding Allowable Traffic

The structural numbers obtained for sections N3 and S12 are larger than that obtained for section N4. Based on these results and the AASHTO 93 pavement design method, some interesting observations can be made. By comparing the results obtained for sections N3 and N4, it may be inferred that the 2-inch increase in AC thickness translates into a 25.7% increase in the structural capacity of the pavement, corresponding to an increase of 1.08 in the calculated SN. Furthermore, based on the AASHTO 93 pavement design method, the allowable traffic the pavement can withstand before failure is 6.6 times greater with the additional 2 inches of AC, increasing from 5.1 million ESALs for section N4 to 33.5 million ESALs for section N3.

The effect of the CTB may be identified by comparing sections N4 and S12, where replacing the 6-inch granular base for an 8-inch CTB produces an 18.1% increase in the structural capacity of the pavement, corresponding to an increase of 1.16 in the calculated SN for section S12. Additionally, based on the AASHTO 93 pavement design method, the

allowable traffic the pavement can withstand before failure is 4 times greater when the granular base is replaced by an 8-inch CTB, increasing from 5.1 million ESALs for section N4 to 20.4 million ESALs for section S12.

Based on the previous results, it was identified that the AASHTO 93 pavement design method attributes most of the structural capacity of the pavement to the AC layers while an improvement in the unbound layers has a much lower impact. Based on the empirical equations of the design method, two additional inches of AC would allow the application of 1.6 times more traffic loads (ESALs) than replacing the granular base by a CTB and increasing its thickness. Consequently, the resulting allowable traffic obtained for section N3 is greater than that obtained for section S12, while the allowable traffic for section N4 is significantly lower than that obtained for other test sections.

According to these results, section N4 would have been expected to fail approximately half way into the first research cycle after 5.1 million ESALs, while section S12 would have been expected to fail by the end of the second research cycle after 20.4 million ESALs. However, by the end of the 2015 research cycle (after over 20 million ESALs) no sign of damage was observed on any of the three test sections. Therefore, the performance of the pavement sections is exceeding the predictions obtained with the AASHTO 93 pavement design method, even after calibrating the structural coefficients using pavement deflection data. The applied traffic exceeds the allowable traffic estimated as part of the design procedure. In the case of these three pavement structures, it was postulated that the AASHTO 93 pavement design method may be over-conservative for determining the pavement thickness.

6.3 MECHANISTIC-EMPIRICAL PAVEMENT DESIGN METHOD

As described before, mechanistic-empirical pavement design is commonly performed using the AASHTOWare Pavement ME Software, supported by AASHTO. The software uses layered elastic analysis to calculate pavement responses such as stresses, strains and deflections under previously defined traffic loads and climate conditions, based on a pavement cross-section and specific material properties defined by the designer. The responses obtained for a great number climatic and traffic combinations are used in location-specific, empirically-derived transfer functions to simulate the performance of the pavement over the design period. If pavement distresses are acceptable, then the proposed pavement structure is deemed adequate for the traffic and climate conditions of the project. However, if pavement distresses exceed the selected design criteria, the pavement structure is modified until adequate results are achieved.

The design process requires a significant number of computations to complete the simulation, which requires software to obtain adequate performance predictions based on the previously mentioned transfer functions coded within the software. Within the software, these empirical transfer functions allow correlating the calculated stresses and strains to the long-term performance of the pavement based on the performance observed and measured for other existing pavements under its corresponding traffic and weather conditions. Currently, the software includes transfer functions that have been calibrated on a national level based on the performance of multiple pavements across the United States. However, most states using the mechanistic-empirical pavement design method have decided to locally-calibrate these transfer functions to account for the state-specific traffic and weather conditions (Timm et al., 2014).

The local calibration of the transfer functions, within the software, requires extensive and costly information on the long-term performance and failure of real pavement test sections. In other words, to calibrate the transfer functions for specific materials, technologies and structural combinations, specific test sections must be built and studied over its entire life cycle. In that way, once the test sections have failed, the observed and measured failure mechanisms can be compared to the performance predicted by the software to adjust the transfer functions so that the measured and predicted performance become similar. At this stage, the local calibration would be appropriate for future pavement designs.

In the case of the three test sections built at the NCAT Test Track, after approximately 20 million ESALs, no damage was observed, making it impossible to perform a local calibration of the CCPR and CTB within the AASHTOWare Pavement ME Software. Even if the pavement structure of the three test sections can be modelled in the software, it would be impossible to attain any significant conclusions based on the computed performance predictions, beyond an evaluation of their predictive capability relative to the excellent performance observed for the three test sections. Robust conclusions on the applicability of the mechanistic-empirical pavement design method for the CCPR and the CTB will only be reached when the test sections begin to show significant signs of failure, attributable to the traffic loading. The only significant observation that could be made at this point would involve comparing the measured and predicted pavement responses, which was already done as part of the analysis presented in the previous section. A more detailed analysis from the perspective of perpetual pavement design, a subcategory of M-E design, will be addressed in the following section of this dissertation.

6.4 PERPETUAL PAVEMENT DESIGN

Perpetual Pavement Design (PPD) is based on a mechanistic-empirical approach. However, instead of correlating pavement responses to damage by means of a transfer function, PPD attempts to define a pavement structure in which the vast majority of expected loads produce stresses, strains and deflections lower than those which would cause structural damage. Most approaches to PPD focus on limiting the pavement responses related to the most common structural pavement distresses; structural rutting and bottom-up fatigue cracking. Although several limiting criteria for PPD have been proposed over the years, most recent studies utilize measured and simulated control strain distributions to evaluate the pavement (Willis and Timm, 2010; Castro et al., 2017).

According to the Asphalt Pavement Alliance, a Perpetual Pavement is defined as "an asphalt pavement designed and built to last longer than 50 years without requiring major structural rehabilitation or reconstruction, and needing only periodic surface renewal in response to distresses confined to the top of the pavement" (Asphalt Pavement Alliance, 2002). Based on this definition, and considering the excellent performance of the three test sections at the Test Track, with no evidence of any deep distress after 20 million ESALs, it was postulated that the pavement structures may be behaving as perpetual pavements. To further investigate this hypothesis, analyses were conducted to evaluate whether these sections may be considered as perpetual pavements with respect to bottom-up fatigue cracking. Although the ultimate failure mechanism of the CCPR and CTB was still unknown, measured and predicted structural responses of the test sections were compared to the limiting criteria developed for each specific condition to assess the applicability of PPD.

6.4.1 Horizontal Strains on the AC/CCPR

Horizontal strains at the bottom of the AC/CCPR layer correlate directly with the capacity of the pavement structure to withstand bottom-up fatigue cracking. The average temperature normalized (68°F) horizontal strains measured over the duration of the two research cycles, and its corresponding standard deviations, are presented in Figure 6.7. Clear differences between the magnitudes of the average tensile strain in the three test sections can be identified. As mentioned previously, the average tensile strain obtained for section N4 is significantly greater than that obtained for section N3, with two additional inches of AC. Similarly, the average strain measured for section S12 is consistent with the presence of the stiffer CTB layer. A Tukey pairwise comparison at a 95% confidence level revealed significant differences between all three test sections. Therefore, the observed decrease in strain for sections N3 and S12 are both practically and statistically significant. A practical comparison between the sections, considering section N4 as the reference, revealed that the additional 2 inches of AC reduced the average measured tensile strain by 33%, while the stiffer CTB layer reduced the average measured tensile strain by 71%.

The lowest average strain was obtained for section S12 and was below the endurance limit of 150 microstrain proposed by Nishizawa et al. (1996), suggesting the test section may be behaving as a perpetual pavement. However, the magnitude of this endurance limit has been greatly discussed in the literature with values ranging from 70 microstrain, as estimated by Monismith and McClean (1972), to 250 microstrain, as allowed by the AASHTOWare Pavement ME Software. For that, a more in-depth analysis based on the overall strain distribution as proposed by Willis and Timm (2009) is required.

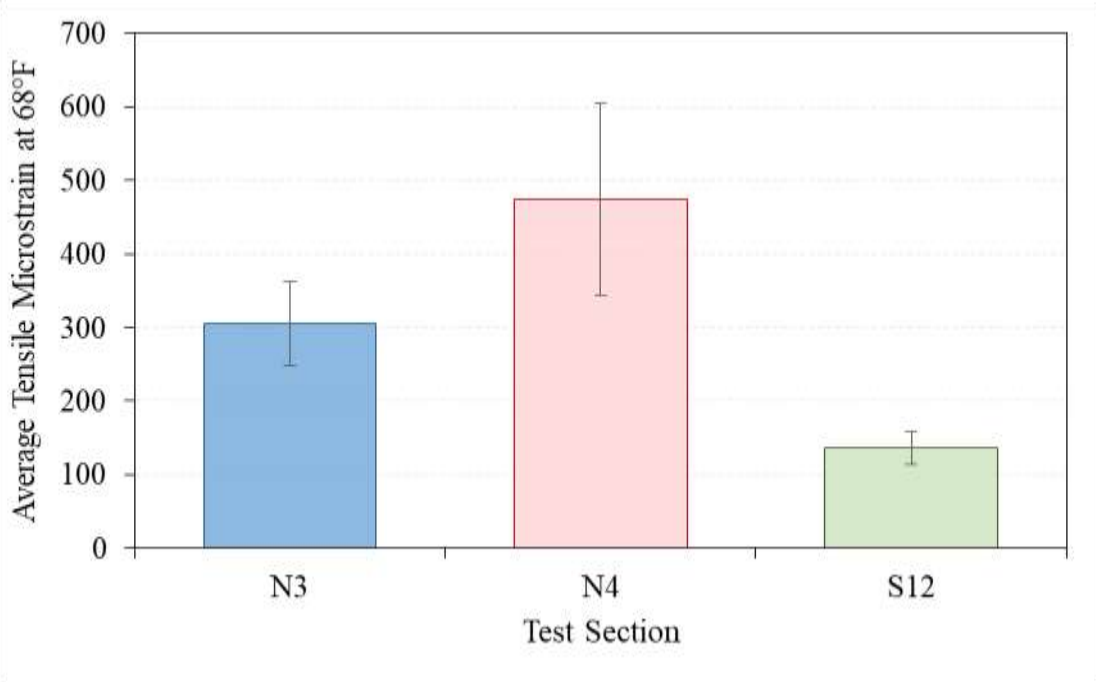

Figure 6.7 Average Measured Tensile Microstrain and Standard Deviation at 68°F

Willis and Timm (2009) developed limiting strain distributions for perpetual pavement design based on measured strain data from a number of test sections at the NCAT Test Track that either did or did not experience bottom-up fatigue cracking. This control distribution serves as an upper limit to the strain response, above which cracking may be expected and below which perpetual performance may be achieved. Simply comparing this limiting threshold distribution with the strain distributions obtained for the test sections included in this study would allow inferring if the test sections are truly behaving as perpetual pavements. It is important to emphasize that the criteria established by Willis and Timm (2009) were not developed from CCPR or CTB pavement sections so it is currently unclear whether they are truly applicable. However, they do allow contrasting the performance of the test sections against conventional flexible pavements.

Figure 6.8 shows the cumulative distribution for the measured strains in the three test sections. The dark continuous line represents the control distribution proposed by Willis and Timm (2009) for field measured strains. The largest strains were obtained for section N4, while the lowest strains observed for in section S12, with intermediate strains for section N3. These results clearly show the benefit of the additional 2 inches of AC, resulting in lower strain levels for section N3 relative to section N4, and the positive effect of the stiffer CTB, resulting in lower strains for section S12 relative to section N4.

Sections N3 and N4 exceed the Willis and Timm (2009) limiting distribution, and based on this criteria, both sections may be expected to experience bottom-up cracking if trafficking is continued. Nonetheless, it is important to mention that at this point, it is still uncertain if these two test sections exceeding the strain limits will truly develop bottom-up cracking since the criteria were not developed from CCPR sections.

The strain distribution obtained for section S12 seems to intersect the Willis and Timm (2009) limiting criteria at a proximately the 30^{th} percentile. The same trend was observed for the measured horizontal strains as well as for the temperature corrected strains. This suggests that section S12, with the CTB, may be expected to be perpetual since its 95^{th} percentile strain distribution is less than the control distribution. Although there still may be a possibility that cracking could develop in section S12, based on the current perpetual pavement design criteria it may be suggested that section S12 is likely perpetual while the other two test sections are not perpetual. Further trafficking of the sections will help validate this hypothesis. Also, construction of thinner CCPR sections could help distinguish between perpetual and non-perpetual CCPR behavior.

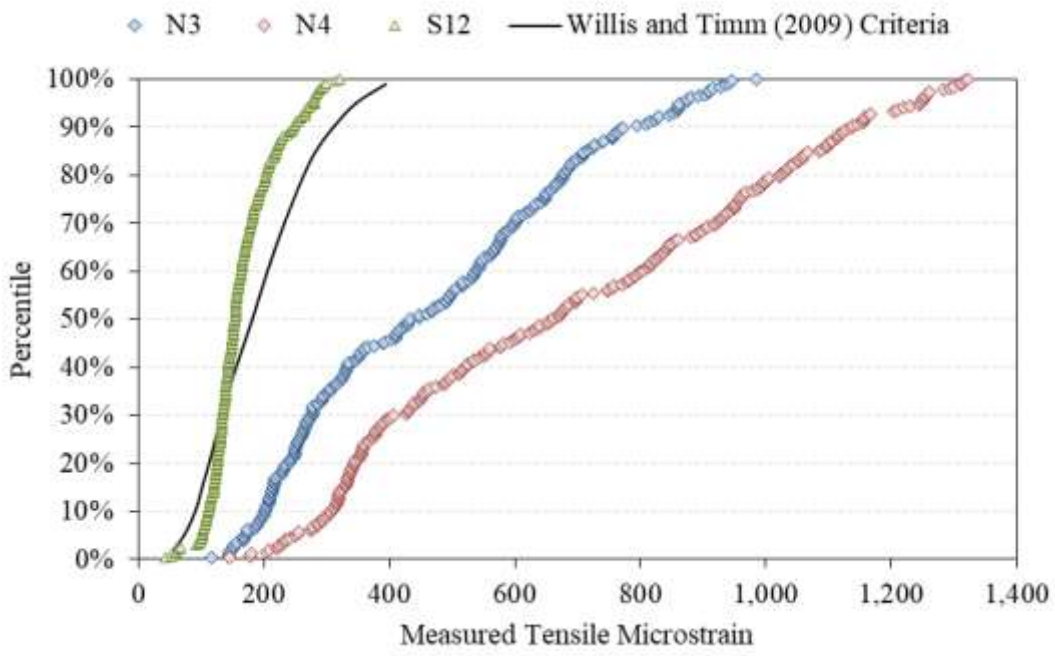

Figure 6.8 Measured Tensile Microstrain Distributions

6.4.2 Vertical Compressive Stresses on the Subgrade

The magnitude of the vertical strains and stresses on top of the subgrade may be considered as an indication of the capacity of the pavement structure to withstand structural rutting (Asphalt Pavement Alliance, 2010). Commonly, the vertical compressive strain of 200 microstrain at the top of the subgrade is used as the limiting design parameter for PPD, as suggested by Harvey et al. (2004) and Walubita et al. (2008). However, at the Test Track, only vertical stresses were measured on top of the subgrade. In fact, measuring vertical deformations within the pavement structure was found to be relatively complicated because of the low vertical strain gauge survivability observed at the Test Track. A different approach, based on the subgrade stress was suggested by the University of Illinois (Asphalt Pavement Alliance, 2010). Although a clear rutting criterion based on this parameter is yet to be established, it may be applicable for the results obtained at the Test Track.

The average vertical stresses on the subgrade, measured over the duration of the two research cycles, and its corresponding standard deviations, are presented in Figure 6.9. As discussed previously, the stresses obtained for section S12 are significantly lower than those observed for sections N3 and N4 demonstrating the effect of the stiffer CTB. Furthermore, the difference between sections N3 and N4 is not significant for practical purposes. A Tukey pairwise comparison at a 95% confidence level revealed significant differences between the average vertical stresses in all three test sections. A practical comparison between the sections, considering section N4 as the reference, revealed that the stiffer CTB layer reduced the average measured vertical stress by 57%, while the additional 2 inches of AC only caused a reduction of 8%, confirming once again the assumptions postulated in the previous section of this dissertation.

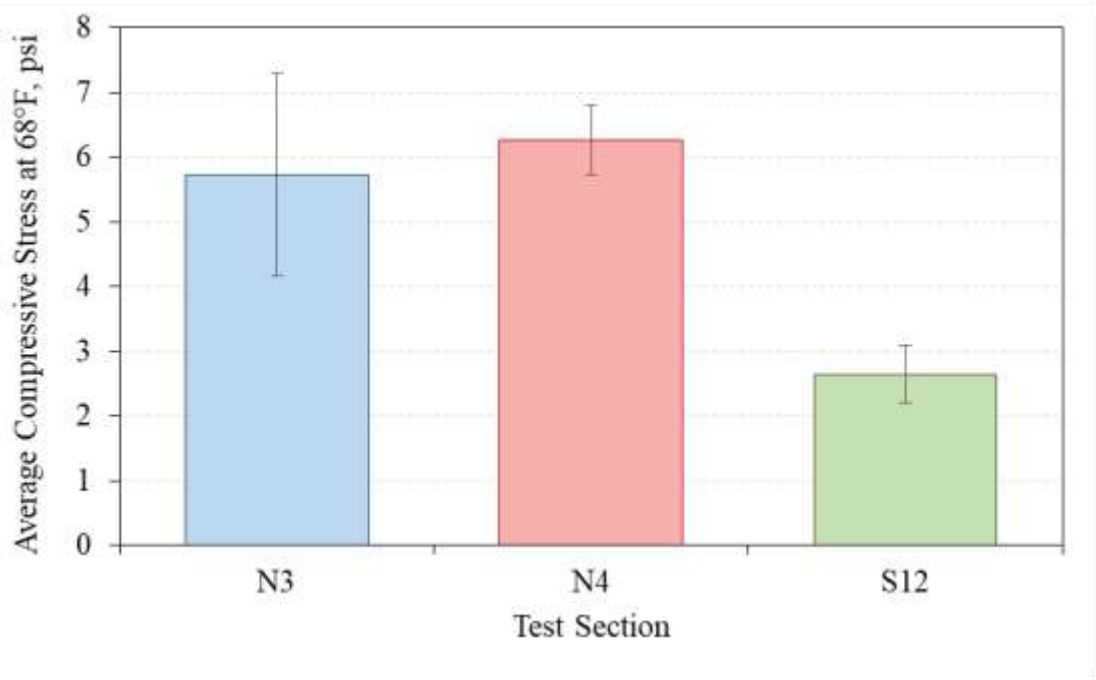

Figure 6.9 Average Measured Compressive Stress and Standard Deviations at 68°F

The approach from the University of Illinois proposed by Bejarano et al. (1999) and Bejarano and Thompson (2001) uses the ratio of the subgrade stress to the unconfined compressive strength of the soil, defined as the Subgrade Stress Ratio (SSR). To analyze the results obtained at the Test Track under this concept, it was necessary to perform a more in-depth analysis. The backcalculated moduli obtained for the subgrade in the previous chapter of this dissertation were used to determine the ultimate unconfined compressive strength based on Equation 6.6, derived from the model established by Hossain and Kim (2014) to correlate resilient modulus to the ultimate compressive strength of fine grained soils with coefficient of determination of 0.73. Although the correlation was originally intended for laboratory measured resilient modulus, an approximation made using the backcalculated modulus values would allow a sufficiently robust comparison for practical purposes.

$$q_u = \left(\frac{1}{143}\right) \times (\mathrm{E} - 4{,}283) \tag{6.6}$$

Where: q_u = Unconfined compressive strength (psi)

E = Modulus of the Subgrade (psi)

An unconfined compressive strength was determined for each backcalculated modulus obtained for the subgrade in the three test sections over the two research cycles. The average unconfined compressive strength, and its corresponding standard deviation, obtained for each test section are presented in Figure 6.10. A Tukey pairwise comparison at a 95% confidence level revealed significant differences between the average vertical stresses in all three test sections.

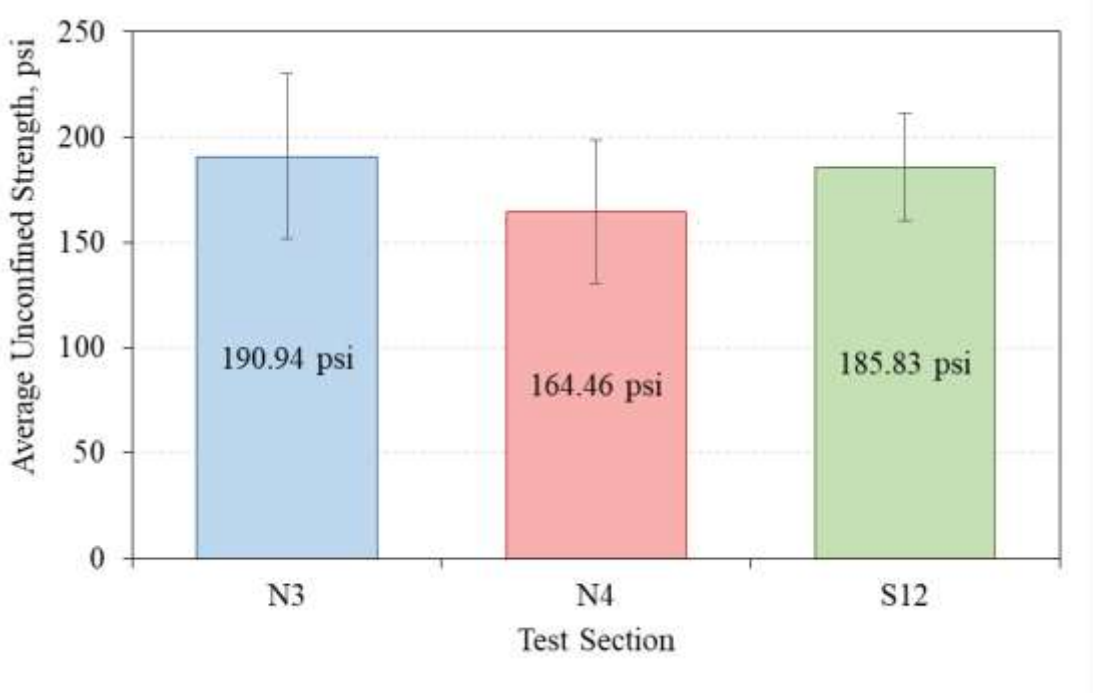

Figure 6.10 Average Unconfined Compressive Strength

The average unconfined strength obtained for each test section was used to calculate individual SSR for each vertical stress measurement performed at the Test Track. The results are presented in the form of a distribution in Figure 6.11. As expected, section N4 shows the highest SSR, indicating the pavement is more susceptible to experience structural rutting. The two additional inches of AC in section N3 represent a 20% reduction in the SSR, while a 66% reduction can be attributed to the CTB. Therefore, structural rutting would be less likely to occur in section S12. A threshold SSR of 0.42 was recommended by Bejarano and Thompson (2001) as the limiting criteria for structural rutting in perpetual pavement design. Based on this criteria, it may be inferred that all three test sections are likely perpetual from the perspective of structural rutting. This is consistent with the observed performance in the field, where all three test sections remained well below the 0.5 inches rutting criteria established at the Test Track.

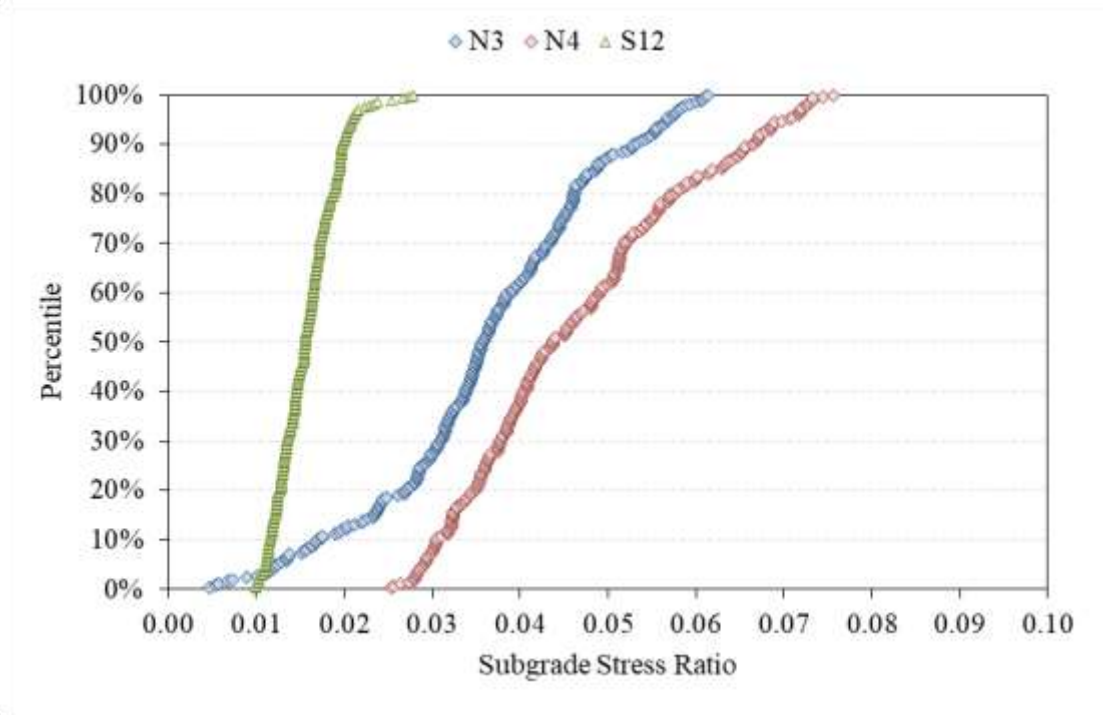

Figure 6.11 Subgrade Stress Ratio Distributions

6.4.3 Perpetual Pavement Analysis

An additional perpetual pavement analysis was performed using the PerRoad software (Version 4.4). Individual mechanistic models of each pavement test section were created in the software based on the layer properties measured at the Test Track during the two research cycles. The test sections were modeled as three layer structures consisting of: (1) an AC/CCPR as the first layer, (2) a granular base for sections N3 and N4 or a CTB for section S12 as the second layer, and (3) the subgrade as the third layer. Figure 6.12 shows the average layer thickness selected for the models and the corresponding layer thickness variability represented as the coefficient of variation (COV) of all the measured thicknesses within each test section, in parenthesis.

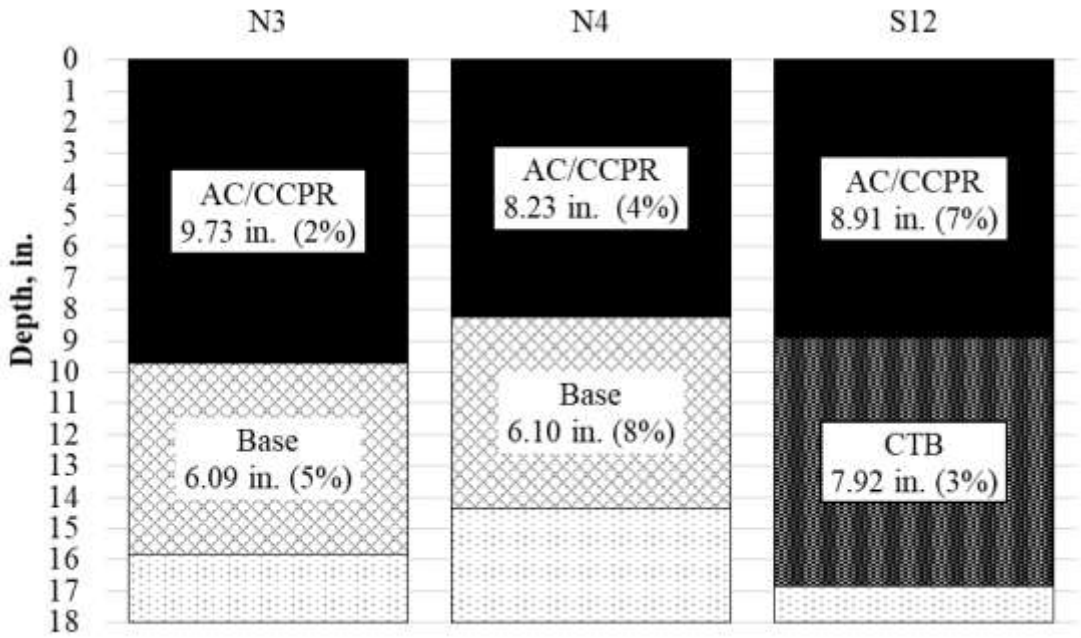

Figure 6.12 Pavement Cross-Sections used for the Mechanistic Models

The properties of each layer were determined based on the backcalculated modulus for each test section, presented in the previous chapter of this dissertation. To simplify the model and to account for the seasonal variability observed in the results, the data was divided into four different seasons identified as: (1) summer, (2) fall, (3) winter and (4) spring, each one lasting approximately 13 weeks. An average backcalculated modulus was obtained for each season and for each layer, carefully selecting the specific dates corresponding to each season within the four-year period over which traffic was applied. Table 6.1 shows the backcalculated modulus for each season-layer-test section combination. Additionally, Table 6.2 includes the average COV for each layer over the duration of the two research cycles.

Table 6.1 Average Backcalculated Modulus used in the Mechanistic Model

Test Section	Season	AC/CCPR E1 (psi)	Base or CTB E2 (psi)	Subgrade E3 (psi)
N3	Summer	579,689	5,000	26,159
	Fall	638,294	11,097	33,230
	Winter	635,105	9,748	35,433
	Spring	570,620	6,205	29,848
N4	Summer	208,794	5,000	23,802
	Fall	382,882	9,020	29,128
	Winter	536,399	8,094	30,386
	Spring	340,006	5,297	26,279
S12	Summer	899,691	215,648	27,442
	Fall	1,011,352	239,218	32,605
	Winter	1,417,626	160,558	32,582
	Spring	1,151,737	142,701	28,850

Table 6.2 Coefficients of Variation used in the Mechanistic Model

Test Section	Backcalculated Modulus COV		
	AC/CCPR	Base or CTB	Subgrade
N3	40%	80%	13%
N4	35%	74%	11%
S12	26%	75%	9%

Using the PerRoad Software, and assigning a normal distribution to each layer modulus based on the previous results, traffic loads were simulated as a 5,000 lb single axle with a tire pressure of 100 psi to emulate the traffic loading conditions at the Test Track. A total of 5,000 Monte Carlo cycles were used for each model to determine: (1) horizontal tensile strains at the bottom of the AC/CCPR, and (2) vertical compressive

strains at the top of the subgrade. Cumulative distributions were generated for each pavement model and for each position.

Figure 6.13 shows the obtained horizontal strain distributions in contrast with the limiting criteria considered by the software. This limiting distribution, developed by Robbins et al. (2015), was developed from simulated strain levels obtained with the PerRoad Software and validated for field-documented perpetual pavements at the NCAT Test Track. The Robbins et al. (2015) limiting strain distribution was especially developed for design purposes and is included as the default design criteria within the PerRoad software (Version 4.4). In practice, if the strain distribution obtained from a specific pavement model is below the limiting distribution at the 55th, 65th, 75th, 85th, and 95th percentiles, it may be inferred that the pavement will behave as perpetual.

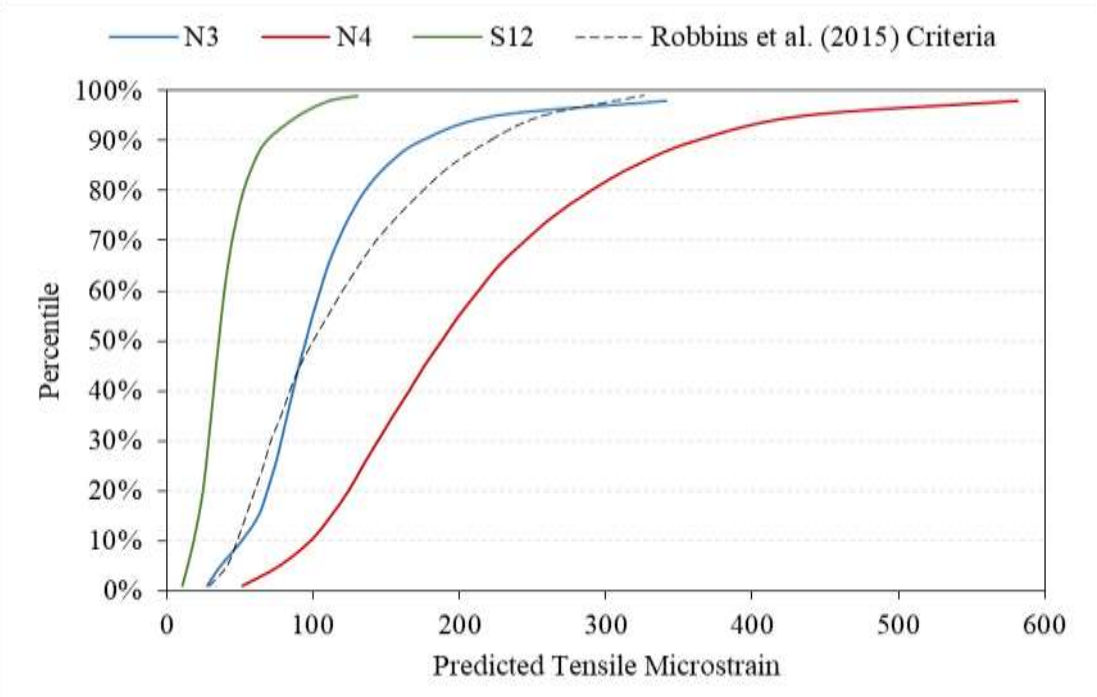

Figure 6.13 PerRoad Simulated Horizontal Strain Distributions

Based on the obtained results, it can be inferred that, from a PPD perspective, section S12 may be expected to be perpetual since its strain distribution is well below the Robbins et al. (2015) control distribution. On the contrary, the horizontal strain distribution obtained for section N4, indicates the pavement is not perpetual and fatigue cracking may appear. Finally, the strain distribution obtained for section N3 seems to cross over the Robbins et al. (2015) limiting distribution. For lower percentiles, the strain distribution is above the limits until approximately the 45th percentile where the strain distribution is below the criteria. At approximately the 96th percentile, the strain distribution exceeds the limiting criteria again. Based on this trend, it may be inferred that section N3 is perpetual as it almost overlaps the limiting strain distribution. In fact, section N3 seems to describe the optimal perpetual pavement for the design conditions based on the horizontal strain criteria.

The Robbins et al. (2015) limiting criteria was not developed for CCPR or CTB materials. At this point, it is unknown whether the sections exceeding the strain limits will truly develop bottom-up cracking since the criteria were not developed from CCPR sections. Likewise, cracking could develop in S12, perhaps from cracking of the cement-stabilized layer reflecting through the CCPR and AC layers. However, application of this perpetual criteria indicates that sections N3 and S12 are likely perpetual and will not suffer from fatigue cracking.

Figure 6.14 shows the vertical compressive strains obtained for each pavement model. A limiting structural rutting criterion of 200 vertical compressive microstrain on top of the subgrade was selected according to the recommendations made by Harvey et al. (2004) and Walubita et al. (2008) and is shown in the figure as a vertical dashed line. Based on these results, section N4 reaches the limiting threshold at approximately the 85th percentile,

indicating there is a low but distinct possibility the pavement may be subjected to structural rutting. Sections N3 and S12 on the contrary are well below the limiting threshold indicating the test sections are perpetual and will not be subject to structural rutting. These results are consistent with the observations made previously based on the horizontal strain distributions in suggesting that, under the traffic and weather conditions at the Test Track, sections N3 and S12 are expected to behave as perpetual pavements according to traditional perpetual pavement design criteria.

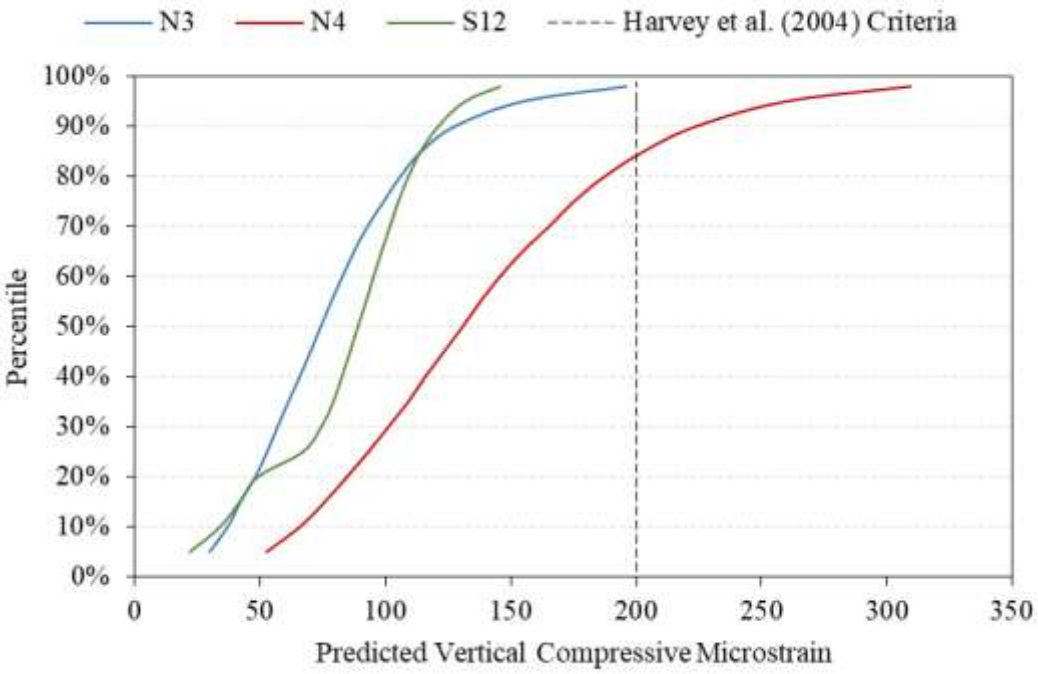

Figure 6.14 PerRoad Simulated Vertical Compressive Strain Distributions

Based on the previous results and considering the specific traffic conditions at the Test Track, the benefits of including two additional inches of AC and replacing the granular base by a CTB, are evident. By comparing the results from sections N3 and N4 it can be inferred that including two additional inches of AC is sufficient to reduce the horizontal

and vertical strains in the structure and achieve a perpetual pavement. Similarly, by comparing the results obtained for sections N4 and S12 it can be postulated that replacing the granular base by a two-inch thicker CTB is also sufficient to achieve a perpetual pavement. Nonetheless, the PPD criteria used in these analyses was not originally developed for CCPR or CTB materials, and all the previous conclusions assume the CCPR layer has the same structural performance on an AC layer. In that way, it is still unknown whether the sections exceeding the strain limits will truly develop bottom-up cracking or structural rutting since the criteria were not developed from CCPR sections.

6.4.4 Perpetual Pavement Design Optimization

The PerRoad model generated for section S12 was gradually modified to optimize the pavement layer thicknesses for the specific conditions at the Test Track during the research cycle. For this, the thickness of the AC/CCPR layer was reduced in 1-inch increments, maintaining all the other properties of the model constant. The horizontal strain distributions obtained for the reduced AC/CCPR thicknesses are shown in Figure 6.15. The Robbins et al. (2015) limiting distribution was slightly exceeded at the 95^{th} percentile when the AC/CCPR thickness was reduced to 4 inches. In that way, 4 inches of AC/CCPR over the 8 inches of CTB, might have been the optimal perpetual pavement for the specific traffic conditions at the Test Track.

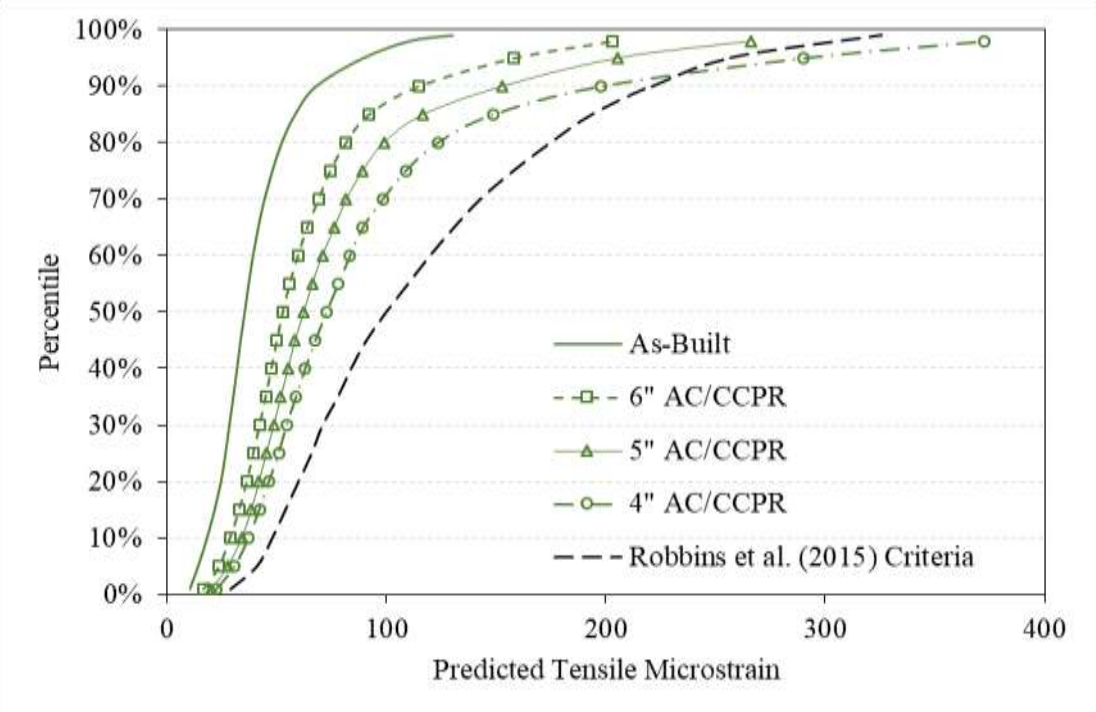

Figure 6.15 Simulated Strains for Reduced AC/CCPR Thicknesses in Section S12

Even if layered elastic analysis within the PerRoad software suggests that an AC/CCPR thickness of 4 inches would still generate horizontal strain distributions below the perpetual pavement design limiting criteria, there is also a concern on the reflective cracking from the CTB which may affect the AC/CCPR layer. Layered elastic modeling of section S12 allowed comparing the as-built pavement with the optimized pavement with a AC/CCPR thickness reduced to 4 inches. The model generated for section S12 was used with the WESLEA layered elastic software to obtain the horizontal strain distributions at different depths within the pavement structure. The results for the as-built and the reduced thickness models are presented in Figure 6.16, where the interface between the AC/CCPR and the CTB layers is identified as CCPR/CTB and the interface of the CTB and the granular base is identified as CTB/GB. In each simulation, the neutral axis (point of zero strain) of the cross-section lies within the AC/CCPR layer with the bottom of the CCPR

and CTB layers both in tension (negative value). The as-built cross-section has nearly equivalent strain levels at the bottom of both layers, but the strains increase significantly as the AC/CCPR thickness is reduced. Reducing the AC/CCPR layer thickness to 4 inches results in a 122% increase in tensile strain at the bottom of the CCPR layer, reaching a relatively higher value of 78 microstrain, which is slightly above the 70 microstrain original perpetual pavement limiting criteria proposed by Monismith and McLean (1972). Similarly, the tensile strain at the interface between the CTB and the granular base increases by 158%, from 45 με to 116 με. The strain tolerance of the CTB is unknown at this point, but this analysis highlights the potential risk of placing too little AC/CCPR over the stabilized base layer where it would be forced to carry significantly greater tensile strains. The fatigue tolerance of the stabilized base should be studied in the future.

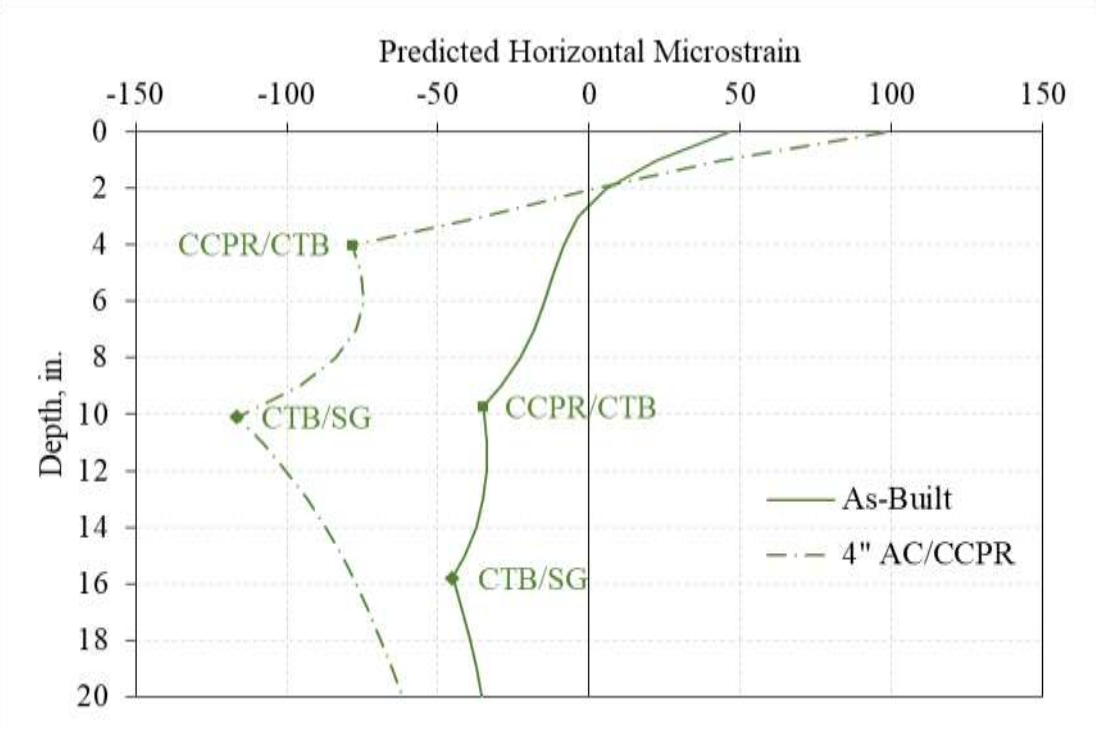

Figure 6.16 Simulated Horizontal Strains versus Depth

From the perspective of continuum mechanics, and assuming the AC/CCPR is indeed a continuous, homogeneous mass, shrinkage cracking in the CTB would reflect on to the upper layer leading to the failure of the pavement structure. However, research conducted by Fu et al. (2010) on the curing mechanisms of foamed asphalt stabilized materials based on micromechanics principles suggested that materials such as the CCPR act as discrete, independent particles. During the foaming process, asphalt is combined with the finer cement particles to create isolated asphalt mastic droplets that bond together the larger particles at specific locations, identified as "spot welds". In that way, the CCPR material would behave as disconnected particles capable of dissipating the stresses induced by cracking of the CTB and acting somewhat like a stress absorbing layer to avoid cracks propagating into the AC layer. More in-depth micromechanics modelling of the crack propagation mechanisms at the CCPR/CTB interface would allow a better understanding of the phenomenon. However, such analyses are beyond the scope of this dissertation and should be the topic of future research at the Test Track.

6.5 SUMMARY

The results obtained from performance monitoring of the test sections were used to characterize the structural performance of the recycled materials from the perspective of different pavement design methods. Analyses were conducted, whenever possible, to identify the structural characteristics of the recycled materials and suggestions were made on how to incorporate them for pavement designs in the future.

The backcalculated modulus values obtained throughout the research cycle were used to determine the structural contribution of each layer based on the AASHTO 93 Pavement

Design Method. For pavement design purposes, it was suggested that the layer coefficients of the CCPR should be considered between 0.30 and 0.35, while the layer coefficients of the CTB should be selected between 0.20 and 0.25. Subsequent pavement design simulations based on the pavement design cross-sections built at the Test Track revealed that field performance of the pavement sections exceeded the predictions obtained with the AASHTO 93 pavement design method. In other words, the applied traffic exceeded the allowable traffic estimated as part of this design procedure. It was therefore postulated that the AASHTO 93 pavement design method may be over-conservative for determining the pavement thickness for CCPR sections.

Since the three test sections included in this study had outstanding performance with no visible damage after over 20 million ESALs, it was fundamentally impossible to conduct any meaningful analyses based on the Mechanistic-Empirical Pavement Design Guide at this stage. The AASHTOWare Pavement ME Software has not yet been calibrated to incorporate recycled materials as CCPR and/or CTB, and based on the fact that no damage was observed at the Test Track, it was not possible to perform any calibrations at this point. Even if the pavement structure of the three test sections could be modelled in the software, it would be impossible to attain any significant conclusions based on the computed performance predictions. Robust conclusions on the applicability of the mechanistic-empirical pavement design method for the CCPR and the CTB will only be reached when the test sections begin to show significant signs of failure, attributable to the traffic loads. The only significant observation that could be made at this point would involve comparing the measured and predicted pavement responses, which was already done as part of the analysis presented in the previous section.

A different M-E analysis was conducted from the perspective of perpetual pavement design. Horizontal and vertical strain measurements performed during the two research cycles were compared to PPD limiting criteria. While all three test sections amply met the structural rutting criteria of a Subgrade Stress Ratio below 0.42 suggested by Bejarano and Thompson (2001), only section S12 met the field PPD criteria defined by Willis and Timm (2009) with horizontal strains well below the limiting strain distributions determined for field measurements. Simulations were conducted using the PPD software PerRoad. The results showed that section N3 seemed to meet the limiting strain distribution on the brink, suggesting the test section has a strong possibility of behaving as a perpetual pavement, while section S12 amply met the PPD criteria. A subsequent optimization of the pavement structure in section S12 revealed that reducing the thickness of the AC/CCPR to only 4 inches would still results in a perpetual pavement. However, the limited knowledge of the cracking mechanisms of the CTB posed some questions regarding the possibility of reflective cracking on a relatively thin AC/CCPR layer.

Based on the analyses presented in this chapter, suggestions were made on how to include recycled materials as CCPR and CTB in different pavement design methodologies. However, additional research on the specific properties of the CCPR and CTB materials and their behavior within the pavement structure is needed to reinforce the findings.

CHAPTER SEVEN

CONCLUSIONS AND RECOMMENDATIONS

7.1 SUMMARY

Pavement recycling techniques such as Cold Central-Plant Recycling (CCPR) and Cement Treated Base (CTB) from a Full Depth Reclamation (FDR) process are becoming popular maintenance and rehabilitation solutions among many state agencies due to their environmental, economic and social benefits (Diefenderfer and Apeagyei, 2011). Both technologies have proven effective in addressing two important needs: (1) recycling the existing pavements and (2) reusing reclaimed materials commonly stockpiled by agencies However, its consistent and widespread use may still be hindered by an apparent lack of long-term performance data from which to derive the expected service life and a lack of understanding of the failure mechanisms in the field. To address this, three test sections were built in 2012 at the National Center for Asphalt Technology (NCAT) Test Track as part of a larger study conducted and sponsored by the Virginia Department of Transportation (VDOT) to evaluate the field performance of these recycled technologies under high traffic conditions and evaluate its structural contribution in a pavement structure.

The test sections were identified as sections N3, N4, and S12. Sections N3 and N4 were adjacent to each other on the north tangent of the Test Track, while the third test

section, S12, was built near the end of the south tangent. Section N3 consisted of three asphalt concrete layers placed over a fourth layer of CCPR. Similarly, sections N4 and S12 consisted of two asphalt concrete layers (top and bottom) placed over a third layer of the same CCPR material. Each section featured stone-matrix asphalt (SMA) surface and Superpave dense-graded AC layers above the CCPR layer. Sections N3 and N4 were constructed on top of a crushed granite aggregate base layer while S12 was built on a CTB layer. The stabilization of the CTB was done in-place where approximately 6" of crushed granite aggregate base and 2" of the subgrade were treated with 4% Type II cement. All three sections were constructed on the same subgrade native to the Test Track and classified as an A-4 soil (Taylor and Timm, 2009). Originally, the VDOT study was formulated to address two specific research objectives with paired test sections. Sections N3 and N4 were designed to evaluate the difference between 4 inches and 6 inches of AC over 5 inches of CCPR, while sections N4 and S12 were designed to determine the differences between aggregate base (6 inches) and the cement stabilized base (SB) layers (8 inches).

A total traffic of 20,055,247 ESALs was applied to each test section by a fleet of special tractor trailer rigs manually operated at a target vehicle speed of 45 mph. The sections were instrumented with an arrangement of asphalt strain gauges, earth pressure cells, and temperature measuring devices, which allowed determining the pavement response under the specific climate and traffic conditions of the test track on a weekly basis. Additionally, the functional and structural performance of each test section was monitored on a routine basis over the duration of the study. Weekly visual inspections and performance measurements of rut depth and ride quality were conducted to maintain current and updated data through slightly different dates over the research cycle. Similarly,

FWD testing was conducted several times per month on each test section. Material samples obtained during construction were tested in the laboratory as part of quality control procedures at the Test Track. Additionally, the CCPR was further evaluated at the Virginia Transportation Research Council (VTRC) Laboratory. The following sections detail conclusions and recommendations that can be derived from this investigation.

7.2 CONCLUSIONS

The results obtained from laboratory testing and performance monitoring were comprehensively analyzed. Based on the observations made and the models studied, the following conclusions can be made regarding the recycled materials used for this investigation.

7.2.1 CCPR and CTB may be used for high traffic applications

After over 20 million ESALs, the functional performance of the three test sections was satisfactory. No surface cracking was detected on any of the test sections. The mean rut depths at the end of the two research cycles was less than two thirds of the rutting failure limit (0.5 inches) established at the NCAT Test Track, indicating the progress of rutting on the test sections is comparable to traditional asphalt concrete pavements. Similarly, despite some rough spots detected since the beginning of trafficking in section S12, the measured IRI in all three test sections was maintained well below the failure threshold of 170 in/mile established at the NCAT Test Track.

The structural performance of the three test sections was evaluated based on the results of FWD testing. Despite some seasonal variability and temperature susceptibility,

observed primarily for the AC and CCPR layers, the variation of backcalculated pavement modulus over time showed no evidence of structural decline in any of the pavement layers. Once normalized to a reference temperature of 68°F, backcalculated pavement modulus remained relatively constant throughout the duration of the study. These results indicate the three pavement structures were capable of withstanding over 20 million ESALs without experiencing any significant structural damage.

Measured pavement response under applied traffic loads remained relatively constant through the two research cycles. Although temperature normalized tensile strains at the bottom of the CCPR showed a slight increase over time in the case of sections N3 and N4, all measured stresses and strains did not seem to indicate any significant signs of damage in any of the test sections. The benefit of the additional 2 inches of AC in section N3 (6 in. AC) as compared to section N4 (4 in. AC) was evident across the temperature spectrum. When normalized at 68°F, section N3 had approximately 40% lower horizontal strains than section N4, while section S12 presented strain magnitudes significantly lower than any other section.

Based on these results, it was established that the two recycled technologies included in this study are adequate for high traffic applications and, if the pavement structure is correctly designed, CCPR and CTB layers may withstand over 20 million ESALs. State agencies and pavement designers should be confident that well designed, well produced, and well maintained pavements with CCPR and CTB are adequate for high traffic roadways.

7.2.2 CCPR is a temperature-dependent material

Laboratory testing showed that the dynamic modulus of the CCPR is affected by temperature and loading frequency. Regardless of the level of confinement, as temperature increased, dynamic modulus of the CCPR decreased, and as test frequency increased, dynamic modulus of the CCPR increased.

Performance monitoring revealed that the FWD backcalculated pavement modulus for the combined AC/CCPR layer was strongly influenced by measured mid-depth pavement temperature. Sections N3 and N4, over the aggregate base, showed a stronger influence of mid-depth pavement temperature on the modulus. Considering only these two test sections allows removing the effect of the CTB from this analysis to focus solely on the structural performance of the CCPR. The test section with a thicker AC layer (N3) was found slightly more temperature sensitive than the thinner AC section (N4), demonstrating the effect of the additional 2 inches of AC in section N3 and the relatively higher percentage of CCPR conforming the AC/CCPR layer in section N4.

Additionally, pavement responses in the test sections having the aggregate base (N3 and N4) showed to be strongly correlated to pavement temperature. A strong correlation was identified between mid-depth pavement temperature and horizontal strains at the bottom of the AC/CCPR layer. Although it was determined that the sensitivity and precision of the pressure measurement was not sufficient to capture the expected reduction in base pressure from the additional AC thickness in section N3 when compared to N4, measured stresses at the top of the base and subgrade showed an evident degree of temperature susceptibility.

Based on these results, it was established that the CCPR is a temperature-dependent material and exhibits a viscoelastic behavior during traffic loading, similar to conventional AC materials. In the field, the modulus of the CCPR layer is influenced by temperature, affecting the stresses and strains induced on the different pavement layers, accordingly. However, the CCPR layer was found less susceptible to temperature than a conventional AC layers.

7.2.3 CTB improved pavement performance

The effect of the CTB on the pavement structure may be observed by comparing sections N4 and S12, with similar pavement structures built over a CTB, in the case of section S12, or an untreated aggregate base, in the case of section N4. Section S12, having the CTB, showed a significantly higher pavement modulus and much less temperature sensitivity than section N4, having the aggregate base. It was postulated that the increased modulus and lower temperature sensitivity was an artifact of the backcalculation process whereby the layers were given a higher apparent modulus to adjust for smaller measured deflections on the CTB. Additionally, the temperature normalized backcalculated modulus values obtained for section S12, over the CTB, showed an increasing trend over time which was attributed to the curing process of the CTB. It was postulated that this behavior may be the result of two different effects. On one hand, the backcalculation process may be attributing higher layer modulus to compensate for the relatively low deflections caused by the presence of the CTB. On the other hand, the CTB may have been curing over time to become a more rigid continuous material, which in turn resulted in increasing backcalculated modulus for all layers.1

Similarly, section S12, having the CTB, presented improved pavement responses with strain and stress magnitudes significantly lower and a response considerably less temperature-sensitive than those obtained for section N4, over the aggregate base. As the tensile strain is a direct function of the underlying supporting material, and the CTB in section S12 is much stiffer than the granular base in sections N3 and N4, it was postulated that the stiffer CTB was limiting, to an extent, the tensile strain in the CCPR layer. Furthermore, measured base and subgrade pressures for section S12 were significantly lower than those obtained for section N4. Based on layered elastic simulations it was established that the increased stiffness of the CTB may have created lower vertical displacements directly above the pressure plate, leading to the significantly lower vertical pressure results obtained for section S12. However, the evolution of temperature-normalized base and subgrade pressures over time in section S12 seemed to indicate some sort of stiffening over time, consistent with a curing process of the CTB.

Based on these results, it was established that the CTB layer had a positive impact on the performance of the pavement structure. The inclusion of stiffer pavement layer underneath a CCPR layer allowed reducing the deflections caused by the application of traffic loads, which in turn translated in reduced strains and stresses in the different pavement layers, and thus an improved structural performance of the pavement.

7.2.4 CCPR and CTB have an acceptable structural contribution

The backcalculated modulus values obtained throughout the research cycle were used to determine the structural contribution of each layer based on the AASHTO 93 Pavement Design Method. For pavement design purposes, it was suggested that the layer coefficients

of the CCPR should be considered between 0.30 and 0.35, while the layer coefficients of the CTB should be selected between 0.20 and 0.25. Subsequent pavement design simulations based on the pavement design cross-sections built at the Test Track revealed that field performance of the pavement sections exceeded the predictions obtained with the AASHTO 93 pavement design method. In other words, the applied traffic exceeded the allowable traffic estimated as part of this design procedure. It was therefore postulated that the AASHTO 93 pavement design method may be over-conservative for determining the pavement thickness for CCPR sections.

Based on these results, it was established that, even if empirical pavement design method may result in over-conservative results, the suggested layer coefficients are adequate from a pavement design perspective. Pavement designers may confidently use the suggested layer coefficients with the AASHTO 93 pavement design method to provide adequate pavement performance, even under high traffic conditions.

7.2.5 The correct combination of CCPR and CTB may result in a Perpetual Pavement

Robust conclusions on the applicability of traditional mechanistic-empirical pavement design method for the CCPR and the CTB could not be reached based on the results from this study. However, a different M-E analysis was conducted from the perspective of perpetual pavement design (PPD). Horizontal and vertical strain measurements performed during the two research cycles were compared to field PPD limiting criteria. While all three test sections amply met the structural rutting criteria of a Subgrade Stress Ratio below 0.42 suggested by Bejarano and Thompson (2001), only section S12 met the field PPD criteria

defined by Willis and Timm (2009) with horizontal strains well below the limiting strain distributions determined for field measurements.

Computer simulations, conducted using the PPD software PerRoad, showed that section S12 amply met the limiting horizontal strain distribution criteria, suggesting the test section could have been designed as perpetual pavement. A subsequent optimization of the pavement structure in section S12 revealed that reducing the thickness of the AC/CCPR to only 4 inches would still results in a perpetual pavement. However, the limited knowledge of the cracking mechanisms of the CTB posed some questions regarding the possibility of reflective cracking on a relatively thin AC/CCPR layer.

Based on these results, it was established that, as observed for section S12, the correct combination of CTB and CCPR may result in a perpetual pavement. On the one hand, the stiffer CTB layer is capable of significantly reducing the stresses and strains within the structure well below the perpetual pavement limiting criteria. On the other, the CCPR layer, besides contributing to the overall pavement structure, also allows absorbing and dissipating the horizontal strains, caused by traffic loads, and the underlying stresses, caused by shrinkage cracking on the CTB, avoiding fatigue and reflective cracking on the pavement surface.

7.3 RECOMMENDATIONS

Continuance of the current research and new supplementary studies would allow validating and expanding the findings from this dissertation. Firstly, continued traffic loading of the three test sections and further monitoring of the functional and structural performance during additional research cycles would allow determining a more accurate rate of deterioration of the built pavement structures. If the pavement sections reach the limiting failure criteria it would be possible to confirm the suggested structural coefficients and perform a local calibration of the transfer functions used for mechanistic-empirical pavement design. Conversely, if the pavement sections continue to exhibit an adequate performance without presenting signs of damage after considerably higher traffic loading, especially in the case of section S12, then the hypothesis of a perpetual pavement may be confirmed.

Furthermore, in the case of failure, forensic analysis of the failed test sections would allow understanding the true failure mechanisms of the CCPR and CTB under traffic loads. Transverse and/or longitudinal trenches at the points of failure may be an adequate starting point for explaining the causes for fatigue cracking and/or structural rutting on the different pavement layers.

Secondly, additional research on the specific properties of the CCPR and CTB materials and their behavior within the pavement structure is needed to reinforce the findings. A better understanding of the cracking mechanisms of the CTB and the effect of the CCPR on dissipating the induced energy caused by the propagation of shrinkage cracks, to ultimately reduce or even eradicate reflective cracking on the pavement surface, is needed.

An in-depth laboratory study of the CCPR would be beneficial to determine its cracking and rutting properties. Bending beam fatigue testing would allow determining the mechanisms for the formation and evolution of fatigue cracks in the CCPR. The susceptibility of the CCPR in comparison to conventional AC materials may be determined by means of Hamburg Wheel or Asphalt Pavement Analyzer testing. The Texas Overlay Tester may also be used to determine the capability of the CCPR to withstand reflective cracking. And many other tests may be conducted for better understanding the failure mechanisms of the CCPR to support and explain with greater detail the conclusions found in this dissertation.

References

AASHTO. (1993). *AASHTO Guide for the Design of Pavement Structures*. Washington, D.C.: AASHTO.

AASHTO. (09/03/2017). *AASHTOWare Pavement ME Design*. https://me-design.com/MEDesign/?AspxAutoDetectCookieSupport=1.

AASHTO. (2009). *AASHTO TP79-09: Standard Method of Test for Determining the Dynamic Modulus and Flow Number for Hot Mix Asphalt (HMA) Using the Asphalt Mixture Performance Tester (AMPT)*. Washington, DC: AASHTO.

Apeagyei, A. & Diefenderfer, B. (2013). Evaluation of Cold In-Place and Cold Central-Plant Recycling Methods Using Laboratory Testing of Field-Cored Specimens. *Journal of Materials in Civil Engineering*, 25(11), 1712-1720.

ARA. (2004). *Guide for Mechanistic–Empirical Design of New and Rehabilitated Pavement Structures*. Washington, D.C.: NCHRP.

Asphalt Academy. (2009). *Bitumen Stabilised Materials, a Guideline for the Design and Construction of Bitumen Emulsion and Foamed Bitumen Stabilised Materials*. Pretoria, South Africa: Asphalt Academy.

APA. (2010). *Perpetual Asphalt Pavements: A Synthesis*. Lanham, MD: Asphalt Pavement Alliance.

APA. (2002). *Perpetual Pavements: A Synthesis*. Lanham, MD: Asphalt Pavement Alliance.

ARRA. (2001). *Basic Asphalt Recycling Manual*. Annapolis, MD: Federal Highway Administration.

Bejarano, M. and Thompson, M. (2001). Subgrade Damage Approach for the Design of Airport Flexible Pavements. *Proceedings of the 27th International Air Transportation Conference*. Chicago, IL.

Bejarano, M. (1999). *Subgrade Damage Approach for the Design of Airport Flexible Pavements.* Urbana, IL: University of Illinois at Urbana-Champaign.

Bemanian, S., Polish P., and Maurer, G. (2006). Cold In-Place Recycling and Full-Depth Reclamation Projects by Nevada Department of Transportation: State of Practice. *Transportation Research Record: Journal of the Transportation Research Board, 1949*, 54-71.

Berthelot, C., Marjerison, B., Houston, G., McCaig, J., Warrener, S., and Gorlick, R. (2007). Mechanistic Comparison of Cement- and Bituminous-Stabilized Granular Base Systems. *Transportation Research Record: Journal of the Transportation Research Board, 2026*, 70-80.

Bonaquist, R. (2011). *NCHRP Report 702 Precision of the Dynamic Modulus and Flow Number Tests Conducted with the Asphalt Mixture Performance Tester*. Washington, D.C.: NCHRP.

Bowering, R. and Martin, C. (1976). Performance of Newly Constructed Full Depth Foamed Bitumen Pavements. *Proceedings of the 8th Australian Road Research Board Conference*. Perth, Australia.

Brown, E., Roberts, F., Lee, D., Kennedy, T., Kim, Y., and Kandhal, P. (2009). *Hot Mix Asphalt - Materials, Mixture Design and Construction*. Lanham, MD: National Center for Asphalt Technology - NAPA Research and Education Foundation.

Castro, A.J., Tran, N., Robbins, M.M., Timm, D.H., and Wagner, C. (2017). Further Evaluation of Limiting Strain Criteria for Perpetual Asphalt Pavement Design. *Transportation Research Record: Journal of the Transportation Research Board, 2640(1)*, 41-48.

Chen, D., Bilyeu, J., Scullion, T., Nazarian, S., and Chiu, C. (2006). Failure Investigation of a Foamed-Asphalt Highway Project. *Journal of Infrastructure Systems,* 12(1), 33-40.

Cho, S., Lee, D., and Kim, N. (2006). Effect of Crack Prevention of Asphalt Pavement Using Geosynthetics. *Proceedings of Geocongress 2006.* Atlanta, GA.

Cross, S.A., and Jakatimath, Y. (2007). *Evaluation of Cold In-Place Recycling for Rehabilitation of Transverse Cracking on US 412, Report No. FHWA/OK 07(04). ,* Oklahoma City, OK.

Díaz-Sánchez, M.A., Timm, D.H., and Diefenderfer, B.K. (2017). Structural Coefficients of Cold Central-Plant Recycled Asphalt Mixtures. *Journal of Transportation Engineering, Part A: Systems*, 143(6), 04017019.

Diefenderfer B.K., Díaz-Sánchez, M., Timm, D.H., and Bowers, B.F. (2016). *Structural Study of Cold Central Plant Recycling Sections at the National Center for Asphalt Technology (NCAT) Test Track*, Report VTRC 17-R9. Charlottesville, VA, 2016.

Diefenderfer, B.K. and Apeagyei, A.K. (2014). *I-81 In-Place Pavement Recycling Project*. Report No. 15-R1, Virginia Center for Transportation Innovation and Research, Virginia Department of Transportation, Charlottesville, 2014.

Diefenderfer, B.K. and Link, S.D. (2014). Temperature and Confinement Effects on the Stiffness of Cold Central-Plant Recycled Mixture. *Proceedings of the 12th international society for asphalt pavements conference on Asphalt pavements.*

Diefenderfer, B. K., Apeagyei, A. K., Gallo, A. A., Dougald, L. E., & Weaver, C. B. (2012). In-place pavement recycling on I-81 in Virginia. *Transportation Research Record*, 2306(1), 21-27.

Diefenderfer, B. K., Bowers, B. F., Schwartz, C. W., Farzaneh, A., and Zhang, Z. (2016). Dynamic modulus of recycled pavement mixtures. *Transportation Research Record*, 2575(1), 19-26.

FHWA. 21/10/2015. Pavement Smoothness. https://www.fhwa.dot.gov/Pavement/smoothness/index.cfm

Fernandez-Almanza, J. (2013). Un Nuevo Modelo de Conservación de Carreteras: Experiencias e Innovaciones Tecnológicas. *Proceedings of Octavo Congreso Mexicano Del Asfalto*, Cancun, Mexico.

Fu, P., Jones, D., Harvey, J. T., and Halles, F. A. (2009). Investigation of the curing mechanism of foamed asphalt mixes based on micromechanics principles. *Journal of Materials in Civil Engineering*, 22(1), 29-38.

Gnanendran, C. and Woodburn, L. (2003). Recycled Aggregate for Pavement Construction and the Influence of Stabilisation. *Proceedings of the 21st ARRB and 11th REAA Conference.* Cairns, Australia.

Guthrie, W. S., Cooley, D., and Eggett, D. L. (2007). Effects of reclaimed asphalt pavement on mechanical properties of base materials. *Transportation Research Record*, 2005(1), 44-52.

Halles, F., Thenoux, G., and Gonzalez, A. (2013). Stiffness Evolution of Granular Materials Stabilized with Foamed Bitumen and Cement. *Transportation Research Record: Journal of the Transportation Research Board*, 2363(1), 105-112.

Hansen, K.R. and Copeland, A. (2013). *Annual Pavement Industry Survey on Recycled Materials and Warm Mix Asphalt Usage: 2009-2012 (No. IS-138).* National Asphalt Pavement Association.

Harvey, J., Monismith, C., Horonjeff, R., Bejarano, M., Tsai, B. W., and Kannekanti, V. (2004). Long-life AC pavements: A discussion of design and construction criteria

based on California experience. *International Symposium on Design and Construction of Long Lasting Asphalt Pavements, 2004*. Auburn, AL.

HRB. (1962). *The AASHO Road Test. Report 5: Pavement Research, Special Report 61E*. Washington, D.C.

Hilbrich, S. and Scullion, T. (2008). Evaluation of Laboratory Mix Design and Field Performance of Asphalt Emulsion and Cement Stabilized Full Depth Reclamation Project in Texas. *Proceedings of 87th annual Meeting of the Transportation Research Board*. Washington, DC.

Hossain, M. and Kim, W. (2014). *Estimation of Subgrade Resilient Modulus Using the Unconfined Compression Test*. Report No. FHWA/VCTIR 15-R12. Charlottesville, VA.

PCA. (09/01/2017). What is a Cement-Treated Base? http://www.cement.org/cement-concrete-applications/paving/cement-treated-base-(ctb).

Janoo, V. (1994). *Layer Coefficients for NHDOT Pavement Materials, Report No. CRREL-SP-94-30*. Hanover, NH.

Jenkins, K. and Van de Ven, M. (2001). Guidelines for the Mix Design and Performance Prediction of Foamed Bitumen Mixes. *Proceedings of the 20th South African Transport Conference*, Pretoria, South Africa.

Jenkins, K., Van de Ven, M., and De Groot, J. (1999). Characterization of Foamed Bitumen. *7th Conference on Asphalt Pavements for Southern Africa*. Pretoria, South Africa.

Jones D., Fu, P., Harvey, J., and Halles, F. (2008). *Full-Depth Pavement Reclamation with Foamed Asphalt: Final Report (No.UCPRC-RR-2008-07)*, University of California Pavement Research Center, Davis and Berkeley, CA.

Khosravifar, S., Schwartz, C. and Goulias, D. (2013). Mechanistic Structural Properties of Foamed Asphalt Stabilized Base Materials. *Proceedings of the 92nd Annual Meeting of the Transportation Research Board*. Washington, D.C.

Kim, Y., Lee, H. D., and Heitzman, M. (2009). Dynamic Modulus and Repeated Load Tests of Cold-in-Place Recycling Mixtures Using Foamed Asphalt. *Journal of Materials in Civil Engineering*, 21(6), 279–285.

Lacrois, A., Underwood, B.S., and Kim, Y.R. (2011). Reduced Testing Protocol for Measuring the Confined Dynamic Modulus of Asphalt Mixtures. *Transportation Research Record: Journal of the Transportation Research Board*, 2210(1), 20-29.

Lane, B. and Kazmierowski, T. (2005). Implementation of Cold In-Place Recycling with Expanded Asphalt Technology in Canada. *Transportation Research Record: Journal of the Transportation Research Board*, 1905(1), 17-24.

Lewis, D., Jared, D., Torres, H., and Mathews, M. (2006). Georgia's use of cement-stabilized reclaimed base in full-depth reclamation. *Transportation Research Record: Journal of the Transportation Research Board,* 1952(1), 125-133.

Lofti, H., and Witczak, M. (1985). Dynamic Characterization of Cement- Treated Base and Sub-Base Materials. *Transportation Research Record: Journal of the Transportation Research Board,* 1031(1), pp. 41-48.

Loizos, A, and Papavasiliou, V. (2006). Evaluation of Foamed Asphalt Cold-in-Place Pavement Recycling Using Nondestructive Techniques. *Journal of Transportation Engineering,* 132(12), 970–978.

Loizos, A., Papavasiliou, V., and Plati C. (2007). Early-Life Performance of Cold-in-Place Pavement Recycling with Foamed Asphalt Technique. *Transportation Research Record: Journal of the Transportation Research Board,* 2005 (1), 36-43.

Marquis, B., Peabody, D., Mallick, R., and Soucie, T. (2003). *Determination of Structural Layer Coefficient for Roadway Recycling Using Foamed Asphalt*. Durham, NH.

Menendez, J., Thenoux, G., and Gonzalez, M. (2013). Premature Cracking in Foamed Asphalt Pavement: Peru Brazil Highway Case Study. P*roceedings of the 92nd Annual Meeting of the Transportation Research Board*. Washington, D.C.

Mohammad, L., Abu-Farsakh, M., Wu, Z., and Abadie, C. (2003). Louisiana Experience with Foamed Recycled Asphalt Pavement Base Materials. *Transportation Research Record: Journal of the Transportation Research Board,* 1832(1), 17-24.

Monismith, C. and McLean, D. (1972). Technology of Thick Lift Construction: Structural Design Considerations. *Asphalt Paving Technology: Journal of the Association of Asphalt Paving Technologists,* 41, 258-304.

Monismith, C.L. (2012). Flexible Pavement Analysis and Design – A Half Century of Achievement. *Geotechnical Engineering State of the Art and Practice,* 187–220.

Nataatmadja, A. (2001). Some characteristics of foamed bitumen mixes. *Transportation Research Record: Journal of the Transportation Research Board,* 1767(1), 120-125.

NCHRP. (09/07/2017). *Material Properties of Cold In-Place Recycled and Full-Depth Reclamation Asphalt Concrete for Pavement Design.* http://apps.trb.org/cmsfeed/TRBNetProjectDisplay.asp?ProjectID=3164.

Newcomb, D.E., Willis, R., and Timm, D.H. (2010). *Perpetual Asphalt Pavements: A Synthesis*, Report IM-40, Asphalt Pavement Alliance.

Nishizawa, T., Shimeno, S., and Sekiguchi, M. (1996). Fatigue Analysis of Asphalt Pavements with Thick Asphalt Mixture Layers. *Proceedings of the 8th International Conference on Asphalt Pavements*. Seattle, WA.

Pellinen, T.K. and Witczak, M.W. (2002). Stress Dependent Master Curve Construction for Dynamic (Complex) Modulus. *Asphalt Paving Technology: Journal of the Association of Asphalt Paving Technologists,* 71, 281-309.

Peters-Davis, K. and Timm, D. (2011). Recalibration of the Asphalt Layer Coefficient. In *Journal of Transportation Engineering*, 137(1), 22–27.

Pierce, L. and McGovern, G. (2014). *Implementation of the AASHTO Mechanistic-Empirical Pavement Design Guide and Software*. NCHRP Synthesis 457. Washington, D.C.

PCA. (09/01/2017). *Cement Treated Base*. http://www.cement.org/docs/default-source/th-paving-pdfs/ctb-cement-treated-base/cement-treated-base-pca-logo.pdf?sfvrsn=2.

Puppala, A., Hoyos, L., and Potturi, A. (2011). Resilient Moduli Response of Moderately Cement-Treated Reclaimed Asphalt Pavement Aggregates. *Journal of Materials Engineering*, 23(7), 990-998.

Robbins, M., Tran, N., Timm, D., Willis, J., and Rodezno, C. (2015). *Refined Limiting Strain Criteria and Approximate Ranges of Maximum Thickness for Designing Long- Life Asphalt Pavements*, *Report No. 15-05*, Auburn University, AL.

Romanoschi, S. A., Hossain, M., Gisi, A., & Heitzman, M. (2004). Accelerated Pavement Testing Evaluation of the Structural Contribution of Full-Depth Reclamation Material Stabilized with Foamed Asphalt. *Transportation Research Record: Journal of the Transportation Research Board*, 1896(1), 199-207.

Saleh, M. F. (2004). New Zealand Experience with Foam Bitumen Stabilization. *Transportation Research Record: Journal of the Transportation Research Board*, 1868(1), 40-49.

Schwartz, C. W., and Khosravifar, S. (2013). *Design and evaluation of foamed asphalt base materials, Final Report, (No. MD-13-SP909B4E)*. Maryland. State Highway Administration. Office of Policy & Research.

Sebaaly, P. E., Bazi, G., Hitti, E., Weitzel, D., and Bemanian, S. (2004). Performance of cold in-place recycling in Nevada. *Transportation Research Record: Journal of the Transportation Research Board*, 1896(1), 162-169.

Sebesta, S. (2006). *Microcracking for Reduced Shrinkage in Cement-Treated Base* (Poject Summary Report 0-4502-S).

Stroup-Gardiner, M. (2011). *Recycling and Reclamation of Asphalt Pavements Using In-Place Methods* (No. Project 20-05 (Topic 40-13)).

Taha, R., Al-Harthy, A., Al-Shamsi, K., and Al-Zubeidi, M. (2002). Cement stabilization of reclaimed asphalt pavement aggregate for road bases and subbases. *Journal of materials in civil engineering*, *14*(3), 239-245.

Taylor, A. and Timm D.H. (2009). *Mechanistic characterization of resilient moduli for unbound pavement layer materials* (Doctoral dissertation).

Thenoux, G., Gonzalez, A., and Dowling, R. (2007). Energy consumption comparison for different asphalt pavements rehabilitation techniques used in Chile. *Resources, Conservation and Recycling*, *49*(4), 325-339.

Tia, M., and Wood, L. E. (1983). Use of asphalt emulsion and foamed asphalt in cold-recycled asphalt paving mixtures. *Transportation Research Record: Journal of the Transportation Research Board*, *898*, 315-321.

Timm, D., and Tutu, K. (2017). Determination of an optimum backcalculation cross section for unconventional pavement profiles. *Transportation Research Record; Journal of the Transportation Research Board*, *2641*(1), 48-57.

Timm, D. H., Diefenderfer, B. K., and Bowers, B. F. (2018). Cold Central Plant Recycled Asphalt Pavements in High Traffic Applications. *Transportation Research Record*, *2672*(40), 291-303.

Timm, D. H., Sánchez, M. D., and Diefenderfer, B. K. (2015). *Field Performance and Structural Characterization of Full-Scale Cold Central Plant Recycled Pavements* (No. 15-0781).

Timm, D. H. (2009). Design, construction and instrumentation of the 2006 test track structural study. *National Center for Asphalt Technology: NCAT Report*, 09-01.

Timm, D. H., Diefenderfer, B. K., and Bowers, B. F. (2017). Cold Central Plant Recycled Asphalt Pavements in High Traffic Applications. *Transportation Research Record*, *2672*(40), 291-303.

Timm, D. H., Robbins, M. M., Tran, N., and Rodezno, C. (2014). *Flexible Pavement Design–State of the Practice* (No. NCAT Report 14-04).

Tran, N., Robbins, M. M., Timm, D. H., Willis, J. R., and Rodezno, C. (2015). *Refined Limiting Strain Criteria and Approximate Ranges of Maximum Thicknesses for Designing Long-Life Asphalt Pavements* (No. NCAT Report 15-05).

Van der Walt, N., Botha, P., Semmelink, C., Engelbrecht, F., and Salminen, N. (1999). The use of foamed bitumen in full-depth in-place recycling of pavement layers illustrating the basic concept of water saturation in the foam process. In *Proceedings of the Seventh Conference on Asphalt Pavements for South Africa*.

Van Wijk, A. and Wood, L. E. (1983). Use of Foamed Asphalt 1n Recycling of an Asphalt Pavement. *Transportation Research Record: Journal of the Transportation Research Board, 911*, 96-103.

Van Wyk, A., Yoder, E. J., and Wood, L. E. (1983). Determination of structural equivalency factors of recycled layers by using field data. *Transportation Research Record: Journal of the Transportation Research Board*, *898*, 122-132.

Vargas-Nordcbeck, A. and Timm, D. (2013). *Physical and structural characterization of sustainable asphalt pavement sections at the NCAT test track* (No. NCAT Report 13-02).

Virginia Department of Transportation, Maintenance Division. (2014). *State of the Pavement Report*.

Virginia Department of Transportation, Materials Division. (2000). *Guidelines for 1993 AASHTO Pavement Design*.

Virginia Department of Transportation. (2015). *Notice of Revision to Materials Division's Manual of Instructions Chapter VI,* Memorandum 386-15.

Walubita, L. F., Liu, W., Scullion, T., and Leidy, J. (2008). *Modeling Perpetual Pavements Using the Flexible Pavement System (FPS) Software* (No. 08-2311).

West R., Timm, D., Powell, B., Heitzman, M., Tran, N., Rodezno, C., Watson, D., Leiva, F., Vargas, A., Willis, R., Vrtis, M., and Díaz, M. (2018). *Phase V (2012-2014) NCAT Test Track Findings.* (No. NCAT Report 16-04).

West, R., Timm, D., Willis, R., Powell, B., Tran, N., Watson, D., and Villacorta, F. L. (2012). *Phase IV NCAT pavement test track findings.* (No. NCAT Report 12-10).

Williams, B, Willis, J., and Carter-Ross, T. (2019). *Asphalt Pavement industry Survey on Recycled Materials and Warm-Mix Asphat Usage* (NAPA IS-138).

Willis, J. and Timm, D. (2009). *Field-based strain thresholds for flexible perpetual pavement design.* (No. NCAT Report 12-10).

Willis, J.R. and Timm, D.H. (2010). Development of Stochastic Perpetual Pavement Design Criteria. *Journal of the Association of Asphalt Paving Technologists,* 79(1), 561-596.

Wirtgen Group. (2002). *Foamed Bitumen – The Innovative Binding Agent for Road Consruction*. Wirtgen GmbH, Windhagen, Germany.

Wirtgen Group. (2012). *Wirtgen Cold Recycling Manual*. First Edition. Wirtgen GmbH, Windhagen, Germany.

Wirtgen Group. (2010). *Wirtgen Cold Recycling Manual*. Wirtgen GmbH, Windhagen, Germany.

Zeiada, W.A., Kaloush, K., Biligiri, K., Reed, J., and Stempihar, J. (2011). Significance of Confined Dynamic Modulus Laboratory Testing for Asphalt Concrete: Conventional, Gap-Graded, and Open-Graded Mixtures. *Transportation Research Record: Journal of the Transportation Research Board*, 2210(1) 9-19.